Advanced Space Concepts Laboratory
Department of Mechanical and Aerospace Engineering
Faculty of Engineering
University of Strathclyde

Exploiting Astrodynamics for the Manipulation and Exploration of Asteroids

Daniel García Yárnoz

Submitted in fulfilment of the requirements for the degree of

Doctor of Philosophy

2015

This thesis is the result of the author's original research. It has been composed by the author and has not been previously submitted for examination which has led to the award of a degree.

Daniel García Yárnoz
Glasgow, Scotland, 23/04/2015

First submission: 14/11/2014
Viva / oral defence: 27/02/2015

Acknowledgements

First of all, I would like to start by thanking Professor Colin McInnes for his guidance during the past 3 years. I honestly could not have asked for a better supervisor; Colin has always been extremely supportive, inspiring and encouraging. I am very grateful as well to Pau, Patricia and Russell for their inputs, constructive criticism and help. Whatever other VisionSpace researchers may say, Theme 3 rules!

I also would like to express my gratitude to the rest of the Advanced Space Concepts Laboratory for creating the perfect environment for research (including of course the always helpful support and administration staff). Big thanks in particular to Garrie and Andreas, from my PhD cohort, with whom I lived through all the stages of the degree. I am also in debt with Jeannette for her countless inputs, ideas, interesting discussions and, above all, poster design tips.

A few side projects have made the past few years even more enjoyable. Doing an internship at Colorado University in Boulder and working under the supervision of Professor Daniel Scheeres was an invaluable experience, professionally and personally. I express my warm thanks to the StrathSat-R kids for the distraction of a completely different project. It was always a source of fresh new ideas, a chance to do some hands-on work, and definitely an exercise for our creativity: could it also be the first time that I actually enjoyed ironing? I am also sincerely grateful to the LightTouch^2 team for their trust with consultant work in their laser deflection proposal to ESA's SysNOVA initiative.

All this would not have been possible without numerous sources of funding that supported me and these projects. In addition to the European Research Council VisionSpace grant, I would like to thank the Royal Society of Edinburgh John Moyes Lessells Travel Scholarship and the Glasgow Mac Robertson Postgraduate Travel Scholarship for their funding of my visit to Boulder, StrathSEDS and ESA's REXUS program for the StrathSat-R support, and the funding provided by the Royal Aeronautical Society, the Institute of Engineering and Technology, the Nanjing University and the PGR scheme of the University of Strathclyde to attend various conferences. Being able to present my research in front of technical audiences around the globe brought me greater insight into my field of research and precious (mostly constructive) feedback.

On a more personal note, I would like to mention my ex co-workers at ESA and GMV for their support during this wonderful but challenging experience, and the ISU family for their vote of confidence, allowing me to manage their engineering department. This taught me precious skills which turned out extremely useful during the last three years. My flatmates in Glasgow also played a major role in lifting up my spirits thanks to our uncounted dinners, laid-back and serious talks over a cuppa or a pint, and the occasional sermon when appropriate!

A heartfelt thanks goes out to my girlfriend Marie: for her always uplifting words, for her patience enduring me during good and bad times, and also for her help in writing these acknowledgements (:P how meta).

Finally, I could never have done it without the support and encouragement of my family (you are the best and you've always been there for me!) and my friends, old and new, even though most of you thought I was crazy for attempting a PhD and leaving a more than good job at ESA after so many years.

A few final words go to Saint-Exupery and his unforgettable *Le Petit Prince*, 'un grand merci'! This inspiring novel truly cheered me up when I felt down. I learnt a great deal from this little boy, in particular how to be both a child and an adult, or in other words, a student in his thirties.

A mamá, papá y Cris.

Abstract

The accessibility of minor bodies, the impact threat they pose, their scientific interest and the theorised potential for material extraction have pinpointed asteroids and comets as attractive targets for current and future space exploration. The manipulation of these minor bodies has been discussed for over a century, mainly with the aim of planetary protection, and in general based on the use of artificial external forces.

Within this thesis, the manipulation of asteroids has been addressed across a range of length-scales, from orbit to dust particle manipulation, placing emphasis on exploiting natural astrodynamics.

On the macro-scale regime, the capture of Near–Earth Objects into libration point orbits of the Sun–Earth system was investigated by exploiting manifold dynamics to obtain low-costs transfers.

At middle scales or meso-scales, this thesis proposes the use of tidal torques acting on captured asteroids during swing-bys to manipulate the asteroid's rotational state. Possibilities included induced asteroid spin-up, de-spin, rotational fragmentation or binary break-up.

In addition, the exploitation of solar radiation pressure was analysed with the purpose of generating new orbiting strategies around minor bodies.

Finally, at the smallest scales or micro-scales, a novel asteroid regolith separation method based on the exploitation of differential solar radiation pressure has been proposed.

Contents

List of Symbols and Acronyms

Constants and Variables

A	Tidal term in the orbit-averaged approach Hamiltonian
a	Semi-major axis
a, b, c	Semi-principal axes of an ellipsoid
A_H	Hamaker coefficient
C	Solar radiation pressure term in the orbit-averaged approach Hamiltonian
c	Speed of light
C_{mn}	Gravitational harmonics coefficients with $m = 0, 1, 2, \ldots$ and $n = 0, 1, \ldots, m$
d	Distance (from the Sun)
e	Eccentricity
f	Aggregate shape or orientation factor
F_c	Cohesive force
G	Gravitational constant
H	Hamiltonian
H_A	Asteroid's absolute magnitude
i	Inclination
I^*	Inertia shape factor
I_{sp}	Specific Impulse
I_{xx}, I_{yy}, I_{zz}	Principal moments of inertia
J	Jacobi Constant
L	Characteristic Length
L_S	Solar luminosity
m	Mass

$minH$	Minimum height over surface
p_v	Albedo
Q	Solar radiation pressure coefficient
R	Body or asteroid radius
r	Particle radius
r	Radial coordinate / radial distance
r^*	Apses radii ratio
r_a	Apocentre radius
r_p	Pericentre radius
r_{eq}	Aggregate equivalent radius
S	Cross-sectional area
S_c	Cleanliness ratio
T	Period
t	Time
T_A	Asteroid rotation period
v	Velocity
v_∞	Hyperbolic excess velocity
WN	Winding number
x or X	X coordinate
y or Y	Y coordinate
z or Z	Z coordinate
$\vec{F}_{SRP}$	Solar radiation pressure force
$\vec{r}$	Position vector / radius vector / state vector
α	Binary pair radii ratio
β	Lightness number
β'	Scaled lightness number
β^*	Aggregate equivalent lightness number
Δv	Delta velocity (velocity change)
η	Normalised Y coordinate

Γ	Normalised Jacobi Constant
γ	Ellipsoid orientation angle
λ_{SUN}	Solar longitude
μ	Gravitational parameter ratio
μ_B	Gravitational parameter body B (see subscripts below)
μ_{log}	Mean of a log-normal distribution
ν	True anomaly
Ω	Right ascension of the ascending node
ω	Argument of pericentre
Ω_O	Diameter of a O^{-2} ion
ω_p	Libration point orbit planar motion frequency
ω_v	Libration point orbit vertical motion frequency
ω_{rot}	Rotational velocity (also indicated as $\dot{\theta}$)
Φ	Porosity
ϕ	Phase space angle
Φ_M	Monodromy matrix
ρ	Density
σ_{log}	Standard deviation of a log-normal distribution
τ	Normalised time
θ	Orientation angle with respect to a reference axis
ϱ	Scaled body or asteroid radius
ξ	Normalised X coordinate
ζ	Normalised Z coordinate
$\vec{\rho}$	Normalised state vector
Ø	Diameter

Subscripts

$_0$	Initial
$_{1,2,3...}$	Indicating a series of events/manoeuvres/bodies...
$_A$	Asteroid (Body)

$_a$	Apocentre
$_B$	Generic solar system body
$_{crit}$	Critical
$_{eject}$	Ejection
$_{eq}$	Equivalent
$_E$	Earth (Body)
$_f$	Final
$_{i,j,...}$	Indexes
$_{loc}$	Local horizontal reference frame
$_M$	Moon (Body)
$_p$	Pericentre
$_{REF}$	Reference
$_{SOI}$	Sphere of influence
$_S$	Sun (Body)
$_t$	Total
$_{x,y,z}$	Relative to the x, y or z coodinate

Additional notation

$\dot{\square}$	First derivative
$\ddot{\square}$	Second derivative
$\partial\square$	Partial
$\Delta\square$	Increment
$\bar{\square}$	Averaged variable
$\tilde{\square}$	Full-dimensional variable
$\vec{\square}$	Vector

Acronyms

2D	Two dimensional
3D	Three dimensional
AIM	Asteroid Impact Monitor
AOCS	Attitude and Orbit Control System
ARM	Asteroid Retrieval Mission

AU	Astronomical Unit
BYORP	Binary YORP effect
CR3BP	Circular Restricted Three–Body Problem
DART	Double Asteroid Redirection Test
ER3BP	Elliptic Restricted Three–Body Problem
ERO	Easily Retrievable Object
ESA	European Space Agency
GEO	Geostationary Earth Orbit or Geosynchronous Equatorial Orbit
ISRU	In-Situ Resource Utilisation
JAXA	Japan Aerospace eXploration Agency
JPL	Jet Propulsion Laboratory
KAM	Kolmogorov-Arnold-Moser
LEO	Low Earth Orbit
LPO	Libration Point Orbit
LSST	Large Synoptic Survey Telescope
MOID	Minimum Orbit Intersection Distance
NASA	National Aeronautics and Space Administration
NEA	Near–Earth Asteroid
NEO	Near–Earth Object
NEOWISE	Near–Earth Object Wide-field Infrared Survey Explorer
NES	Natural Earth Satellites
NHATS	Near–Earth Object Human Space Flight Accessible Targets Study
OCC	Orbit Conditioning Code
OSIRIS-REx	Origins Spectral Interpretation Resource Identification Security Regolith Explorer
Pan-STARRS	Panoramic Survey Telescope And Rapid Response System
QTO	Quasi-Terminator Orbit
RPA	Radiation Pressure Approximation
SC	Spacecraft
SEA	Small Earth–Approachers

SRP	Solar Radiation Pressure
TCO	Temporarily Captured Orbiter
WAC	Wide Angle Camera
YORP	Yarkovsky-O'Keefe-Radzievskii-Paddack effect

List of Figures

List of Tables

Chapter 1

Introduction

"One only understands the things that one tames"

Saint-Exupéry (1943), *The Little Prince*

This chapter introduces the scope and main objectives of the thesis, and provides the necessary background to understand the need for Near–Earth Object (NEO) manipulation research. The concept of *exploitation of natural astrodynamics* and the possibilities associated to *asteorid manipulation* are also discussed.

1.1 NEO: Threat, challenges and opportunities

Recently, significant interest has been devoted to the understanding of minor bodies of the solar system, including near-Earth and main belt asteroids and comets (Bottke et al., 2002a). Near–Earth Objects in particular (asteroids and comets with perihelion distance smaller than 1.3 AU) have grown in prominence because of two important points: they are among the easiest bodies to reach from Earth (Abell et al., 2012; Adamo et al., 2010; Barbee et al., 2010) and they represent a potential impact threat (Chesley et al., 2002).

In addition to their accessibility and threat, as witnesses of the early solar system, asteroids and comets could cast light onto unresolved questions concerning the formation of the planets from the proto-planetary disc (Bottke et al., 2002a), and perhaps settle debates on the origin of water on Earth and panspermian theories, among others. This scientific importance has translated into an increasing number of robotic probes sent to minor bodies, with many more planned over

the coming decades. NASA, ESA and JAXA have conceived a series of scientific missions (a brief description of past and future missions can be found in Scheeres, 2012b), having in mind that minor body research not only provides a deeper insight into the formation and evolution of the solar system, but also represents a technological challenge for space exploration. The Chinese National Space Administration recently became the fourth space agency to visit a minor body with an end-of-life extension to their probe Chang'e 2 to perform a flyby of asteroid Toutatis (Zoua et al., 2014), further demonstrating the scientific interest of the international community in these objects. Science and knowledge gain, however, are not the only benefits of asteroid and comet characterisation, and mission concepts exploring synergies with science, planetary protection and space resource utilisation are becoming important. A classical reference in the matter of resource extraction is the book by Lewis (1996). Finally, asteroid's low gravity wells are also one of the most promising and feasible "planetary" surfaces that can be visited by crewed missions under NASA's flexible path plan (Augustine et al., 2009). These new mission concepts go beyond remote sensing and in-situ characterisation, requiring more complex forms of interaction with minor bodies.

These complex interactions are intrinsically linked to and conditioned by our level of understanding of minor bodies. The suggestion in the opening quote that to truly understand something one must first *"tame"* it is backed up by the history of humanity and its interaction with the environment. From the literal taming of flora and fauna, to phenomena such as fire, or even larger scale modifications of geography itself, such as shifting of riverbeds, understanding and taming (or manipulation) have always gone hand in hand. Scientists and engineers attempt to control nature and physical phenomena which leads to a better understanding of them, and vice-versa, growing knowledge and discoveries result in novel techniques to modify or manipulate the world around us.

In the case of asteroids and comets, the benefits of a deeper understanding are clear, and indeed the first daring attempts to manipulate them have already taken place, with mixed success. Examples of this are NASA's Deep Impact kinetic impactor mission (A'Hearn et al., 2005), JAXA's sample return mission to asteroid Hayabusa (Kawaguchi et al., 2008), or ESA's Rosetta mission featuring a lander with harpoons (Glassmeier et al., 2007). Future sample return mission studies include ESA's discontinued candidate missions MarcoPolo (Barucci et al., 2009) and MarcoPolo-R (Barucci et al., 2012), and JAXA's follow-up mission

Hayabusa-2 (see again Kawaguchi et al., 2008). In addition, recent NASA and ESA studies on kinetic impact demonstrator missions plan on taking asteroid manipulation one step further. Building on the blocks of the cancelled Don Quixote proposal to deflect an asteroid (Carnelli et al., 2006), the joint binary object orbit modification study AIDA (Murdoch et al., 2012), comprising the DART and AIM spacecraft, intends to demonstrate and validate the concept of kinetic impactor for orbit modification of the binary system Dydimos.

Further advances could be made by exploiting natural astrodynamics and other dynamical features of the solar system, and in particular of these minor bodies, to reduce the cost of manipulation, enhance its engineering intervention effects, or devise new applications. The aim of this thesis will therefore be to form the basis for novel concepts of asteroid manipulation, focusing mainly on NEOs and taking advantage of these natural dynamics.

1.2 Exploitation of natural astrodynamics

The term *exploitation* is usually associated with making use of tangible resources for some benefit. In this thesis exploitation is used in a broader way, with resources including more abstract concepts such as gravity, sun-light, and in general any force or environmental characteristic.

This loosely defined term of "exploitation of astrodynamics" is by no means a new notion. It is the same concept as taking advantage of Earth's gravity and rotational period to define Geostationary (GEO) orbit (Clarke, 1945), or exploiting perturbations such as the oblateness of the Earth to devise Molniya orbits for high latitude coverage, already in the 1970s (Kidder and Vonder Haar, 1990), or to generate Sun-synchronous orbits for Earth observation and other applications (see for example Vallado, 2007, pp. 786-791). Much bolder schemes of exploitation of natural dynamical features have been successfully flown. Placing spacecraft in libration point orbits could soon be considered as routine, with over seven spacecraft already flown from the ISEE-3 mission (Richardson, 1980) or the SOHO observatory (Domingo et al., 1995) to the recent ESA Herschel and Planck telescopes (Doyle et al., 2009) or the already mentioned Chang'e 2 (Zoua et al., 2014). Many more are indeed planned for the near future (e.g. GAIA, JWST, Euclid, ATHENA ...). Manifold dynamics have also been used to recover spacecraft (Belló et al., 2010), and novel propellantless propulsion methods such as

solar sailing have already been demonstrated (Funase et al., 2010). Solar sailing, for example, exploits solar radiation pressure (SRP) perturbations for propulsion (McInnes, 1999), and could potentially widen the spectrum of achievable highly non-Keplerian orbits, from displaced GEO (Heiligers et al., 2011) to heliotropic orbits (Colombo et al., 2011).

These same techniques can be applied to the case of asteroids and other minor bodies, with the advantage of their very low-gravity and near vacuum environment, which increases the relative effect of perturbations. However, due to the diversity of asteroids and comets in their type of orbits (Bottke et al., 2002a), size, spin state (Pravec et al., 2002), structure (Britt et al., 2002), and composition (Binzel et al., 2002; Clark et al., 2002), most of these techniques will need to be tailored for each particular case. The dynamical effects that the manipulation methods are based on are generic, although their relative importance will vary for each case with asteroid characteristics and the intended application.

1.3 Forces on NEOS

In order to exploit natural astrodynamics, it is important to determine the forces acting on Near–Earth Objects and their environment, and in which time-frame and length-scale they operate. Scheeres et al. (2010) provide a comprehensive review of the forces affecting regolith material and spacecraft in the vicinity of asteroids, and their relative scaling. In addition to these, in this thesis forces that affect the asteroid itself, its orbit, spin and structure will also be considered. Figure 1.1 shows a schematic of the main forces acting on NEOs, represented in a time-scale vs. length-scale plot. The various effects have been colour-coded according to their origin. Forces based on gravity are coloured in blue, radiation induced effects in yellow, and material related forces in green. The boundaries in this classification are somewhat fuzzy and should not be taken as fixed. For example, cohesive forces between particles, indicated on the graph as a material related force, are explained by the electromagnetic attraction of molecules, so it could be argued that they belong in the same group as electrostatic forces.

Highlighted with red text are three specific effects that will be the main focus of this thesis: manifold dynamics, tidal forces, and solar radiation pressure perturbations. They were selected because of the practical time-scales they act on, and their potential for manipulation.

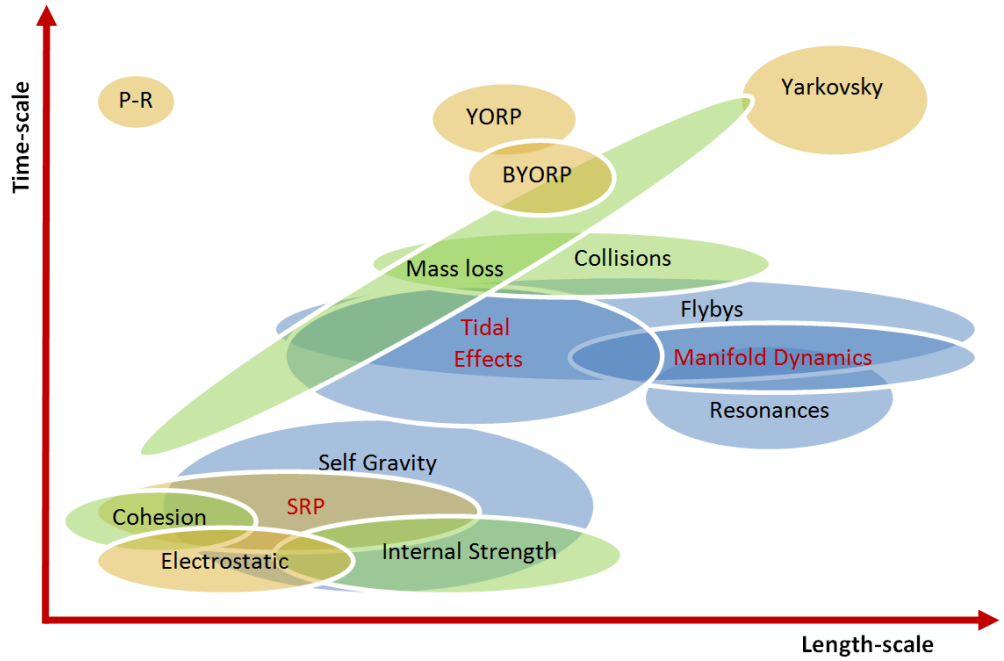

Figure 1.1: Summary of forces acting on asteroids at different time and length scales.

1.3.1 Gravitational forces

Near–Earth Objects are all subject to the gravitational attraction of the Sun, and their usual state is in orbits about it that regularly bring them relatively close to the Earth. In addition, third-body perturbations due to other major bodies in the solar system play an important role to explain their orbit evolution and migration between orbiting regions. In particular, resonances with Jupiter and other major planets can explain the gaps formed in the main asteroid belt (Moons, 1996), and is one of the sources of re-population of the near–Earth space (Bottke et al., 2002b).

Closer encounters with planets or moons, referred to in this thesis indistinctly as flybys or swing-bys, are also common (on astronomical time-scales) during a NEO lifetime (Bottke et al., 1994). These result in large orbit modifications and further migration either to the inner or outer solar system, or impacts on the surface of the Sun, planets or moons, in some cases generating craters (Brown et al., 2002). These encounters also affect NEOs on meso-scales or intermediate scales (Walsh et al., 2011), causing rotation (Scheeres et al., 2005), structure and configuration upheaval (Davidsson, 2001a,b; Richardson, 1995; Richardson et al.,

1998), possibly creating and separating binaries (Fang and Margot, 2012; Melosh and Stansberry, 1991), due to tidal torques during swing-bys. A distinct type of close encounter effects is indicated in Fig. 1.1 as "manifold dynamics". It refers to orbits on or close to the unstable hyperbolic manifolds associated with the libration points of planets. They can explain transfers of comets between the outer and inner regions of Jupiter orbit (Belbruno and Marsden, 1997) and are also responsible, among other orbital effects, for temporary capture of asteroids by the Earth (Granvik et al., 2011).

Finally, self-gravity is what holds asteroids and comets together, most of them having a loose rubble pile structure (Britt et al., 2002). Due to their irregular shape and density distribution, NEOs can have complex gravity fields (Scheeres, 2012c), and in the case of binaries (or triplets), the gravitational and tidal interactions between components of an irregular shape can modify their rotation axes and speed. Because of this, it can be shown that tidally locked binaries are expected to be usual (Scheeres et al., 2002). These irregular gravity fields also have a significant influence on the orbiting regimes and surface movement of dust and of course spacecraft (Hu and Scheeres, 2002; Scheeres et al., 1998, 1996). In addition to dominating dust and regolith migration and sedimentation (Miyamoto et al., 2007; Robinson et al., 2001), the spin state and gravity field of NEOs need to be taken into account for spacecraft operations on the surface (Chacin and Tunstel, 2012; Richter, 1998) or in close orbits (Scheeres et al., 2003).

1.3.2 Solar and radiation induced forces

Aside from resonances and swing-bys, the main mechanism for the migration of main belt objects to the Near–Earth space is the solar radiation induced Yarkovsky effect (Öpik, 1951), theorised as early as 1901 but unconfirmed by observations until much later (Chesley et al., 2003). Albeit acting on much longer time-scales than gravitational interactions (changes in semi-major axis of the order of 10^{-3} AU per million of years for kilometer size objects, see Nugent et al. (2012)), the Yarkovsky effect can slowly modify the orbit of a rotating asteroid (Bottke et al., 2001) until it falls into some resonance or has a close encounter with a planet which pumps up or down their orbit further (Morbidelli and Vokrouhlický, 2003). Additional seasonal effects associated with thermal drag can contribute further to orbit shrinking depending on the asteroid's spin state (Rubincam, 1995).

Related to the Yarkovsky effect, there are two other effects that act on the meso-scale properties of asteroids: YORP and BYORP. The Yarkovsky-O'Keefe-Radzievskii-Paddack effect, thankfully shortened to YORP effect, is responsible for the spin-up and spin-down of irregular-shaped asteroids, due to torques generated by differential infrared radiation over their surface (Rubincam, 2000). Ultimately, YORP can lead up to structure reconfiguration and total fragmentation of asteroids and comets through rotational fission (Cuk, 2007; Jacobson and Scheeres, 2011), or slow them down to chaotic tumbling spin states. In a similar fashion, the Binary YORP effect, or BYORP (Steinberg and Sari, 2011), can disrupt the separation between components of a tidally locked binary, causing them to separate or collide. As with their "parent" Yarkovsky effect, both YORP and BYORP act on very long time-scales of hundred-thousands to millions of years (for example, Rubincam (2000) showed that YORP can double or halve the spin of a 5 km object in 100 million years), although for very small asteroids their effects could be significantly faster. YORP is as well highly dependent on the irregularity of the shape of the object.

A similarly slow effect, radiation-related but of relativistic origin, is the Poynting-Robertson drag (Poynting, 1904; Robertson, 1937), which causes small particles or dust grains in orbit to spiral down around the Sun. Due to the long time-scales the Poynting-Robertson effect requires and the small length-scales it acts on (tens of thousands of years for spiralling down of particles of less than 1 μm), it does not have a straightforward application for manipulation.

Of greater interest are electrostatic forces on the surfaces of an asteroid (Hughes et al., 2008). Solar radiation charges the regolith on the sunlit region of an asteroid, and due to the asteroid rotation and build-up of differential charge along the terminator, these electrostatic forces can generate electric discharges and dust particles ejection and levitation (Lee, 1996). Electrostatic levitation may be responsible for the migration of small particles and formation of dust ponds (Robinson et al., 2001).

Finally, the most obvious radiation-related force is the direct solar radiation pressure perturbation (Scheeres, 2012d). Although its effect on the asteroid itself is limited, it is one of the most relevant perturbations experienced by dust particles (Richter and Keller, 1995) or spacecraft in orbit about a NEO (Byram and Scheeres, 2008; Dankowicz, 1993).

1.3.3 Material related forces

Most asteroids are believed to consist of rubble piles loosely held together by gravity, with regolith of different sizes across their surface (Britt et al., 2002; Michel, 2013). However, some of the spin states from known asteroids could only be explained if they were monolithic structures, with some internal material strength avoiding mass shedding or surface disruption by centrifugal forces (Walsh et al., 2011). For smaller asteroids, inter-particle forces, namely cohesion, could also explain their consistency even at high spin rates (Sánchez and Scheeres, 2013; Scheeres et al., 2010). Due to their vacuum environment (which implies cleaner surfaces) and their low gravity, cohesive strength has a greater relative importance than on Earth.

Of relevance across all length-scales are the effects caused by mass loss. Be it through ejecta by micro-meteoroid impacts (Scheeres et al., 2002), mass shedding caused by high spin rates (Hirabayashi and Scheeres, 2012), or ejecta plumes in the case of comets approaching the inner solar system, mass loss can generate transient or quasi-permanent dust atmospheres, affect the rotation and structure of the asteroid, possibly seed the secondary of a binary or even multiple body systems (Jacobson and Scheeres, 2011; Walsh et al., 2012), and ultimately change the orbit of the NEO (most significantly in the case of comets).

One final effect that could be considered material-related, or possibly an external force, are collisions with other asteroids or minor bodies (Paolicchi et al., 2002). However, these are uncommon in the NEO population, and the time-scales in other asteroid families such as main belt objects can arguably be of the same order or even longer than other effects such as YORP (Marzari et al., 2011).

1.3.4 External forces

Up to this point, all forces and effects described exist naturally on asteroids. On the other hand, for the popular type of asteroid manipulation that is asteroid deflection, numerous techniques involving external forces or interaction with external bodies have been proposed. These techniques, such as laser ablation (Gibbings et al., 2012), low-thrust engines (Scheeres and Schweickart, 2004), or nuclear explosions (Kleiman, 1968), could also be applied to other types of manipulation, for example to asteroid capture, spin-up, de-spin, or break-up. Tech-

niques that combine an applied external force enhanced by natural dynamical features or forces will be most efficient for the purpose of manipulation.

1.4 Types of manipulation

Having described the various perturbing forces acting on NEOs, several types of manipulations can be envisaged, which exploit one or a combination of the forces and phenomena described above. This section briefly lists possible manipulation concepts, but as asteroid manipulation is a relatively new research theme, the list cannot be exhaustive nor detailed enough to consider all possibilities.

The manipulation techniques have been sorted in three different length-scale ranges according to their effect: **macro-scale** or very large scales for manipulations that affect a NEO in scales of the order of their orbit, **meso-scale** or intermediate scales for NEO sizes or binary pair distances, and **micro-scale** or small scales for manipulations affecting dust or elements smaller than the asteroid itself. Again the quantification of the scale at which a type of manipulation acts is subject to interpretation, and some could indeed affect the asteroid across multiple length-scale ranges, which often overlap.

1.4.1 Macro-scale

The most well known type of macro-scale manipulation is asteroid deflection. Given the undeniable threat that NEOs pose to life on Earth as we know it (Baileya et al., 2006), there has been numerous proposals and studies on deflection methods for decades (Kleiman, 1968; Melosh et al., 1994). A more recent discussion and multi-criteria comparison of various of these methods can for example be found in Sanchez Cuartielles et al. (2009). Because of the numerous previous studies on NEO deflection, asteroid deflection techniques have been explicitly excluded from this thesis.

However, all deflection methods that impart a change of velocity to an asteroid to modify its orbit can in principle also be applied with the aim of asteroid capture. Proposals for asteroid capture have gained momentum recently (Brophy et al., 2012; Hasnain et al., 2012; Massonnet and Meyssignac, 2006). Capturing can thus be considered a variation of deflection, but to a different target orbit, with the advantage that the judicious use of key dynamical features, such as unstable

manifolds, aid in reducing the costs of orbit manipulation. New methods for capture are regularly being proposed, such as the possibility of a binary exchange mechanism (Borum et al., 2012), extending temporary captures (Urrutxua et al., 2014), or a low energy capture into Kolmogorov–Arnold–Moser (KAM) tori (Verrier and McInnes, 2015). Owing to this interest, a novel proposal for asteroid capture and a more detailed literature review on the subject will be presented in Chapter 3.

Other types of orbit manipulation could also be of interest in the long term, for example asteroid shepherding into other types of orbits, not necessarily around a planet, such as cycler orbits between the Earth and Mars (Lewis, 1996, pp.115). The less ambitious possibility of extending the duration of the capture of naturally occurring temporary moons of the Earth has also been suggested (Urrutxua et al., 2014).

1.4.2 Meso-scale

For intermediate scales of the order of the NEO itself, some of the deflection methods could again be used for the purpose of binary orbit modification, as proposed by the kinetic impactor demonstrator DART and AIM (Murdoch et al., 2012). Two additional studies for the SysNOVA initiative, KABOOM (Bombardelli et al., 2013) and BEAST (Gil-Fernandez et al., 2013), also analysed the possibility of modifying the orbit of a binary system. The external forces associated with deflection methods could be used for the purpose of de-spinning a NEO prior to capture (for example by off-setting the low-thrust engine direction (Scheeres and Schweickart, 2004) or the application of a laser beam away from the centre of gravity), or for break-up (for example with a nuclear blast).

Indeed spin-up, de-spin or break-up analysis of NEOs by artificial or natural forces have received considerable attention in the literature. The most common cause of spin modification or fragmentation are tidal interactions (e.g. Davidsson, 2001a; Melosh and Stansberry, 1991; Toth et al., 2011). Other phenomena that can explain the formation and destruction of binary or multiple systems are the already mentioned YORP spin-up and induced disruption through rotational fission, leading to the generation of a secondary seed which grows by accretion into a circular synchronous secondary, later migrating due to BYORP (Cuk, 2007; Jacobson and Scheeres, 2011). An example of a more exotic proposal suggests

the use of tethers for artificial spin-up and fragmentation (Bombardelli, 2007). In this thesis, the possibility of a controlled spin modification through tidal torques during a swing-by is further discussed and analysed in Chapter 4.

The modification of spacecraft orbits around asteroids exploiting natural dynamics, although not strictly a manipulation of the asteroid per se, can also be considered a meso-scale effect, and is of direct application for exploration. Examples of this are the well-known terminator orbits (Byram and Scheeres, 2008; Dankowicz, 1993; Scheeres, 2007), and other associated highly non-Keplerian orbits (Broschart et al., 2014; Lantoine et al., 2013). The exploitation of solar radiation pressure around very small asteroids for the generation of novel orbits, to complement terminator orbit families, is the focus of Chapter 5.

1.4.3 Micro-scale

Finally, on the smallest scales, the study of ejecta (Scheeres et al., 2002; Scheeres and Marzari, 2000), natural dust levitation (Lee, 1996) and binary seeding (Cuk, 2007) can be a precursor for possible manipulation techniques, such as artificial binary or multiple asteroid system seeding, transient atmosphere avoidance or neutralisation, or other types of manipulation associated for example with asteroid mining (Lewis, 1996).

In that respect, novel techniques for material separation need be designed taking into account the exotic environment of NEOs. Lunar regolith processing methods and material sorting techniques have already been suggested and tested in the laboratory (Graham et al., 2010; Haskin et al., 1986; Stoeser et al., 2011), and some of these techniques may be extended to asteroids. Further literature review on the matter is provided in Chapter 6, and a new material sorting technique is proposed, inspired in natural dust levitation and utilising SRP for material separation.

1.5 Thesis research objectives

The main objective of this thesis is to study novel concepts for the manipulation of asteroids and other NEOs across a range of length-scales, from orbital to particle sizes. Based on the previous discussion on the natural forces acting on asteroids,

and the types of manipulation over different length-scales, the following research objectives have been defined:

- Investigate the benefits of **manifold dynamics** associated with the colinear libration points of the Sun–Earth system for the **capture** of small Near–Earth Objects.
- Study the effect of **tidal interactions** on an asteroid's **rotational state and structure** during swing-bys and close approaches to massive bodies.
- Study the potential of the **solar radiation pressure** perturbation to devise **highly non-Keplerian orbits** around asteroids for exploration.
- Propose novel methods for **material separation** on asteroids exploiting the **solar radiation pressure** perturbation.

The proposed asteroid manipulation concepts were selected because of their potential and the practical time-scales they act on.

1.6 Contributions of thesis

Asteroid manipulation can be considered a research field in its infancy, with most of the previous literature concentrating on the possibility of asteroid deflection and planetary defence. As such, the concepts proposed and analysed in this thesis contain a high degree of novelty and try to unlock the potential of the astrodynamics research applied to asteroid manipulation, establishing connections between the study of dynamics and engineering applications. This section lists this main contributions of the research reported.

On the **macro-scale** regime, for the first time exploiting manifold dynamics has been analysed for the capture of asteroids on libration point orbits. A new family of Near–Earth Objects, termed Easily Retrievable Objects (ERO), has been defined, and an associated objective, quantifiable and ordered classification based on their potential for capture has been established. The first 12 candidates for the catalogue of EROs have already been identified and low-cost transfers calculated. A novel method for pruning the Minor Planet Centre database based on capture cost estimates has been developed, and a robust methodology to find

optimal trajectories for inserting onto manifolds leading to target libration point orbits has been implemented and tested.

Bridging the gap between **macro- and meso-scales**, the novel concept of exploiting tidal toques to manipulate the spin state and the structure of a captured asteroid during a swing-by has been proposed. Capture strategies that employ one or more swing-bys to reduce the cost of insertion into final target orbits need consider the orbit-attitude coupling during these phases. Various recommendations are provided to avoid undesired spin-up, fragmentation of the asteroid, or separation of a binary during the close approach, and the range of initial spin states at which effective de-spin or spin-up though tidal torques can be achieved has been calculated.

For the range of **meso- to micro-scales**, the exploitation of solar radiation pressure to devise new orbiting strategies and families of orbits in the vicinity of asteroids has been considered. An alternative strategy to the traditional hovering or multiple flyby concepts has been presented. It consists of an alternating orbiter that reverses its orbit direction after a number of revolutions. Analysis shows that it provides complementary coverage to terminator associated orbits, and it saves fuel with respect to hovering and pseudo-hovering strategies. As the spacecraft is effectively in orbit, it is suggested that this strategy is also more beneficial for the characterisation of the gravity field than hovering or multiple flybys. Moreover, the well-known symmetric periodic planar a and $g - g'$ families of the Hill problem have been extended for the first time to higher levels of solar radiation pressure characteristic of asteroids. The evolution of these families, their stability, their applicability to very small asteroids and the effect of eclipses have been studied. Variable effective surface or variable reflectivity devices are identified as key technologies to enable these SRP dominated orbiting concepts.

Finally, on the **micro-scale** regime, a radical new concept to separate material on asteroids as a function of density or particle size by exploiting solar radiation pressure has been proposed. The potential of this method, analogous to winnowing on Earth but using differential SRP instead of differential drag, has been studied with simplified models to describe the behaviour of dust in the low-gravity and high SRP environment of an asteroid. Because of the method's potential for high throughput, possible applications for an initial pre-concentration of regolith sizes or materials prior to more complex processing methods are suggested.

1.7 List of publications and outcomes of the PhD research

The main contributions of this thesis have been published in the following journal papers, book chapters and conference papers.

1.7.1 Peer-reviewed journal publications

García Yárnoz D., Scheeres D. J., McInnes C. R. (2015), 'On the a and g families of orbits in the Hill problem with solar radiation pressure and their application to asteroid orbiters,' *Celestial Mechanics and Dynamical Astronomy*, **121**(4) pp. 280-291
doi:10.1007/s10569-015-9604-9

García Yárnoz D., Sánchez Cuartielles J. P., McInnes C. R. (2015), 'Alternating orbiter strategy for asteroid exploration,' *Journal of Guidance, Control, and Dynamics*, **38**(2) pp. 280-291
doi:10.2514/1.G000562

García Yárnoz D., Sánchez Cuartielles J. P., McInnes C. R. (2014), 'Passive sorting of asteroid material using solar radiation pressure,' *Journal of Guidance, Control, and Dynamics* **37**(4) pp. 1223-1235
doi:10.2514/1.62412

García Yárnoz D., Sanchez J. P., McInnes C. R. (2013), 'Easily Retrievable Objects among the NEO Population,' *Celestial Mechanics and Dynamical Astronomy* **116**(4), pp. 367-388
doi:10.1007/s10569-013-9495-6

1.7.2 Peer-reviewed book chapters

García Yárnoz D., Sanchez J. P., McInnes C. R. (2013), 'Opportunities for Asteroid Retrieval Missions,' in V. Badescu (ed.), *Asteroids. Prospective Energy and Material Resources*, Springer-Verlag Berlin Heidelberg, pp. 479-505
doi:10.1007/978-3-642-39244-3_21

1.7.3 Conference papers

1.7.3.1 Authored

García Yárnoz D., McInnes C. R. (2014), 'Coupled orbit–attitude dynamics of a captured asteroid during swing-bys,' IAC-14.C1.2.13, *65th International Astronautical Congress*, Toronto, Canada

García Yárnoz D., Scheeres D. J., McInnes C. R. (2014), 'On the a and g families of symmetric periodic orbits in the photo-gravitational Hill problem and their application to asteroids,' AIAA-2014-4120, *SPACE2014 – AIAA/AAS Astrodynamics Specialist Conference*, San Diego, CA, USA

García Yárnoz D., Sanchez Cuartielles J. P., McInnes C. R. (2013), 'Applications of solar radiation pressure dominated highly non-Keplerian trajectories around minor bodies,' IAC-13.C1.9.6, *64th International Astronautical Congress*, Beijing, China

García Yárnoz D., Sánchez Cuartielles J. P., McInnes C. (2013), 'Passive sorting of asteroid material using solar radiation pressure,' AAS 13-484, *23rd AAS/AIAA Space Flight Mechanics Conference*, Lihue, HI, USA

1.7.3.2 Co-authored

Parry T., Brown R., Hammond P., Clark C., García Yárnoz D. (2014), 'Deployable structures demonstrator StrathSat-R: A second chance,' IAC-14.A2.3.12, *65th International Astronautical Congress*, Toronto, Canada

Sanchez Cuartielles J. P., Alessi E. M., García-Yárnoz D., McInnes C. (2013), 'Earth resonant gravity assists for asteroid retrieval missions,' IAC-13.C1.7.8, *64th International Astronautical Congress*, Beijing, China

Donaldson D., Parry T., Sinn T., Garcia Yarnoz D., Lowe C. J., Clark R. (2013), 'Ejection and recovery system for CubeSat sized ejectables on sounding rockets,' IAC-13-A2.3.3, *64th International Astronautical Congress*, Beijing, China

Sinn T., Brown R., McRobb M., Wujek A., Lowe C., Weppler J., Parry T., Garcia Yarnoz D. et al. (2013), 'Lessons learned from three university experiments onboard the REXUS/BEXUS sounding rockets and stratosphere balloons,' IAC-13-D1.5.3, *64th International Astronautical Congress*, Beijing, China

Vetrisano M., Branco J., Garcia Yarnoz D. (2013), 'Effective approach navigation prior to small body deflection,' *12th Annual Space Generation Congress*, Beijing, China.
Winning paper of Move an Asteroid 2013 Competition, BIS

Vetrisano M., Branco J., Sanchez Cuartielles J. P., Garcia Yarnoz D., Vasile M. (2013), 'Deflecting small asteroids using laser ablation: Deep space navigation and asteroid orbit control for LightTouch^2 Mission,' *AIAA Guidance, Navigation and Control Conference 2013*, Boston, MA, USA
doi:10.2514/6.2013-5250

Vasile M., Vetrisano M., Gibbings A., Garcia Yarnoz D. et al. (2013), 'LightTouch^2: A Laser-Based Solution for the Deflection, Manipulation and Exploitation of Small Asteroids,' IAA-PDC13-04-22, *Planetary Defense Conference 2013*, Flagstaff, AZ, USA

Sanchez Cuartielles J. P., Garcia Yarnoz D., Alessi E. M., McInnes C. (2012), 'Gravitational capture opportunities for asteroid retrieval missions', IAC-12.C1.5.13, *63rd International Astronautical Congress*, Naples, Italy

Sanchez J. P., Garcia Yarnoz D., McInnes C. (2012), 'Near–Earth Asteroid Resource Accessibility and Future Capture Mission Opportunities,' GLEX-2012.11.1.5, *Global Space Exploration Conference*, Washington DC, USA

1.8 Thesis layout

The outputs of the research has been structured in this thesis as follows.

This first Chapter 1 contains the introduction of the research topic, including a short overview of the concepts, a general literature review, and an outline of the research objectives and contributions of the thesis.

In Chapter 2, the main dynamical models that are used throughout the thesis and are common to more than one technical chapter are briefly presented. Other models and extensions that are specific to a particular technical chapter are described directly in them, for continuity and for ease of reading.

Building on this background information, Chapters 3 to 6 contain the main new contributions of the thesis. They have been divided and ordered according to the length-scale of the type of manipulation proposed: from macro-scale to micro-scale, corresponding to each of the research objectives defined in Section 1.5.

Each chapter contains a background section and a literature review applicable to the method proposed, as well as final sections with discussion, model limitations and a summary of the research outputs.

- **Chapter 3** focuses on one of the extremes of the length scale, the **macro-scale** or orbit-scale manipulation, and presents the results of the analysis to exploit manifold dynamics for asteroid capture, and the definition of the new family of Easily Retrievable Objects (ERO).
- **Chapter 4** continues with manipulations acting on **macro- to meso-scales**, of sizes of the order of the asteroid itself. It contains the results of tidal torque exploitation to manipulate the spin of an asteroid or a binary configuration during swing-bys and close approaches to massive bodies.
- **Chapter 5** follows with manipulations on scales ranging from **meso- to micro-scale**. It introduces the manipulation and generation of asteroid exploration orbiting strategies about minor bodies in regimes dominated by the solar radiation pressure perturbation.
- **Chapter 6** closes the main contributions of the thesis with the other extreme of the length-scale: **micro-scales**. In it, the winnowing-like method to manipulate dust and regolith particles on asteroids for material separation by exploiting solar radiation pressure is presented.

Finally, Chapter 7 sums up the main findings of the thesis, containing general conclusive remarks and a discussion on future work.

Chapter 2

Dynamical Models

This chapter briefly introduces the general dynamical models that will be used throughout the thesis. It is not intended to be an exhaustive description of the methods of astrodynamics. For that purpose, the reader can refer to works such as those by Szebehely (1967), Battin (1999) or Vallado (2007). More specific models only relevant for a particular analysis in the thesis will be described in the context of each chapter when required.

2.1 Gravitational two-body problem

As a first approximation, the orbits of a spacecraft or an asteroid about the Sun or other massive body can be modelled with the classical two body problem (e.g., Battin, 1999, chap. 2):

$$\ddot{\vec{r}} = -\frac{\mu_1 + \mu_2}{r^3}\vec{r} \tag{2.1}$$

where $\vec{r}$ is the radius-vector from body 1 (or primary) to body 2 (or secondary), with modulus r, and $\mu_i = Gm_i$ is the gravitational parameter of body i of mass m_i, with G the universal gravitational constant.

This system is completely integrable and has an analytical solution. The solutions to the previous equation of motion are conic sections and are usually referred to as Keplerian motion. Pure Keplerian motion and the two-body problem will be assumed in this thesis for asteroid ephemeris with respect to the Sun between two close encounters with the Earth, as well as test cases for propagation of an asteroid trajectory inside the sphere of influence of the Earth or Moon during swing-bys of these bodies.

2.2 Gravitational three-body problems

In general, n-body problems with more than one attractive body are a more realistic representation of dynamical systems in astrodynamics. When the mass of the n^{th} body (a particle, spacecraft or even an asteroid) is considered negligible with respect to that of the rest of the attractive bodies, the model is termed "restricted". In the case of a restricted three-body problem, the motion of the two massive bodies can be solved analytically with the traditional two-body problem (see Section 2.1), leaving just the motion of the third non-massive object to be integrated.

Restricted three-body problems involving two massive bodies such as the Sun and the Earth, or the Sun and an asteroid, will be utilised throughout this thesis, with additional perturbations in some instances. The two massive bodies will be referred to as the primary and secondary.

2.2.1 Circular Restricted 3-Body Problem (CR3BP)

A particular case of the restricted three-body problem is the Circular Restricted 3-Body Problem (CR3BP), in which the secondary is assumed to follow a circular orbit of radius d about the primary (or alternatively both bodies move on circular orbits about their common barycentre).

The equations of motion can be expressed in a co-rotating frame (or synodic frame) with origin at the barycentre of the system and with the x-axis pointing towards the secondary (see schematic for a Sun–asteroid system in Fig. 2.1). The Sun, primary, or more massive body is assumed on the negative x-axis (contrary to the convention used in Szebehely, 1967). The two bodies, as well as the reference frame, rotate around the barycentre with a frequency Ω_R given by:

$$\Omega_R = \sqrt{\frac{\mu_1 + \mu_2}{d^3}} \tag{2.2}$$

Defining the mass ratio μ:

$$\mu = \frac{\mu_2}{\mu_1 + \mu_2} \tag{2.3}$$

the positions of the primary and secondary along the x axis are $-\mu$ and $1 - \mu$ respectively, where distances have been normalised with respect to the circular orbit radius d.

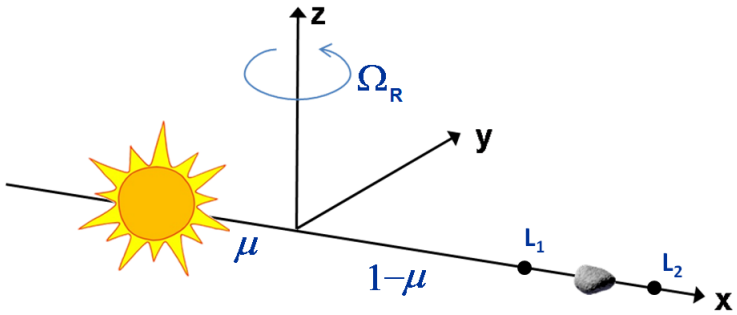

Figure 2.1: Schematic representation of the co-rotating synodic frame with the origin at the barycentre of the Sun–asteroid system (not to scale).

The equations of motion for the third body are then given in normalised coordinates by:

$$\begin{cases} \ddot{x} - 2\Omega_R\dot{y} &= {\Omega_R}^2\left(x - \frac{(1-\mu)(x+\mu)}{((x+\mu)^2+y^2+z^2)^{3/2}} - \frac{\mu(x+\mu-1)}{((x+\mu-1)^2+y^2+z^2)^{3/2}}\right) \\ \ddot{y} + 2\Omega_R\dot{x} &= {\Omega_R}^2\left(y - \frac{(1-\mu)y}{((x+\mu)^2+y^2+z^2)^{3/2}} - \frac{\mu y}{((x+\mu-1)^2+y^2+z^2)^{3/2}}\right) \\ \ddot{z} &= {\Omega_R}^2\left(-\frac{(1-\mu)z}{((x+\mu)^2+y^2+z^2)^{3/2}} - \frac{\mu z}{((x+\mu-1)^2+y^2+z^2)^{3/2}}\right) \end{cases} \tag{2.4}$$

This system of equations allows an integral of motion, the Jacobi constant J:

$$J = -2E = 2U - 2T \tag{2.5}$$

where U and T are the potential and kinetic energy, which can be expressed as:

$$U = \frac{1}{2}{\Omega_R}^2(x^2+y^2) - \frac{1-\mu}{((x+\mu)^2+y^2+z^2)^{1/2}} \tag{2.6}$$

$$T = \frac{1}{2}(\dot{x}^2+\dot{y}^2+\dot{z}^2) \tag{2.7}$$

This model is a useful representation for the motion of an asteroid in a simplified Sun-Earth system (where the orbit of the Earth is assumed circular). An extension not considered in this thesis is to take into account the eccentricity of the orbit of the secondary, using the the Elliptic Restricted 3-Body Problem model (ER3BP, see for example Broucke, 1969). Give the low eccentricity of the Earth, the solutions presented are good first approximation of the real world dynamics.

2.2.2 Hill problem

The classical Hill problem is one of the two limiting cases of the CR3BP (Hénon, 1969), when the mass of the secondary tends to zero ($\mu \to 0$). Normalising the independent variable time with the rotational frequency ($\tau = \Omega_R t$), displacing the

origin of coordinates to the centre of the secondary, scaling all distance with $\mu^{1/3}$ and neglecting all terms of the order of $\mu^{2/3}$ or higher, the equations of motion of the Hill problem take the well known form:

$$\begin{cases} \ddot{\xi} &= 2\dot{\eta} + 3\xi - \frac{\xi}{(\xi^2+\eta^2+\zeta^2)^{3/2}} \\ \ddot{\eta} &= -2\dot{\xi} - \frac{\eta}{(\xi^2+\eta^2+\zeta^2)^{3/2}} \\ \ddot{\zeta} &= -\zeta - \frac{\zeta}{(\xi^2+\eta^2+\zeta^2)^{3/2}} \end{cases} \tag{2.8}$$

where the scaled state vector $(\xi, \eta, \zeta) = (x - 1 + \mu, y, z)/\mu^{1/3}$. These equations also allow an integral of motion, a scaled Jacobi constant Γ given by:

$$\Gamma = 3\xi^2 - \zeta^2 + \frac{2}{\sqrt{\xi^2 + \eta^2 + \zeta^2}} - \dot{\xi}^2 - \dot{\eta}^2 - \dot{\zeta}^2 \tag{2.9}$$

where constant terms and terms of order higher than $\mu^{2/3}$ are neglected.

Due to the small size and low gravity of asteroids the Hill problem is a good starting point to study orbital dynamics in their vicinity. However, other perturbations, in particular solar radiation pressure (SRP), become important when the size of the minor body decreases, which can lead to highly non-Keplerian orbits. Similar to the ER3BP, an extension again not considered here is eccentric orbits of asteroids, such as in the elliptic Hill problem (Ichtiaroglou, 1980). For short duration orbits around asteroids, or for bodies with low eccentricity, the implications of using a simplified model are small.

2.3 Models with Solar Radiation Pressure

For very small bodies, SRP is arguably the largest non-gravitational perturbing force affecting the orbital motion of a spacecraft with typical effective area and mass in the vicinity of an asteroid. In this thesis, the SRP acting on a particle or spacecraft is modelled assuming the classical so-called 'cannon-ball' model. This model is representative of how SRP would affect a spherical cannon-ball of uniform reflective properties, and it was first developed for the cannon-ball looking satellites LAGEOS (Andrés de la Fuente, 2007). It thus assumes the SRP force only has a radial component, with the effective surface of the spacecraft always perpendicular to the Sun–spacecraft line. The solar radiation pressure force can be expressed as (see for example Pater and Lissauer, 2010, section 2.7.1):

$$\vec{F}_{SRP} = \frac{L_S Q S}{4\pi c} \frac{\vec{r}_S}{|\vec{r}_S|^3} \tag{2.10}$$

where L_S is the solar luminosity, Q the solar radiation pressure coefficient, which depends on the reflectivity of the body surface, S the cross-sectional area of the particle or spacecraft, c is the speed of light and $\vec{r}_S$ is the radius-vector from the Sun to the spacecraft. The solar radiation pressure coefficient Q is 1 for a perfectly absorbing surface, and is equal to 2 for the case of ideal specular reflection. Unless otherwise stated, for most analyses the (conservative) value of $Q = 1$ is assumed. For higher Q, the effective areas required would be smaller for the same effect.

Both the SRP force and the gravitational attraction of the Sun scale with the inverse of the distance squared. The ratio between both forces defines the lightness number β (McInnes, 1999, Section 2.3.3) given by:

$$\beta = \frac{F_{SRP}}{F_{2BP}} = \frac{L_S Q}{4\pi c \mu_S} \frac{S}{m} \tag{2.11}$$

where F_{2BP} is the two-body problem gravitational force (see Section 2.1) assuming the Sun as the central body, with μ_S its gravitational constant. The lightness number is clearly proportional to the area-to-mass ratio S/m. It is a relevant parameter to illustrate the relative importance of both forces, and it will be used in different forms throughout the thesis.

Several dynamical models that incorporate SRP and are put to use in the following chapters are described in the following subsections.

2.3.1 Photo-gravitational CR3BP

For simplicity, most problems involving spacecraft or particles in the vicinity of asteroids can be modelled, in a first approximation, by the well-known photo-gravitational circular restricted three-body problem (Chernikov, 1970; Schuerman, 1980; Simmons et al., 1985), a direct extension of the CR3BP (see Section 2.2.1). A spherical or point-mass asteroid not affected by SRP in a circular orbit of heliocentric distance d about the Sun is assumed. In the co-rotating frame defined above, the extended CR3BP equations of motion are:

$$\begin{cases} \ddot{x} - 2\Omega_R \dot{y} &= {\Omega_R}^2 \left(x - \frac{(1-\mu)(1-\beta)(x+\mu)}{((x+\mu)^2+y^2+z^2)^{3/2}} - \frac{\mu(x+\mu-1)}{((x+\mu-1)^2+y^2+z^2)^{3/2}} \right) \\ \ddot{y} + 2\Omega_R \dot{x} &= {\Omega_R}^2 \left(y - \frac{(1-\mu)(1-\beta)y}{((x+\mu)^2+y^2+z^2)^{3/2}} - \frac{\mu y}{((x+\mu-1)^2+y^2+z^2)^{3/2}} \right) \\ \ddot{z} &= {\Omega_R}^2 \left(- \frac{(1-\mu)(1-\beta)z}{((x+\mu)^2+y^2+z^2)^{3/2}} - \frac{\mu z}{((x+\mu-1)^2+y^2+z^2)^{3/2}} \right) \end{cases} \tag{2.12}$$

where the main difference with the classical CR3BP is the lightness number term $(1-\beta)$, effectively reducing the gravitational attraction of the Sun on the particle or spacecraft.

The Jacobi constant is again given by Eq. 2.5, with the potential energy U now being:

$$U = \frac{1}{2}{\Omega_R}^2(x^2+y^2) - \frac{(1-\mu)(1-\beta)}{((x+\mu)^2+y^2+z^2)^{1/2}} \tag{2.13}$$

2.3.2 Photo-gravitational Hill problem

As noted before, due to their low mass, the Hill approximation and notably its photo-gravitational extension are well suited for the study of the dynamics in the vicinity of asteroids. The equations of motion of the Hill problem with solar radiation pressure in a synodic co-rotating frame centred in the secondary can be expressed as (Papadakis, 2006):

$$\begin{cases} \ddot{\xi} &= 2\dot{\eta} + 3\xi - \frac{\xi}{(\xi^2+\eta^2+\zeta^2)^{3/2}} + \beta' \\ \ddot{\eta} &= -2\dot{\xi} - \frac{\eta}{(\xi^2+\eta^2+\zeta^2)^{3/2}} \\ \ddot{\zeta} &= -\zeta - \frac{\zeta}{(\xi^2+\eta^2+\zeta^2)^{3/2}} \end{cases} \tag{2.14}$$

where distances are again normalised by d and scaled by $\mu^{1/3}$, the lightness number is scaled in a similar fashion $\beta' = \beta/\mu^{1/3}$, and time is normalized by $1/\Omega_R$.

These are equivalent to the equations of motion defined in Byram and Scheeres (2008) or Broschart et al. (2014). They allow an integral of motion Γ, equivalent to Hénon's modified Jacobi constant (see Eq. 2.9 above), where the constant terms have been excluded:

$$\Gamma = \frac{J-3-2\mu^{1/3}\beta'}{\mu^{2/3}} = 3\xi^2 - \zeta^2 + 2\beta'\xi + \frac{2}{\sqrt{\xi^2+\eta^2+\zeta^2}} - \dot{\xi}^2 - \dot{\eta}^2 - \dot{\zeta}^2 \tag{2.15}$$

2.3.3 Comparison of non-scaled and scaled lightness numbers

This thesis uses both the non-scaled lightness number β as defined in Eq. 2.11, and the scaled lightness number β', which depends on the mass ratio of the system. In order to illustrate the ranges in which these two parameters vary, and familiarize the reader with the expected values in each case, Table 2.1 presents a few characteristic examples.

For each example, three lightness numbers are provided: a non-scaled β and two scaled β', one assuming the Earth as secondary, and one assuming an asteroid of similar mass to Rosetta's target comet 67P/Churyumov-Gerasimenko. The first example consists of a spherical dust or regolith particle of radius 100 μm and density 3.2 g/cm^3. The second example is a Rosetta-type spacecraft, with effective area 64 m^2 and mass 1230 kg.* The third case corresponds to a higher area-to-mass ratio spacecraft, such as the one foreseen for the Sunjammer mission, with effective area 1444 m^2 and mass 45 kg (Heiligers et al., 2014).

Table 2.1: Characteristic lightness number examples.

	Non-scaled	Scaled β'	
	β	Earth	Asteroid
Mass parameter $[kg^3/s^2]$		398600	6.7×10^{-7}
Mass ratio μ		3×10^{-6}	5×10^{-18}
Particle	0.0018	0.12	1031
$r = 100\ \mu m, \rho = 3.2\ g/cm^3$			
Rosetta SC	3.9×10^{-5}	0.0027	22.9
$S = 64\ m^2,\ m = 1230\ kg$			
Sunjammer SC	0.024	1.67	14139
$S = 1444\ m^2,\ m = 45\ kg$			

The previous lightness numbers have been calculated assuming a solar radiation pressure coefficient $Q = 1$, which underestimates the realistic values, especially for a reflective sail such as Sunjammer's. Nevertheless, this table highlights the importance of differentiating between scaled and non-scaled lightness numbers. For most solar sailing applications, non-scaled lightness numbers β of the order of 0.02 or smaller are usually quoted. Most current missions to asteroids refer instead to scaled lightness numbers β' of the order of 20–30 (Scheeres, 2012d). These scaled lightness numbers are associated with relatively large asteroids (larger than a few hundred metres diameter). As the scaled lightness number is inversely proportional to the radius of the asteroid ($\mu^{1/3} \propto R$), for an asteroid size of tens of metres, lightness numbers between 10 and a 100 times larger are feasible.

* http://sci.esa.int/rosetta/47366-fact-sheet/ Last accessed 05/11/2014

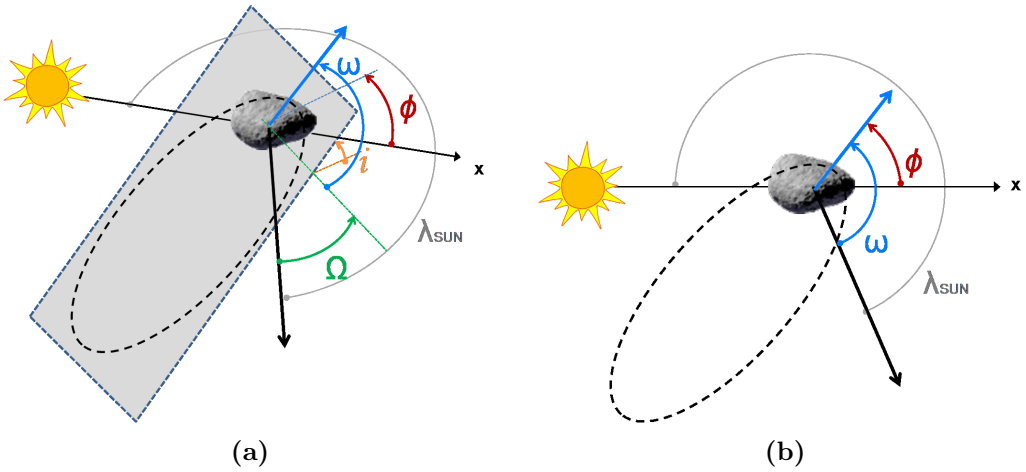

Figure 2.2: Definition of phase angle ϕ in the 3D case (a) and planar case (b).

2.3.4 Orbit averaged equations

In addition to the previously described models, an orbit-averaged approximation approach provides useful tools for graphical representation of trajectories.

Hamilton and Krikov (1996) proposed the use of orbit-averaged Lagrange planetary equations to study the behaviour of circumplanetary dust in the planar case. This method was later used to describe applications for high-area-to-mass ratio spacecraft for Earth geomagnetic tail exploration (McInnes et al., 2001; Oyama et al., 2008), passive de-orbiting, and heliotropic orbits applications (Colombo et al., 2011). It can be shown that it is also well-suited to describe dynamics in the vicinity of asteroids under certain assumptions.

Following loosely Hamilton and Krikov's methodology, a planar case is assumed, in which the asteroid's rotational axis is perpendicular to the plane of movement of both the asteroid around the Sun and the spacecraft or particle around the asteroid. The solar phase angle ϕ is defined as (see Fig. 2.2a):

$$\phi = \Omega + \arctan\left(\frac{\cos i \sin \omega}{\cos \omega}\right) - \lambda_{SUN} + \pi \tag{2.16}$$

where Ω represents the right ascension of the ascending node of an orbit about the asteroid, i and ω are the inclination and argument of the pericentre, and λ_{SUN} is the solar longitude. This phase angle ϕ between the anti-solar direction and the periapsis line is in the planar case given simply by $\phi = \omega - \lambda_{SUN} + \pi$ (see Fig. 2.2b).

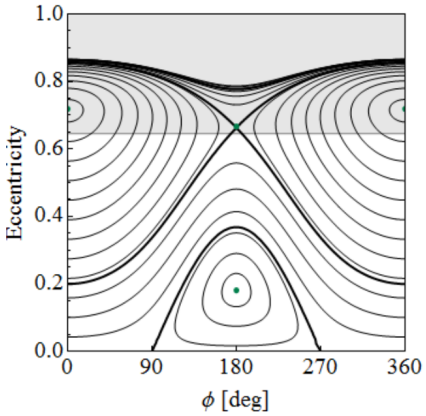

Figure 2.3: Example of iso-hamiltonian lines in an eccentricity-ϕ phase space map (Credit: Colombo et al., 2011).

The dynamics under the influence of the solar radiation pressure perturbation and tidal forces caused by solar gravity can be described by the Hamiltonian (Hamilton and Krikov, 1996):

$$H = \sqrt{1-\bar{e}^2} + \frac{1}{2}A\bar{e}^2\left(1+5\cos(2\phi)\right) - C\bar{e}\cos\phi \tag{2.17}$$

where the coefficients C and A correspond to the solar radiation pressure and tidal term respectively, and they can be expressed with the nomenclature followed by this thesis as:

$$C = \frac{3}{2}\beta\sqrt{\frac{\mu_S}{\mu_A}\frac{\bar{a}}{d}} \qquad A = \frac{3}{4}\sqrt{\frac{\mu_S}{\mu_A}\frac{\bar{a}^3}{d^3}} \tag{2.18}$$

The eccentricity $\bar{e}$ and semi-major axis $\bar{a}$ in Eq. 2.17 and Eq. 2.18 are orbit averaged values. This is an acceptable assumption in the case of circumplanetary dust, as the variation of the semi-major axis over one revolution is zero (Hamilton and Krikov, 1996) and the eccentricity changes slowly.

In the case of asteroid dynamics, the excursions of the osculating semi-major axis from the mean and the variations in eccentricity in one revolution are much larger, introducing deviations from the analytical approximation, but the overall behaviour of the system is still well described with the Hamiltonian approach. The evolution of the eccentricity e and angle ϕ is then given by the following Hamiltonian system in non-canonical form, which uses the solar longitude as its independent variable:

$$\begin{cases} \dfrac{\partial \bar{e}}{\partial \lambda_{SUN}} &= -\dfrac{\sqrt{1-\bar{e}^2}}{\bar{e}} \dfrac{\partial H}{\partial \phi} \\ \dfrac{\partial \phi}{\partial \lambda_{SUN}} &= \dfrac{\sqrt{1-\bar{e}^2}}{\bar{e}} \dfrac{\partial H}{\partial \bar{e}} \end{cases} \tag{2.19}$$

Phase space plots (with the phase angle ϕ in the horizontal axis and eccentricity e in the vertical axis) are useful graphical tools to display the evolution of the orbit under perturbations. Trajectories follow isolines of constant Hamiltonian H in the phase space plot, as depicted in the example in Fig. 2.3. For further examples of their use, see Colombo et al. (2011); Oyama et al. (2008).

Chapter 3

MACRO-SCALE: Easily Retrievable Objects

"Five-hundred-and-one million, six-hundred-twenty-two thousand, seven-hundred-thirty-one. I am concerned with matters of consequence: I am accurate."

"And what do you do with these stars?"

"What do I do with them?"

"Yes."

"Nothing. I own them."

"You own the stars?"

"But I have already seen a king who–"

"Kings do not own, they reign over. It is a very different matter."

"And what good does it do you to own the stars?"

"It does me the good of making me rich."

"And what good does it do you to be rich?"

"It makes it possible for me to buy more stars, if any are discovered."

"This man," the little prince said to himself, "reasons a little like my poor tippler..."

Nevertheless, he still had some more questions. "How is it possible for one to own the stars?"

"To whom do they belong?" the businessman retorted, peevishly.

"I don't know. To nobody."

"Then they belong to me, because I was the first person to think of it."

Saint-Exupéry (1943), *The Little Prince*

Ownership and appropriation issues aside, the utilisation and exploitation of resources on minor bodies has been a matter of discussion since the early rocketry pioneers. (For more information on the legal implications, see Pop (2013), or his former work on extra-terrestrial property rights (Pop, 2006, 2008)). The opening extract uses the term "*stars*", although they might well be referring to asteroids and comets, judging from the response of the Little Prince, who mentions the "*king*" that reigned over a minor planet or asteroid. The "businessman" seems only concerned with the possession of these minor bodies, not paying attention to the potential resources on them or how to reach them, which leaves him with a rather poorly argued business plan. In this respect, Near-Earth Objects (NEOs) are of particular interest because of their accessibility from Earth, and also because of their speculated wealth of material resources. The exploitation of these resources has long been discussed as a means to lower the cost of future space endeavours. Capturing or retrieving small asteroids can be envisaged as a first step and a technology demonstrator which will be needed to actually make the "businessman" rich, along with the associated scientific return of such a project.

In this chapter, the surveyed NEO population as of July 2012 is considered and a family of so-called Easily Retrievable Objects (EROs) is defined: objects that can be transported from accessible heliocentric orbits into the Earth's neighbourhood at affordable costs. The asteroid retrieval opportunities are sought from the continuum of low-energy transfers enabled by the dynamics of invariant manifolds. Specifically, the retrieval transfers target planar, vertical Lyapunov and halo orbit families associated with the collinear equilibrium points of the Sun–Earth Circular Restricted 3–Body problem. The judicious use of these manifolds provides an opportunity to find extremely low energy Earth transfers for asteroid material. A catalogue of asteroid retrieval candidates is then presented. Despite the highly incomplete census of very small asteroids, the ERO catalogue can already be populated with 12 different objects retrievable with a Δv of less than 500 m/s. Moreover, the approach proposed represents a robust search and ranking methodology for future retrieval candidates that can be automatically applied to the growing survey of NEOs.

The "businessman" also raises another point often overlooked, when he states *"if any are discovered."* In the case of Solar System minor bodies, detection and proper tracking is indeed an issue that needs to be addressed in the coming decades, not only for exploitation purposes, but also for threat mitigation. The implications to the problem of capture will be further discussed in this chapter.

3.1 Motivation and background

With the recent interest in asteroid capture, as evidenced by the Keck's study report (Brophy et al., 2012) and the follow-up NASA's Asteroid initiative (Gates et al., 2014; Mazanek et al., 2014), a classification of NEOs distinct from the traditional families and based on retrievability is desirable. This section discusses the rationale for such a classification, the possible applications, and some of the enabling technologies and challenges faced.

3.1.1 Old and new families of Near Earth Objects

NEOs have traditionally been classified into three families according to their orbital elements: Atens, Apollos and Amors, with Atens and Apollos being Earth-crossers, and Amors having orbits completely outside the orbit of the Earth. In the recent literature (Greenstreet et al., 2011; Michel et al., 2000), further emphasis has been placed on the cataloguing of asteroids inside the Earth's orbit, and a fourth group, the symmetric equivalent of Amors, has been added to the list. The new family has been named Atira after the first confirmed object of its kind in 2003, 163693 Atira*. This is a useful classification for NEOs into 4 distinct families, and it is possible to draw some conclusions from this classification regarding the origin and evolution of these objects and their detectability. However, it provides little information in terms of the accessibility of their orbits.

Because of current interest in the science and exploration of NEOs, other classifications have arisen. Some of them have somewhat arbitrary or imprecise definitions: Arjunas have been defined as NEOs in extremely Earth-like orbits (Bombardelli et al., 2012), with low eccentricity, low inclination and a semi-major axis close to that of the Earth; while Brasser and Wiegert (2008) proposed a similar Small Earth-Approachers (SEA) definition for objects with diameters less than 50 m and a semi-major axis, eccentricity and inclination within the ranges of [0.95 AU, 1.05 AU], [0, 0.1] and [0°, 10°] respectively.

Other definitions concern objects that follow very particular trajectories, such as objects on horseshoe orbits, Earth trojans, or objects that for a short period of time naturally become weakly captured by the Earth, referred to as Natural Earth Satellites (NES), or Temporarily Captured Orbiters (TCO) (Granvik et al., 2011).

*Minor Planet Circular 61768 (2008), *Minor Planet Center*, ISSN 0736-6884, Cambridge, USA

The number of known NEOs in each of these categories is however small, with a single confirmed TCO, one Earth trojan, and a handful of asteroids observed in horseshoe orbits to date.

In order to provide a systematic classification of accessible objects, NASA began publishing in 2012 the Near-Earth Object Human Space Flight Accessible Target Study (NHATS) list (Abell et al., 2012), which will be continuously updated and identifies potential candidate objects for human missions to asteroids. NEOs in NASA's NHATS list are ranked according to the number of feasible return trajectories to that object found by an automated search within certain constraints. This provides an objective, quantifiable and ordered classification of the objects in NEO space that allow feasible return missions.

Further classification involving impact hazards by NEOs have also resulted in the generation of an objective scale, the Palermo scale (Chesley et al., 2002), for the ranking of a subset of these objects: the Potentially Hazardous Objects (PHOs). This subset is defined according to orbit and size parameters that are related to the threat they pose: PHOs have a minimum orbit intersection distance (MOID) with respect to Earth of less than 0.05 AU, and their absolute magnitude is less than 22.0 (corresponding roughly to objects larger than 140 m diameter assuming a typical S-class asteroid albedo).

Inspired by this, and considering the growing interest in the capture of small NEOs (Borum et al., 2012; Brophy et al., 2012; Hasnain et al., 2012; Sanchez and McInnes, 2011a), a new objective, quantifiable and ordered classification of NEOs is proposed: the sub-category of Easily Retrievable Objects (EROs). EROs are defined as objects that can be gravitationally captured in bound periodic orbits around the collinear libration points L_1 and L_2 of the Sun–Earth system under a certain Δv threshold, set for this work at 500 m/s. Deep space and insertion manoeuvres of that order have been performed by various spacecrafts. However, in the case of an asteroid, the mass to be accelerated is much larger, increasing fuel costs dramatically. This value should thus only be considered a very conservative upper limit for capture. EROs can then be ranked according to the required Δv cost.

3.1.2 Enabling technologies for capture

Proposed technologies and methods for the deflection of potentially Earth impacting objects have experienced significant advances, along with increasing knowledge of the asteroid population. While initially devised to mitigate the hazard posed by global impact threats, at the moment the impact risk is largely posed by the population of small undiscovered objects (Shapiro et al., 2010). Thus, methods have been proposed to provide subtle changes to the orbits of small objects, as opposed to large-scale interventions such as the use of nuclear devices (Kleiman, 1968). This latter batch of deflection methods, including but not limited to the low thrust tugboat (Scheeres and Schweickart, 2004), the gravity tractor (Edward and Stanley, 2005) or a small kinetic impactor (Sanchez and Colombo, 2013), are moreover based on physical principles that have already been demonstrated in the space environment. As such they can render the apparently ambitious scenario of manipulating asteroid trajectories a likely option for the coming decades, although extensive technological development is still required.

Current interplanetary spacecraft have masses on the order of 10^3 kg, while an asteroid of 10 metres diameter will most likely have a mass of the order of 10^6 kg. Hence, already moving such a small object, or an even larger one, with the same ease that a scientific payload is transported would demand propulsion systems orders of magnitudes more powerful and efficient; or alternatively, orbital transfers orders of magnitude less demanding than those to reach other bodies in the solar system.

Therefore, advances in both asteroid deflection technologies and dynamical system theory, which allow new and cheaper means of space transportation, are now enabling radically new mission concepts, such as low-energy asteroid retrieval missions (Brophy et al., 2012). These envisage a spacecraft reaching a suitable object, coupling itself to the surface and returning it, or a portion of it, to the Earth's orbital neighbourhood. Moving an entire asteroid into an orbit in the vicinity of Earth entails obvious engineering challenges, but may also allow much more flexible resource extraction in the Earth's neighbourhood, in addition to other advantages such as enhanced scientific return.

3.1.3 Projects requiring asteroid retrieval

The increased interest in NEOs has encouraged the community to put forward further engineering projects related to asteroid retrieval missions, taking advantage of the synergies with search campaigns of minor bodies and asteroid manipulation technology development initiatives.

Various space macro-engineering projects have as a primary requirement the capture or shepherding of a portion of, or a full asteroid, into useful orbits in the solar system (see Table 3.1).

For example, early proposals for the space elevator concept involve the capture of a small body in an orbit close to GEO to serve as counterweight. The size of the counterweight required depends on the radius of the orbit where the asteroid would be placed, with size decreasing exponentially with altitude above GEO, resulting in a 50 ton asteroid (about 3.3 m diameter) for a counterweight at a circular orbit of radius 100,000 km (Aravind, 2007).

Similarly, the use of captured asteroids has also been proposed for geo-engineering purposes as means of reducing solar insolation at Earth by generating dust rings or clouds. Depending on the position of the dust cloud, either an Earth ring (Pearson et al., 2006), Sun–Earth L_1 cloud (Bewick et al., 2012), or Earth–Moon L_4/L_5 region cloud (Struck, 2007), and the desired reduction in insulation, the asteroid mass requirements and the complexity and cost of the capture transfer vary, but the minimum size for a target asteroid is never below 500 metres diameter. Retrieving objects of this size is doubtless far beyond current technological capabilities. Pearson et al. (2006) suggests the use of space manufactured solar reflectors instead of dust rings or clouds, which would reduce the mass required by more than one order of magnitude. However, that would involve a large manufacturing infrastructure on orbit.

Much smaller asteroids are already of interest for resource exploitation. The in-situ utilisation of resources in space has long been suggested as the means of lowering the cost of space missions, for example by providing bulk mass for radiation shielding or distilling rocket propellant for interplanetary transfers (Lewis, 1996). The development of technologies for in-situ resource utilisation (ISRU) could become a potentially disruptive innovation for space exploration and utilisation and, for example, enable large-scale space ventures that could today be considered far-fetched, such as large space solar power satellites or sustaining

Table 3.1: Macro-engineering projects proposing asteroid capture. To estimate asteroid sizes, given in diameter, an average NEO density of 2.6 g/cm^3 (Chesley et al., 2002) was used when necessary.

Project	Target orbit(s)	Size or mass required	Reference
Space Elevator	~GEO	$52 \cdot 10^3$ kg (> 3.3 m)	Aravind (2007)
Geo-engineering: Dust ring LEO	~LEO	$2.3 \cdot 10^{12}$ kg (> 1190 m)	Pearson et al. (2006)
Geo-engineering: Dust cloud L_1	Sun–Earth L_1	$1.9 \cdot 10^{11}$ kg (> 515 m)	Bewick et al. (2012)
Geo-engineering: Dust cloud $L_{4/5}$	Earth–Moon L_4/L_5	$2.1 \cdot 10^{14}$ kg (> 5.3 km)	Struck (2007)
Tech. demo ISRU/Fuel depot	L_1, L_2, Moon orbit...	> 2 m	Brophy et al. (2012)
Space station	L_1, L_2, L_4, L_5	> 10 m	
NEO shield	Sun–Earth L_1, L_2	20–40 m	Massonnet and Meyssignac (2006)
Cyclers	Earth–Mars resonant orbit	> 100 m	Lewis (1996, p. 115)

communities in space. Although the concept of asteroid mining dates back to Tsiolkovsky (1903), a pioneer of astronautics, evidence of a renewed interest can be found in the growing body of literature on the topic (Baoyin et al., 2010; Hasnain et al., 2012; Sanchez and McInnes, 2011a), as well as in high profile private enterprise announcements by Planetary Resources Inc.* or Deep Space Industries.†

A recent asteroid retrieval mission study (Brophy et al., 2012) proposed the capture of a 2–4 m diameter asteroid around the Moon with current technologies, which could serve as test-bed for the development of in-situ resource utilisation (ISRU) technologies and methods. Other proposals (Massonnet and Meyssignac, 2006) suggest a larger asteroid, to be used as a NEO shield in combination with resource exploitation. Fuel depots or permanent space stations that use a small asteroid as a base can also be envisaged in the near future. Finally, the use of asteroids in cycler orbits to provide structural support and radiation shielding for

*http://www.planetaryresources.com/
†http://deepspaceindustries.com/

interplanetary transfers can be considered a more futuristic enterprise that can also be found in literature (Lewis, 1996, p. 115).

In all of these studies, the Sun–Earth Lagrangian points repeatedly appear as one of the preferred destinations for captured asteroids. This is relevant as they can also serve as natural gateways to other destinations in the Earth–Moon system through the use of heteroclinic connections (Koon et al., 2000). There are however several key challenges to overcome: the development of techniques to modify asteroid trajectories, the improvement in the minor body census in order to find the most suitable candidates of the appropriate size, and the design of low-cost transfers to the desired final orbits.

This chapter aims to provide a feasibility assessment of the capture mission concept by defining a set of preliminary mission opportunities that could be enabled by invariant manifold dynamics. Missions delivering a large quantity of material to the Lagrangian points are of particular interest. This material can be used in a first stage as a test bed for ISRU technology demonstration missions and material processing at affordable costs. The science return is also greatly improved, with an asteroid permanently, or for a long duration, available for study and accessible to telescopes, probes and even crewed missions to the Lagrangian points. Finally, it sets the stage for other future endeavours, such as those listed in Table 3.1.

3.1.4 Resource availability

With regards to the availability of the required asteroid resources for such macro-engineering projects, recent work by Sanchez and McInnes (2011a, 2013) demonstrates that a substantial quantity of resources can indeed be accessed at relatively low energy. On the order of 10^{14} kg of material could potentially be harvested at an energy cost lower than that required to access resources from the surface of the Moon. More importantly, asteroid resources could be accessed across a wide spectrum of energies, and thus, current technologies could be adapted to return to the Earth's neighbourhood small objects from 2 to 30 meters diameter for scientific exploration and resource utilisation purposes. In their work, the accessibility of asteroid material is estimated by analysing the volume of Keplerian orbital element space from which the Earth can be reached under a given energy threshold by means of a bi-impulsive transfer. This volume of Keplerian element space is then mapped into existing NEO orbital (Bottke et al., 2002b) and size distribution models (Mainzer et al., 2011).

3.1.5 The issue of detection

One of the main challenges for capture resides with the difficulties inherent in the detection of small objects. Thus, for example, only one out of every million objects with a diameter between 5 to 10 meters is currently known and this ratio is unlikely to change significantly in the coming years (Veres et al., 2009). As of December 21^{st} 2012, 9432 NEOs were known. The smallest object among the surveyed asteroids is estimated to be of only a few meters in diameter, while the largest is of 32 km diameter (i.e., Ganymed). However, the surveyed portion of the NEO population is only a fraction of the total existing population, especially at very small sizes, on the order of a few meters in diameter, for which the surveyed fraction is well below 1% (Shapiro et al., 2010). The knowledge of the orbital parameters of already surveyed objects of that size is not very precise, and subsequent re-detections during future close approaches are in most cases not guaranteed. For the vast majority of known asteroids only the orbital elements and the absolute magnitude H_A (i.e., intrinsic brightness) of the object are available, and in most cases with large associated uncertainties. Given the absolute magnitude, a simple formula provides a first insight into the asteroid size in terms of equivalent diameter Ø:

$$Ø = 1329\ km\ \times 10^{-H_A/5} p_v^{-1/2} \tag{3.1}$$

where the absolute magnitude H_A is provided in JPL's Small–Body Database Browser,* and the asteroid's albedo p_v can be assumed to be 0.154 as the average value for the standard near Earth asteroid (Chesley et al., 2002). However, this rough estimate can easily be inaccurate by an order of magnitude, and light curve analysis, radar campaigns or spacecraft encounter data would always be more reliable, but they are rarely available.

The implications of such a reduced census of objects, and the uncertainties in their orbits and size on the manipulation and capture are better illustrated through a case study. ESA's SysNova initiative, bearing the NEO threat in mind, proposed a challenge consisting on contactless asteroid orbit modification. The main specifications of the challenge were to impart at least 1 m/s Δv over the course of three years to a small asteroid of size 2–4 meters diameter. Further constraints limited the target asteroid's orbital elements to have a perihelion (r_p) larger than 0.7 AU, an aphelion (r_a) smaller than 1.4 AU and an inclination i smaller than 5 degrees.

* http://ssd.jpl.nasa.gov/sbdb.cgi (last accessed 27/07/12)

Table 3.2: Possible candidates for the SysNova challenge

Designation	H_A	r_p [AU]	r_a [AU]	i [deg]
2012 AQ	30.698	0.9598	1.1821	2.856
2011 CA7	30.319	0.7686	1.3930	0.121
2012 FS35	30.286	0.9686	1.2290	2.338
2008 WO2	29.779	0.8323	1.2182	2.010
2011 JV10	29.706	0.9095	1.3701	1.404
2011 AM37	29.690	0.9385	1.2626	2.629
2008 JL24	29.572	0.9276	1.1489	0.550
2006 RH120	29.527	1.0080	1.0585	0.595
2008 UA202	29.440	0.9624	1.1042	0.264
2012 EP10	29.165	0.9285	1.1721	1.033

Several solutions were proposed, among them a laser ablation demonstrator called LightTouch[2] (Vasile et al., 2013).

At the time of the challenge, 189 NEOs were known in the required range of orbital elements according to JPL Small–Body Database Browser, and only ten of which fall within the range of sizes of the SysNova challenge, assuming the above mentioned albedo to calculate the equivalent spherical diameter for their magnitude. Table 3.2 shows the orbital elements, absolute magnitude and estimated size of these objects. If brighter bodies are assumed, the number of NEOs in that region under 5 meters increases to 13 for an albedo of 0.25, and to 40 NEOs for very bright objects of albedo 0.50 (intended for icy objects).

According to the latest near Earth object population estimates, i.e., NEOWISE (Mainzer et al., 2011), close to 2×10^{10} NEOs with diameter ranging from 2 to 4 meter diameter should exist. From these, close to 1 million should also have orbital elements within the specified operational orbit constraints. Since only 10 were known at the time of the challenge, from which 6 were discovered over the course of the previous year, this represents a large deficit of small objects that could be targeted for capture, but also a great potential for discovery of new asteroids. Moreover, a consequence of the goal to catalogue 90% of all the 140 meters NEOs by 2020,* and the effort by the new generation of all sky surveys

*National Aeronautics and Space Administration Authorization Act of 2005 (Public Law 109–155), January 4, 2005, Section 321, George E. Brown, Jr. Near–Earth Object Survey Act.

Table 3.3: Estimated density and albedo of 2008 JL24 and 2006 RH120 for SysNova. The values are also compared with typical asteroid data as in Chesley et al. (2002)

	ρ [kg/m^3]	p_v
C-class	1,300	0.06
S-class	2,700	0.18
2008 JL24	**3,879.4**	**0.1637**
2006 RH120	**3,879.4**	**0.1707**
M-class	5,300	0.12
Standard NEO	2,600	0.154

such as Pan-STARRS and LSST to fulfil this, is that an enormous increase of the population of small objects should be expected over the next years (Shapiro et al., 2010).

The Minor Planet Centre defines an Orbit Condition Code (OCC) which gives an indication of the uncertainty in a perturbed orbital solution for a minor planet. It is expressed as an integer between 0 and 9 indicating how well an object's orbit is known on a logarithmic scale, with 0 indicating an extremely low uncertainty, and 9 a very high one. Objects with OCC larger than 5 can be considered effectively "lost" for the purpose of a rendezvous mission, unless new radar or optical observations become available, as the uncertainty on the position would increase significantly with time.

Considering only objects with OCC below 4 (to be conservative), only two can be short-listed as the most suitable targets for a deflection demonstrator: 2008 JL24 (OCC=3) and 2006 RH120 (OCC=1). These objects will both undergo a very close approach to Earth in the coming decades: asteroid 2008 JL24's closest approach occurs during 5^{th} March 2026 with a minimum distance to Earth of only 0.061 AU; while asteroid 2006 RH120's closest approach occurs during 9^{th} October 2028 with a minimum distance of 0.027 AU. In line with SysNova requirements, both objects are assumed to be 4 m diameter asteroids with a mass of 130 tons. Given this mass and size the estimated average density is 3879.4 kg/m^3 for both objects, somewhat higher than S-class asteroids and lower that M-class asteroids. Table 3.3 reports the typical density of S-class, C-class and M-class asteroids and their albedos along with the estimated density and albedos of the selected targets.

Table 3.4: NEO properties and next observation opportunities predicted by NHATS (http://neo.jpl.nasa.gov/nhats/ last accessed 09/12/2012)

DESIGNATION	2008 JL24	2006 RH120
H_A [mag]	29.6	29.5
Estimated Diameter [m]	2.1–9.5	2.2–10
OCC	3	1
Next Optical Opportunity [yyyy-mm (visual mag.)]	none	2028-06 (23.9)
Next Arecibo Radar Opportunity [yyyy-mm]	none	none
Next Goldstone Radar Opportunity [yyyy-mm]	none	none

The assumed characteristics appear to correspond to a somewhat denser S-type asteroid, and are well within realistic values.

Even with their low OCC, the ephemerides of both objects are relatively uncertain and a rendezvous may pose a serious challenge. If the asteroids were observable from Earth before the rendezvous, the ephemerides of these objects may be updated and the uncertainty significantly reduced. Physical characteristics, such as its shape and rotation, can be extracted from radar observations. Unfortunately, as shown in Table 3.4, no radar observations will be possible in the coming two decades and only 2006 RH120 will be visible from Earth during June 2028.

Assuming the above estimated sizes and albedos, a more detailed account of the visual magnitude of the objects as seen from both the Earth and a spacecraft during a possible rendezvous trajectory is shown in Fig. 3.1. The spacecraft trajectories correspond to low-thrust transfers calculated during the course of the study (the final proposal argued for a high-thrust mission, but both low-thrust and impulsive transfers were generated, see Vasile et al. (2013)). It can be observed, for example, that asteroid 2008 JL24 approaches the Earth twice during 2026. The best transfer opportunity for 2008 JL24 requires departing from Earth just before the second close approach, and as the spacecraft approaches the asteroid the visual magnitude of the asteroid as seen from the spacecraft (red line) decreases very quickly. Asteroid 2008 JL24 reaches only a minimum magnitude around 25 as seen from Earth, slightly above the minimum required to be detected by Earth-based surveys with current standard assets (*horizontal blue dashed line*). Assuming a wide angle camera for acquisition from the spacecraft similar to the Osiris instrument on-board Rossetta (Keller et al., 2007), with a limiting apparent visual magnitude of 13–14 (*horizontal orange dashed line*), the

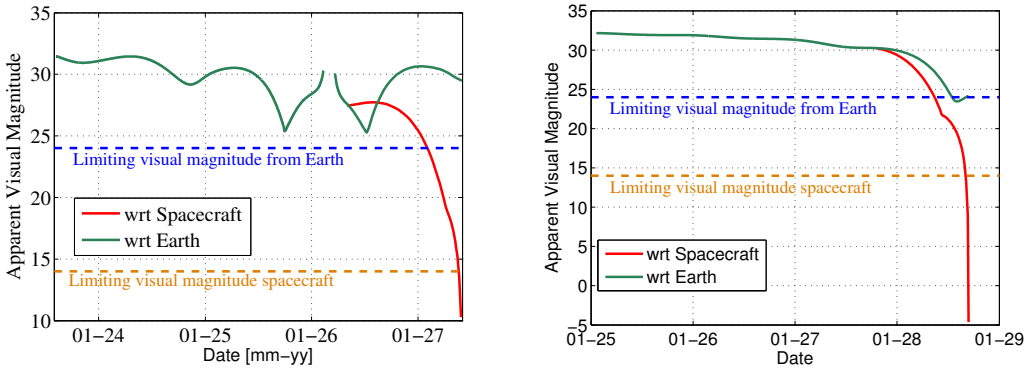

(a) **(b)**

Figure 3.1: Visual magnitude of 2008 JL24 (a) and 2006 RH120 (b) from Earth and from a spacecraft on a preliminary transfer trajectory

spacecraft would be capable of acquiring the asteroid only during the last few days before rendezvous. On the other hand, 2006 RH120 appears to be a more advantageous target since the asteroid is visible from Earth during the approach.

Both distance and relative Sun–asteroid–spacecraft geometry play a crucial role during acquisition. Figure 3.2 shows the region around the spacecraft where an asteroid of 4 meters diameter will be visible by a standard wide angle camera at 1 AU distance from the Sun (approximately that of the spacecraft during the transfer for these two particular asteroids). In the figure the spacecraft is at the origin, the Sun direction is towards the negative x-axis, and the blue curve encloses the region where an asteroid 4 meters in diameter would be seen from the spacecraft. The area where the asteroid can be seen lies mostly away from the Sun, as the Sun is illuminating the asteroid. It can thus be understood that not only will the asteroid be visible during the final days of approach, when at very close distances, but also the approach needs to ensure a certain geometrical configuration with respect to the Sun and the asteroid.

Similar rendezvous trajectories would be required during an asteroid retrieval mission. The above example therefore illustrates the challenges associated with detection that any mission to a small body will face. Based on these concerns of a reduced census of small bodies, and the poor orbit quality of most of them, which limits the applicability of any manipulation or even approach strategy, an extensive campaign of observations and follow-ups of small bodies would be highly recommended. For simplicity, in what follows detection issues are assumed

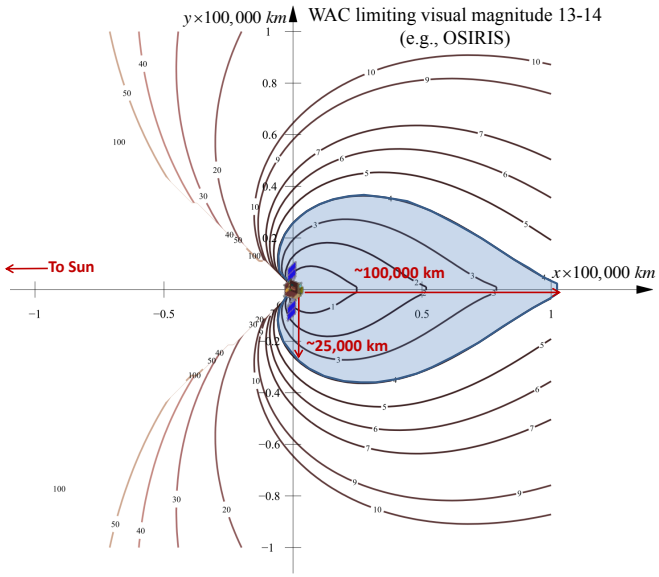

Figure 3.2: Observability diagram of a faint object from a vantage point at 1 AU (Vasile et al., 2013). Contour lines indicate the size of the observable object from the origin of coordinates (spacecraft).

solved by such a campaign, and the ephemeris of the target orbits for capture are considered well determined.

3.2 Low energy transport conduits

Solar system transport phenomena, such as the rapid orbital transitions experienced by comets Oterma and Gehrels 3 (Belbruno and Marsden, 1997), from heliocentric orbits with periapsis outside Jupiter's orbit to apoapsis within Jupiter's orbit, or the Kirkwood gaps in the main asteroid belt (Moons, 1996), are some manifestations of the sensitivities of multi-body dynamics. The same underlying principles that enable these phenomena also allow excellent opportunities to design surprisingly low energy transfers.

It has been known for some time that the hyperbolic invariant manifold structures associated with periodic orbits around the L_1 and L_2 collinear points of the Three Body Problem provide a general mechanism that controls the aforementioned solar system transport phenomena (Belbruno and Marsden, 1997; Koon et al., 2000; Lo and Ross, 1999). In this chapter, these mathematical constructs are utilised to find *low-cost* trajectories to retrieve asteroid material to the Earth's vicinity.

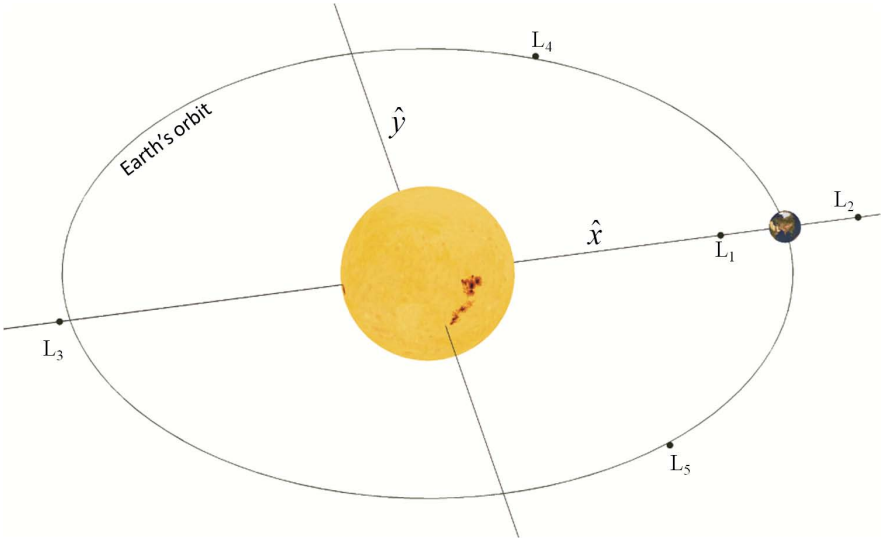

Figure 3.3: Schematic of the CR3BP and its equilibrium points.

3.2.1 Periodic orbits and manifold structures

This chapter now concentrates on the dynamics concerning the Sun–Earth L_1 and L_2 points (see Fig. 3.3), as they are the *gate keepers* for potential ballistic capture of asteroids in the Earth's vicinity. The work performed assumes the motion of the spacecraft and asteroid under the gravitational influence of the Sun and Earth, within the framework of the Circular Restricted Three–Body Problem (CR3BP, see Section 2.2.1), following closely the approach by Koon et al. (2008). The well known equilibrium points of the system are shown in Fig. 3.3. The mass parameter μ is taken as $3.0032080443\times10^{-6}$, which neglects the mass of the Moon. Note that the usual normalised units are used when citing Jacobi constant values.

There has been a long and intense effort to catalogue all bounded motion near the libration points of the Circular Restricted 3–Body Problem (Howell, 2001). The principal families of bounded motion that have been thoroughly studied are planar and vertical families of Lyapunov periodic orbits, quasi-periodic Lissajous orbits, and periodic and quasi-periodic halo orbits (Gómez et al., 2000; Koon et al., 2008). Some other families of periodic orbits can be found by exploring bifurcations in the aforementioned main families (Howell, 2001).

Theoretically, an asteroid transported onto one of these orbits would remain near the libration point for an indefinite period of time. In practice, however, these orbits are unstable, and an infinitesimal deviation from the periodic orbit

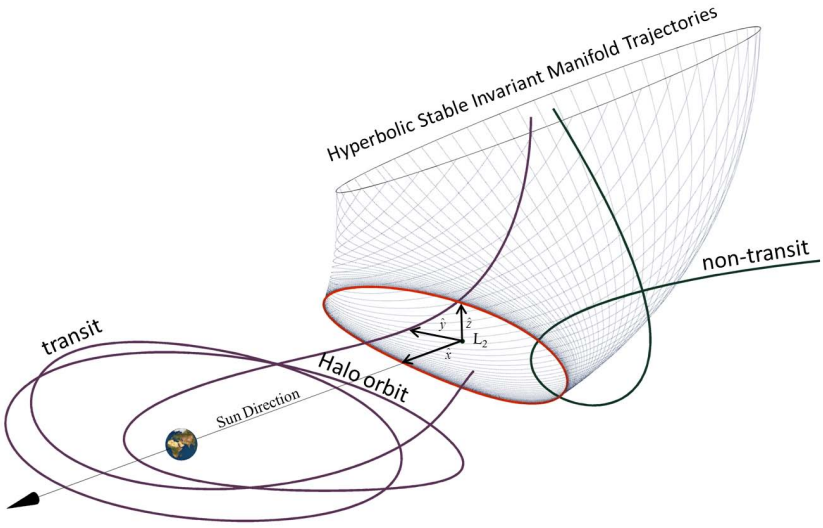

Figure 3.4: Schematic representation of the four categories of motion near the L_2 point (represented by the set of axes in the figure): periodic motion around L_2 (e.g., halo orbit), hyperbolic invariant manifold structure (i.e., set of stable hyperbolic invariant manifold trajectories), transit trajectory, and non-transit trajectory.

will make the asteroid depart asymptotically from the libration point regions. Nevertheless, small correction manoeuvres can be assumed to be able to keep the asteroid in the vicinity of the periodic orbit (Howell and Pernicka, 1993; Simó et al., 1987).

The linear behaviour of the motion near the libration points is of the type *centre* × *centre* × *saddle*, which is also a characteristic of all bounded motion near these points (Szebehely, 1967). This particular dynamical behaviour ensures that, inherent to any bounded orbit near the libration points, an infinite number of trajectories exist that asymptotically approach, or depart from, the bounded motion. Each set of trajectories asymptotically approaching, or departing, a periodic or quasi-periodic orbit near the L_1 or L_2 points forms a hyperbolic invariant manifold structure.

It is well known that the phase space near the equilibrium regions can be divided into four broad classes of motion: bound motion near the equilibrium position (i.e., periodic and quasi-periodic orbits), asymptotic trajectories that approach or depart from the latter, transit trajectories, and, non-transit trajectories (see Fig. 3.4). A transit orbit is a trajectory such that its motion undergoes a rapid transition between such regions. In the Sun–Earth case depicted in Fig. 3.4, for

example, the transit orbit approaches the Earth following a heliocentric trajectory, transits through the bottle neck delimited by the halo orbit and becomes temporarily captured at Earth. An important observation from dynamical system theory is that the hyperbolic invariant manifold structure defined by the set of asymptotic trajectories forms a phase space separatrix between transit and non-transit orbits for a given energy. Asteroids close to this separatrix will be sought as the most likely candidates for capture.

It follows from the four categories of motion near the libration points that periodic orbits near the Sun–Earth L_1 and L_2 points cannot only be targeted as the final destination of asteroid retrieval missions, but also as natural gateways of low energy trajectories to Earth–centred temporarily captured trajectories or transfers to other locations of the cis-lunar space, such as the Earth–Moon Lagrangian points (Canalias and Masdemont, 2006; Lo and Ross, 2001).

In this section, three distinct classes of periodic motion to be used as target orbits for capture near the Sun–Earth L_1 and L_2 points are described: Planar and Vertical Lyapunov and Halo Orbits, herein referred to as a whole as libration point orbits (LPO).

3.2.1.1 Lyapunov Orbits

The *centre* × *centre* part of the linearised motion in the vicinity of a collinear equilibrium point generates a 4-dimensional central invariant manifold when all energy levels are considered. For a given energy level the central invariant manifold is a 3-dimensional set of periodic and quasi-periodic solutions lying on an invariant torus, together with some stochastic regions in between (Gómez and Mondelo, 2001). There exist families of periodic orbits with frequencies related to both centres: ω_p and ω_v (Alessi, 2010), where the subscripts p and v indicate an associated planar or vertical motion. They are known as *planar Lyapunov family* and *vertical Lyapunov family*, see Fig. 3.5a, and their existence is ensured by the Lyapunov centre theorem. Halo orbits are 3-dimensional periodic orbits that emerge from the first bifurcation of the planar Lyapunov family.

To generate the entire family of planar and vertical Lyapunov periodic orbits, an approximate solution is generated in a very close neighbourhood of the libration point (see for example Howell, 2001). This initial solution is corrected in the nonlinear dynamics of the problem by means of a differential correction algorithm

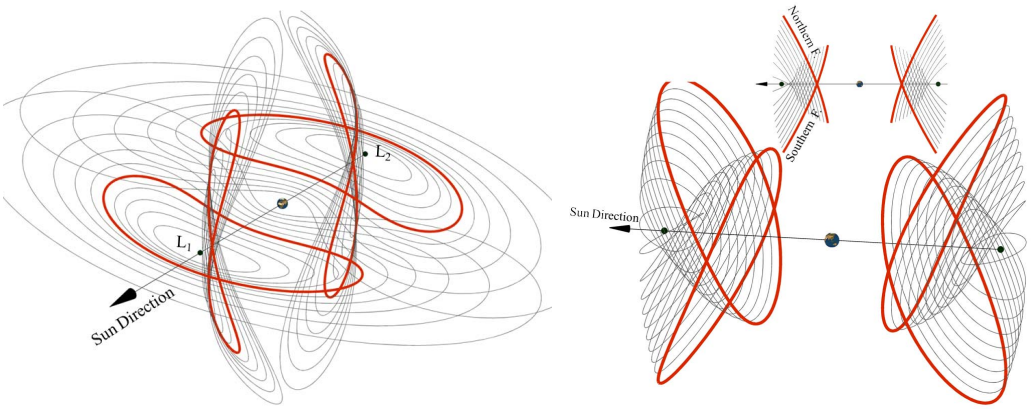

(a) **(b)**

Figure 3.5: Series of planar and vertical Lyapunov orbits (a) and northern and southern halo orbits (b) associated with the Sun–Earth L_1 and L_2 points. Lyapunov orbits are plotted ranging from Jacobi constant 3.0007982727 to 3.0000030032. Halo orbits are plotted ranging from Jacobi constant of 3.0008189806 to 3.0004448196. The *thicker red line* has a Jacobi constant of 3.0004448196, which corresponds to half the distance between the energy at equilibrium in L_2 and L_3.

(Koon et al., 2008) over a suitable plane section that takes advantage of the known symmetries of these orbits (Zagouras and Markellos, 1977). Once one periodic solution has been computed, the complete family can be generated by means of a numerical continuation process that uses the previous solution as an initial guess. By properly choosing the phase space direction in which to extend the solution by numerical continuation, and repeating the process iteratively, one can build a family of periodic orbits with increasing Jacobi constant, as shown in Fig. 3.5.

3.2.1.2 Halo Orbits

The term halo orbit was coined by Robert Farquhar, who advocated the use of these orbits near the Earth–Moon L_2 point to provide a continuous communication relay with the far side of the Moon (Farquhar, 1967).

As previously noted, this type of orbit emerges from a bifurcation in the family of planar Lyapunov orbits. As the amplitude of planar Lyapunov orbits increases, eventually a critical amplitude is reached where the planar orbits become vertical critical, as defined by Hénon (1973a), and new three-dimensional families of periodic orbits bifurcate. The minimum possible size for halo orbits in the Sun–Earth system is approximately $(240 \times 660) \cdot 10^3$ km at L_1 and $(250 \times 675) \cdot 10^3$ km

at L_2, sizes denoting the maximum excursion from the libration point in the x and y directions respectively (considering a rotating frame as shown in Fig. 3.4). At the bifurcation point, two symmetric families of halo orbits emerge for each libration point, here referred to as the northern and southern family depending on whether the maximum out-of-plane z displacement is achieved in the northern (i.e., $z > 0$) or southern (i.e., $z < 0$) direction, respectively (see Fig. 3.5b).

Similarly to planar and vertical Lyapunov orbits, the set of halo orbits was computed by means of the continuation of a predictor–corrector process. The initial seed was computed by means of Richardson's (1980) third order approximation of a halo orbit. A differential corrector procedure is then used to trim Richardson's prediction and obtain the smallest halo orbit possible (Koon et al., 2008; Zagouras and Markellos, 1977). The process is then continued by feeding the next iteration with a prediction of a slightly larger displacement in z. Repeating this process provides a series of halo orbits with increasing energy, or decreasing Jacobi constant.

A more extended explanation on the generation of the families of LPOs can be found in Sanchez et al. (2012a). It details the process to generate the target orbits for the asteroid retrieval missions presented here, and also studies the access to the required Lyapunov orbits from Earth.

3.3 Asteroid retrieval opportunities

In the past few years, several space missions have already attempted to return samples from the asteroid population , e.g., Hayabusa (Kawaguchi et al., 2008), and others are planned for the near future.* As shown by Sanchez and McInnes (2011a), given the low transport cost expected for the most accessible objects, it is possible to envisage returning to Earth entire small objects with current or near-term technology.

In this section, the surveyed population of asteroids will be scanned to search for the most accessible candidates for near-term asteroid retrieval missions by means of invariant hyperbolic stable manifold trajectories, the so-called Easily Retrievable Objects.

*http://www.nasa.gov/topics/solarsystem/features/osiris-rex.html (last accessed 02/05/12)

For this purpose, a systematic search of capture candidates among catalogued NEOs was carried out, selecting the L_1 and L_2 regions as the target destination for the captured material. This gives a grasp and better understanding of the possibilities of capturing entire NEOs or portions of them in a useful orbit. It also demonstrates a method that can be applied to categorise newly discovered small bodies in the future when detection technologies improve and rank them according to their retrievability.

3.3.1 Invariant manifold trajectories to L_1 and L_2

In order to provide a simple but robust method for categorizing EROs, the design of the transfer from the asteroid orbit to the L_1 and L_2 LPO consists of a ballistic arc, with two impulsive burns at the start and end, intersecting a hyperbolic stable invariant manifold asymptotically approaching the desired periodic orbits. This analysis only considers the inbound leg of a full capture mission.

Planar Lyapunov, vertical Lyapunov, and halo orbits around L_1 and L_2 generated with the methods described in the previous section were considered as target orbits. The invariant stable manifold trajectories were computed by perturbing the target orbit periodic solutions around the Lagrangian point on the stable eigenvector direction (Koon et al., 2008) by a magnitude of 10^{-6}, in normalised units. These initial conditions were propagated backwards in the Circular Restricted 3-Body Problem (Section 2.2.1) until they reached the desired fixed section in the Sun–Earth rotating frame. This propagation time is referred to as the manifold transfer time. The section was arbitrarily selected as the one forming an angle of $\pm\pi/8$ with the Sun–Earth line ($\pi/8$ for the L_2 orbits, see Fig. 3.6, the symmetrical section at $-\pi/8$ for those targeting L_1). This corresponds roughly to a distance to Earth of the order of 0.4 AU, where the gravitational influence of the planet is considered small. No additional perturbations were assumed in the backward propagation.

In this analysis, Earth is assumed to be in a circular orbit of 1 AU heliocentric distance. This simplification allows the conditions of the manifold trajectories (and in particular in the selected section) to be independent of the insertion time into the final orbit. The only exception is the longitude of the perihelion, i.e., the sum of the right ascension of the ascending node and the argument of perihelion, which varies with the insertion time with respect to a reference time with the following relation:

$$(\Omega + \omega) = (\Omega_{REF} + \omega_{REF}) + \frac{2\pi}{T}(t - t_{REF}) \tag{3.2}$$

where Ω_{REF} and ω_{REF} are the right ascension of the ascending node and the argument of perihelion at the $\pm\pi/8$ section, for an insertion into a target orbit at reference time t_{REF}, and T is the period of the Earth. For orbits with non-zero inclination, the argument of perihelion of the manifolds is also independent of the insertion time and the above equation indicates a variation in Ω. However, in the case of planar Lyapunov orbits with zero inclination, Ω is not defined and an arbitrary value of zero can be selected, resulting in the equation representing a change in argument of perihelion.

The transfer between the NEO orbit and the manifold is then calculated as a heliocentric Lambert arc (implemented following Simó (1973)) of a restricted two–body problem (section 2.1) with two impulsive burns, one to depart from the NEO and the final burn for insertion into the manifold, with the insertion constrained to take place before or at the $\pm\pi/8$ section.

Thus, the problem can be defined with 5 variables: the Lambert arc transfer time, the manifold transfer time, the insertion date at the target periodic orbit, the energy of the final orbit, and a fifth parameter determining the point in the target orbit where the insertion takes place.

The benefit of such an approach is that the asteroid is asymptotically captured into a bound orbit around a collinear Lagrangian point, with no need for a final insertion burn at arrival. All burns are performed far from the Earth, so no large gravity losses need to be taken into account. Furthermore, this provides additional time for orbit corrections, as the dynamics in the manifold are "slow" when compared to a traditional hyperbolic approach. Finally, this type of trajectory is then easily extendable to a low-thrust trajectory if the burns required are small.

The shape of the manifolds projected onto the $r - \dot{r}$ phase space (with r being the radial distance from the Sun) at the intersection with the $\pm\pi/8$ section is shown in Fig. 3.7 for a particular Jacobi constant. For an orbit with exactly the energy of L_1 or L_2, the intersection is a single point; while for lower Jacobi constants, the shape of the intersection is a closed loop. The intersection corresponding to the bifurcation between planar and halo orbits is also plotted. A few capture candidate asteroids have been included in the plot (+ markers) at their intersection with the $\pi/8$ plane around their next closest approach to the Earth. It is

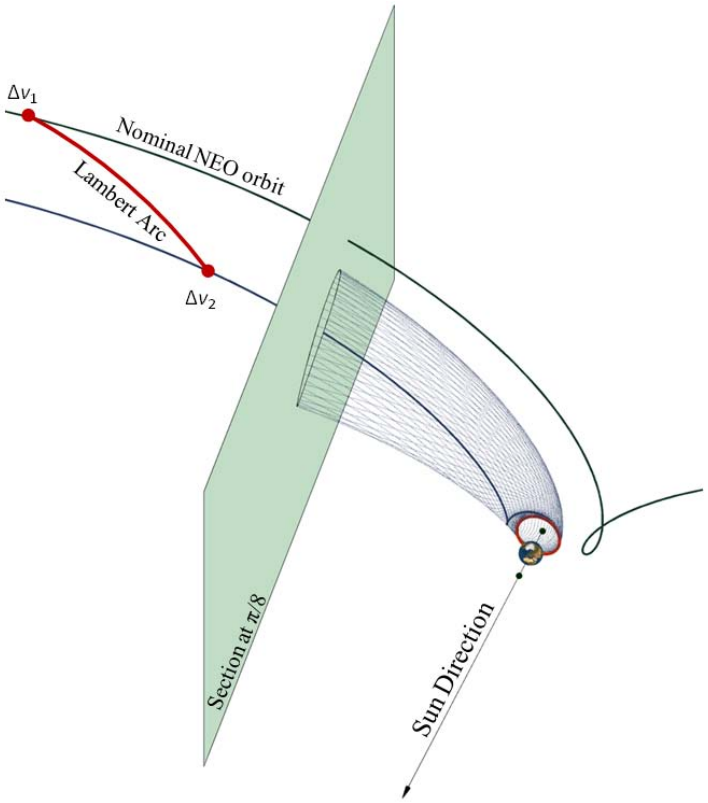

Figure 3.6: Schematic representation of a bi-impulsive transfer to a libration point orbit around L_2

worth noting that the epoch of the next encounter, and thus of the intersection, is different for each particular asteroid. In a planar case, this would already provide a good measure of the distance of the asteroid to the manifolds. However, when considering the 3D problem, information on the z component or the inclination would also be necessary.

Figure 3.8 provides a more useful representation of the manifolds in terms of perihelion and aphelion radii, as well as inclination for the two collinear points. The point of bifurcation between the planar Lyapunov and halo orbits, when they begin to grow in inclination, can easily be identified. Halo manifold trajectories extend a smaller range in aphelion and perihelion radius when compared to planar Lyapunov manifolds. Vertical Lyapunov manifold orbits have even smaller excursions in radius from a central point, as can already be seen in the smaller loops corresponding to vertical Lyapunov orbits in Fig. 3.7, but they extend to much lower values of the Jacobi constant and cover a wider range of inclinations.

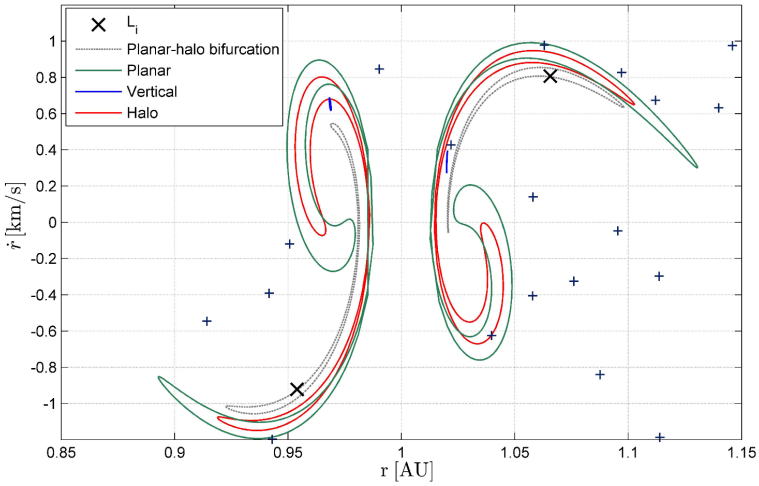

Figure 3.7: Projection of the manifolds onto the $r - \dot{r}$ phase space for a Jacobi constant of 3.0004448196. The manifolds are represented at their intersection with a plane forming a $\pm\pi/8$ angle with the Sun–Earth line in the rotating frame. Manifolds on the left correspond to L_1, on the right to L_2. Capture candidates are indicated with a + marker.

Several asteroids are also plotted with small markers in the graphs. Their Jacobi constant J is approximated by the Tisserand parameter defined as (e.g., Murray and Dermott, 1999, pp. 71-73):

$$J \approx \frac{1}{a} + 2\sqrt{a(1-e^2)\cos i} \tag{3.3}$$

where a, e and i are the semi-major axis (in AU), eccentricity and inclination of the asteroid orbit.

This illustrates the proximity to the manifolds of a number of NEOs. In particular, asteroid 2006 RH120 has been highlighted, due to its proximity to the L_2 manifolds. From these graphs, and ignoring any phasing issues, it can already be pinpointed as a good retrieval mission candidate, as its perihelion and aphelion radius are close to or within the range of all the three types of manifolds, and its inclination also lies close to the halo orbit manifolds. The manifold orbital elements appear to be good filter parameters to prune the list of NEOs to be captured.

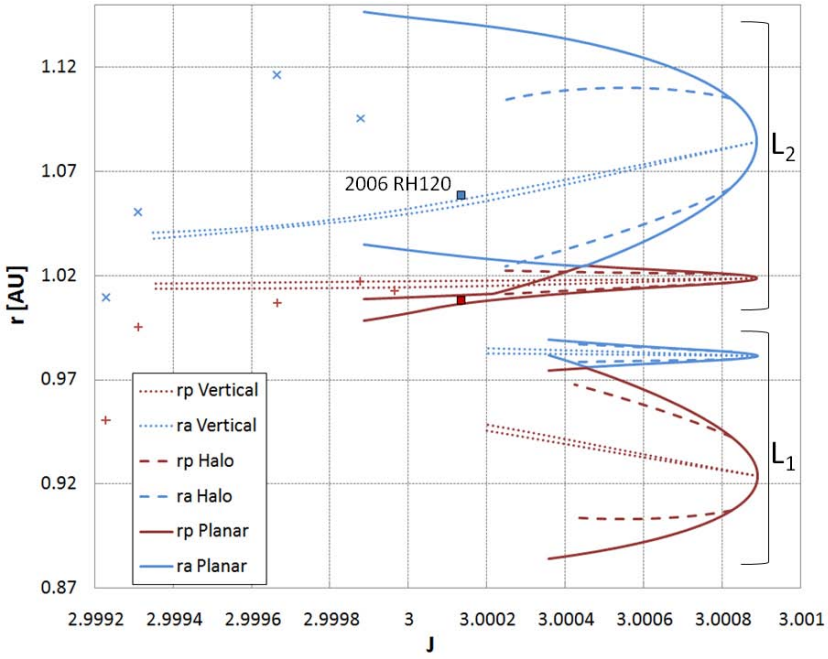

(a)

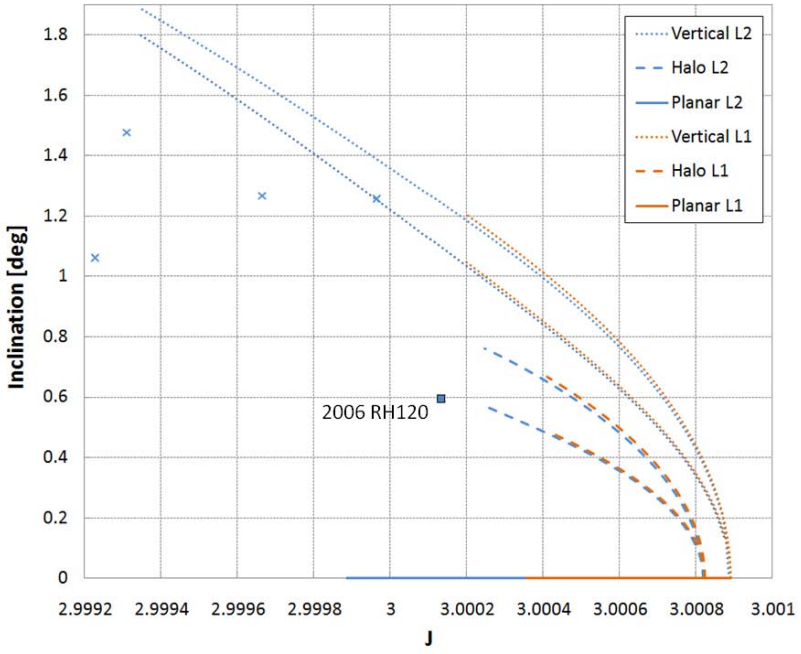

(b)

Figure 3.8: Minimum and maximum perihelion and aphelion radii (a) and inclination (b) of the manifolds leading to planar Lyapunov, vertical Lyapunov and halo orbits around L_1 and L_2.

3.3.2 Asteroid catalogue pruning

For the calculation of capture opportunities, the NEO sample used for the analysis is JPL's Small–Body Database Browser,* downloaded as of July 27^{th} 2012. This database represents the catalogued NEOs up to that date, and as such it is a biased population, most importantly in size, as already noted. A large number of asteroids of the most ideal size for capture have not yet been detected, as current detection methods favour larger asteroids. Secondly, there is an additional detection bias related to the type of orbits, with preference for Amors and Apollos in detriment to Atens, as objects in Aten orbits spend more time in the exclusion zone due to the Sun.

Even with this reduced list, it is a computationally expensive problem and preliminary pruning becomes necessary. Previous work by Sanchez et al. (2012b) showed that the number of known asteroids that could be captured from a hyperbolic approach with a total Δv less than 400 m/s is of the order of 10. Although the hyperbolic capture approach in their work and the manifold capture are inherently different, the number of bodies that could be captured in manifold orbits at low cost is expected to be of the same order. Without loss of generality, it is possible to immediately discard NEOs with semi-major axis (and thus energy) far from the Earth's, as well as NEOs in highly inclined orbits. However, a more systematic filter needed to be devised.

As a first approximation of the expected total cost in terms of Δv, a bi-impulsive cost prediction with both burns assumed at aphelion and perihelion was implemented. Either of the two burns is also responsible for correcting the inclination. The Δv required to modify the semi-major axis can be expressed as:

$$\Delta v_a = \sqrt{\mu_S \left(\frac{2}{r} - \frac{1}{a_f}\right)} - \sqrt{\mu_S \left(\frac{2}{r} - \frac{1}{a_0}\right)} \tag{3.4}$$

where μ_S is the Sun's gravitational constant, a_0 and a_f are the initial and final semi-major axis before and after the burn, and r is the distance to the Sun at which the burn is made (perihelion or aphelion distance). On the other hand the Δv required to modify the inclination at either apsis can be approximated by:

$$\Delta v_i = 2\sqrt{\frac{\mu_S}{a_0} r^*} sin\left(\Delta i/2\right) \tag{3.5}$$

* http://ssd.jpl.nasa.gov/sbdb.cgi (last accessed 27/07/12)

where Δi is the required inclination change, and r^* corresponds to the ratio of perihelion and aphelion distance if the burn is performed at aphelion, or its inverse if performed at perihelion.

Note that these formulas are only first order approximations intended for the pruning of the database, and they will not be used to calculate the final transfers. Particularly, the plane change is only valid for small corrections in inclination and large deviations from the values provided by the filter are expected to be observed for higher inclinations. Nevertheless, emphasis is on low cost transfers, which imply a small plane change, so this approximation is acceptable as a first estimate. Also, these formulas only take into consideration the shape and inclination of the orbits, ignoring the rest of the orbital elements: right ascension of the ascending node and argument of pericentre. It is then implicitly assumed that the line of nodes coincides with the line of apsis and the inclination change can be performed at pericentre or apocentre. Finally, no phasing penalty is implemented.

The total estimated cost for pruning is then calculated as:

$$\Delta v_t = \sqrt{\Delta v_{a1}^2 + \Delta v_{i1}^2} + \sqrt{\Delta v_{a2}^2 + \Delta v_{i2}^2} \tag{3.6}$$

with one burn performed at each of the apsis, and one of the two inclination change Δv assumed zero.

The estimated transfer Δv thus corresponds to the minimum of four cases: aphelion burn modifying perihelion and inclination, followed by a perihelion burn modifying aphelion; perihelion burn modifying aphelion and inclination, followed by an aphelion burn modifying perihelion; and the equivalent sequences in which the inclination change is done in the second burn.

For simplicity, the target manifold final perihelion, aphelion and inclination values are selected as ranges or bands obtained from Fig. 3.8. For example, planar Lyapunov manifolds at L_2 correspond to a range of $\{r_p, r_a, i\} \in \{1.00–1.02, 1.02–1.15, 0\}$, or $\{1.01–1.02, 1.025–1.11, 0.59–0.78\}$ for halo manifolds at L_2. Note that the inclination range for halo orbits was given as the one that corresponds to the highest energy. This is due to the fact that most candidate asteroids have higher energies than the manifolds, and the lowest cost is assumed to take place where the energy difference is minimum. In the case of vertical Lyapunov orbits, due to the narrow ranges and strong dependency with J, polynomial fits for $\{r_p, r_a, i\}$ as a function of $\tilde{J} = 1000(J - 3)$ were used.

The polynomial functions for L_2 vertical Lyapunov are:

$$\begin{aligned} r_p = &\quad 0.00249738\tilde{J} \ + 1.01613263 \\ r_a = &\quad 0.01219016\tilde{J}^2 + 0.02763935\tilde{J} + 1.05140802 \\ i_{max} = &- 0.62451343\tilde{J}^4 - 0.13878871\tilde{J}^3 + 0.10102862\tilde{J}^2 \\ &- 0.84803389\tilde{J} \ + 1.35088139 \\ i_{min} = &- 0.49047751\tilde{J}^4 - 0.03290418\tilde{J}^3 + 0.10993911\tilde{J}^2 \\ &- 0.92599955\tilde{J} \ + 1.21594836 \end{aligned} \tag{3.7}$$

While for L_1 vertical Lyapunov the following polynomial fits are used:

$$\begin{aligned} r_p = &- 0.03390248\tilde{J} \ + 0.95380418 \\ r_a = &- 0.00343782\tilde{J} \ + 0.98459020 \\ i_{max} = &- 7.55405731\tilde{J}^4 + 12.73627312\tilde{J}^3 - 8.01136805\tilde{J}^2 \\ &+ 1.15327811\tilde{J} \ + 1.20636876 \\ i_{min} = &- 5.91931368\tilde{J}^4 + 10.04069997\tilde{J}^3 - 6.20674370\tilde{J}^2 \\ &+ 0.61312357\tilde{J} \ + 1.10434916 \end{aligned} \tag{3.8}$$

With this filter, it is then possible to calculate the regions of a three-dimensional orbital element space (in semi-major axis, eccentricity and inclination) that can be potentially captured under a certain Δv threshold. These regions are plotted in Fig. 3.9 for transfers to LPOs around L_2 with a Δv of 500 m/s, and any asteroid with orbital elements inside them could in principle be captured at that cost. The figure shows a three-dimensional view of the surfaces that delimit the regions for planar Lyapunov, vertical Lyapunov and halo, as well as two-dimensional projections in the $a - i$ and $e - i$ planes. There is a significant overlap between the regions of different LPO target orbits. Therefore, it is expected that several asteroids would allow low-cost captures to more than one family of LPO. A similar plot can be generated for the case of L_1. Figure 3.10 presents the regions for L_1 and L_2 compared to the definitions of the 4 families of NEOs. Objects from all four families seem to be adequate candidates for the new category of Easily Retrievable Objects, particularly those close to the Apollo–Amor and Aten–Atira divides. The boundaries for the Small Earth–Approachers subset is also depicted with a dashed line, and shows that this definition is not particularly useful for the purpose of pruning candidates for asteroid retrieval.

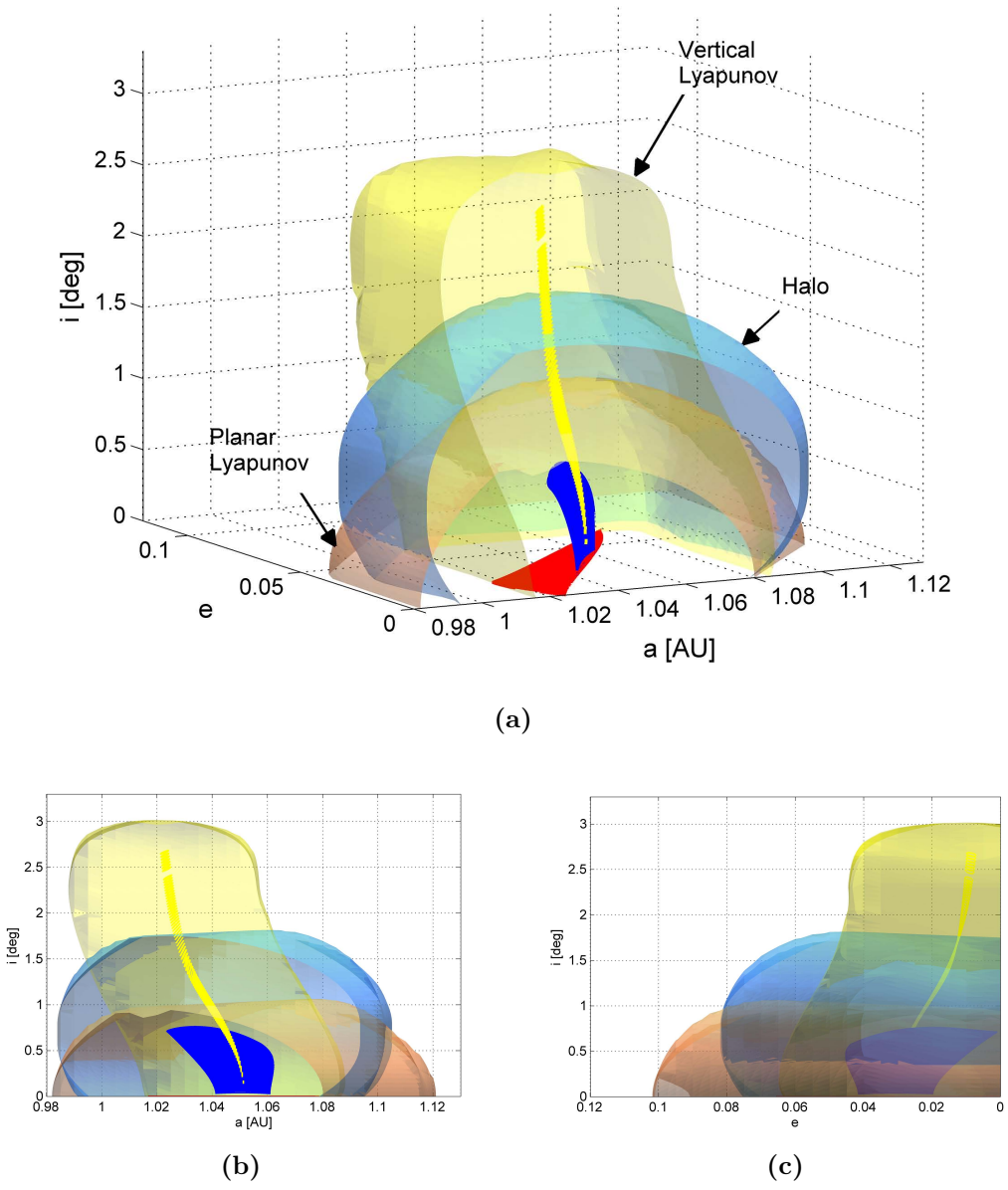

Figure 3.9: Regions in the orbital element space with total estimated cost for capture into an LPO around L_2 below 500 m/s. The manifolds corresponding to the LPOs are plotted in solid colours.

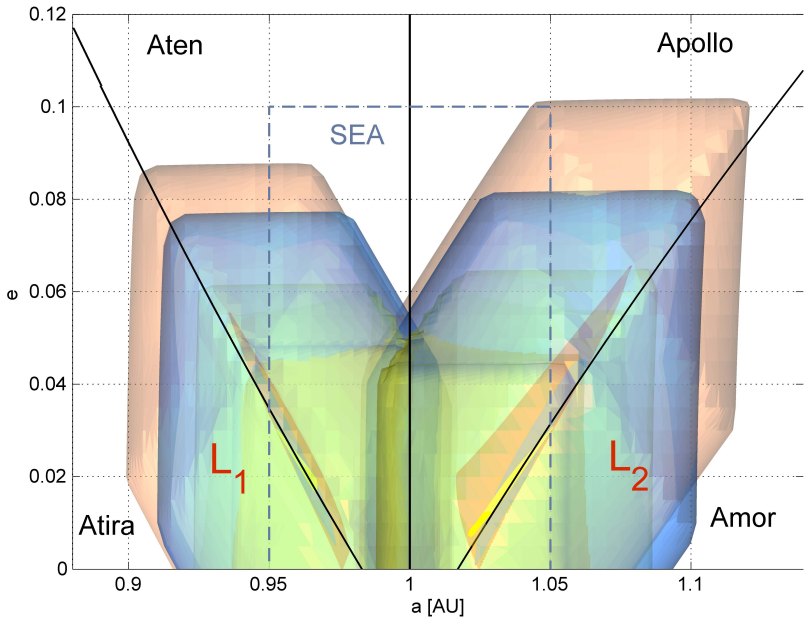

Figure 3.10: Semi-major axis and eccentricity map of the capturable regions for L_1 and L_2. The boundaries of the main 4 families of NEOs and the Small Earth–Approachers subset are indicated. The manifold orbital elements are enclosed in the capturable regions and closely follow the Apollo–Amor and Aten–Atira divides.

The filter approximation provides in general a lower bound Δv estimate, as it ignores any phasing issues, and assumes the burns can be performed at apocentre or pericentre. Moreover, there is no guarantee, and in fact it is quite unlikely, that a combination of the extremes of the ranges of $\{r_p,\ r_a,\ i\}$ used in the filter correspond to proper manifold trajectories. Finally, the plane change does not include a modification in right ascension of the ascending node Ω. Although the final value of Ω can be tuned by modifying the phasing with the Earth, this is not completely free as the final insertion will take place around a natural close approach of the asteroid. The combination of this constrained phasing and the plane change will incur additional costs. North and south halo obits provide two opportunities with opposite Ω for each transfer, which should result in two different costs, while the filter provides a single value.

For a few cases, with high initial inclination and associated plane change cost, the filter can over-estimate the Δv. As the inclination increases, solutions splitting the large plane change into the two burns can potentially result in a lower cost. In cases where the filter favours solutions with larger burns at pericentre, it can also result in higher costs estimates for the plane change compared with the optimal solution.

3.4 Capture transfer results

As the main objective of this chapter is to catalogue objects that can be captured under a threshold of 500 m/s, the focus will be on the asteroids with estimated Δv below 1 km/s as provided by the filter, to be conservative. For each of these NEOs, feasible capture transfers with arrival dates in the interval 2016–2100 were obtained. The NEO orbital elements are only considered valid until their next close encounter with Earth. The Lambert transfers between the asteroid initial orbit and the manifolds were optimised using EPIC, a global optimisation method that uses a stochastic search blended with an automatic solution space decomposition technique (Vasile and Locatelli, 2009). Single objective optimisations with total transfer Δv as the cost function were carried out. Trajectories obtained with EPIC were locally optimised with MATLAB's built-in constrained optimisation function *fmincon*. Lambert arcs with up to 3 complete revolutions before insertion into the manifold were considered. For cases with at least one complete revolution, the two possible solutions of the Lambert problem were optimised. This implies that seven full problem optimisations needed to be run for each NEO. In order to limit the total duration of the transfers, the insertion into the manifold was arbitrarily constrained to take place not earlier than 1000 days before the $\pi/8$ section during the global search. This constraint was released in the local optimisation.

Figure 3.11 plots the results of the optimisation for L_2 and L_1 together with the Δv estimates. It can be observed that the filter provides, in general, a good approximation of the total cost. As expected, the larger the inclination, the larger the deviation of the results from the filter's predicted cost. It is nevertheless a useful tool to select candidates and prioritise lists of asteroids for optimisation, and to quickly predict if any newly discovered asteroid is expected to have low capture costs. Dotted lines have been added to the plot as indicators of the ideal cost of performing just the inclination change at a circular orbit at 1 AU. Predicted and optimised results are expected to fall above or close to these lines. EROs with capture costs smaller than 500 m/s are identified in the plots.

Table 3.5 shows the EROs with capture costs lower than the selected Δv threshold. Twelve asteroids out of the whole NEO catalogue can be retrieved at this cost, ten of them around L_2 and two Atens around L_1. The table provides the orbital elements, minimum orbit intersection distance (MOID) according to the

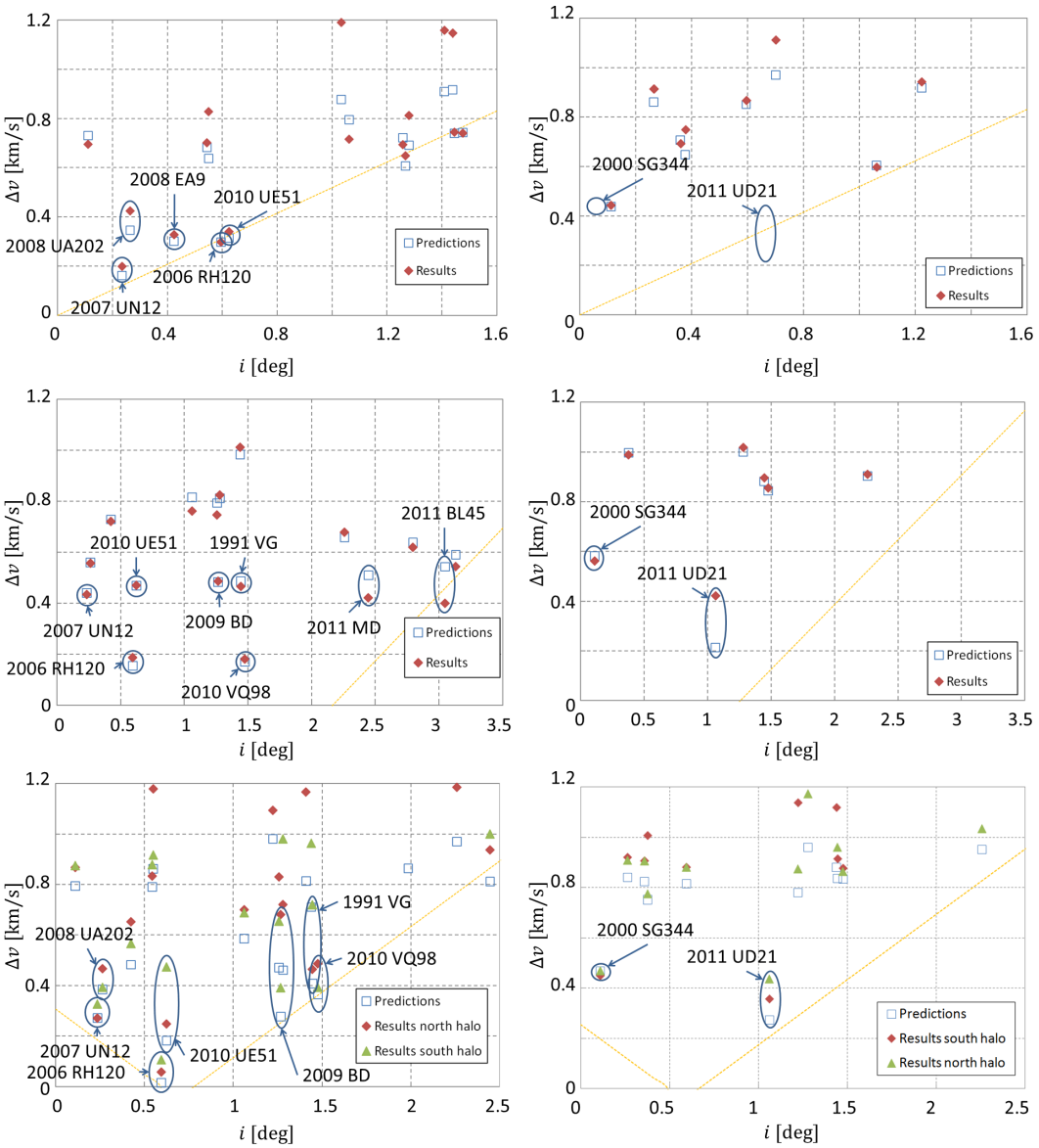

Figure 3.11: Filter cost estimates and results of the optimisation for planar Lyapunov (*top*), vertical Lyapunov (*middle*) and halo orbits (*bottom*) around L_2 (*left*) and L_1 (*right*). *Dotted lines* indicate the cost of changing just the inclination.

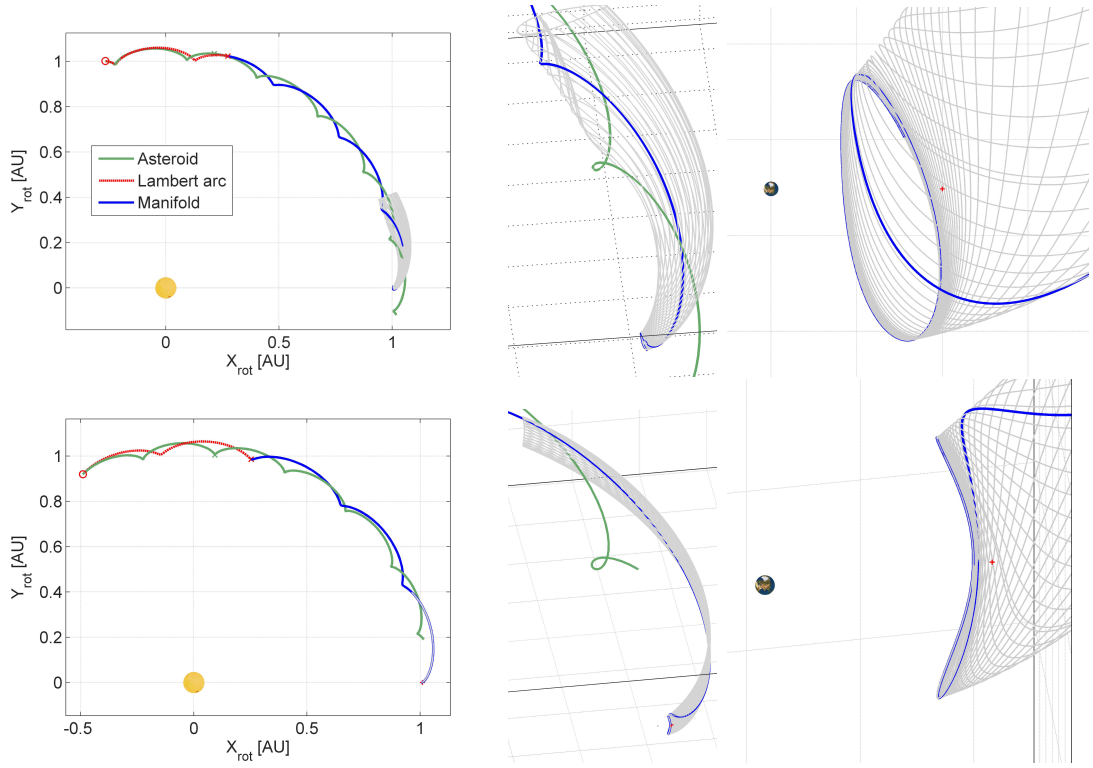

Figure 3.12: Capture trajectories for asteroid 2006 RH120 to a south halo (*top*) and vertical Lyapunov (*bottom*). The unperturbed original orbit of the asteroid is plotted in *dark green*. Sun and Earth are not to scale; they are plotted 10 times their size.

JPL Small–Body Database, and an estimate of the size of the object. This estimate is calculated with Eq. (3.1), where the albedo p_v is assumed to range from 0.05 (dark) to 0.50 (very bright icy object).

Not surprisingly, planar Lyapunov orbits are optimal for lower inclination NEOs, while NEOs with higher inclination favour transfers to vertical Lyapunov orbits. Figure 3.12 shows two example trajectories in a co-rotating frame, where the Sun–Earth line is fixed for a transfer of asteroid 2006 RH120 to LPOs around L_2. Both trajectories correspond to the same close approach of the asteroid to Earth in 2028. Close-ups of the final parts of the trajectory are plotted in a three-dimensional view in order to appreciate the shape of the final orbit and manifolds.

Table 3.6 presents the best trajectory for each type of target orbit for L_2 and L_1. The cheapest transfer, below 60 m/s, corresponds to a trajectory inserting asteroid 2006 RH120 into a halo orbit. Solutions to planar and vertical Lyapunov

Table 3.5: NEO characteristics for transfer trajectories with Δv below 500 m/s. The type of transfer is indicated by a 1 or 2 indicating L_1 or L_2 plus the letter P for planar Lyapunov, V for vertical Lyapunov, and Hn or Hs for north and south halo.

Rank #	Designation	a [AU]	e	i [°]	MOID [AU]	Ø [m]	Type	Δv [km/s]
1	2006 RH120	1.033	0.024	0.595	0.0171	2.3–7.4	2Hs	0.058
							2Hn	0.107
							2V	0.187
							2P	0.298
2	2010 VQ98	1.023	0.027	1.476	0.0048	4.3–13.6	2V	0.181
							2Hn	0.393
							2Hs	0.487
3	2007 UN12	1.054	0.060	0.235	0.0011	3.4–10.6	2P	0.199
							2Hs	0.271
							2Hn	0.327
							2V	0.434
4	2010 UE51	1.055	0.060	0.624	0.0084	4.1-12.9	2Hs	0.249
							2P	0.340
							2V	0.470
							2Hn	0.474
5	2008 EA9	1.059	0.080	0.424	0.0014	5.6–16.9	2P	0.328
6	2011 UD21	0.980	0.030	1.062	0.0043	3.8–12.0	1Hs	0.356
							1V	0.421
							1Hn	0.436
7	2009 BD	1.062	0.052	1.267	0.0053	4.2–13.4	2Hn	0.392
							2V	0.487
8	2008 UA202	1.033	0.069	0.264	2.510^{-4}	2.4- 7.7	2Hn	0.393
							2P	0.425
							2Hs	0.467
9	2011 BL45	1.033	0.069	3.049	0.0040	6.9–22.0	2V	0.400
10	2011 MD	1.056	0.037	2.446	0.0018	4.6–14.4	2V	0.422
11	2000 SG344	0.978	0.067	0.111	8.310^{-4}	20.7–65.5	1P	0.443
							1Hs	0.449
							1Hn	0.468
12	1991 VG	1.027	0.049	1.445	0.0037	3.9–12.5	2Hs	0.465
							2V	0.466

Table 3.6: Capture trajectories and mass estimates for the lowest cost asteroid for each type of transfer.

Designation		Date [yy/mm/dd]			J	ToF	Δv		I_{sp}=300 s	
		Asteroid	Manifold	L_i	manifold	[yr]	[m/s]		Mass	Ø
		departure	insertion	arrival			Dep	Ins	[ton]	[m]
2006 RH120	2Hs	21/02/01		28/08/05	3.000421	7.51	58	0	153.6	4.83
2006 RH120	2Hn	23/05/11	24/02/20	28/08/31	3.000548	5.31	52	55	82.3	3.92
2010 VQ98	2V	35/02/14	35/09/01	39/11/15	3.000016	4.75	177	4	46.8	3.25
2007 UN12	2P	13/10/22		21/02/19	3.000069	7.33	199	0	42.3	3.14
2011 UD21	1Hs	37/11/20	38/07/03	42/07/19	3.000411	4.66	149	207	21.9	2.52
2011 UD21	1V	36/07/20	38/11/16	41/06/21	3.000667	4.92	226	196	17.9	2.36
2011 UD21	1Hn	39/10/24	40/06/15	43/08/30	3.000504	3.85	210	226	17.2	2.33
2000 SG344	1P	24/02/11	25/03/11	27/06/18	3.000357	3.35	195	248	16.8	2.04

orbits were also found for 2006 RH120 at higher costs (see Table 3.5). This is in agreement with the interpretation of Fig. 3.8. The pruning method was also predicting that this transfer would be the cheapest, with a minimum estimated Δv of 15 m/s. It is important to emphasise that the total Δv comprises both burns at departure from the asteroid and insertion into the manifold. The NEO orbit may intersect the manifold directly, and in that case the transfer to the target orbit can be done with a single burn, as for this particular asteroid.

The total duration or time of flight of the transfers ranges from 3 to 7.5 years. For the longer transfers it is possible to find faster solutions with fewer revolutions in the Lambert arc at a small Δv penalty.

3.5 Discussion

3.5.1 Retrievable mass with current space technology

The results presented in the previous section could be used to calculate a limit on the mass that can be retrieved with current space technology. In order to obtain a first estimate of the mass and size of capturable asteroids, a basic system mass budget exercise can be performed. The Keck study report for asteroid retrieval (Brophy et al., 2012) proposes a low-thrust mission involving a spacecraft of 5500 kg dry mass and 8100 kg of propellant already at the NEO encounter. With a spacecraft of that size but assuming high thrust with a specific impulse of 300 s, the total asteroid mass that could be transferred with the trajectories described

in this chapter is close to 400 tons. However, the launch mass required would be close to 16 tons. Such a high launch mass would imply either a long escape strategy from LEO, or a heavy launcher not yet developed, or multiple launches and assembly in space. A more modest mission of the size of Cassini can be considered (2442 kg dry mass and 3132 kg propellant mass*) at the NEO. A full system budget would require a larger fuel mass at launch to deliver the spacecraft to the target, and thus an analysis of the outbound leg. However, preliminary analysis for asteroid 2006 RH120, performed in the frame of LightTouch[2] deflection demonstrator mission (Vasile et al., 2013), show trajectories with low departure velocities from Earth (well below 1 km/s) and transfer Δv budgets lower than 450 m/s, though the arrival times at the asteroid are not appropriate for the type of capture transfers here proposed. These figures correspond to a spacecraft of mass 6300 kg departing Earth with an escape velocity of approximately 500 m/s, within the capabilities of current launch systems such as Ariane 5 ECA. Multiple burn escape strategies from a HEO orbit are also feasible.

Assuming the Cassini-like mass budgets, results are appended for each trajectory on Table 3.6 for a standard high-thrust propulsion system. The total retrievable mass for a high thrust engine of specific impulse (I_{sp}) 300 s ranges from 17 to 154 tons, which represents 3–28 times the wet mass of the spacecraft at arrival at the NEO. The trajectories presented assume impulsive burns, so in principle they are not suitable for low-thrust transfers. However, due to their low Δv and long time of flight, transformation of these trajectories to low-thrust is in principle feasible, and can be considered in future work. If a similar cost trajectory could be flown with a low-thrust engine of higher specific impulse (e.g., 3000 s) the asteroid retrieved mass would be over ten times that of the high-thrust case, up to 1500 tons or over 10 m diameter in the case of a hypothetical transfer from the orbit of 2006 RH120 to a halo orbit.

For an average NEO density of 2.6 g/cm^3 (Chesley et al., 2002), the equivalent diameter of the asteroid that can be captured is also included in the table. This shows that reasonably sized boulders of 2–5 m diameter, or entire small asteroids of that size, could be captured with this method. The capture of entire bodies of larger size is still challenging, but the derived sizes of a few of the candidates fall within this range. The ERO 2000 SG344, with a derived size in the range of

* http://saturn.jpl.nasa.gov/multimedia/products/pdfs/cassini_msn_overview.pdf (last accessed 05/09/12).

20–65 m, is the only asteroid that completely fails to meet the capturable range shown in Table 3.6, even with the hypothetical higher specific impulse transfer.

3.5.2 Safety considerations

Regarding the safety of such a project, there could be a justified concern regarding the possibility of an uncontrolled re-entry of a temporary captured asteroid into Earth's atmosphere. A migration through the unstable invariant manifold leading towards the inner region around Earth could result in homoclinic or heteroclinic transits between L_1 and L_2 (Canalias and Masdemont, 2006; Koon et al., 2000), some of which intersect the planet. Active control would be required to ensure that all deviations from the target periodic or quasi-periodic orbits are in the direction of the unstable manifolds leading to the outside (for L_2) or inside (L_1) heliocentric regions. It is however a less serious concern due to the small size of the EROs considered. Objects smaller than 5 m have a low impact energy (specially the lower velocity impacts that would result from a transit orbit when compared to a hyperbolic trajectory), and a relatively high impact frequency with Earth (Chesley et al., 2002). Statistically, one object of a similar size impacts the Earth every 1–3 years with limited consequences. If larger objects were considered, additional mitigation measures would be required. The Keck study report (Brophy et al., 2012) suggests a lunar orbit as the final destination for their captured object, to circumvent this problem.

3.5.3 Overview of the catalogue of EROs

All identified EROs are of small size (perhaps with the exception of 2000 SG344), which is ideal for a technology demonstrator retrieval mission. In fact, seven of them fit the previously mentioned SEA definition by Brasser and Wiegert (2008). They showed, focusing on object 1991 VG, that the orbit evolution of these type of objects is dominated by close encounters with Earth, with a chaotic variation in the semi-major axis over long periods of time. A direct consequence of this is that reliable capture transfers can only be designed with accuracy over one synodic period, before the next encounter with Earth changes the orbital elements significantly. The fact that EROs are close to the hyperbolic manifolds, makes them a particularly interesting subset of NEOs with regards to dynamics, since they represent objects with potential for high sensitivity to

gravitational perturbation during these future Earth encounters. One could argue that finely tuning these encounters could also be used to shepherd these objects into trajectories that have a lower cost to be inserted into a manifold (Sanchez and McInnes, 2011b).

The NEOs in Table 3.5 are well-known, and there has been speculation about the origin of a few of them, including the possibility that they were man-made objects (spent upper stages) or lunar ejecta after an impact (Brasser and Wiegert, 2008; Chodas and Chesley, 2001; Kwiatkowski et al., 2009; Tancredi, 1997). In particular object 2006 RH120 has been thoroughly studied (Granvik et al., 2011; Kwiatkowski et al., 2009), as it was a temporarily captured object that was considered the "second moon of the Earth" until it finally escaped the Earth in July 2007. Granvik shows that the orbital elements of 2006 RH120 changed from being an asteroid of the Atens family pre-capture, to an Apollo post-capture, having followed what is referred to in this chapter as a transit orbit inside Earth's Hill sphere. Thus, it must have orbited inside the separatrix surface of the hyperbolic stable manifold. One more object of the list, 2007 UN12, is also pointed out by Granvik as a possible candidate to become a Temporarily Captured Orbiter, or TCO.

Regarding their accessibility, a recent series of publications (Adamo et al., 2010; Barbee et al., 2010; Hopkins et al., 2010) considered up to seven of the above objects as possible destinations for the first crewed mission to a NEO (it is worth noting that the other five were not discovered at the time). They proposed human missions during the same close approaches as the capture opportunities calculated. However, the arrival dates at the asteroids are later than the required departure date for the capture, so their outbound legs could not apply to the proposed capture trajectories. In a similar fashion, the outbound legs calculated for the aforementioned LightTouch^2 deflection demonstrator (Vasile et al., 2013) for 2006 RH120 all arrive too late. The second asteroid in that study, 2008 JL24, has a minimum estimated cost after pruning of 637 m/s. After optimisation the real cost went up to over 800 m/s and it did not make the list of EROs. The calculated outbound transfers were, regardless of the costs, not applicable due to late arrival as well. An additional study by Landau and Strange (2011) presents crewed mission trajectories to over 50 asteroids. It shows that a mission to 6 of the considered asteroids is possible with a low-thrust Δv budget between 1.7 and 4.3 km/s. The costs presented are for a return mission of a spacecraft with a dry mass of 36 tons (including habitat) in less than 270 days. A longer duration

robotic mission with a final mass at the NEO of less than 10 tons and a manifold capture as proposed here would result in much lower fuel costs as the thrust-to-mass ratio increases. Moreover, eleven of these 12 capturable objects appear in the top 25 of NASA's NHATS list as of September 2012, seven of them in the top 10. This indicates that the objects found by the pruning and optimisation are indeed easily accessible, even if the outbound part of the trajectory was not considered in the calculations.

The ERO list presented has been capped at 500 m/s but could be extended further if required, in order to have a ranking analogous to the NHATS list for capturable asteroids.

3.5.4 Follow-up work on EROs and other capture analyses

The Easily Retrievable Objects family has generated a series of papers following up on the work here presented. Sanchez Cuartielles et al. (2013) and Alessi et al. (2013) looked into the possibility of using a series of very high-altitude resonant flybys to reduce the energy required for capture, in a two-dimensional approximation first, and subsequently including the effects on inclination as well. This can, though, extend the captures to several decades, depending on the synodic period. Ceriotti and Cuartielles (2013) analysed the control requirements for an asteroid capture mission during the transfer to a libration point orbit and once inserted into it. They concluded that for some cases the control is infeasible, while in others the trajectories are very robust against errors in Δv. Related to the type of capture here proposed, new algorithms have been developed to optimize manifold dynamics transfers with impulsive manoeuvres (Tsirogiannis and Markellos, 2013). The method is applied for test cases in the Earth–Moon system, but applications to optimise the capture of EROs are also proposed. In a completely different approach, Urrutxua et al. (2014) analyses the possibility of extending the natural temporary capture of the most attractive candidate ERO, 2006 RH120, by means of a single impulsive burn, with very promising results: an extension of the captured phase of over 5 years can be achieved with only 31.2 m/s. Verrier and McInnes (2015) propose the long-lived capture of similar asteroids into KAM tori, essentially obtaining an almost permanent chaos-assisted capture at low-costs.

Regarding accessibility, Qiao (2014) presents a very preliminary study of impulsive outbound legs from Earth to the candidate EROs in this chapter. While this chapter assumes impulsive manoeuvres for the transfer, other authors have since focused on low-thrust propulsion strategies, best suited to impart the required impulse to the large mass associated to an asteroid capture project. Little and Choueiri (2013) developed an analytical semi-empirical approach to size the propulsion system, and estimate mission time and mass constraints. Cardiff and Englander (2013) studied full missions from launch till capture for 10 of the EROs presented in this chapter, plus two additional asteroids of interest. They managed to generate full mission profiles for 6 of the EROs. In a similar fashion, Mingotti et al. (2014) obtained low-thrust trajectories to LPO and Moon distant prograde and retrograde orbits for all 12 ERO candidates, although three of them were considered non-viable. These two independent results indicate that the impulsive approach is a good initial guess for low-thrust missions, but the mass of the target needs to be taken into consideration as some asteroids were found to be too large to capture with a realistic level of thrust under their assumptions and constraints.

Focusing on the challenge of detection, Shah et al. (2013) and Ruprecht et al. (2014) outline the requirements for detection of small asteroids, such as the potential TCOs, or the most likely candidate EROs. Concerning profitability, Elvis (2014) and Elvis and Esty (2014) provide estimates on the number of asteroids rich enough to justify mining missions, and the number of characterisation probes that would be required to find such asteroids. Finally, a further example of the interest in asteroid deflection and exploitation, with special mention to EROs, can be found in a recently published informative book (Lunan, 2014).

3.5.5 Method limitations

One of the first objections that can be raised to the approach presented involves some of the simplifications in the model. The main simplifying assumptions are placing the Earth in a circular orbit, assuming Keplerian propagation for the NEOs orbital elements until the next close encounter with Earth without considering any uncertainties in their ephemerides, and not including other types of perturbations, in particular the Moon as a third body perturbation. While the influence of the first two assumptions on the general behaviour of the trajectories should be relatively small, and the transfers obtained can be used as first guesses

for a local optimisation with a more complex model with full Earth and NEO ephemerides, not including the Moon as a perturbing body can have a much greater influence. Granvik et al. (2011) show that the Moon plays an important role in the capture of TCO, and the trajectories of the manifolds would be also affected by it. The lunar third body perturbation can also strongly influence the stability of LPOs, in particular large planar Lyapunov orbits, and it could render some of them unsuitable for target orbits. Trajectories calculated with full dynamics may no longer be optimal, since the final orbits are no longer strictly periodic in an Elliptical Restricted 3-Body Problem, and they can also be highly unstable. A control strategy would also be required to maintain a captured object in an orbit around a Lagrangian point. However, the asymptotic behaviour of the manifolds and the type of NEOs that can be captured are not expected to change. The family of EROs presented are also of significant scientific interest as they are the most likely candidates to suffer natural transitions through the L_1/L_2 regions and migrations between NEO families. Other perturbations, such as the changes in the orbits of small bodies induced by the Yarkovsky effect are of little relevance within the timescales considered.

Even if unstable, the target libration point orbits presented here can serve as either observation points for the temporarily captured EROs, or as gateways to other Sun–Earth–Moon system orbits of interest, through the transit orbits inside Earth's Hill sphere and heteroclinic connections between libration points. Other capture possibilities, e.g., by means of a single or double lunar swing-bys, or multiple resonant Earth swing-bys, have not been studied and are outside of the scope of this thesis, but they could potentially increase the number of retrievable objects available.

A final limitation was already advanced in Section 3.1.5, that is, the additional challenges posed by the detection and the uncertainty in orbit and size of these small objects. This limitation is not restricted to EROs or to trajectories to the selected target orbits, but to any minor body mission in general.

3.6 Summary

The possibility of capturing a small NEO or a segment from a larger object would be of great scientific and technological interest in the coming decades. It is a logical stepping stone towards more ambitious scenarios of asteroid exploration

and exploitation, and possibly the easiest feasible attempt for humans to modify the solar system environment outside of Earth, or attempt a large-scale macro-engineering project.

This chapter has shown that the retrieval of a full asteroid is well within today's technological capabilities, and that there exists a series of objects that can be easily captured into libration point orbits. These objects are termed Easily Retrievable Objects (EROs). Their orbits lie close to a stable hyperbolic invariant manifold such that a small Δv transfer may link the nominal trajectory of the asteroid with an asymptotic trajectory leading to a periodic orbit near the Sun–Earth L_1/L_2 points. Under certain conditions, these transfers can be achieved with costs below 500 m/s. Indeed, the analysis presents a list of 12 EROs, with a total of 25 trajectories to periodic orbits near L_2 and six near L_1 below a cost of 500 m/s. The lowest cost is of 58 m/s to transfer asteroid 2006 RH120 to a southern halo orbit with a single burn on 1^{st} February 2021. All the capture transfer opportunities to Earth's vicinity have been identified for the currently catalogued NEOs during the next 30 years, and enable capture of bodies within 3–7 metres diameter with low propellant costs.

Taking advantage of these transfer opportunities and the unique dynamical characteristics of the identified EROs, the utilisation of asteroid resources may become a viable means of providing substantial mass in Earth orbit for future space ventures. Despite the largely incomplete survey of very small objects, the surveyed population of asteroids provides a good starting platform to begin the search for easily capturable objects. With this goal, a robust methodology for systematic pruning of a NEO database and optimisation of capture trajectories through the hyperbolic invariant stable manifold into different types of LPO around L_1 and L_2 has been implemented and tested.

The proposed method can be easily automated to prune the NEO database on a regular basis, as the number of EROs in orbits of interest is expected to grow with the new efforts in asteroid detection. Any new occurrence of a low-cost candidate asteroid can be optimised to obtain the next available phasing and transfer opportunities and the optimal target LPO.

Moreover, Sun–Earth LPOs can also be considered as natural gateways to the Earth system. Thus, the problem to transfer an asteroid to an Earth or Moon centred orbit can be decoupled into the initial phase of inserting the asteroid into a stable invariant manifold and then providing the very small manoeuvres

required to continue the transit into the Earth system. While a method to find optimal LPO capture trajectories and possible targets has been defined, the transit trajectories can potentially allow the asteroid to move to the Earth–Moon L_1/L_2 or other locations within cis-lunar space taking advantage of heteroclinic connections between collinear points.

Chapter 4

MACRO to MESO: Spin modification during capture

"I follow a terrible profession. In the old days it was reasonable. I put the lamp out in the morning, and in the evening I lighted it again. I had the rest of the day for relaxation and the rest of the night for sleep."

"And the orders have been changed since that time?"

"The orders have not been changed," said the lamplighter. "That is the tragedy! From year to year the planet has turned more rapidly and the orders have not been changed!"

"Then what?" asked the little prince.

"Then the planet now makes a complete turn every minute, and I no longer have a single second for repose. Once every minute I have to light my lamp and put it out!"

"That is very funny! A day lasts only one minute, here where you live!"

[. . .]

The little prince went on with his explanation: "Your planet is so small that three strides will take you all the way around it. To be always in the sunshine, you need only walk along rather slowly. When you want to rest, you will walk and the day will last as long as you like."

"That doesn't do me much good," said the lamplighter. "The one thing I love in life is to sleep."

"Then you're unlucky," said the little prince.

Saint-Exupéry (1943), *The Little Prince*

The above extract is the first documented description (to our knowledge) of the YORP effect on a small asteroid, more than a decade before Radzievskii, Paddack and O'Keefe theorised the spin-up and spin-down of irregular bodies due to radiative effects (Rubincam, 2000). The rotation of minor bodies of irregular shapes has been known to change due to absorption and re-emission of thermal radiation. In fact, by erecting a lamppost on one of the sides of the asteroid, it could well be that the asymmetries of the body were exacerbated and the YORP effect increased.

Operations on the surfaces of minor bodies (such as thrusting at a particular direction, or mining operations at appropriate solar longitudes) are obviously greatly affected by the shape and rotational state. One of the first phases of a capture strategy would normally involve matching the rotation of the asteroid before gripping it or bagging it, and then de-spinning it (Brophy et al., 2012). This sort of asteroid manipulation has never been attempted, and represents a challenge in cost and complexity due to their large mass, associated moments of inertia, and usually loose internal structure.

In the case of the extract, the period of the asteroid has decreased over time from one day to just one minute, to speeds well beyond any rotational breakup limit that one could imagine, irrespective of how dense the lamplighter's fictional asteroid is. In a real-world scenario, this would imply that the asteroid is monolithic, as any loose regolith or boulder would have already been ejected from the surface (except perhaps close to the rotational poles).

The rotational spin-up and spin-down due to YORP is however a slow process (Rubincam, 2000). Out of the three theorised main causes of rotational state disruption on asteroids, namely YORP, collisions with other minor bodies (Marzari et al., 2011; Paolicchi et al., 2002), and tidal interactions with major bodies, only the latter could deliver fast spin changes taking place in practical time-scales (i.e., decades) for Near–Earth Objects. Thus, they will be the focus of this chapter.

The rotational state and structure of minor bodies can undergo fast and major disruptions during close encounters with massive bodies (Hirabayashi and Scheeres, 2012; Walsh et al., 2011). These tidal interactions during a swing-by can in principle be used to modify or manipulate the spin and possibly the structure of asteroids, primarily during capture. The possibility of avoiding or inducing the de-spin, spin-up, or the controlled break-up of a captured asteroid is considered in the following sections.

4.1 Motivation and background

Recent interest in the capture of asteroids for scientific purposes or exploitation has generated a series of proposals for asteroid retrieval missions to various target orbits, as discussed in Chapter 3. A number of these proposals utilise swing-bys of the Moon or Earth to reduce the asteroid hyperbolic excess velocity and the associated insertion burns into the final capture orbit.

NASA's Asteroid Redirect Mission, loosely based in the Keck's study report (Brophy et al., 2012), foresees using a lunar swing-by to reduce the capture energy into a lunar Distant Retrograde Orbit as the final destination for the retrieved asteroid. Strange et al. (2014) study capturable asteroids with this strategy, imposing a lunar swing-by height constraint as low as 50 km above the lunar surface. Following a slightly different approach, Sanchez Cuartielles et al. (2013) suggest the use of multiple Earth passes (at large distances) to reduce the capture costs of small asteroids. Although they consider only weak interactions far from what is normally referred to as a swing-by, the possibility of using high altitude Earth gravity assists may reduce even further the required energy for capture. More relevantly, the extended lifetime trajectories of Temporarily Captured Orbiters (TCO) proposed by Urrutxua et al. (2014) do comprise much closer Earth passes in their weakly captured trajectories.

Given the large mass and inertia of asteroids, and the usually irregular shape of the smallest bodies in the NEO family, which represent the best candidates for capture or TCO lifetime extension with current technology, a close swing-by of a massive body, be it the Earth or the Moon, will induce large variations in the rotational state and possibly disruption of the structure of the asteroid. These interactions may pose serious challenges for the attitude control of asteroids during capture. Whether they are bagged, firmly attached to a spacecraft or not, large quantities of fuel may be required to counteract the torque build-up. On the other hand, if engineered, the disruption events can be seen as opportunities to modify the spin or structure of the asteroid at zero or low costs. This chapter proposes the utilisation of the tidal induced torques during a swing-by for rotational state manipulation, separation of contacts binaries or even (partial) disintegration of rubble piles.

To this end, the effect of the coupling between attitude and orbit dynamics for this particular case has been studied with a series of simple planar models. They

provide insight into the rotational state upheaval and the chance of break-up of the asteroid during the close approach. Three different dynamic models (and a combination of two of them) are considered:

1. A dumbbell of two equal point-masses connected with a massless rod to demonstrate coupled orbit-attitude dynamics during close passes
2. A simplified rigid body (of various shapes) in which the attitude and rotation evolution is decoupled from the orbit propagation
3. A binary pair with two small asteroids with mutual gravitational attraction and initially rotating around their common barycentre
4. An equal mass contact binary (model 2) with the possibility of separation as the rotation rate increases into a binary pair (model 3)

In order to observe the dependence with the swing-by conditions, the well studied asteroids 2004 MN4 (also known as Apophis) and 2006 RH120 are selected as test cases for these three simple models. The hyperbolic excess velocity for the swing-bys is thus selected as that of their close approaches to Earth on years 2029 and 2028 respectively. Their size, shape, rotational state and structure are however modified to match the assumptions of the different models. The evolution of the rotational state and structure of the asteroids is then studied for the hypothetical cases of a single lunar or Earth swing-by prior to capture. The final conditions are shown to be highly dependent on the initial rotational state, the distance to the swing-by body, and, most importantly, the relative attitude of the asteroid to the local vertical at pericentre.

4.2 Asteroid rotation and structure disruption during planetary swing-bys

Figure 4.1 displays the rotation period as a function of the size for asteroids for which there is an estimate of their spin. Most of these asteroids are uniform rotators about their axis of maximum moment of inertia (minimum energy state) with periods above a clearly defined limit. The associated rotational speed limit $\dot{\theta}_{shed}$, sometimes referred to as the rubble pile spin barrier, is the spin rate at

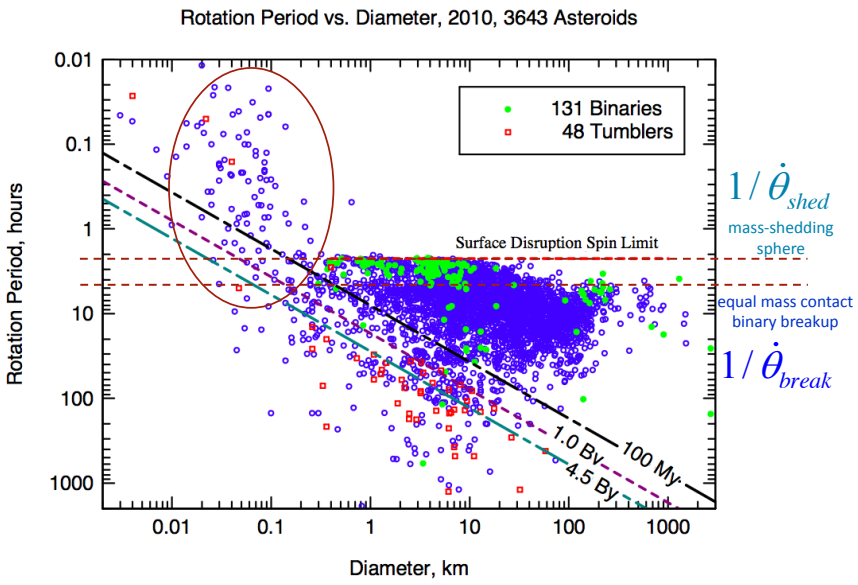

Figure 4.1: Rotation period of asteroids and spin limits. Fast rotators are circled. (Credit: A. W. Harris via Scheeres, 2012c)

which a rotating sphere (with no internal strength or other cohesive forces between particles) would start shedding mass at its equator. It is given by:

$$\dot{\theta}_{shed} = 2\sqrt{\pi G \rho / 3} \tag{4.1}$$

and it is only a function of the density of the orbiting body ρ, with G being the universal gravitational constant.

This mass shedding limit (in the case of the period is the inverse of the rotational speed) has been plotted in Fig. 4.1 for the case of an average asteroid density of 2.1 g/cm^3, which corresponds roughly to a period of 2.3 hours. For large rubble pile asteroids, it represents a maximum spin rate before they start shedding mass, while for smaller ones, higher spin rates have been observed (see circled fast rotators in Fig. 4.1), which can be explained either by a monolithic structure or by cohesive forces that bind them together and hinder the mass shedding (Sánchez and Scheeres, 2013; Scheeres, 2012c). An additional useful limit is the rotational speed at which an equal mass double-sphere contact binary would split if no internal forces or cohesion are considered. This rotational speed $\dot{\theta}_{break}$ is exactly half the mass shedding limit (a period of approximately 4.6 hours, twice the mass shedding limit period, shown again in Fig. 4.1). For contact binaries of different size the break-up speed without cohesion would lie between the former two.

It is important to highlight, thought, that these asteroid spin states are not static and they evolve with time. The evolution and changes of rotation rate can be explained through YORP effect, encounters with planets or larger bodies, and collisions (Marzari et al., 2011; Rubincam, 2000). In addition, comets have spin changes due to out-gassing. The fragmentation of comets due to rotational fission is thus more common, but in 2013, for the very first time, a main belt asteroid was observed to break up into more than 10 pieces (Jewitt et al., 2014), possibly caused by YORP spin-up. However, given the larger time-scales for the YORP effect (Jacobson and Scheeres, 2011), fast or abrupt alterations of the rotational state are mainly caused by a swing-by of a major body of the solar system. They may induce tumbling and place them in complex rotational states, and they can also cause a disruption of their structure through tidal torques (Schunová et al., 2014).

One of the earliest results related to tidal disruption is the Roche limit (Chandrasekhar, 1963), defined as the distance below which tidal forces will disintegrate an orbiting object held together only by self-gravity. Since the original definition for a fluid satellite in 1848 by Roche, there has been numerous definitions of such a tidal break-up limit for various types of internal strength, rigidity and material properties. Davidsson (2001a,b) provides a good overview of previous analysis and calculates varying Roche limits for rotating asteroids with internal strength, showing that for very small asteroids the Roche limit decreases considerably.

However, Roche limits normally refer to orbiting satellites. For a single swing-by event, it provides an initial estimate of the distances below which tidal disruption is significant, but the outcome of a swing-by depends on the particular geometry of the encounter and the structure and characteristics of the body. The effect on the rotation state of the asteroid can also be felt at much greater distances than the Roche limit. Scheeres et al. (2000) provide a semi-analytic set of formulas to estimate these rotation state changes. In a later paper, Scheeres et al. (2005) show that swing-bys radically affect the spin state of asteroids and can induce asteroids that previously had uniform rotation into a tumbling state. Richardson et al. (1998) demonstrate with a multi-particle model with self-gravity that for low-velocity encounters at distances less than 3 Earth radii the structure of a rubble pile can be completely distorted. This may lead to the formation of very elongated bodies, double-lobed asteroids or contact binaries (Walsh et al., 2011). Similar processes may explain crater chains in the Moon.

Doublet and multiple crater impacts have also been explained by binary asteroids generated by previous encounters with Earth, or multiple fragment break-up during the approach (Schunová et al., 2014; Toth et al., 2011). Farinella and Chauvineau (1993) studied such close encounters of binaries with Earth, first with a linear approximation, and then with a more general hyperbolic trajectory. They conclude that disruptions during these encounters may explain doublet craters, as proposed also by Melosh and Stansberry (1991), the formation of contact binaries as one stable outcome, as well as slow rotators or binaries with wide distances between the components of the pair. Energy dissipation may play an important role to achieve stable configurations after the disruption caused by a swing-by. Fang and Margot (2012) argue that these close encounters can increase or decrease the semi-major axis of a binary and break tidal locks, and they may also affect BYORP, shutting it down. In principle, binary encounters with Earth could also result in one of the components of the binary being captured with the other ejected back in a hyperbolic trajectory (Borum et al., 2012).

All these effects can be explained by the coupling of the attitude and orbit of non-symmetric bodies, and the tidal torques generated. These torques are also the cause of tidally locked satellites, and can be used for attitude control by gravity gradient. Sincarsin and Hughes (1983) studied this coupling for very large spacecraft, and their conclusions are partly applicable to asteroids, if deformations or restructuring are not considered. In the frame of an asteroid capture mission, this coupling will need to be taken into account, to avoid undesired rotation rate changes or break-up, or to be used instead to control the rotation rate and induce an intended break-up.

4.3 Dynamical models

This section presents the dynamical models employed in the chapter, and the test cases used to validate them. All models presented are planar, with the rotational axis of the asteroid or binary pair perpendicular to the orbital plane. This is a considerable simplifying assumption, as it avoids any instance of tumbling, complex rotation or off-plane forces. However, the tidal torques experienced by the asteroid or the binary are greatest in the planar case. It thus still represents a limiting case of interest where the stronger tidal torques will cause larger variations in the rotation state.

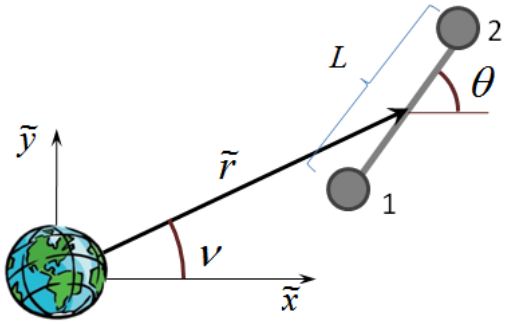

Figure 4.2: Schematic of the dumbbell planar problem definition.

4.3.1 Coupled dynamics of point-mass dumbbell

The simplest of models to study the coupled dynamics of a non-spherical satellite around a spherical massive body is an ideal equal mass dumbbell, assuming point-masses linked with a massless rod of given length L. The dumbbell rotates along an axis of maximum moment of inertia, and this axis is assumed perpendicular to the orbital motion. The coupled orbit-attitude equations of motion for the planar case of such a dumbbell (modified from Borggräfe et al. (2012) removing the solar radiation pressure and normalizing), are given by:

$$\begin{aligned}
\ddot{r} - r\dot{\nu}^2 + \frac{\frac{\mu_B}{2}\left(r - \frac{1}{2}\cos(\theta-\nu)\right)}{\left[r^2 - r\cos(\theta-\nu) + \frac{1}{4}\right]^{\frac{3}{2}}} + \frac{\frac{\mu_B}{2}\left(r + \frac{1}{2}\cos(\theta-\nu)\right)}{\left[r^2 + r\cos(\theta-\nu) + \frac{1}{4}\right]^{\frac{3}{2}}} &= 0 \\
\ddot{\nu} + 2\frac{\dot{r}\dot{\nu}}{r} + \frac{\frac{\mu_B}{4r}\sin(\theta-\nu)}{\left[r^2 + r\cos(\theta-\nu) + \frac{1}{4}\right]^{\frac{3}{2}}} + \frac{\frac{\mu_B}{4r}\sin(\theta-\nu)}{\left[r^2 - r\cos(\theta-\nu) + \frac{1}{4}\right]^{\frac{3}{2}}} &= 0 \\
\ddot{\theta} + \frac{\mu_B r\sin(\theta-\nu)}{\left[r^2 - r\cos(\theta-\nu) + \frac{1}{4}\right]^{\frac{3}{2}}} + \frac{\mu_B r\sin(\theta-\nu)}{\left[r^2 + r\cos(\theta-\nu) + \frac{1}{4}\right]^{\frac{3}{2}}} &= 0
\end{aligned} \tag{4.2}$$

where r is the distance from the massive body to the centre of mass of the dumbbell, ν is the true anomaly or an equivalent angle between the position vector of the dumbbell and a reference direction in an inertial frame, and θ is the angle the dumbbell forms with the same reference direction. All distances have been normalised by the length of the dumbbell L , and thus $r = \tilde{r}/L$ and the mass parameter $\mu_B = \tilde{\mu}_B/L^3$, where tilde variables represent fully dimensional variables. Figure 4.2 shows a schematic of the dumbbell and the state vector variables definition for this particular problem.

The equations can be rewritten as:

$$\begin{aligned} \ddot{r} - r\dot{\nu}^2 + \frac{\mu_B}{2}\frac{r_1}{{d_1}^3} + \frac{\mu}{2}\frac{r_2}{{d_2}^3} &= 0 \\ \ddot{\nu} + 2\frac{\dot{r}\dot{\nu}}{r} + \frac{\mu_B}{4r}\sin(\theta-\nu)\left(\frac{1}{{d_2}^3} - \frac{1}{{d_1}^3}\right) &= 0 \\ \ddot{\theta} + \mu_B r \sin(\theta-\nu)\left(\frac{1}{{d_1}^3} - \frac{1}{{d_2}^3}\right) &= 0 \end{aligned} \tag{4.3}$$

in which r_1 and r_2 are given by:

$$r_1 = r - \frac{1}{2}\cos(\theta-\nu); r_2 = r + \frac{1}{2}\cos(\theta-\nu) \tag{4.4}$$

and d_i is:

$$d_i|_{i=1,2} = {r_i}^2 + \frac{1}{4}\sin^2(\theta-\nu) \tag{4.5}$$

The three coordinates r, ν and θ are all interdependent, and rotational energy can be transferred to orbital energy and vice-versa, as shown in Borggräfe et al. (2012). There is a clear dependence with the relative attitude through the angular difference $\theta - \nu$, which is the angle between the dumbbell and the local vertical. The evolution of this angle is a function of the orbit and the rotation of the asteroid, be it prograde or retrograde. The term prograde rotators will be used throughout this chapter for bodies rotating in the same direction as the orbital motion ($\dot{\theta} > 0$). They are more susceptible to tidal torques disturbances than retrograde rotators, as they are more likely to enter into resonance with the orbital motion.

As a particular example, a test case is selected consisting of an asteroid composed of 2 constant density spheres of 50 m radius, separated by just 100 m (so in essence a solid double sphere contact binary, but modelled as a point-mass dumbbell). This captured asteroid is assumed to be located on a very high eccentricity orbit with an apocentre radius equal to the mean lunar distance from the Earth, and a pericentre radius of 2 Earth radii. This is a relevant case if a Moon swing-by followed by an Earth close passage is to be used as the first step to capture an object in an Earth bound orbit. The final rotation rate at the next apocentre at this quasi-Moon distance is shown in Fig. 4.3 for various initial rotation rates $\dot{\theta}_0$ as a function of $\theta - \nu$ at pericentre. Initial prograde rotation rates are plotted with solid lines, while retrograde rotation rates are dashed.

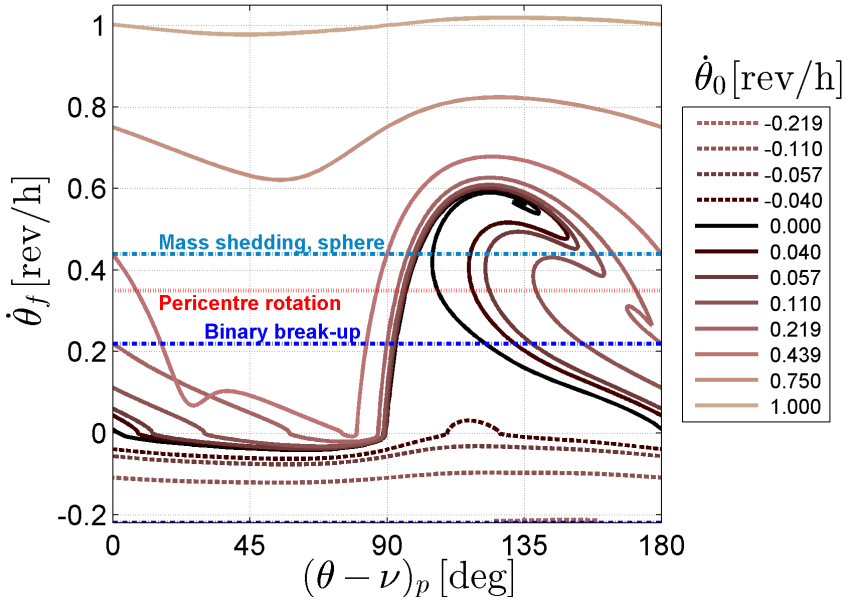

Figure 4.3: Final rotation rate for a point-mass dumbbell as a function of the angle with the local vertical at pericentre.

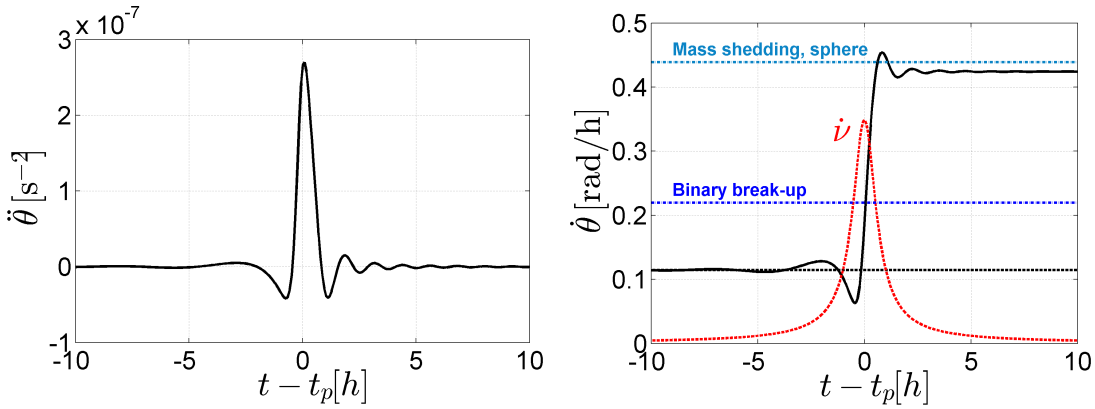

Figure 4.4: Instantaneous angular acceleration and rotational speed evolution due to tidal torque for a point-mass dumbbell in a highly elliptical orbit with pericentre at 2 Earth radii.

Three horizontal lines mark rotation rates of note, including the mass shedding spin rate $\dot{\theta}_{shed}$, the contact binary break-up limit $\dot{\theta}_{break}$, and a third line, in this case intermediate between the previous two, which is the maximum true anomaly variation rate for the orbit $\dot{\nu}_p$. This maximum true anomaly rate always takes place at the pericentre. It depends on the orbit of the asteroid, and for a hyperbolic trajectory it can be expressed as:

$$\dot{\nu}_p = \sqrt{2\frac{\mu_B}{{r_p}^3} + \left(\frac{v_{\inf}}{r_p}\right)^2} \tag{4.6}$$

It can be observed in Fig. 4.3 that the spin of fast prograde rotators (of more than one revolution per hour) and retrograde rotators (*dashed lines*) is not strongly affected by the tidal torques during a pericentre passage. Slow prograde rotators and non-rotating dumbbells can however be effectively de-spun, or spun up above the binary break-up or mass shedding limit depending on the configuration at pericentre. The spin rates acquired can be higher that the rotation rate at pericentre $\dot{\nu}_p$. In general, the dumbbell is spun up when $\theta - \nu$ is the range $90 - 180°$ (positive torque at pericentre), and de-spun for angles in the range $0 - 90°$.

A low spin rate at the end of the propagation does not discard the possibility that any of these limits was surpassed during the pericentre passage. Figure 4.4 presents the evolution of the torque acceleration and the rotational state for a particular case with an initial rotation period of 5.8 hours. As expected, most of the interaction takes place at pericentre in a bracket of 4 hours around the closest approach. Due to the configuration at the pericentre with a $\theta - \nu$ angle of 165°, the net result is an acceleration in the rotation of the dumbbell. Even though the final spin state is below the mass shedding limit, this is surpassed right after pericentre and mass loss could have occurred.

4.3.2 Decoupled dynamics of a rigid body

The coupling between attitude and orbit in the case of the dumbbell shown above (or any other rigid body) is weak (Sincarsin and Hughes, 1983), resulting in only small perturbations to the in-plane orbital elements. The predominant effect is thus changes in the rotational state. As such, the system of equations can be considered decoupled for characteristics lengths of the body much smaller than the orbital radius. Then, the asteroid can be modelled as a rigid body rotating

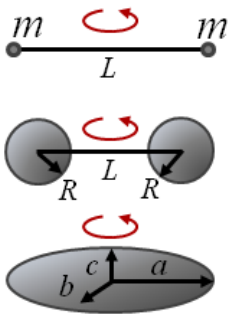

$$I^* = \frac{I_{yy}-I_{xx}}{I_{zz}} = 1$$

$$I^* = \frac{5}{8(R/L)^2+5}$$

$$I^* = \frac{1-(b/a)^2}{1+(b/a)^2}$$

Figure 4.5: Rigid body configurations and associated moments of inertia ratios

around the axis of largest moment of inertia (minimum energy configuration), which is assumed again perpendicular to the orbital plane. As in the previous dumbbell case, deformations or any type of reconfiguration are ignored.

In addition to solving the traditional orbital equations of motion for the centre-of-mass of the rigid body (in the simplest of cases with the two-body problem, see Section 2.1), the attitude of the asteroid is propagated by integrating the equation for the torque acceleration, which can be expressed by (adapted from Blackburn et al., 1969):

$$\ddot{\theta} + \frac{3\mu_B}{2r^3}\frac{I_{yy} - I_{xx}}{I_{zz}}\sin 2(\theta - \nu) = 0 \tag{4.7}$$

where $I_{zz} > I_{yy} > I_{xx}$ are the principal moments of inertia of the body. This differential equation depends only on a "shape" parameter I^* given by the ratio of the body's moments of inertia, and is independent of the size of the object. For several simple shapes I^* can be calculated with the expressions given in Fig. 4.5. The extreme case of an ideal "point-mass" dumbbell has a value of 1 (very elongated object), while a spherical body would result in a shape factor of zero.

Figure 4.6 plots the final spin state of a rigid body after a test case equivalent to a close encounter at 2 Earth radii as described in the previous section. The "point-mass" dumbbell shape reproduces almost exactly the results of the coupled orbit-attitude dumbbell equations. For less elongated shapes, the smaller shape factor reduces the effect of the gravitational torque on the final rotational rate. Similar conclusions to Section 4.3.1 can be drawn: fast prograde rotators and retrogade rotators are least affected.

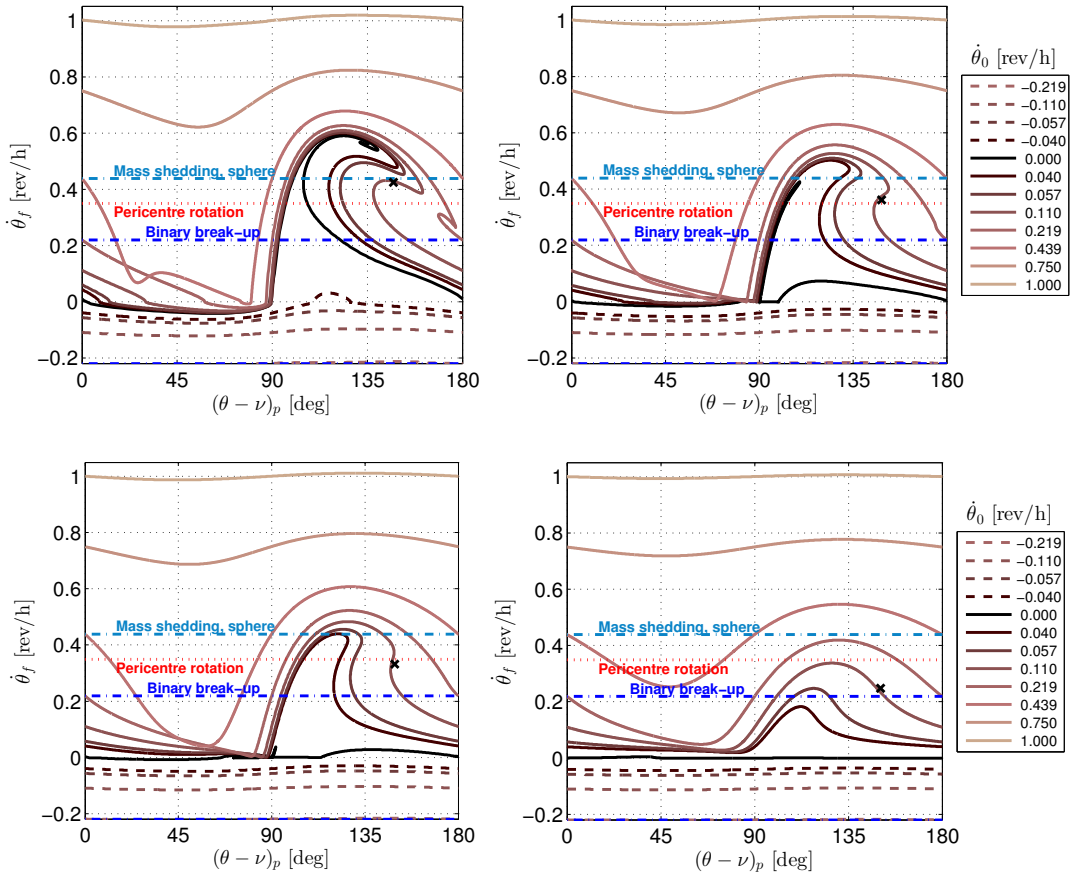

Figure 4.6: Final rotation rate for rigid bodies with point-mass dumbbell shape (top-left, $I^* = 1$), equal spherical masses contact binary (assumed rigidly bound, top-right, $I^* \approx 0.71$), and two cases of tri-axial ellipsoids with $a = 2b$ and $a = \sqrt{2}b$ (bottom, $I^* = 0.6$ and $I^* \approx 0.33$ respectively)

Figure 4.7 compares a particular case (indicated with $\times$ *markers* in Fig. 4.6) with an initial rotation rate of half of the binary break-up spin limit for different rigid body shapes. The torque and its effects are considerably reduced for less elongated, more spherical bodies.

4.3.3 Binary pair

Finally, the case of a binary system performing a swing-by of a massive body is considered, modelling the gravitational attraction between the two components of the binary (the 1+N body problem with N=2).

The equations of motion for each of the two components of the binary pair are

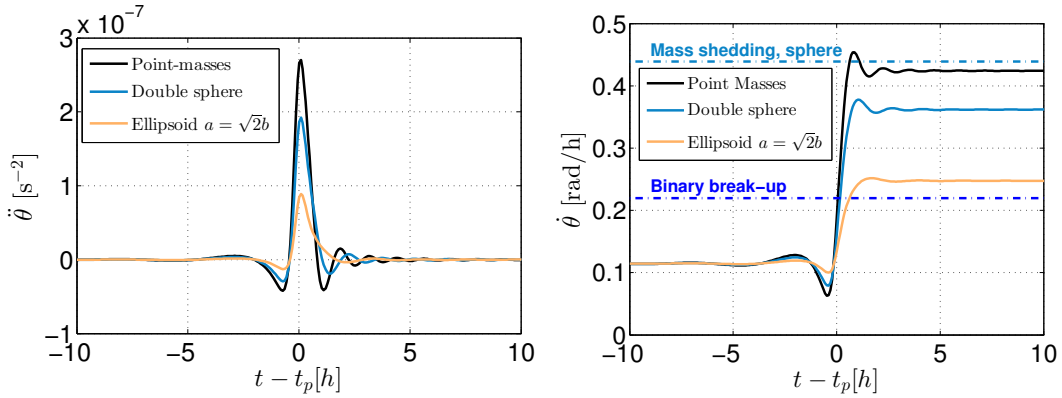

Figure 4.7: Comparison of the tidal torque acceleration and rotational speed evolution for three different rigid body shapes.

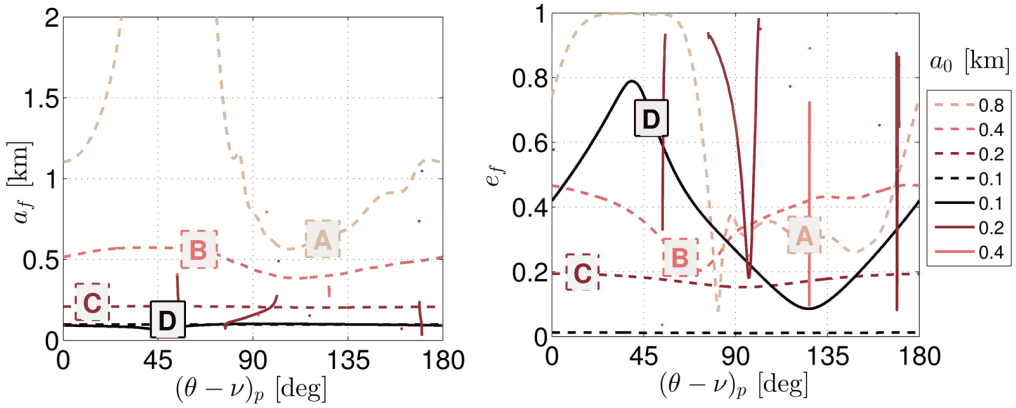

Figure 4.8: Final semi-major axis a and eccentricity e for an equal mass binary pair after a pericentre passage at 5 Earth radii. *Dashed and solid lines* indicate retrograde and prograde rotating binaries.

given by:

$$\ddot{\vec{r}}_i = -\mu_B \frac{\vec{r}_i}{{r_i}^3} - \frac{2}{3}\alpha\pi\rho G \frac{\vec{r}_i - \vec{r}_j}{|\vec{r}_i - \vec{r}_j|^3} \tag{4.8}$$

where α is a function of the ratio of the radii of the binary pair:

$$\alpha = \frac{{R_1}^3 + {R_2}^3}{L^3} \tag{4.9}$$

Distances are again normalised with a reference length $L = R_1 + R_2$, where R_i are the radius of each of the elements of the binary, assumed spherical. For the case of an equal mass binary Eq. 4.8 results in:

$$\ddot{\vec{r}}_i = -\mu_B \frac{\vec{r}_i}{{r_i}^3} - \frac{1}{6}\pi\rho G \frac{\vec{r}_i - \vec{r}_j}{|\vec{r}_i - \vec{r}_j|^3} \tag{4.10}$$

As a test case, an equal sized circular binary with a range of semi-major axes is assumed to perform a close encounter with Earth at pericentre distances of 2, 5 and 10 Earth radii. The components of the binary are assumed point masses, which implies that no impact is computed when the normalized distance between the binary centres is smaller than 1.

Figure 4.8 plots the semi-major axis and eccentricity of the binary system after a close encounter for the intermediate pericentre case (5 Earth radii). Similar plots have been generated for cases with both lower and higher pericentre radius. For the 2 Earth radii case, mostly retrograde rotating binaries with a small initial semi-major axis survive the close approach without a break-up and escape. There are a few single cases of geometrical configurations that allow prograde binaries to survive. For higher pericentres (for example the 5 Earth radii shown in Fig. 4.8) some prograde rotating binaries (*solid lines*) manage to maintain their binary structure and do not escape from each other. However, the initial semi-major axis is in most cases small (of the order of 100 m, a particular case is indicated as "D") and they suffer large variations in the binary orbit eccentricity. It can be observed in Fig. 4.8 that retrograde binaries (*dashed lines*) fare better: for initial semi-majors axis smaller than 400 m, the disruption introduced by the gravitational torque does not manage to break the binary pair. This limit increases to over 800 m for the case of a pericentre passage over 10 Earth radii.

Figure 4.9 shows the semi-major axis and eccentricity evolution, as well as a binary trajectory plot centred on one of the components of the pair, for 4 particular cases identified with letters in Fig. 4.8. Case "A" through "C" correspond to retrograde binaries of decreasing initial semi-major axis of 800, 400 and 200 m. It is clear that the disruption is smallest for the closest binary pair "C", with no apparent change in semi-major axis and a small increase in eccentricity. In cases "A" and "B" the binary pair is technically broken at the pericentre passage (eccentricity larger than 1), but then gravitationally bound together again in an elliptical orbit when the gravitational torques reduce away from the closest approach. Case "D" represents one of the few cases of a surviving prograde close binary. However, it can be observed that the orbit shape suffers a dramatic change. No case of binary exchange was obtained (one of the components being captured and the other ejected). This is not surprising, as Borum et al. (2012) report the binary exchange mechanism only takes place at much lower velocity swing-bys, on asteroids with almost parabolic trajectories with hyperbolic excess velocities lower than 50-100 m/s.

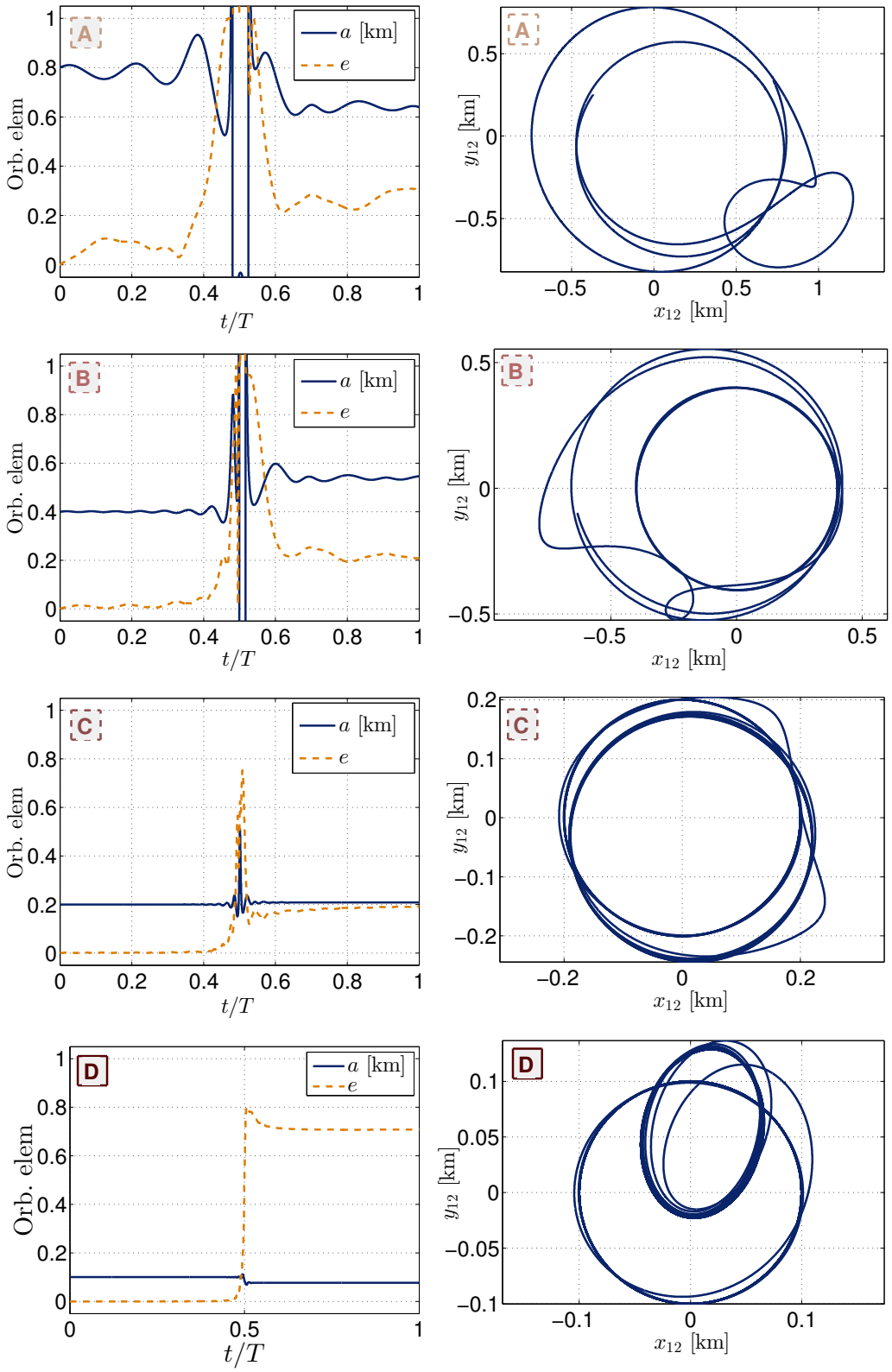

Figure 4.9: Binary semi-major axis a and eccentricity e evolution for an equal mass binary pair during a close approach (*left*), and trajectories of one of the components of the binary with respect to its companion (*right*). Initial trajectories are circular ($e = 0$).

4.3.4 Equal mass contact binary

This model combines rigid body propagation and the binary pair model (see sections 4.3.2 and 4.3.3), with switching events triggered by a limit rotational rate for break-up, and re-impact of the components. It will be used in Section 4.4.3 to investigate the behaviour of a contact binary during a lunar flyby.

For the rigid body propagation the shape factor of two spheres in contact is used. No sliding between boulders, independent boulder rotation, or other type of relative movement between the two components of the contact binary is considered. If the contact binary rotation speed reaches the binary break-up rotation limit, the pair splits and propagation continues with the binary pair model. This implies only self-gravity is considered, with no cohesion between the components of the contact binary. Reconfiguration of the binary takes place when the distance between the two components drops below two radii. No collision or reconfiguration due to the impact is computed.

4.4 Application to capture

In the event of an asteroid retrieval mission that requires a lunar swing-by (such as in Brophy et al., 2012; Strange et al., 2014), or an Earth encounter at lower distances than those proposed in Sanchez Cuartielles et al. (2013), the consequences of the swing-by on the minor body can be investigated with the models described in Section 4.3.

In this section, both isolated single Earth and lunar swing-bys are considered, for different pericentre radii. No third body perturbation is included in the propagation of the trajectories. Two test cases are considered: a low velocity swing-by with hyperbolic excess velocity $v_\infty = 0.6479$ km/s, and a high velocity swing-by with $v_\infty = 5.851$ km/s. They correspond to the asymptotic velocities of the predicted encounters with Earth of asteroids 2006 RH120 and 2004 MN4 (Apophis) in the years 2028 and 2029 (from JPL's Small–Body Database Browser*). Candidate asteroids for capture are more likely to have low hyperbolic excess velocities, the reason being that asteroids with orbits close to that of the Earth will have relatively modest energy requirements for capture.

* http://ssd.jpl.nasa.gov/sbdb.cgi Last accessed 20/06/2014

4.4.1 Isolated Earth swing-by

Figures 4.10 and 4.11 plot the maximum rotation rate changes achievable with an Earth swing-by for the two swing-by velocities assumed, as a function of their initial rotation rate. Positive variations correspond to the maximum achievable asteroid spin-up, while negative variations are the maximum de-spin. The pericentre radius ranges from two to ten Earth radii.

The dashed diagonal red line represents the mass shedding rotation limit: $\Delta\dot{\theta} = \dot{\theta}_{shed} - \dot{\theta}_0$. Any point above this line corresponds to a rotation rate in which mass is being lost at the equator of the asteroid (assumed spherical) if no cohesion is taken into account. Similar lines can be plotted for the binary break-up limit ($\Delta\dot{\theta} = \dot{\theta}_{break} - \dot{\theta}_0$, parallel to the mass shedding line half the distance from the origin of coordinates) and for zero spin rate ($\Delta\dot{\theta} = -\dot{\theta}_0$, again parallel through the origin of coordinates).

The plots on the right have been normalised with respect to the rate of variation of the true anomaly at pericentre $\dot{\nu}_p$. It can be observed that in the case of the low velocity swing-by all lines for various pericentre radii in the normalised plots are superimposed. This indicates that both axes, the maximum rotation rate changes and the initial rotation rate, seem to scale with this value, and the results can thus be easily generalised to even higher pericentre radius. For the high velocity swing-by, however, the vertical axes scaling is no longer accurate, and the maximum normalised values decrease noticeably with the pericentre radius.

Several key conclusions can be drawn from these plots. Consistent with the results for the test cases in Section 4.3, no rotation rate variation of practical relevance can be achieved for retrograde asteroids, or for asteroids rotating initially at speeds higher that three times the true anomaly variation at pericentre $\dot{\nu}_p$. The maximum de-spin for low positive (prograde) initial spin rates follows the zero spin rate line $\Delta\dot{\theta} = -\dot{\theta}_0$ for the cases with a high shape factor. This indicates elongated objects can be completely de-spun for a certain range of initial rotation rates. Variations larger than $\dot{\nu}_p$ can be achieved for elongated shapes.

The maximum spin-up occurs for prograde initial rotation rates close to zero, while the maximum de-spin is for asteroids initially rotating at speeds close to $\dot{\nu}_p$. These maxima increase with the elongation of the asteroid shape, and the location of the rotation for maximum spin-up on the horizontal axis moves away

from zero initial rotation rate with the swing-by speed, while at the same time the initial rotation for maximum de-spin decreases.

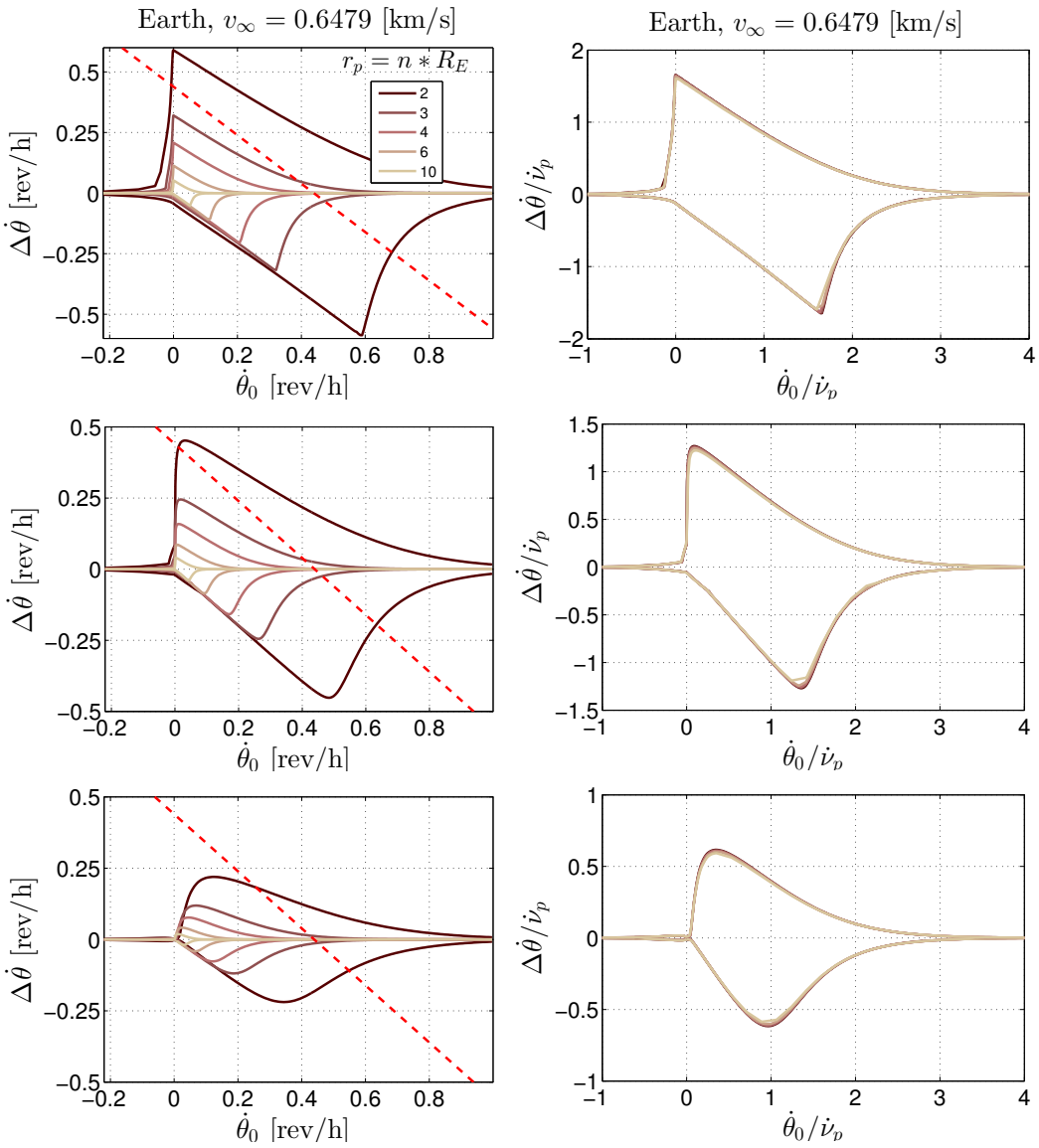

Figure 4.10: Maximum spin-up and de-spin achievable for a low-velocity Earth swing-by for various shape factors: point-mass dumbbell (*top*), equal mass contact binary (*middle*) and ellipsoid with $a = \sqrt{2}b$ (*bottom*). Right plots have been normalised with the true anomaly rate at pericentre $\dot{\nu}_p$.

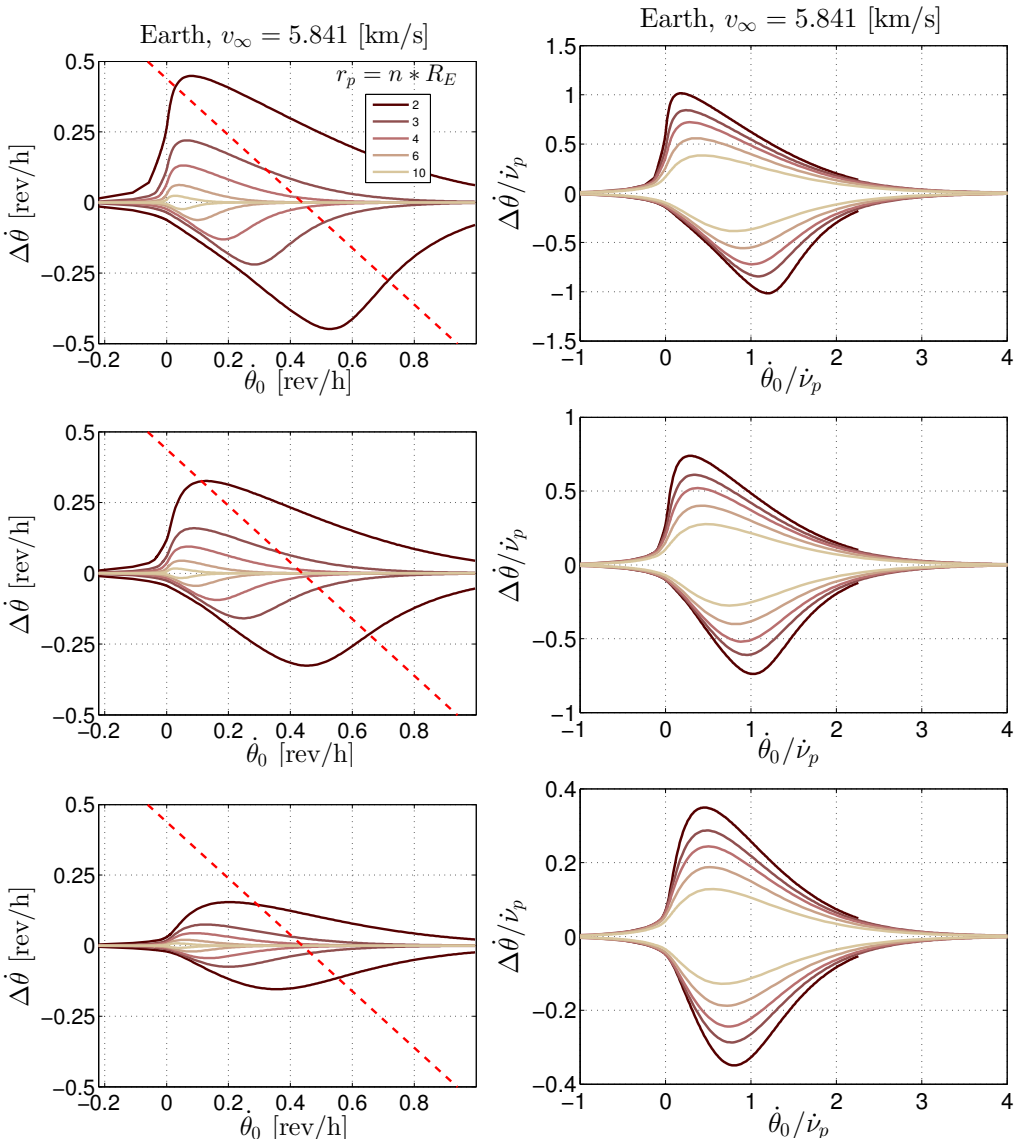

Figure 4.11: Maximum spin-up and de-spin achievable for a high-velocity Earth swing-by for various shape factors: point-mass dumbbell (*top*), equal mass contact binary (*middle*) and ellipsoid with $a = \sqrt{2}b$ (*bottom*). Right plots have been normalised with the true anomaly rate at pericentre $\dot{\nu}_p$.

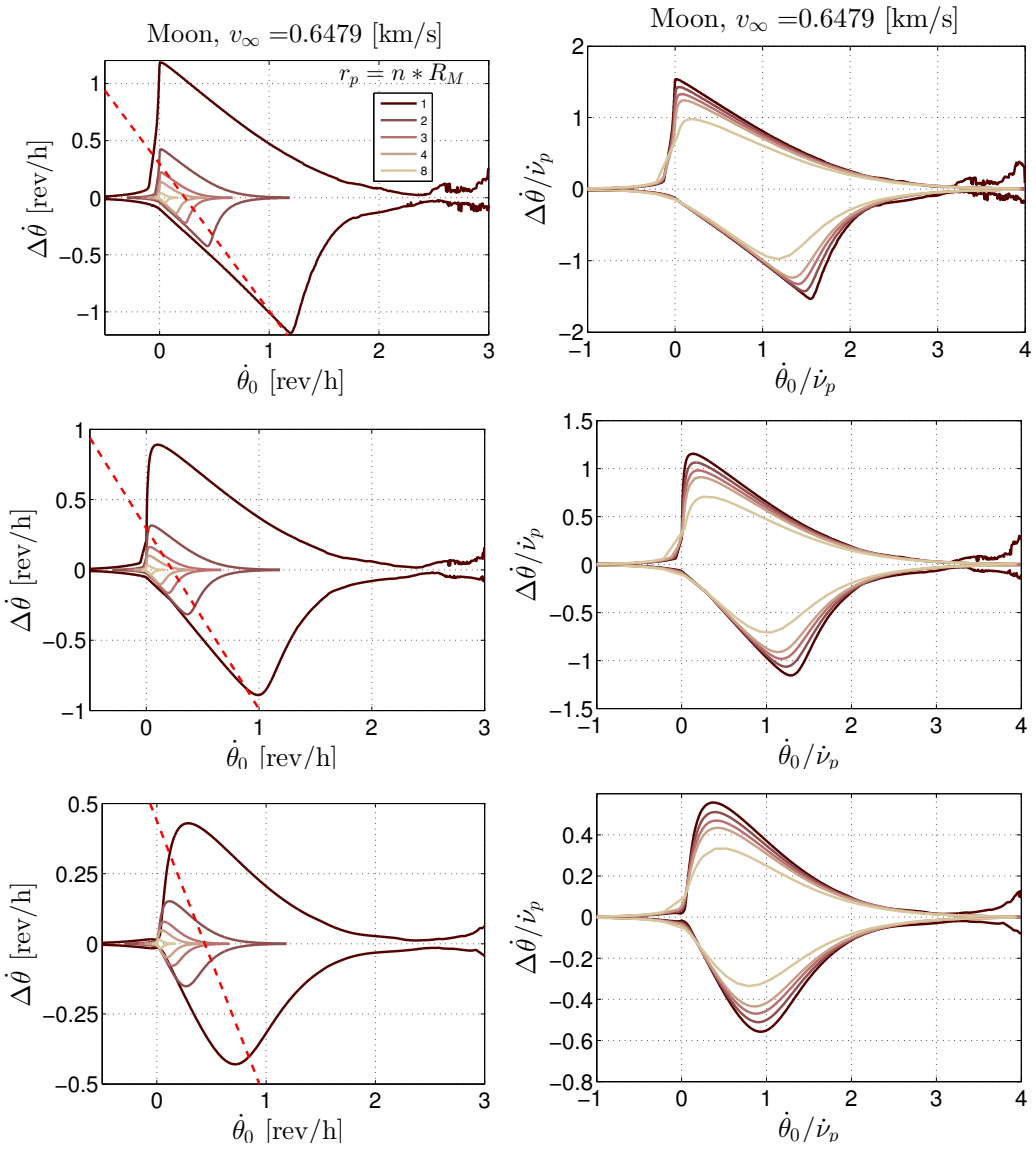

Figure 4.12: Maximum spin-up and de-spin achievable for a low-velocity Moon swing-by for various shape factors: point-mass dumbbell (*top*), equal mass contact binary (*middle*) and ellipsoid with $a = \sqrt{2}b$ (*bottom*). Right plots have been normalised with the true anomaly rate at pericentre $\dot{\nu}_p$.

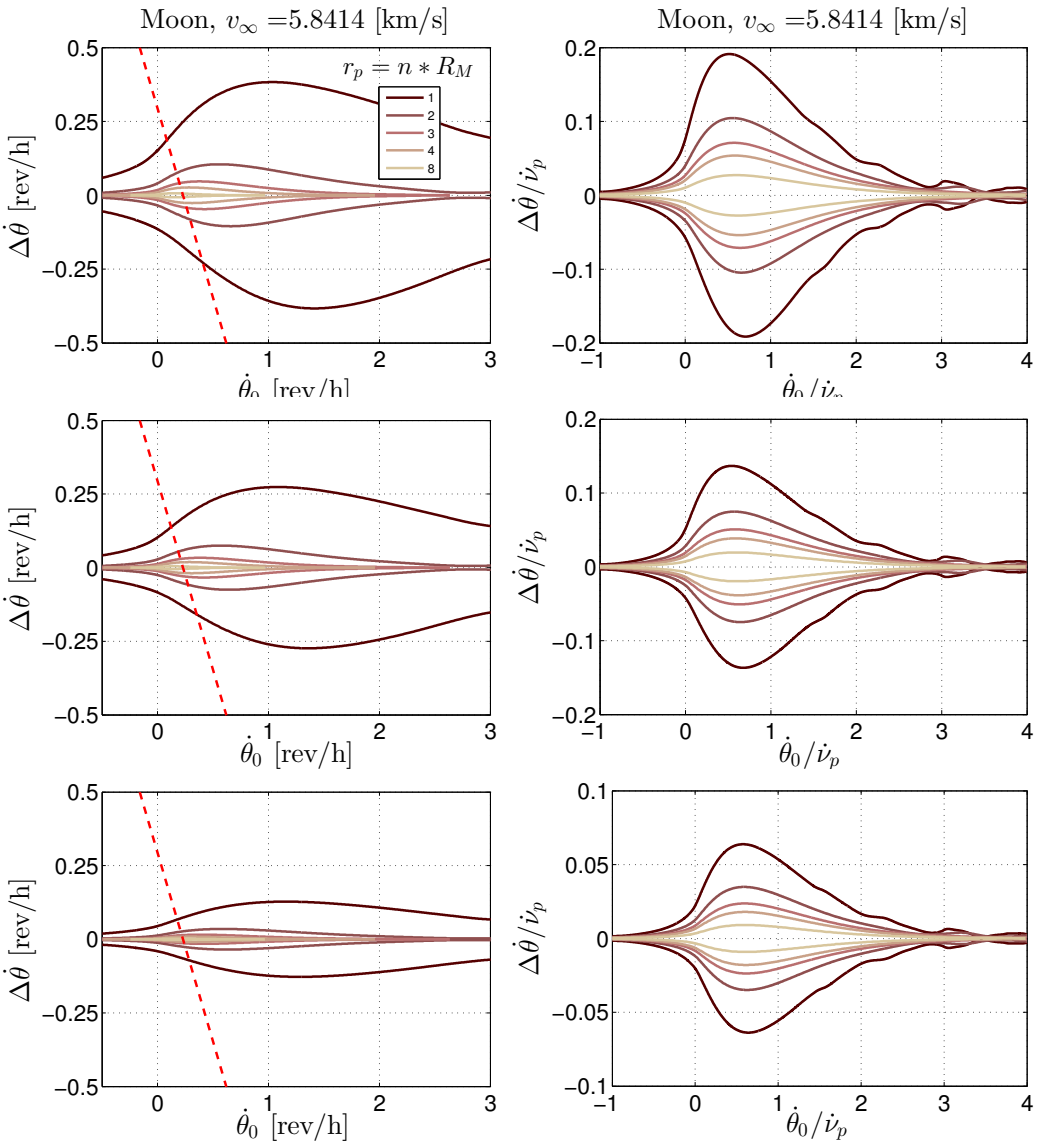

Figure 4.13: Maximum spin-up and de-spin achievable for a high-velocity Moon swing-by for various shape factors: point-mass dumbbell (*top*), equal mass contact binary (*middle*) and ellipsoid with $a = \sqrt{2}b$ (*bottom*). Right plots have been normalised with the true anomaly rate at pericentre $\dot{\nu}_p$.

4.4.2 Isolated lunar swing-by

For the lunar swing-by case, pericentre radii as low as 1800 km are considered (approximately 63 km above the lunar surface), and up to 8 lunar radii. Figure 4.12 and 4.13 show the maximum rotation rate variation for the lunar swing-by cases. The results are analogous to those of Section 4.4.1, although the effects in the lunar swing-bys, particularly for the high-velocity case, are much smaller than in the Earth swing-by for a similar pericentre radius.

Rotation rate changes of the order of the true anomaly rate at pericentre $\dot{\nu}_p$ can still be achieved for the low velocity flyby. However, for the lunar swing-by, a slowly rotating prograde asteroid cannot be completely de-spun: the maximum de-spin does not follow the $\Delta\dot{\theta} = -\dot{\theta}_0$ line (it is not parallel to the red dashed line). For the high speed swing-by, the maximum spin-up and de-spin lines appear to be almost symmetric with respect to the horizontal axis, indicating that there is an initial rotation rate for which the largest change can be achieved in either direction depending on the geometric configuration at pericentre. The magnitude of the spin-up and de-spin is much reduced in this case. As a side note, there are small oscillating variations at higher speeds, indicating higher order resonances, but the effects are limited.

4.4.3 Equal mass contact binary break-up

As a final case study, the possibility of break-up of a contact binary was analysed for a low velocity lunar swing-by with a pericentre at two lunar radii. The contact binary is assumed to rotate initially in a prograde direction at half the binary break-up limit.

The results are again very much dependent on the geometry at pericentre passage, and thus the initial conditions. Figure 4.14 presents three examples of different outcomes. The rotation rates have been scaled with the binary break-up limit, and the time with the total time within the lunar sphere of influence t_{SOI}.

In the first case (Fig. 4.14a), the contact binary reaches the break-up limit, and the distance between the binary pair d_{1-2} increases due to tidal torques until they effectively break apart from each other. A second case shows a separation into a binary pair that collapses once again into a contact binary during the swing-by (Fig. 4.14b). The maximum separation between the two components is larger

than 6 times their radius. Finally, there are cases in which the contact binary survives the swing-by without breaking apart at any time, as shown in Fig. 4.14c.

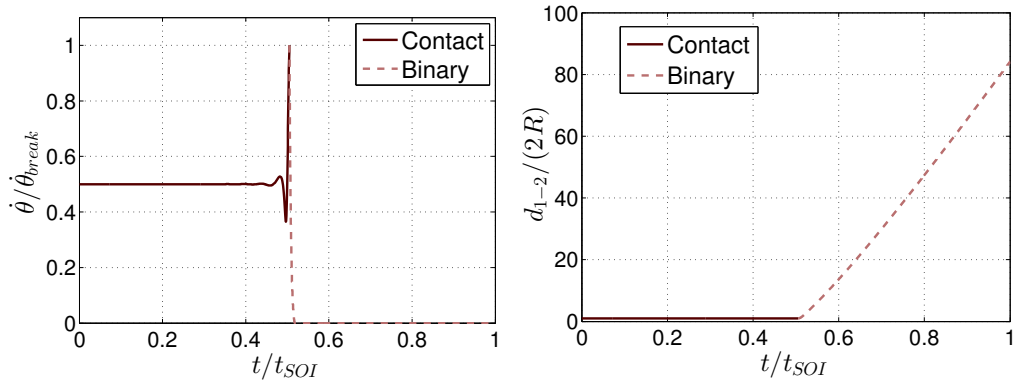

(a)

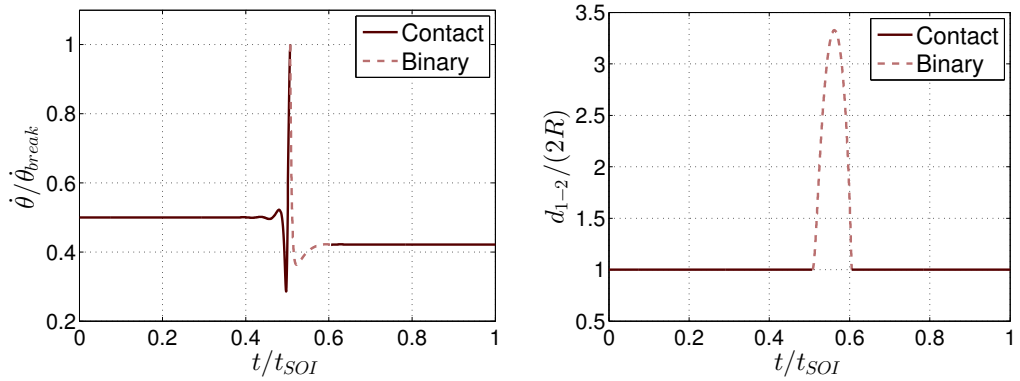

(b)

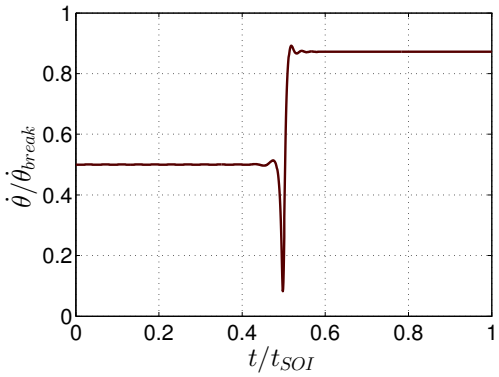

(c)

Figure 4.14: Examples of binary disruption: contact binary break-up (a), binary pair generation and collapse to contact binary again (b), and contact binary surviving the swing-by (c).

4.5 Discussion and model limitations

The modification of the rotational state and structure of an asteroid during a close encounter with a planet or moon taking advantage of tidal torques has been proven to be feasible in a simplified planar model. However, this is only a preliminary analysis, and more complex models need to be implemented, starting with multi-body systems (Earth-Moon-asteroid).

Most importantly, non-planar models in which the rotation is not constrained to be perpendicular to the orbital plane should be considered. These will introduce the possibility of tumbling and complex rotation states, but possibly also the opportunity to use tidal toques to de-tumble or stabilize the rotation of an asteroid.

In addition, introducing internal strength and cohesion will significantly affect the outcome of the break-up analysis. As a further step, complex models of asteroid rubble piles, with multiple size and shape mass concentrations held together by self-gravity and cohesion could be devised.

Finally, as shown in the previous analysis, the outcomes of a tidal interaction during a swing-by are very sensitive to variations in the geometry of the encounter, and small errors may cause large deviations in the final state. Devising control strategies and studying their feasibility is left here for future work.

4.6 Summary

Swing-bys during the capture phase of an asteroid retrieval mission could be effectively used to de-spin the asteroid, or spin-up and break-up of rubble piles. Several recommendations can be formulated from the previous analysis, limited to planar models for swing-bys around the Earth or the Moon.

Assuming a target captured asteroid has been de-tumbled or de-spun after grappling and bagging (as in the proposal of the Keck study report, Brophy et al., 2012), and no induced rotation during the capture swing-by phase is desired, introducing a small retrograde rotation for the asteroid (with periods as large as 25 hours) will effectively avoid undesired spin-up effects. This requires very little control, which should be within the capabilities of the retrieval spacecraft if a complete de-spin was performed after bagging. Fast rotators (faster than three

times the true anomaly variation at pericentre) are also not affected, but having a controlled fast rotating asteroid is less likely to be feasible or of practical use.

Conversely, assuming a residual prograde rotation of the asteroid at the time of the swing-by that needs to be reduced, small modifications in the time of pericentre passage or in the rotational state would allow a change in the relative attitude of the asteroid at pericentre. Tuning this geometry can completely de-spin the captured asteroid depending on its shape. This is effective for rotation rates slower or of the order of the true anomaly variation at pericentre $\dot{\nu}_p$.

Further spin control techniques can be envisaged. If spin-up of the captured asteroid is desired for some practical purpose, a similar strategy can be proposed to increase the rotation rate of a slowly rotating asteroid to levels of the order of $\dot{\nu}_p$. Induced spin-up can be employed ultimately to break-up a contact binary or fragment a rubble pile, for scientific reasons or in the case it would be beneficial for exploitation.

Chapter 5

MESO to MICRO: Solar radiation pressure enabled orbits around asteroids

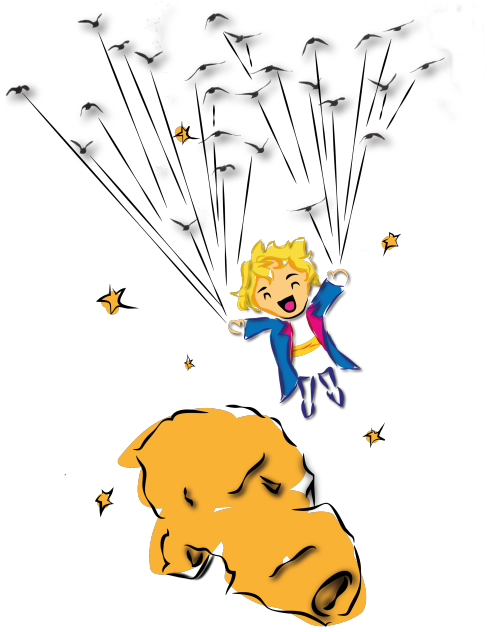

"I had thus learned a second fact of great importance: this was that the planet the little prince came from was scarcely any larger than a house!

[. . .]

I believe that for his escape he took advantage of the migration of a flock of wild birds.

Saint-Exupéry (1943), *The Little Prince*

Indeed one fact of great importance in asteroid research is the diversity in the size of Near-Earth Objects. As already noted in Chapter 3, the currently known population ranges from sizes of a few meters (limited by current detection capabilities), to tens of kilometres. Asteroids "*scarcely larger than a house*" are extremely abundant in the NEO population according to well-accepted size distribution models, even if the surveyed population in those sizes is small (Shapiro et al., 2010).

As gravity scales with the volume of the attracting body in questions, these "house-size" objects of the order of 10 m diameter, would have 10 to 30 million times lower gravity than for example comet 67P/Churyumov–Gerasimenko, visited by Rosetta (depending on the density, quite low for the comet in question). The little prince takes advantage in the above extract of a "*migrating flock of birds*" to escape his fictional asteroid. Similarly, in the low-gravity environment of real-world asteroids, very small forces, such as the solar radiation pressure perturbation, third-body gravity perturbations, or very low-thrust, regain importance and could go a long way to allow exotic orbits, quick escape trajectories, or other exploration strategies.

This chapter proposes the use of highly non-Keplerian trajectories enabled by solar radiation pressure and devices with variable area or reflectivity to map and characterise small asteroids. Strategies alternative to hovering involving a combination of retrograde and prograde orbits together with inversions of the orbit direction by either manoeuvres, or exploiting the natural dynamics are presented and analysed. As opposed to terminator orbits, these strategies allow orbits that remain in the orbital plane of the asteroid, and allow direct overflies of the sub-solar point and other equatorial regions.

5.1 Motivation and background

The influence of a large solar radiation pressure perturbation (SRP) on spacecraft dynamics is of great importance for asteroid exploration missions. For large asteroids, such as Eros and Vesta, various relatively stable orbiting regimes can be achieved (Scheeres, 1994; Scheeres et al., 2003). This is not the case for much smaller objects (of a diameter of less than a few hundreds of metres), where SRP destabilises most orbits. The well-known terminator orbits (Byram and Scheeres, 2008; Dankowicz, 1993; Scheeres, 2007) have been proposed for spacecraft orbiting these bodies. They are currently the most studied long-term stable orbits around asteroids when SRP is dominant. Most other bound orbits experience large excursions in eccentricity, which cause the spacecraft to impact or escape after a small number of revolutions, or have reduced stability. However, some of these orbits which experience large eccentricity changes present interesting possibilities, and will be the focus of this chapter.

One of the main drawbacks of terminator orbits is precisely the reduced or partial coverage that they provide of the asteroid. Because of their geometry, on the terminator plane and slightly displaced towards the anti-sun direction, their observation of features of the asteroid is constrained to regions along the terminator line, which implies long shadows and is not optimal for optical observations. The sub-solar point and other areas in the sunlit hemisphere are not directly accessible, and neither is the anti-solar point at small Sun-spacecraft-asteroid angles.

Various solutions have already been proposed in literature to circumvent this problem. Using the classical Stark problem, it was demonstrated that trajectories remain confined between paraboloids when small perturbations are applied to terminator orbits (Bookless and McInnes, 2006; Bookless, 2006). One set of paraboloids extends towards the Sun direction, which would allow partial coverage of the sunlit side of the asteroid, while the second set extends towards the anti-Sun direction. One subset of this latter type of orbit, a family of periodic orbits confined to the sunward paraboloid, were proposed to provide partial coverage of the sunlit side (Broschart et al., 2014; Lantoine et al., 2013). These trajectories were termed Quasi-Terminator Orbits (QTO), as they extend the terminator orbit families they originate from. Nevertheless, their coverage of the region around the sub-solar point is still far from optimal.

Other solutions for sunlit hemisphere coverage include direct hovering in a quasi inertial frame or co-rotating frame (Broschart and Scheeres, 2005, 2007), or pseudo-hovering solutions where the spacecraft stays in a control box, with regular manoeuvres reversing the velocity vector (Scheeres, 2012a). Because of the cost of orbit maintenance, hovering solutions are feasible for small asteroids only.

Another possible strategy is the use of multiple low-velocity flybys of the asteroid (Takahashi and Scheeres, 2011). This was suggested as a means to characterise the gravity field of a small asteroid without inserting into orbit about it, but it could also be used for monitoring various regions of interest on the surface of an asteroid.

Two novel solutions that provide a more comprehensive coverage of equatorial regions perpendicular to the terminator are discussed in this chapter:

- Alternating orbiter: an intermediate strategy between control box hovering and multiple flybys in which the spacecraft stays in orbit around the

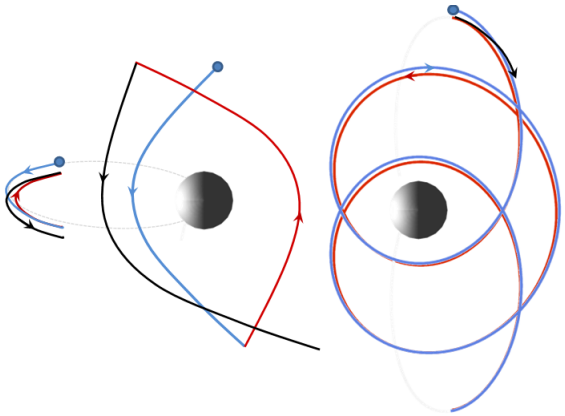

Figure 5.1: Schematic representation of sub-solar point mapping strategies: control box pseudo-hovering scheme and multiple low-velocity flybys (left), and the proposed SRP enabled alternating orbiter (right).

asteroid performing regular manoeuvres to reverse the velocity vector and orbit direction after a few revolutions (see Fig. 5.1). These inversions are intended to avoid impact due to the increase in eccentricity caused by SRP.

- Symmetric planar periodic orbits: certain planar solutions of the Hill problem extended with SRP perturbation, in particular the a and $g-g$' families, present a more comprehensive coverage of the equatorial regions, as well as interesting properties for asteroid exploration.

On one hand, the cost for orbit maintenance for these strategies is expected to be lower than hovering solutions previously investigated. Even if regular manoeuvres are scheduled, or small corrections required to avoid escape or impact due to their stability properties, the orbit maintenance costs and frequency of manoeuvres would be greatly reduced. In addition, having an orbiting solution will allow for a faster characterisation of the gravity field, and more comprehensive coverage than multiple flybys.

The following sections present the results of the analysis for these two solutions, as well as some initial work on the effect of eclipses and non-sphericity perturbation. Additional orbits of interest for hopper spacecraft are also briefly discussed. Finally, in terms of system implementation, various possible implementations of variable area spacecraft that could provide the required SRP control are suggested and discussed for the above strategies.

5.2 Alternating orbiter strategy for asteroid exploration

In order to select feasible orbits for the proposed strategy, this section analyses the evolution of the orbit properties of a high-area-to-mass ratio spacecraft moving in the orbital plane of the asteroid, perpendicular to the terminator. In what follows, the dynamical models described in detail in Section 2.3 will be used, with extensions to account for eclipses or perturbations when indicated. Both the lightness number β, as defined in Eq. 2.11 or in its scaled form β', and the cross-sectional area S (once the spacecraft mass is fixed) will be used interchangeably in this chapter to describe the different orbiting regimes.

5.2.1 Phase-space graphs from orbit-averaged equations

In the following subsections, the photo-gravitational CR3BP equations of motion will be used for the propagation of trajectories. However, the phase space plots of the orbit-averaged Hamiltonian approach (Section 2.3.4) still provide an intuitive analytical tool to explain the evolution of the orbital elements in a high-SRP and low gravity environment. Phase space graphs of the numerical trajectories will be plotted in order to understand the different orbiting regimes, and to observe the deviations with respect to the expected analytical averaged behaviour.

Contrary to the cases investigated around Earth (Colombo et al., 2011; Oyama et al., 2008), there are no equilibrium points in the Hamiltonian for the case of high SRP around very small asteroids. Scheeres (1999) reports that planar equilibria are still feasible for Eros-size asteroids but become impractical for smaller bodies, of a few kilometres diameter, such as the target of Rosetta. For the even smaller asteroids which are the focus of this chapter, of size of the order of tens or hundreds of metres, the equilibrium point shifts to an eccentricity of almost unity. This implies that the isolines of constant Hamiltonian H all reach at some point the critical eccentricity value of 1, which results in most trajectories either escaping or impacting the surface eventually. The shape of the isolines is represented in Fig. 5.2 for prograde orbit cases (i.e. rotating counter-clockwise). As predicted by theory (Colombo et al., 2011), for constant H the eccentricity decreases for phase angles lower than 180°, and increases for phase angles larger than 180°. They are similar to the limiting case for an infinite SRP coefficient

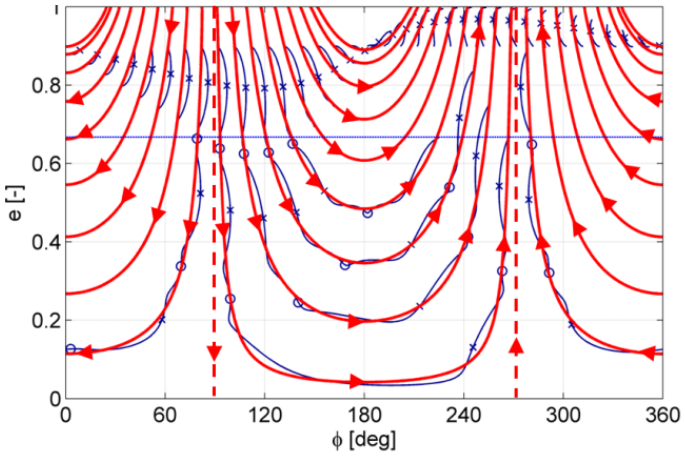

Figure 5.2: Eccentricity-ϕ plot comparing numerical propagated trajectories *(thin blue lines)* and the isolines of constant Hamiltonian *(thick red lines)*. Apocentres and pericentres of the numerical trajectories are indicated with $\times$ and $\circ$ markers respectively.

as reported in Oyama et al. (2008). Fig. 5.2 shows that there are orbits that, starting with very high eccentricities, become almost circular due to the effect of SRP before the eccentricity grows again back to values beyond 1. For retrograde orbits (rotating clockwise) the phase space would be flipped horizontally with respect to $\phi = 180°$, and the direction of the isolines is reversed. A few example, numerically propagated trajectories are shown overlapped in the figure. They closely follow the Hamiltonian isolines, demonstrating the usefulness of the phase-space plot. Chapter 6 includes further detailed analysis of these particular trajectories.

The phase-space plot also indicates a critical eccentricity (*horizontal line*) above which all pericentres are below the asteroid surface. This critical eccentricity varies along the orbit with the osculating semi-major axis. If there is a pericentre passage above this line it implies an impact with the asteroid. If instead no pericentre passage takes place, the eccentricity can grow up to values greater than 1, and the resulting trajectory corresponds in principle to an escape trajectory.

In most cases the trajectories studied in this chapter will have initial phase angle of 90° or 270° (vertical dashed isolines in Fig. 5.2), which correspond to orbits with an initial pericentre on the positive or negative Y-axis of the co-rotating frame. They are of particular interest as the eccentricity reaches smaller values close to 0 (circular orbits) and as a general rule tend to remain longer in orbit (they require more time for the eccentricity to grow back to critical values).

5.2.2 Extensions of the photo-gravitational CR3BP

This subsection presents extensions to the photo-gravitational Circular Restricted 3-Body Problem presented in Section 2.3.1, to include the effect of eclipses and non-sphericity of the asteroid.

5.2.2.1 Eclipses

The original definition of the photo-gravitational CR3BP (or the orbit-averaged Hamiltonian approach) does not take eclipses into account. For the trajectories considered in this section, eclipses, though short in duration, have a significant effect on the evolution of the orbit elements.

A first simple approximation is to model eclipses as a cylindrical shadow projected by a spherical asteroid of radius R, and assuming the lightness number β becomes zero whenever the eclipse conditions are satisfied:

$$\left.\begin{array}{c} \vec{r}\cdot\vec{r}_{S-A} > 0 \\ \left|\vec{r}\cdot\frac{\vec{r}_{S-A}\times(\vec{r}\times\vec{r}_{S-A})}{\left|\vec{r}_{S-A}\times(\vec{r}\times\vec{r}_{S-A})\right|}\right| < R \end{array}\right\} \implies \beta = 0 \tag{5.1}$$

with $\vec{r}$ and $\vec{r}_{S-A}$ the asteroid-to-spacecraft and Sun-to-asteroid radius vectors respectively.

The previous model does not consider any umbra or penumbra effects, implying that SRP is either active or not. A slightly more complex model was implemented, with the lightness number varying with the area of the Sun occulted by the asteroid, accounting for umbra and penumbra. Extensive testing showed that the difference between both models is negligible.

Figures 5.3 and 5.4 illustrate the importance of including eclipses in the orbit propagation. The number of complete revolutions, the impact and escape conditions vary significantly with eclipse conditions. For instance, if no eclipses are considered there is a final pericentre ($\circ$ markers in the phase space plot) taking place before the eccentricity grows back to critical levels, resulting in an additional revolution before impact. The same trajectory with eclipses does not clear the surface in this final pericentre passage and impacts 15 hours earlier. The phase space plot 5.3b trajectories do not differ significantly, but on plotting the eccentricity (see Fig. 5.4), three eclipse phases can be clearly pinpointed, where the SRP is not active and the eccentricity does not vary.

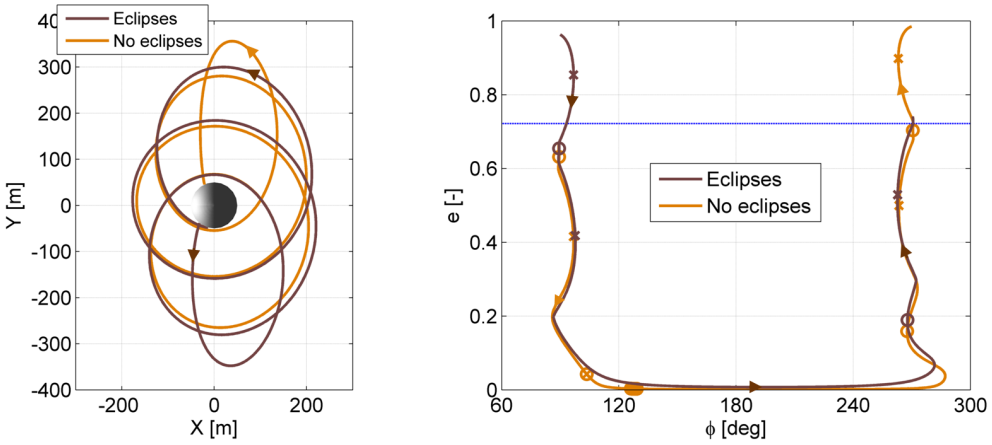

Figure 5.3: Differences in propagation with and without eclipses in the co-rotating frame (a) and the phase space (b). Apocentres and pericentres are indicated with $\times$ and $\circ$ markers respectively in the phase space. When no eclipses are considered there is an additional revolution.

5.2.2.2 Non-sphericity perturbation

When spacecraft orbit in close proximity to an asteroid, its irregular shape and non-sphericity of its gravitational field introduces large perturbations in the spacecraft trajectory.

For the purpose of studying the influence of non-sphericity, the asteroid has been modelled as a constant density tri-axial ellipsoid rotating uniformly in a *prograde* direction about an axis corresponding to its maximum moment of inertia (see Fig. 5.5a). The ratio between the ellipsoid semi-major axes is assumed to be $\sqrt{2}$, and the total volume and mass is equal to that of a spherical asteroid of equivalent radius R. The rotation axis direction is constant and assumed aligned with the Z-axis of the co-rotating frame, and the state of the asteroid can be thus defined by a single variable γ, the angle between the X-axis of the co-rotating frame (Sun-asteroid direction) and the principal axis associated with the ellipsoid's minimum moment of inertia.

The gravitational field of the ellipsoid is modelled as a spherical harmonic potential up to order 4 for simplicity. The spherical harmonic's coefficients in dimensionless form in the body frame up to 4^{th} order can be calculated using the relations provided by Balmino (1994) as:

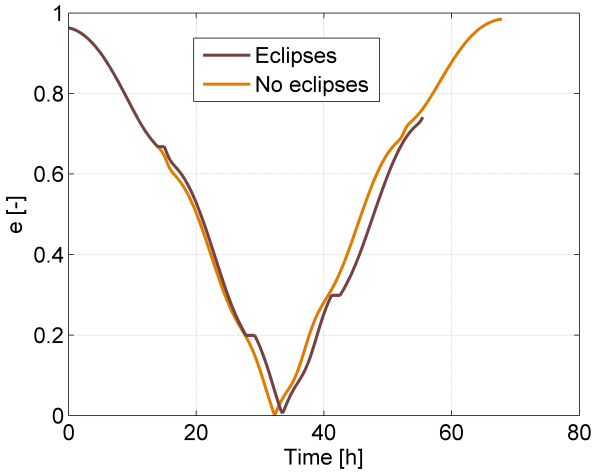

Figure 5.4: Eccentricity evolution with and without eclipses for an equatorial trajectory departing from the surface of the asteroid.

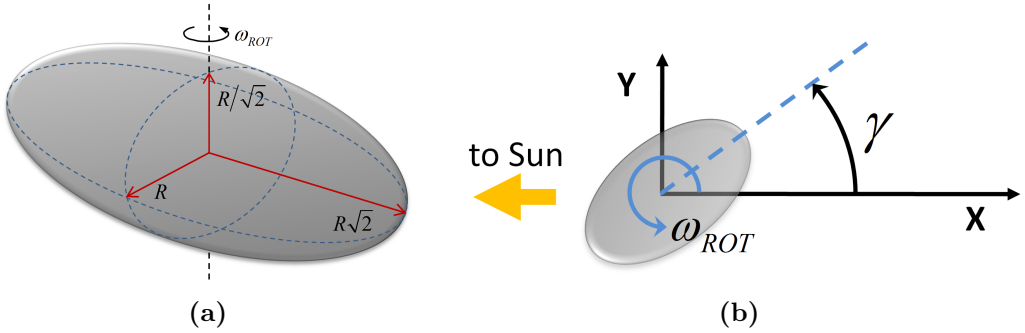

Figure 5.5: Tri-axial ellipsoid dimensions (a) and angle γ definition (b).

$$\begin{aligned} C_{20} &= \frac{1}{5R^2}\left(c^2 - \frac{a^2+b^2}{2}\right) &&= -\frac{1}{5} \\ C_{22} &= \frac{1}{20R^2}\left(a^2 - b^2\right) &&= \frac{1}{20} \\ C_{40} &= \frac{15}{7}\left({C_{20}}^2 + 2{C_{22}}^2\right) &&= \frac{27}{280} \\ C_{42} &= \frac{5}{7}C_{20}C_{22} &&= -\frac{1}{140} \\ C_{44} &= \frac{5}{28}{C_{22}}^2 &&= \frac{1}{2240} \end{aligned} \tag{5.2}$$

where the ellipsoid semi-principal axes $a = \sqrt{2}R$, $b = R$, and $c = R/\sqrt{2}$, as shown in Fig. 5.5a, and the reference radius for normalization is chosen as the mean radius of the asteroid and is equal to R.

The assumption of rotation around the Z-axis results in the largest in-plane perturbations for the equatorial case, which is in principle conservative. However, other rotational states not aligned with the orbit normal would additionally induce out-of plane perturbations which would in turn generate more complex trajectories. For other ellipsoids or more complicated asteroid geometries, the gravitational harmonics coefficients will change, resulting in different trajectories.

Figure 5.6 shows an example of the effect of the additional gravity terms on the evolution of two trajectories. The position of the ellipsoid is plotted at the initial time. It can be easily observed that prograde trajectories (Fig. 5.6a), which orbit in the same direction as the asteroid rotation, are much more strongly perturbed than retrograde trajectories (Fig. 5.6b). Prograde orbits may enter in resonance with the asteroid rotation, become hyperbolic and escape as in the example, or have dramatic changes in semi-major axis and eccentricity and prematurely impact. The eccentricity evolution in retrograde trajectories also has peculiar features, but in general they are more stable and reproduce more closely the behaviour of the spherical asteroid case.

5.2.3 SRP enabled trajectories

Using the models described above, the search for useful SRP dominated highly non-Keplerian trajectories was performed for hoppers and orbiters around a hypothetical asteroid of 50 m radius, a constant density of 2.6 g/cm^3 (corresponding to an average near-Earth asteroid as reported in Chesley et al. (2002)), and a 4 hour rotational period on a circular orbit at 1 AU around the Sun. The rotational axis is assumed perpendicular to the orbital plane, and the direction of rotation is the same as the orbit direction. The initial preliminary analysis is carried out for a spherical asteroid, and the effect of higher order gravitational harmonic terms is discussed in Section 5.2.3.6.

A spacecraft mass of 100 kg is assumed. Orbiting regimes will be discussed as a function of the variable effective surface area S instead of the lightness number, as it allows a better grasp of the spacecraft solar sail or reflective surface involved.

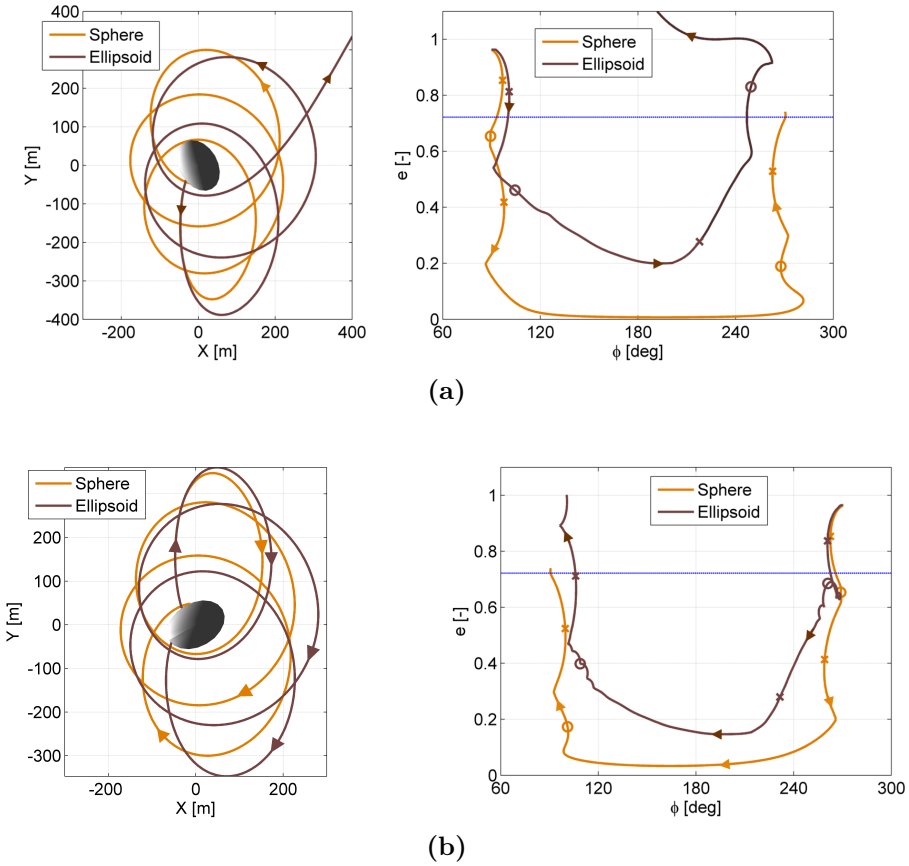

Figure 5.6: Differences in propagation including higher order gravitational terms in the co-rotating frame and the phase space. Prograde trajectories (a) are much more strongly affected when compared to retrograde ones (b).

5.2.3.1 Winding number definition

In order to adequately categorise the trajectories around the minor body it is useful to define the winding number WN as the number of revolutions that the XY projection of a trajectory onto the co-rotating frame performs around the centre of the asteroid, measured counter-clockwise from a hypothetical ejection point to its impact or escape point, such that:

$$WN = \left(\theta(t_f) - \theta(t_0)\right)/2\pi \tag{5.3}$$

The angle θ can be measured from any arbitrary direction in the XY plane (e.g. the X-axis) and must be continuous (no jumps of $\pm 2\pi$). Prograde and retrograde trajectories have positive and negative winding numbers respectively.

The winding number is a more useful geometrical definition than the commonly used number of complete orbits, as the argument of pericentre varies greatly in

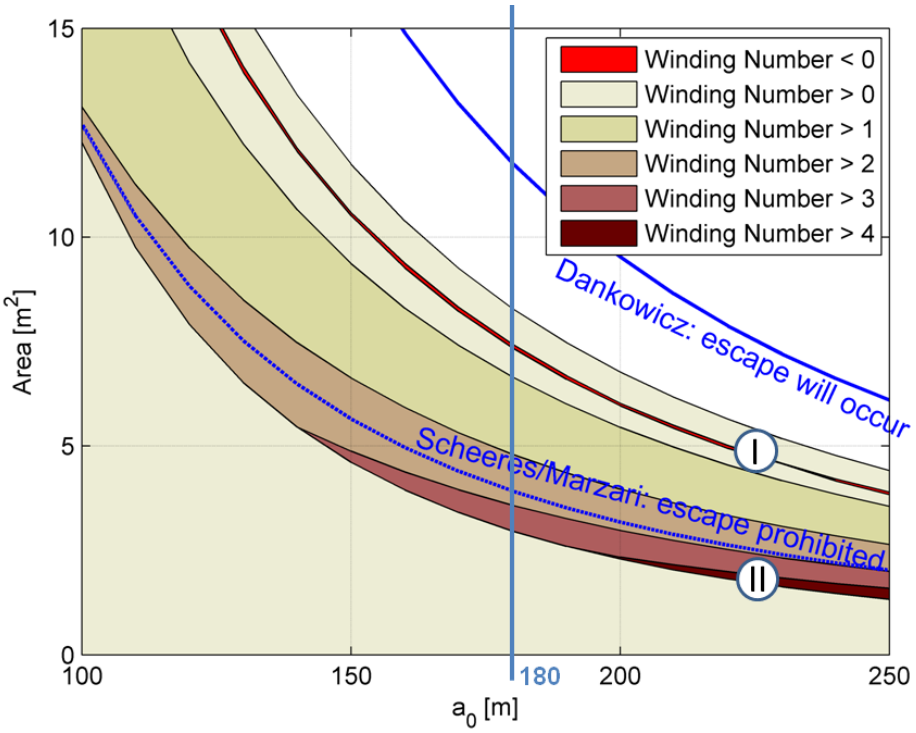

Figure 5.7: Winding number as a function of the initial semi-major axis and effective area, for prograde trajectories with $\phi = 90°$ departing perpendicularly to the surface of a spherical asteroid of radius 50 m and 4 hour rotation period.

these trajectories, and they can also become parabolic or hyperbolic and invert the orbit direction. In the case of escaping hyperbolic trajectories, they are propagated until they reach 15 asteroid radii, and the winding number is calculated up to this point.

Figure 5.7 represents the winding number for trajectories departing vertically (relative velocity perpendicular to the surface) from a spherical asteroid with phase angle $\phi = 90°$. Given an initial osculating semi-major axis a_0 and considering the asteroid rotational angular velocity ω_{rot}, the corresponding initial osculating eccentricity that satisfies the vertical relative departure velocity condition is given by:

$$e_0 = \sqrt{1 - \frac{{\omega_{rot}}^2 R^4}{\mu_A a_0}} \tag{5.4}$$

The condition of vertical departure can be of importance for hopper spacecraft that may preferably leave and return to the surface with no horizontal velocity with respect to it. Orbiter trajectories not intending to impact can in principle be calculated for any other departure condition.

The *blank area* in Fig. 5.7 corresponds to trajectories that escape directly due to SRP and the 3^{rd} body perturbation of the Sun before an apocentre passage takes place. The *light area* at the bottom contains trajectories that impact directly before performing a single revolution. If the SRP perturbation is large enough to ensure clearing the surface at the first pericentre passage, multiple revolution trajectories can be obtained (*darker shades*).

The *bright red narrow area* (a particular point in this region is also marked with Ⓘ) corresponds to trajectories that crash or escape with negative winding numbers. Given that the initial conditions are for a prograde trajectory, it implies that the orbiting direction has been reversed at some point. The sensitivity to small variations in the spacecraft effective area in this region and above is high. Trajectories above the red narrow area, which perform less than one prograde revolution but have at least one apocentre passage, may impact or escape for small variations of the initial conditions.

The region of interest roughly corresponds to the limits in semi-major axis that ensure escape (Dankowicz, 1993) or where escape is prohibited and ensures impact (Scheeres and Marzari, 2000). These limits are also plotted for comparison, and are given in Eq. 5.5. In principle, they apply only to terminator orbits.

$$a_{impact} = \frac{|\vec{r}_{S-A}|}{4}\sqrt{\frac{\mu_A}{\beta\mu_S}} \qquad a_{escape} = \frac{\sqrt{3}|\vec{r}_{S-A}|}{4}\sqrt{\frac{\mu_A}{\beta\mu_S}} \tag{5.5}$$

As a variety of orbiting regimes with physically meaningful and realistic areas for a lightweight spacecraft are sought, a minimum semi-major axis can be selected from Fig. 5.7. Several trajectories of interest enabled by the SRP perturbation are described in the following sections: a hopper returning to the initial solar longitude Ⓘ, multi-revolution trajectories (II), and the study of the proposed alternating orbiter for coverage of the sub-solar point. An initial semi-major axis of 180 m (*vertical lin*e in Fig. 5.7) has been selected for this last case.

5.2.3.2 Hopper free-return trajectories

The orbiting regime with negative winding numbers Ⓘ requires an inversion of the orbit direction. This can only take place if the eccentricity reaches values equal to or larger than one and the orbit meets the zero-velocity curves, with instantaneous zero angular momentum. Exploiting this fact, it is possible to design trajectories for a hopper that depart from the surface of the asteroid, reach zero-velocity

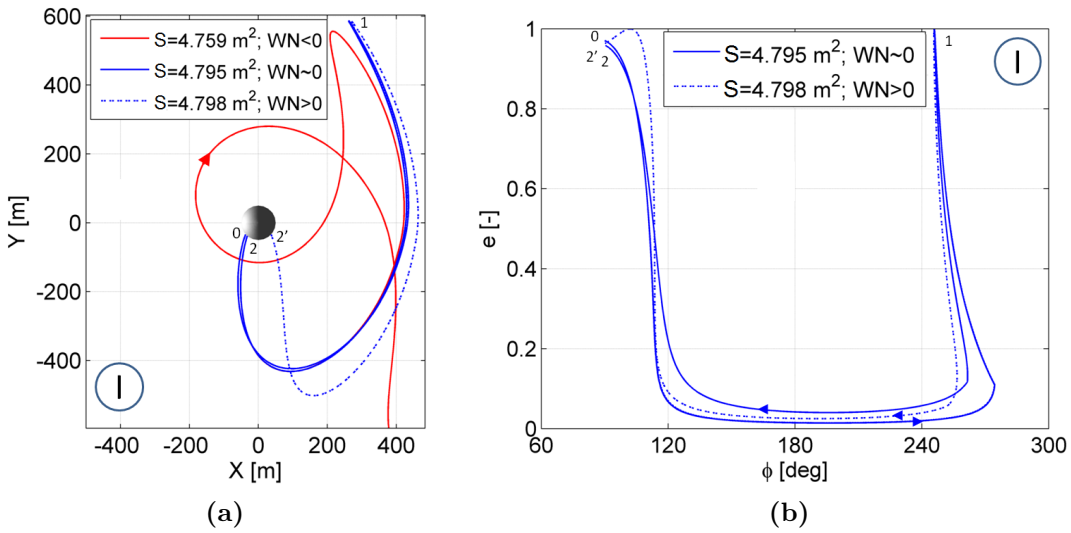

Figure 5.8: Example case with winding number close to 0 for a 225 m initial semi-major axis, in the co-rotating frame (a) and the phase space (b). The orbit direction is inverted at eccentricity 1 (*point 1*). For small variations of the effective area it is possible to obtain trajectories ranging from a hopper returning to the initial solar longitude to escape trajectories.

conditions, and then return back to the surface of the asteroid at the same solar longitude (corresponding to winding number $WN \sim 0$, which can be obtained with a simple Newton iterative method). An example is plotted in Fig. 5.8 (*blue line*) for an initial semi-major axis of 225 m, returning back to the original point after over 80 hours, or more than 20 asteroid revolutions. The left figure shows the sensitivity of the solution for this regime of high SRP perturbation, with an escape trajectory (*red line*) after the orbit direction inversion with the same initial conditions and only 360 cm^2 less effective area.

The trajectory returning to the original solar longitude (*blue solid line*) has however a residual relative horizontal velocity (see Fig. 5.9) when returning to the surface of the asteroid (*point 2*), which may not be well suited to a hopper, if sliding in the asteroid's low-gravity environment needs to be avoided.

Fine tuning the spacecraft area can lead to a trajectory with a second inversion of the orbit direction (eccentricity reaching again a value of 1 at inversion). This trajectory returns to the surface (*point 2'*) in a prograde orbit with the same eccentricity and phase angle as in the initial conditions, and only a vertical component of the relative velocity with respect to the surface (see again Fig. 5.9).

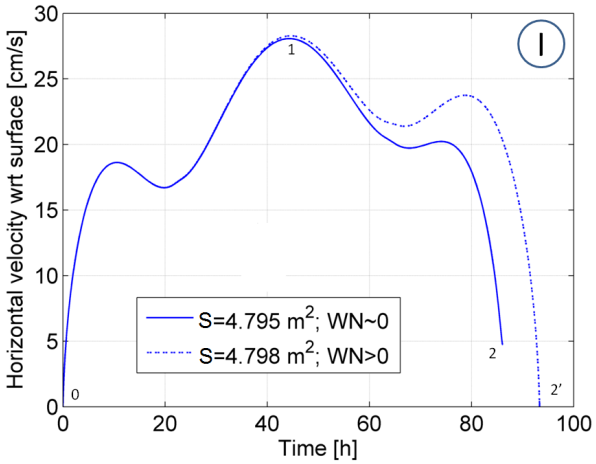

Figure 5.9: Horizontal velocity with respect to the asteroid surface for a returning hopper. Trajectories that depart and return vertically to the asteroid surface can be designed, i.e. trajectories that return with negligible horizontal velocity (*dashed line*).

5.2.3.3 Multiple revolution trajectories

Figure 5.10 presents an extreme case of a trajectory with close to 5 revolutions for a departure semi-major axis of 225 m (point (II) in Fig. 5.7). The evolution of the eccentricity in the phase space clearly follows the behaviour predicted by the Hamiltonian isolines in Section 5.2.1. Similar trajectories could be employed to observe the sub-solar point of the asteroid while at the same time improving the gravity field characterisation of the asteroid. This inspired the trajectories presented in the following section, where a spacecraft reverses the orbiting direction after a number of revolutions.

Such trajectories with a high number of revolutions have however the drawback of experiencing extremely close passes skimming the asteroid surface. In a more realistic case with a full shape and gravitational model, they would likely result in an impact or large subsequent perturbations to the orbit.

5.2.3.4 Alternating orbiter with apocentre manoeuvres

An alternating orbiter that reverses its velocity vector with a small manoeuvre at apocentre after a number of revolutions is now presented. This interesting solution is proposed as an alternative to hovering, and would allow direct overflies of the sub-solar point, and indeed the whole equatorial region. In addition, it

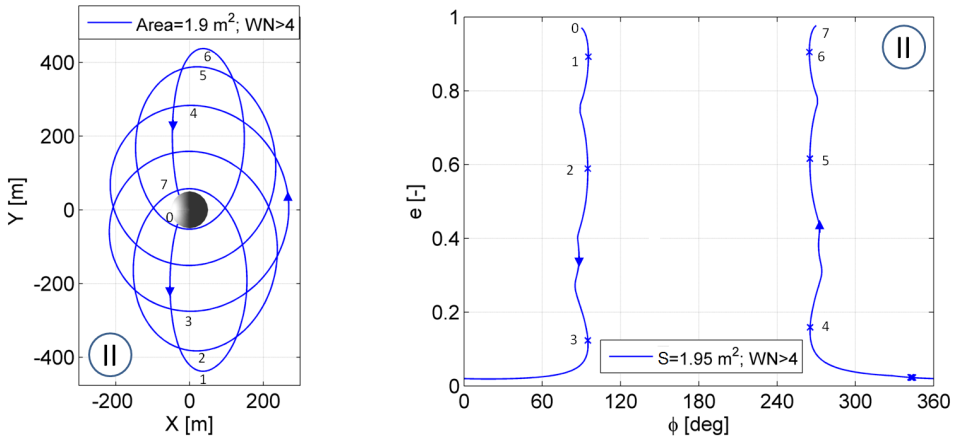

Figure 5.10: Illustrative case for winding number larger than 4 for a 225 m initial semi-major axis, in the co-rotating frame (a) and phase space (b). Trajectories with almost five full revolutions can be obtained. Apocentres are indicated with numbers *1-6* and × *markers* on the right plot.

may improve the characterisation of the gravity field and shape model of the asteroid while at safe distances. The solution consists of symmetric single or multi-revolution trajectories that alternate prograde with retrograde orbits. The trajectories start at apocentre and perform an inversion of the velocity vector at the last apocentre before an impact with the surface. Trajectories similar to that presented in the previous section could also be devised, performing the inversion of the velocity vector two apocentres before impact (from points 2 to 5 in Fig. 5.10) for safety reasons.

Figure 5.11 presents a close-up of Fig. 5.7 around the region of the selected semi-major axis of 180 m. Symmetric trajectories with respect to the X-axis with less than 1 to 4 revolutions (∘, ×, △ *and* □ *markers*) have been identified as possible candidates for the alternating orbiter operational orbit. Symmetry is desirable in order to ensure both inversion manoeuvres of the same size, but it is not a strong requirement. Plots of representative example trajectories for each marker type are also included. Inversion manoeuvres should take place at the marked apocentres. Manoeuvres take place from every 16 hours for the case with less than one revolution, up to every 53 hours for the case with close to four orbits.

The solution with almost one revolution (∘ *marker*) does not provide coverage to the sunlit hemisphere. It could nonetheless be a safe starting orbit to perform

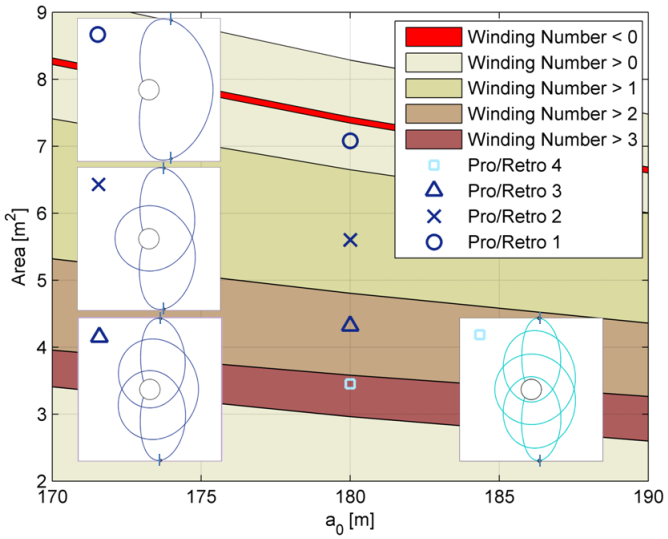

Figure 5.11: For any arbitrarily selected initial semi-major axis symmetric trajectories can be found with one or several revolutions. Alternating orbiter solutions with manoeuvres at the extreme apocentres allow coverage of the whole asteroid equatorial region.

the first characterisation of the asteroid before transferring to one of the multi-revolution options. On the other hand, the solution with close to 4 revolutions (□ *marker*) has again the drawback of very low altitude pericentres, and may not be suitable for a realistic case.

Figure 5.12 presents the intermediate solutions for an alternative orbiter with over one ((a), × *marker*) and over two ((b), △ *marker*) complete revolutions. The trajectories in the co-rotating frame have been numerically propagated until the fifth inversion of the velocity vector with no additional control or correction manoeuvres. Key points in the orbit are indicated both in these plots and on the phase space, where it is possible to observe the almost symmetric behaviour of the Hamiltonian for prograde and retrograde trajectories.

5.2.3.5 Comparison with direct hovering

Assuming there is a requirement to fly over the sub-solar point, the cost of the strategy proposed can be easily compared with more traditional hovering strategies. As already noted, the alternating orbiter solution requires small manoeuvres every 16 to 53 hours. The size of these manoeuvres is small (less than 2 cm/s for each), which would amount to a total cost over a period of one year of 2 to

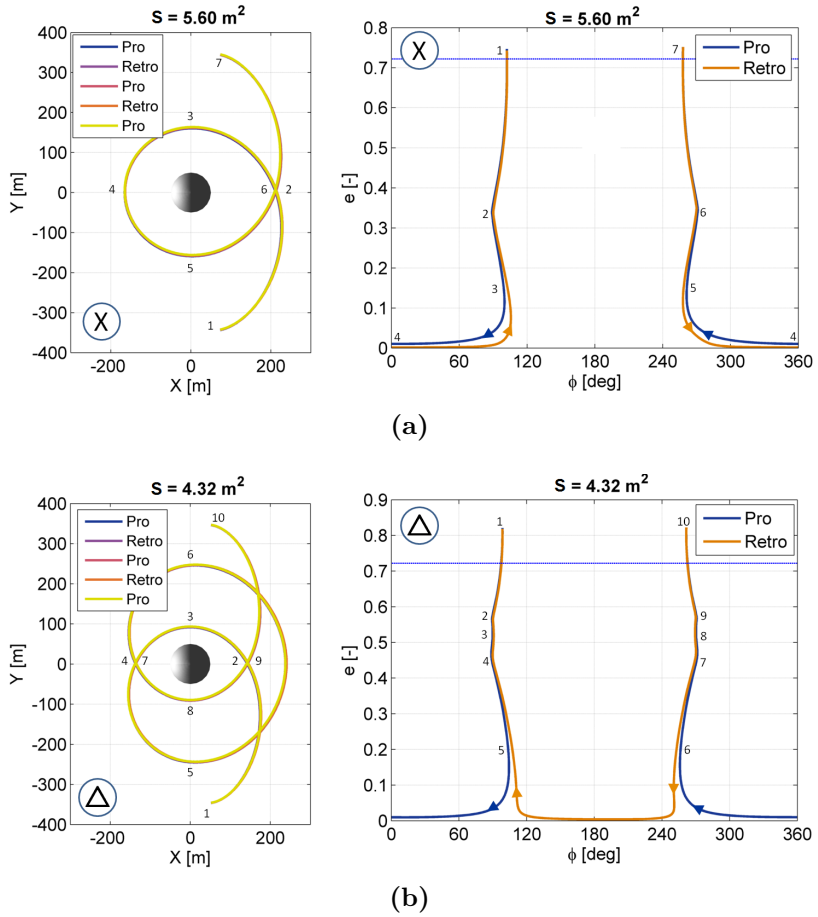

Figure 5.12: Two alternating orbiter solutions with more than one (a) and two (b) revolutions in the co-rotating frame and the phase space. Sub-solar point is covered at distances ranging from 90 to 120 metres.

10 m/s depending on the case. Missions around asteroids are unlikely to perform such long-duration phases, but this period is chosen as reference for comparison, with monthly costs being one twelfth of the reported values. Table 5.1 compares the frequency and size of manoeuvres required, and the total annual fuel costs for three different orbit maintenance strategies.

The first case consists of continuous fixed point hovering in the co-rotating frame at a constant distance over the sub-solar point. In this strategy there are no manoeuvres per se, but a constant acceleration needs to be applied. The total costs over a full year of hovering would be of the order of 50 m/s for a hovering point 200 m above the sub-solar point for an assumed effective area of the spacecraft of 3 m^2, rising to 130 m/s if this distance is halved. The required Δv changes slightly with the spacecraft area, but even assuming no SRP, the annual costs would be over 40 m/s for the 200 m hovering point.

The second set of results corresponds to a simple box control hovering strategy, in which the spacecraft velocity is reversed every time it falls below a certain height. This is a simplified version of the strategy proposed by Scheeres (2012a). Two semi-major axes and three different control box lower height limits have been selected. The eccentricity is calculated using Eq. 5.4, that is, the shape of the orbits selected is similar to the ones used in the alternating orbiter. No SRP perturbation has been taken into account to estimate the frequency and size of the manoeuvres (Keplerian propagation is assumed). Depending on the selected parameters, the size of the manoeuvres ranges from 1.7 to 3.6 cm/s and one manoeuvre is required every 7 to 13 hours. The total accumulated costs over one year would be equivalent to 16 to 31 m/s, lower than for fixed point hovering.

Finally, the estimated costs over a year are presented for the alternating orbiter solution with its 4 cases with varying numbers of revolutions. The manoeuvre size is smaller than the previous case, as all manoeuvres are performed at apocentre, and the frequency is also lower: manoeuvres need to take place only every 16 to 53 hours. The total cost over one year is thus reduced. In the two intermediate cases of interest presented in Fig. 5.12, the total Δv over one year will be between 2.8 and 5.0 m/s.

Table 5.1: Frequency and size of manoeuvres required for each type of control.

	a_0 [m]	S [m^2]	Burn periodicity [h]	Δv One burn [cm/s] (or accel. [cm/s^2])	Annual [m/s]
Hover fix H=100 m	150	3.00	continuous	(4.2×10^{-4})	131.64
Hover fix H=200 m	250	3.00	continuous	(1.6×10^{-4})	50.10
Hover Box H>50 m	150	N/A	9.6	3.48	31.92
	180	N/A	12.9	3.62	24.56
Hover Box H>100 m	150	N/A	8.6	2.46	25.22
	180	N/A	12.0	2.66	19.44
Hover Box H>150 m	150	N/A	7.1	1.74	21.35
	180	N/A	10.7	2.01	16.41
Altern. Orbiter <1 rev	180	7.08	16	1.92	10.52
Altern. Orbiter <2 rev	180	5.60	28	1.61	5.04
Altern. Orbiter <3 rev	180	4.32	42	1.36	2.84
Altern. Orbiter <4 rev	180	3.45	53	1.20	1.98

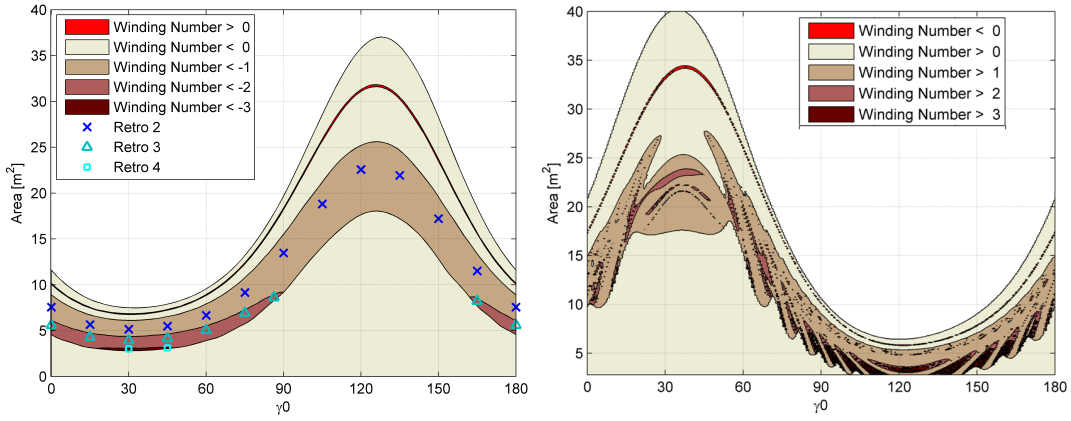

(a) **(b)**

Figure 5.13: Winding number for a retrograde orbiter (a) and a prograde orbit (b) around a rotating ellipsoid, as a function of the initial relative geometry and the area. Symmetric solutions for the retrograde case are indicated with markers.

The benefits of such a strategy are not only lower fuel and operational costs, but also the possibility of direct overfly of other points along the equator (anti-solar point, terminator crossings, etc.), the variation in height over distinct passes, and possibly a better determination of the gravity field and shape model of the asteroid. As the cost of orbit maintenance scales linearly with the asteroid radius, the savings in Δv would increase for larger asteroids. For a 500 m radius asteroid, these costs would be multiplied by 10, and the total Δv savings become significant. However, if there are no requirements on the sub-solar point region coverage, terminator orbits and associated QTO would still be the preferred solution for small asteroids as the required corrections would be negligible when compared to the above strategies. For large asteroids the eccentricity variations are smaller and slower, and other alternative control sequences to ensure the eccentricity is constrained can be devised (Wallace and Broschart, 2013).

5.2.3.6 Effect of higher order gravitational harmonics

Contrary to the case of the point mass or spherical mass distribution, for any irregular shape the spacecraft effective areas required to perform a trajectory with a certain winding number varies with the initial attitude of the asteroid. For the tri-axial ellipsoid model described in Section 5.2.2.2, the winding number for an osculating departure semi-major axis a_0 of 180 m is plotted for different initial γ_0 (defined in Fig. 5.5) for a retrograde orbiter (Fig. 5.13a) and prograde orbiter

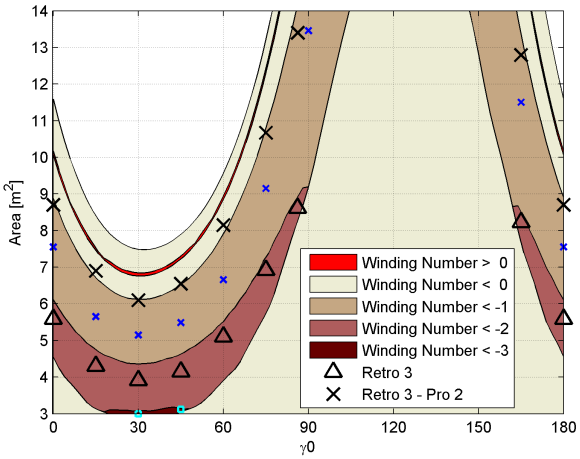

Figure 5.14: Proposed solution combining a 3 revolution retrograde orbit (*black triangular markers*) and a 2 revolution prograde orbit (*black* × *markers*)

(Fig. 5.13b). The retrograde orbits are more stable, as expected. Prograde orbits have wider variations on the winding numbers larger than 2 for small changes in the initial attitude of the asteroid.

The symmetric solutions with more than one revolution that were the basis for the alternating orbiter strategy have been indicated with markers for the retrograde case. In the prograde case only solutions with less than two revolutions can be guaranteed to exist for a wide range of initial conditions.

It is nonetheless possible to combine a retrograde solution with close to 3 revolutions, with a prograde one of close to two. This maximises the number of passes over the sub-solar point (2+1) while avoiding the chaotic behaviour introduced when prograde orbits enter in resonance with the rotation of the asteroid. However, the effective area required for each phase would be different. Figure 5.14 indicates the required areas for the proposed solutions with a 3-revolution retrograde orbit (*black* △ *marker*), and the associated return 2-revolution prograde orbit (*black* × *marker*). The ratio between both areas is of the order of 1.6.

The time between manoeuvres performed at apocentre to reverse the velocity vector is also different for each of the two phases. Figure 5.15 plots one particular case for a starting γ_0 of zero in the co-rotating frame and the phase space. The ellipsoid orientation is plotted at the initial time. The prograde orbit is always further away from the surface of the asteroid, to avoid undesired escape or impact. Two manoeuvres of size 1.52 cm/s are required every 59 hours (one after 36 hours, the other after 22.6 hours), amounting to an annual cost of 4.47 m/s.

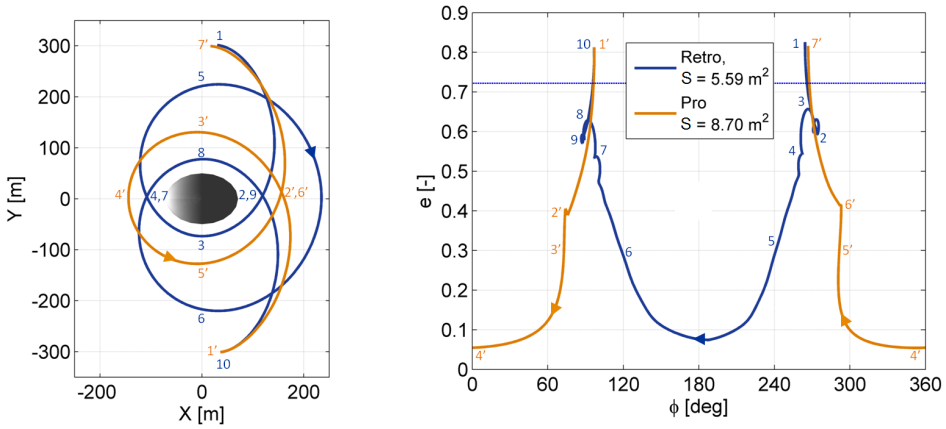

(a) (b)

Figure 5.15: Alternating orbiter for the 3-retrograde / 2-prograde case with an initial γ_0 angle of zero degrees. Plots in co-rotating frame (a) and phase space (b).

Another example solution has been propagated in Fig. 5.16 until the fifth velocity inversion for a different starting γ_0 of 60°. The areas required in this case are 5.1 m^2 and 8.15 m^2 for retrograde and prograde orbits respectively; and two manoeuvres of similar size (1.5 cm/s) are required every 56 hours. There has not been any fine control trying to reduce the errors by modifying the manoeuvres at subsequent apocentre passages. The areas are also kept constant for the two orbiting directions. If finer control is desired, the manoeuvre size and direction could be optimised and the areas could be tuned each revolution to stay as close as possible to the nominal original trajectory with minor extra Δv costs.

Depending on the initial state of the asteroid the size of the manoeuvres ranges from 1.2 to 1.8 cm/s, the total duration of a retro-pro phase can be from 40 to 70 hours and the annual costs are in the range of 3 to 8 m/s. The analysis of an optimal control strategy is out of the scope of this thesis.

5.2.4 Discussion and model limitations

The alternating orbiter strategy introduced represents an alternative solution to the hovering and orbiting solutions around small minor bodies. For certain purposes, these orbits can present advantages in terms of coverage and cost. However, the dynamical models implemented are very simplified and active control strategies have not been implemented or discussed in detail. Further work is required to analyse the stability of these orbits, in particular with more irregular gravity

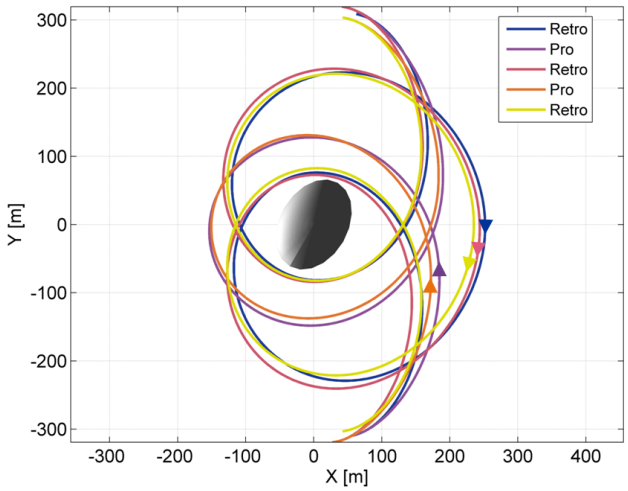

Figure 5.16: Multiple velocity inversions for an alternating orbiter for the 3-retrograde / 2-prograde case with an initial γ_0 angle of 60°.

fields. This section discusses the limitations of the models and possible extensions for detailed analysis.

The trajectories analysed correspond to orbits with zero inclination, assuming the equator of the asteroid coincides with the orbital plane of the asteroid around the Sun. These trajectories remain in the same orbital plane, as there are no external out-of-plane forces. However, the propagation tools coded can handle 3-dimensional trajectories, and extension to out-of-plane motion is possible. Various tests show that the evolution of eccentricity e and phase angle ϕ follows the same pattern (e decreasing for prograde orbits with $\phi < 180°$ and increasing for $\phi > 180°$) for trajectories with inclinations as high as 60°. The evolution of the inclination has a similar behaviour, decreasing for $\phi < 180°$ and increasing for $\phi > 180°$ in prograde orbits. A full problem extension to out-of-plane dynamics is left for future work.

One of the most significant simplifications in the model is considering the orbit of the asteroid around the Sun as being circular. However, if the time the spacecraft remains in the alternating orbiter configuration is small, the effect of the asteroid orbit eccentricity is small and can be counteracted by tuning each inversion manoeuvre. For long term orbit maintenance however, higher fidelity models including the eccentricity of the orbit need to be implemented, such as the eccentric augmented normalised Hill three-body problem (Lantoine et al., 2013). Additional gravitational perturbations, in particular more complex and irregular

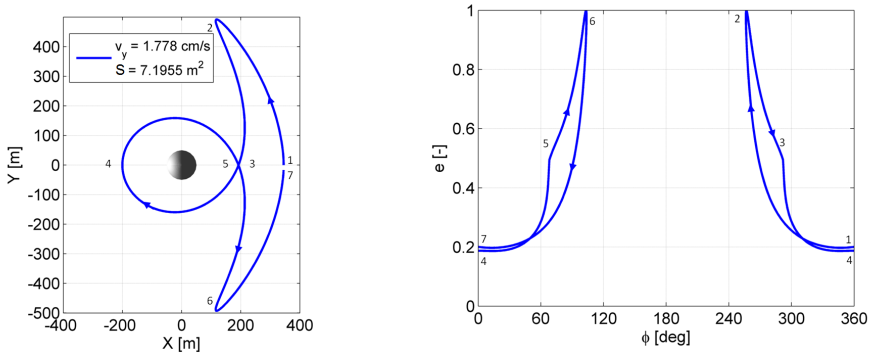

(a) (b)

Figure 5.17: Planar symmetric periodic solution in a co-rotating synodic frame (a) and phase space (b).

shapes and mass distributions, as well as different rotational states, would need to be analysed on a case-by-case basis for each particular asteroid.

5.3 Symmetric solutions

Motivated by the natural inversion of the orbit direction that takes place for areas in the red "chaotic" region in Fig. 5.7, a grid search was performed for solutions that feature two or more of these natural inversions and return to the initial departure point. Solutions departing from the positive X-axis with a given perpendicular velocity along the Y-axis v_y were sought, optimising the required surface area S to obtain a closed orbit.

These solutions represent closed periodic orbits contained in the orbital plane of the asteroid that perform part of the rotation in the prograde direction and part in the retrograde direction. They are symmetric with respect to the X-axis in a synodic frame co-rotating with the asteroid around the Sun. Fig. 5.17 plots one such solution for the 50 m diameter asteroid analysed in Section 5.2. It displays two natural inversions of the orbit direction when the eccentricity reaches the value of 1 (see phase space plot in Fig. 5.17b). The total period of the orbit is 67.2 hours and the spacecraft spends over 12 hours at altitudes lower than 160 m. Another interesting characteristic of this solution in particular is that the spacecraft performs the inner loop in a retrograde direction, and the outer loop in a prograde direction. This hints at the possibility of finding similar orbits in a more complex model with non-sphericity perturbations, as retrograde orbits were

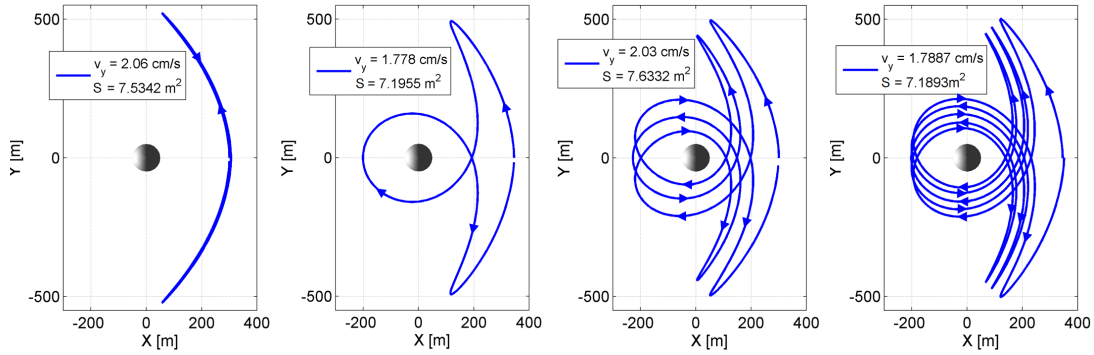

Figure 5.18: Families of solutions in a co-rotating synodic frame.

least affected by the non-sphericity of a rotating asteroid (assuming prograde rotation of the asteroid).

A wider range of solutions are shown in Fig. 5.18, with different numbers of orbit direction inversion points. The first two classes of orbits were identified as members of the a and g' families described by Hénon (1969). These families of orbits are a well-known set of solutions of the Circular Restricted Three Body Problem (CR3BP), and of the Hill problem (see Section 2.2.2), as one of its limiting cases. In particular, the top branch of Hénon's g' family greatly resembles the type of orbits with one loop and two inversions that were found in this preliminary search.

5.3.1 Families of planar symmetric periodic orbits in the CR3BP and the Hill problem

In his 1969 paper, Hénon explored families of symmetric periodic orbits in the planar case of the CR3BP for a very small secondary (limiting case of Hill). Hénon concentrated on simple-periodic cases (orbits with only two crossings of the x-axis), although the aforementioned branch of the g' family has 4 crossings and is thus double-periodic according to Hénon's own definition. N-periodic orbits, or orbits of multiplicity N, are defined as orbits with 2N crossings of the x-axis. With this definition, the type of trajectories presented in Fig. 5.18 are simple-periodic, double periodic, 5-periodic, and 8-periodic (2, 4, 10 and 16 crossings of the x-axis respectively). Hénon systematically mapped the planar problem, studied the in-plane stability, and cross-checked the validity of previous solutions reported by Hill himself, Lord Kelvin, Jackson and the outputs of the more thorough searches by Matukuma (1930, 1932, 1933).

These families have been extensively studied but are still of great interest. Besides the references used by Hénon in his classical series of papers, other authors came across orbits of the a, g and g' family, albeit for different mass ratios. Darwin (1897) generated an incomplete map of various classes of orbits for a mass ratio of 1/11 (a fictitious Sun–Jupiter case with a much larger mass for Jupiter), which corresponds to sections of the $g - g$' family. Broucke (1968) presented results for orbit families in the Earth–Moon system. Szebehely and Nacozy (1967) worked on these same sets of periodic obits. Szebehely's book *Theory of Orbits* (Szebehely, 1967) indeed remains to date a classic reference with an extensive study on different families in the CR3BP, mostly for equal masses (the so-called Copenhagen problem), but also reviewing and completing Darwin's and Broucke's work. Hénon also studied, prior to the Hill problem, planar symmetric families in the Copenhagen problem as the other limiting case of the CR3BP (Hénon, 1965). In fact, the naming convention assigning letters for the orbit families actually spawns from the nomenclature Strömgren introduced for families of solutions for the Copenhagen problem decades before (Strömgren, 1922).

Hénon continued studying the vertical stability in the equal masses case (Hénon, 1973a) and the Hill problem (Hénon, 1973b). Michalodimitrakis (1980) extended this work by studying some 3-dimensional families of orbits branching off from the vertical critical orbits in the planar case. Perko (1982) established the existence of the families a, c, f, g, g', g"... for the case of small mass ratio $\mu > 0$, although it had already been established that they existed for larger mass ratios. He overlays his families over Hénon's, showing their similarity. An additional paper of Hénon (2003), in which he came back to the same problem after over 30 years, expanded his search to orbits of higher multiplicity. A few years later, Hénon (2005) revisited once more the Hill problem to study asymmetric periodic solutions.

Finally, Lara and Russell (2006) performed a comprehensive review of the g family for different mass ratios (explaining and comparing, among others, Darwin's (1897) results for the fictitious Sun–Jupiter case or Broucke's (1968) for the Earth–Moon system), and analysed applications of planar and three-dimensional periodic orbits for a Jupiter–Europa mission (Lara et al., 2007; Russell, 2006). Very recently, two papers by Batkhin (2013a,b) presented an algorithm with regularised coordinates to systematically obtain all families of orbits reported by Hénon for the Hill problem and a set of additional families including multiple collisions with the secondary body. In conversations with Verrier (2013) to discuss

the branching and connections between two-dimensional and three-dimensional families, she reported that she was studying families of period-doubling bifurcations from halo orbits for the Earth-Moon mass ratio (which she denotes U1 and U2), that resemble planar g' orbits. She reports a connection with the g' family and has proved the existence of this connection also in the Hill problem.

5.3.2 Extending Hill problem with a radiating primary

Hill's limiting case of the CR3BP is particularly suited to the study of asteroids, as the mass of the asteroid can be considered negligible with respect to the Sun, leading to very low mass ratios. However, SRP plays an important role around these minor bodies. Its effect on the well-known symmetric periodic orbit solutions of the CR3BP has not been studied in detail.

Approaching the classical photo-gravitational CR3BP (see section 2.3.1), Papadakis (1996) studied the evolution of planar symmetric families in the equal masses case (Copenhagen problem) with two radiating bodies. This approximation has interesting applications in the study of accretion disks around binary stars. Markellos et al. (2000) studied the limiting case of Hill for different configurations of the radiating bodies, and later analysed the evolution of families of periodic orbits up to high multiplicity (16-periodic) and their stability (Kanavos et al., 2002). A more comprehensive analysis using regularised coordinates and covering symmetric periodic orbits up to multiplicity 81 can be found in Papadakis (2006). These studies limit themselves though to modest solar radiation pressure perturbation, applicable to a star–planet case, but falling short for the case of asteroids.

A simple model of the extended Hill problem with solar radiation pressure allows the study of the evolution of Hénon's simple and double-periodic families with SRP increasing from the classical Hill problem to levels characteristic of current and future planned missions to minor bodies.

5.3.3 Symmetric periodic orbit families evolution

Recalling the photo-gravitational Hill problem equations of motion (Eq. 2.14), and neglecting eclipses at this stage:

$$\begin{cases} \ddot{\xi} &= 2\dot{\eta} + 3\xi - \frac{\xi}{(\xi^2+\eta^2+\zeta^2)^{3/2}} + \beta' \\ \ddot{\eta} &= -2\dot{\xi} - \frac{\eta}{(\xi^2+\eta^2+\zeta^2)^{3/2}} \\ \ddot{\zeta} &= -\zeta - \frac{\zeta}{(\xi^2+\eta^2+\zeta^2)^{3/2}} \end{cases} \tag{5.6}$$

They are invariant under the following symmetries (Miele, 2010; Villac, 2003):

$$\begin{array}{lrcl} \Sigma_1: & (\zeta, \dot{\zeta}) & \leftrightarrow & (-\zeta, -\dot{\zeta}) \\ \Sigma_2: & (t, \eta, \dot{\xi}, \dot{\zeta}) & \leftrightarrow & (-t, -\eta, -\dot{\xi}, -\dot{\zeta}) \\ \Sigma_1\Sigma_2: & (t, \eta, \zeta, \dot{\xi}) & \leftrightarrow & (-t, -\eta, -\zeta, -\dot{\xi}) \end{array} \tag{5.7}$$

All symmetries with respect to the η-axis are lost. The first symmetry is just an inversion of the third coordinate, indicating that a mirror trajectory with respect to the $\xi\eta$-plane always exists. From the last two symmetries, which comprise a time inversion, if a trajectory satisfies either of the two following conditions at two different times, the resulting orbit will be periodic:

$$\begin{array}{l} (\eta, \dot{\xi}, \dot{\zeta}) = 0 \\ (\eta, \zeta, \dot{\xi}) = 0 \end{array} \tag{5.8}$$

The first condition translates into finding two perpendicular crossings of the $\xi - \zeta$ plane, and corresponds to three-dimensional periodic families that are out of the scope of this chapter, but are covered in detail in Giancotti et al. (2014).

Assuming a planar trajectory ($\zeta = 0$), the second condition implies finding two perpendicular ($\dot{\xi} = 0$) crossings of the ξ-axis. This property is used in this section to find periodic orbits in the extended Hill problem with SRP. Initial conditions are selected as a perpendicular crossing point of the ξ-axis with arbitrarily positive $\dot{\eta}_0$. Trajectories are integrated with a Runge-Kutta solver of order 4-5 (Dormand and Prince, 1980) and the initial value of $\dot{\eta}_0$ is optimised with a Sequential Quadratic Programming optimisation algorithm (Nocedal and Wright, 2006) as implemented in MATLAB's internal functions *ode45* and *fmincon*. The stopping conditions are selected as a second perpendicular ξ-axis crossing, with tolerance on the perpendicularity boundary constraint $\dot{\xi} = 0$ of 10^{-9}. In order to avoid orbits with N-multiplicity higher that 2, trajectories with more than one ξ-axis crossing before reaching the stopping condition are discarded.

5.3.3.1 The *a* and *g-g'* families in the original Hill problem

The former equations of motion reduce to the classical Hill problem (see Section 2.2.2) when equating the lightness number β' to zero. This set of equations does not depend then on any additional parameter. The same planar periodic families of orbits symmetric with respect to the ξ-axis were reproduced using Hénon's reported values as initial guesses.

The families in the vicinity of the L_2 region are of particular interest due to their possible application to small asteroid exploration. With the introduction of SRP, this region is reduced in size and is closer to the secondary, while the L_1 point migrates far away in the direction of the radiating primary and its associated families of orbits are thus of less interest for close observations of an asteroid. Only simple-periodic families (and a double-periodic branch) were considered as in the original paper by Hénon. Figure 5.19 represents for reference the traditional Hill problem solution map in the $\Gamma - \xi_0$ space, with ξ_0 representing the initial position along the ξ-axis. The shaded patches represent the forbidden region, given by $\Gamma > 3{\xi_0}^2 + 2\beta'\xi_0 + 2/\xi_0$. An orbit in these regionn would require negative kinetic energy.

Figure 5.20 presents examples of orbits for the three families analysed: family *a* (more commonly referred to in literature as planar Lyapunov orbits (a)), originating from L_2; family *g* (b), also termed Distant Prograde Orbits (DPOs), evolving from large ribbon-type orbits to circular orbits of decreasing size around the secondary; and subfamily *g'* (c), emanating from a bifurcation point (*black dot marker*) and including oval-shaped orbits near the bifurcation (*right*) and double periodic orbits (with 4 intersections with the horizontal axis, *left*) after a collision with the secondary (*black + marker*). This section follows closely the *a* family in the $\Gamma - \xi_0$ space. Below the bifurcation point the *g'* oval orbits continue extending towards the left until their shape starts deforming with ribbon-like loops again until a second collision point with the secondary at $\xi_0 = 0$. The *g'* family branch shown in the negative Γ quadrant corresponds to the second crossing of the double periodic *g'* orbits aforementioned. Families *f* and *c* have been included in the plot for completeness. They consist of the sometimes called Distant Retrograde Orbits (DROs), and planar Lyapunov orbits around L_1 (the symmetric equivalent to family *a* for L_2) respectively. They will not be the focus of this section, though, as their distance to the secondary increases rapidly with

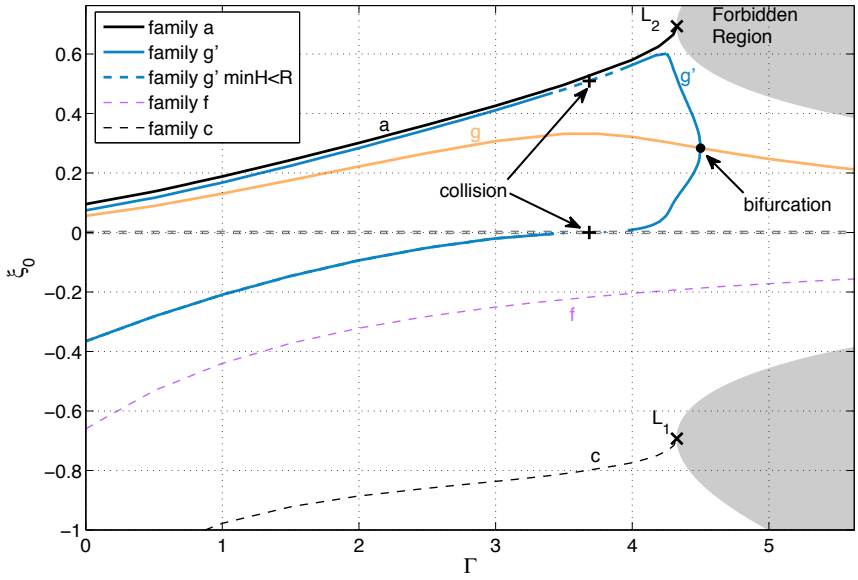

Figure 5.19: Solution map of the symmetric periodic families in the original Hill problem

lightness number, and thus their usefulness is limited for asteroid observation. From this point on, only the positive plane is plotted.

Some of the orbits would intersect the secondary if it is not considered a point mass. The asteroid radius (assumed a spherical body) in scaled coordinates ϱ, independent of the size of the secondary, is fixed for a given density ρ and heliocentric distance d:

$$\varrho = \frac{1}{d}\sqrt[3]{\frac{3\mu_S}{4\pi\rho G}} \tag{5.9}$$

where G is the gravitational constant.

Family g' orbits intersecting the secondary body surface for an average asteroid density of 2.6 g/cm^3 (Chesley et al., 2002) and a heliocentric distance of 1 AU are indicated with a dashed blue line in Fig. 5.19. It is not surprising that these regions contain the collision points.

5.3.3.2 Evolution with lightness number

By means of a continuation method, the value of β' is increased up to lightness numbers characteristic of asteroid missions. For currently flying and planned minor body orbiters the scaled lightness number β' is usually of the order of 20-30 (Scheeres, 2012d). An extreme case with a β' value of approximately 684 is

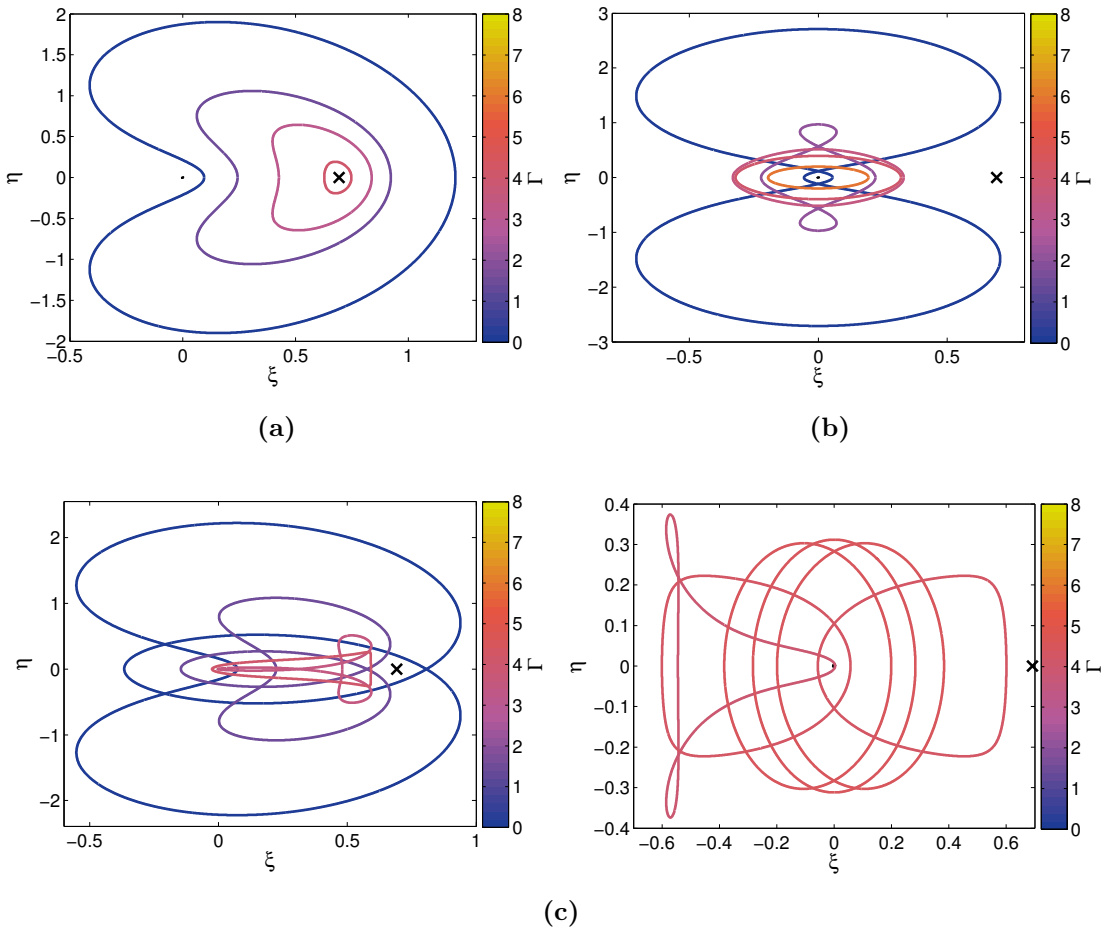

Figure 5.20: Families a (a), g (b) and g' (c), split in two, in the Hill problem with no SRP. A *black* $\times$ *marker* indicates the position of the L_2 point.

also considered (corresponding to a small 50 m radius asteroid at 1 AU, average asteroid density of 2.6 g/cm^3, 100 kg spacecraft mass and 8 m^2 effective area, similar to the cases studied for the alternating orbiter in Section 5.2).

Figure 5.21 shows the evolution of the families with positive ξ_0 with increasing β'. Dashed sections of the families correspond to orbits intersecting the secondary body surface for average NEO asteroid and distance of 1 AU. The horizontal grey dashed line indicates the scaled radius of the secondary. As the lightness number increases, the L_2 point position on the ξ-axis decreases, while its Jacobi constant Γ increases. The bifurcation point of the $g - g$' families disappears immediately for small lightness numbers resulting in two unconnected families (in the plane, there could still be connections through intermediate three-dimensional families). This bifurcation disappears as well in the CR3BP for the case of very small μ, as reported by Perko (1982) and shown for the case of the Jupiter-Europa system by Russell (2006). However, the connection of the branches of the families in the case of small μ is exactly the opposite of the case here presented.

Arbitrarily, the g family was assumed now to contain the branch of the original g family left of the bifurcation point, and the branch of the original g' family to the bottom of the bifurcation point (see Fig. 5.21). The g' family now contains the top branch of the original g', which includes the collision point and the double-periodic section, and the right branch of the original g family including decreasingly smaller orbits around the secondary. The new g family reduces its size and the maximum ξ_0 crossing decreases rapidly. It then disappears for large lightness numbers. The right branch of the new g' family on the other hand quickly tends to skirt the border of the forbidden region, tending to linear degenerate orbits along the ξ-axis. Meanwhile, the collision point that separates the simple and double periodic portions of the new g' family migrates towards the L_2 point.

This behaviour is similar to the one observed in the study of radiating equal masses (Papadakis, 1996), and continues the results obtained in Kanavos et al. (2002) for small lightness numbers up to 0.33.

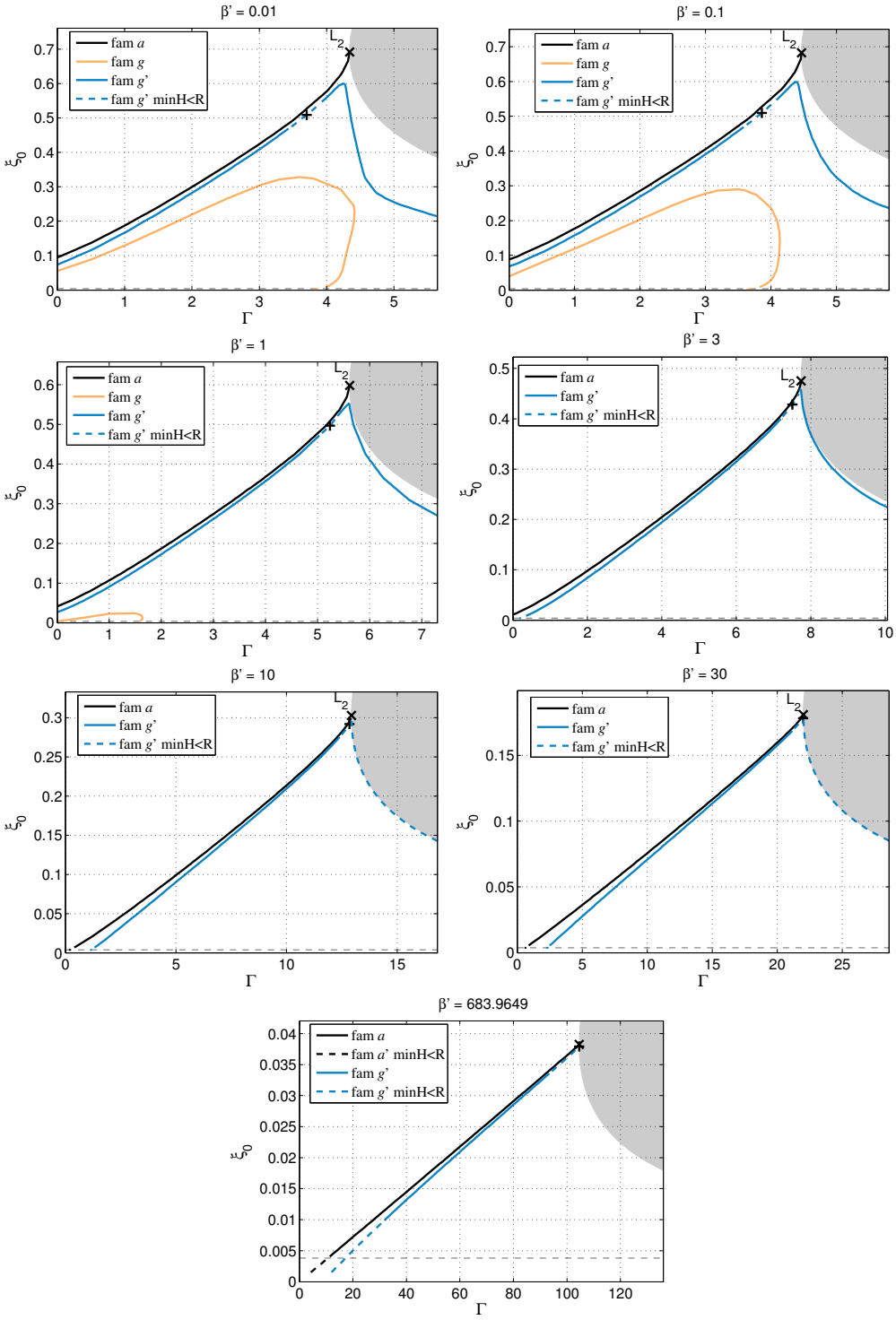

Figure 5.21: Solution map evolution with increasing lightness number β'. The dashed horizontal line shows the radius of the secondary assuming average NEO density and 1 AU distance from the Sun.

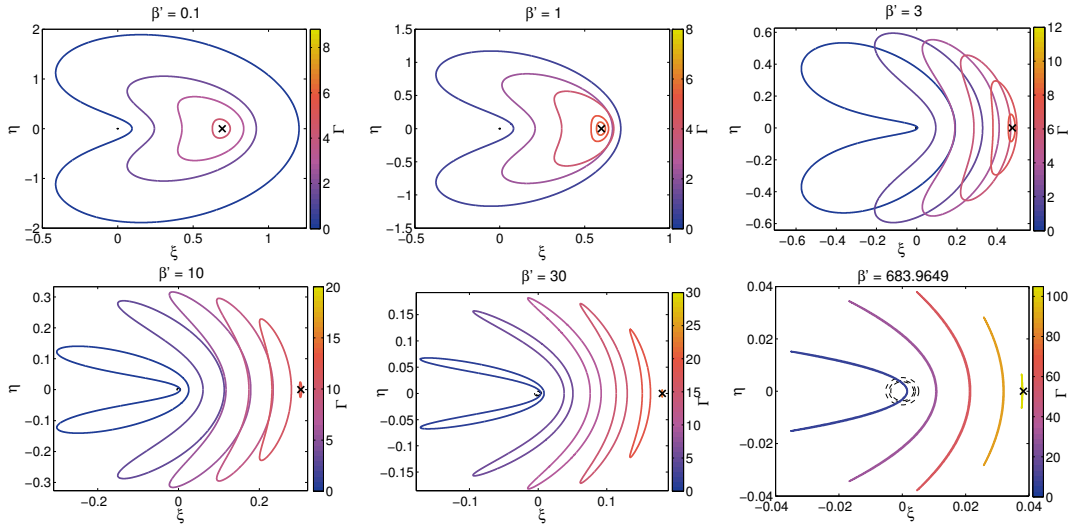

Figure 5.22: Family a evolution with increasing lightness number. *Dashed black circles* indicate the asteroid surface for densities of 1, 2 and 3 g/cm^3 and 1 AU distance from the Sun.

Family *a*

Figure 5.22 shows the evolution of the a family from bean-shaped to boomerang-like orbits. To easily display possible intersections with the surface of the secondary, dashed grey circles represent the asteroid surface for densities of 1, 2 and 3 g/cm^3 (circles of decreasing size as the density grows), assuming a heliocentric distance of 1 AU. They are mostly noticeable for the extreme case with high SRP.

Family *g*–*g'*

Figure 5.23 plots orbits of the left branch of the g' family up to the maximum value of ξ_0 crossing for various Jacobi constants. This includes the double periodic branch left of the collision point along with several oval-shaped simple periodic orbits.

Figure 5.24 plots orbits of the right branch of the g' family from the maximum value of ξ_0 crossing for various Jacobi constants. In the case of no SRP (see Fig. 5.20c, right), family g' continued with oval-shaped orbits oriented towards the left until the collision point at $\xi_0 = 0$. In Fig. 5.24, the branch now includes the former part of the g family which consisted of direct orbits around the secondary of reducing size. With increasing lightness number β', this branch tends towards degenerate linear orbits along the ξ axis.

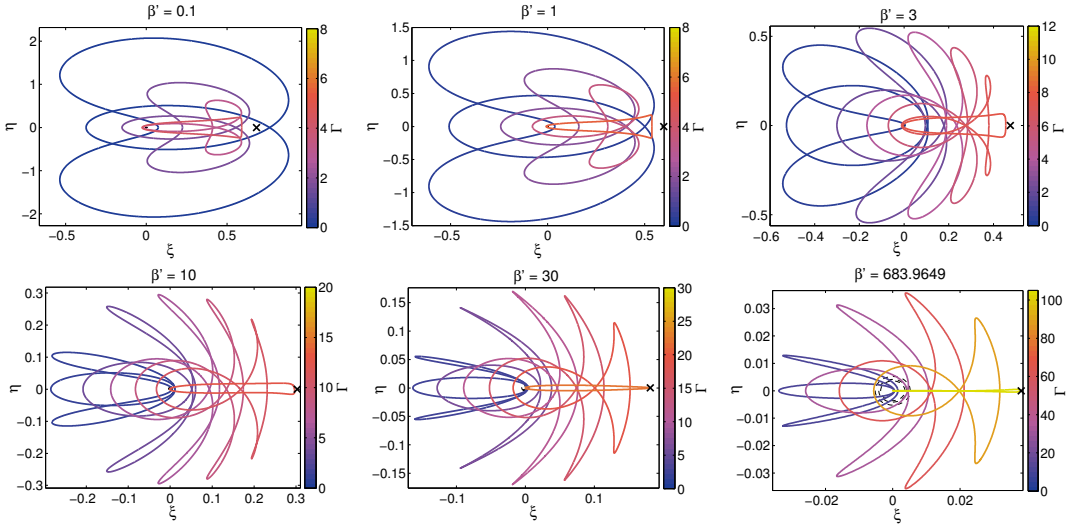

Figure 5.23: Family g' left branch evolution with increasing lightness number. *Dashed black circles* indicate the asteroid surface for densities of 1, 2 and 3 g/cm^3 and 1 AU distance from the Sun.

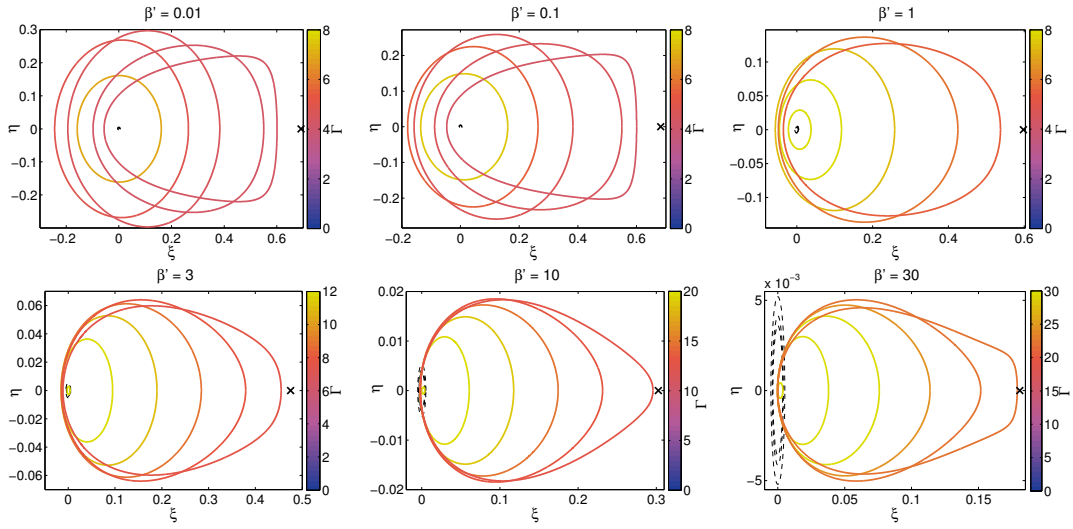

Figure 5.24: Family g' right branch evolution with increasing lightness number. *Dashed black circles* indicate the asteroid surface for densities of 1, 2 and 3 g/cm^3 and 1 AU distance from the Sun.

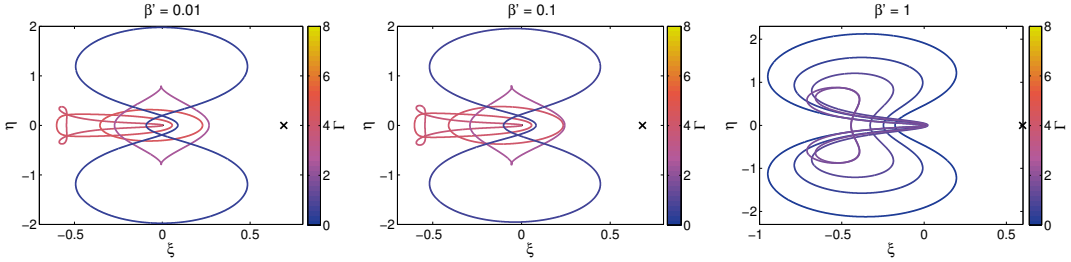

Figure 5.25: Family g evolution with increasing lightness number

Finally, Figure 5.25 plots orbits of the g family for various Jacobi constants. Family g now transitions from the ribbon-type orbits in the original g family to the left-extending oval-shape orbits in the original g'. For a lightness number of 1 the orbits transition between the two ribbon-type orbits without an oval-shape phase.

5.3.4 Application to small asteroids

The above results are an extension of the generic Hill problem with solar radiation pressure, of interest by itself as a dynamical system, and applicable to a variety of problems. When used to model the dynamics of a spacecraft around a small minor body or asteroid, some of the families cease to exist or are significantly modified when the asteroid is not considered as a point mass, due to intersections with the asteroid surface, or eclipses. The influence of considering a spherical asteroid is more relevant for higher lightness numbers.

5.3.4.1 Feasibility considering physical constraints

The feasibility of some branches of the reported families is questionable when physical constraints such as the body radius are considered. The right section of the new g' family appears to always intersect the asteroid surface for any realistic density at high lightness numbers (see dashed circles in Fig 5.24). It is particularly noticeable for the bottom right plot.

In Fig. 5.26 the maximum pericentre height for the right branch of the new g' family and the maximum ξ_0 crossing of the g family have been plotted as a function of the scaled lightness number. Horizontal lines indicate radius of the secondary for different densities ranging from 1 to 7 g/cm^3, this last density much larger than the expected values for minor bodies. The distance between the asteroid and the Sun is assumed again to be 1 AU. For lightness numbers higher than 8 the whole right branch of the g' family intersects the surface. The lightness number for a few representative asteroid missions are also indicated, showing that only for missions to very large asteroids such as Eros, where low lightness numbers are realistic, is this right branch feasible.

The maximum crossing of the g family decreases even more rapidly, falling below the asteroid surface already for values as low as 2. This would render both these

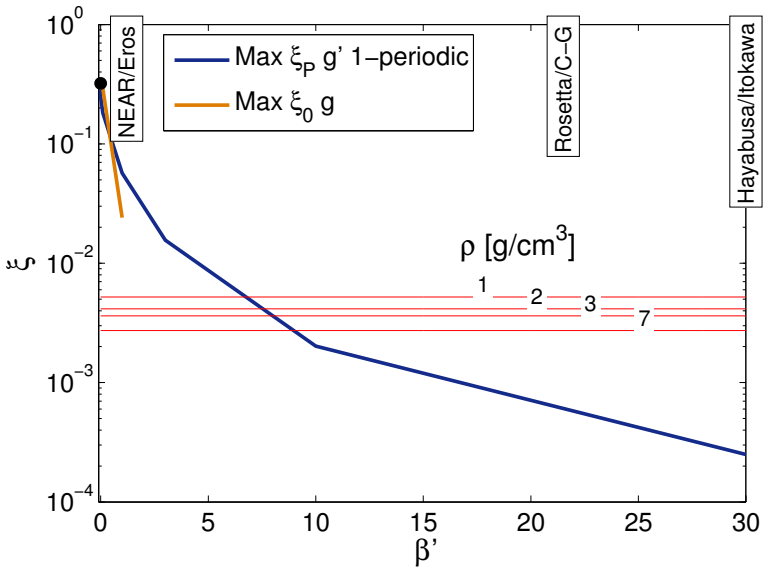

Figure 5.26: Maximum pericentre height of the simple-periodic g' branch and maximum ξ_0 crossing of the g family. For large β' they fall below the body surface. Horizontal lines indicate radius of the secondary for different asteroid densities ranging from 1 to 7 g/cm^3.

family sections unusable for the small bodies that are targeted by future missions such as Hayabusa 2 or OSIRIS-REx.

5.3.4.2 Effect of eclipses

The consideration of the secondary as a spherical asteroid instead of a point mass has an additional implication on the dynamics due to eclipses. All trajectories of the a and $g - g$' family have portions of the orbit in eclipse, and these last a larger portion of the orbit the larger the lightness number (as can be observed in Figs. 5.23 and 5.24).

Modifying the solar radiation pressure term assuming a simple cylindrical shadow, Eq. 5.1 can be given in scaled coordinates:

$$\left.\begin{array}{r} \xi > 0 \\ \\ \eta^2 + \zeta^2 < \varrho^2 \end{array}\right\} \implies \beta' = 0 \tag{5.10}$$

and in the planar case the second condition reduces to $\eta < \varrho$. The a and g' families were recalculated for high lightness numbers with the addition of eclipses. A distance of 1 AU and an average asteroid density of 2.6 g/cm^{3}are again assumed to fix the size of the asteroid.

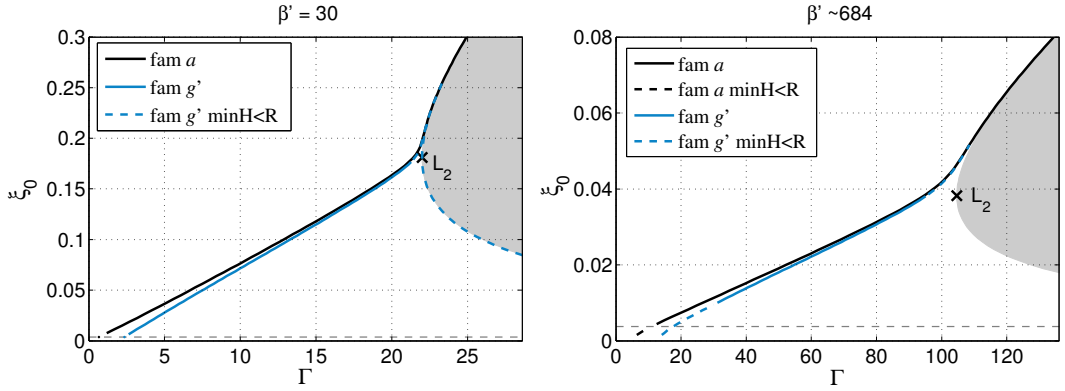

Figure 5.27: Solution map for the numerical propagation with eclipses. The *dashed horizontal line* shows the radius of the secondary assuming average NEO density and 1 AU distance from the Sun.

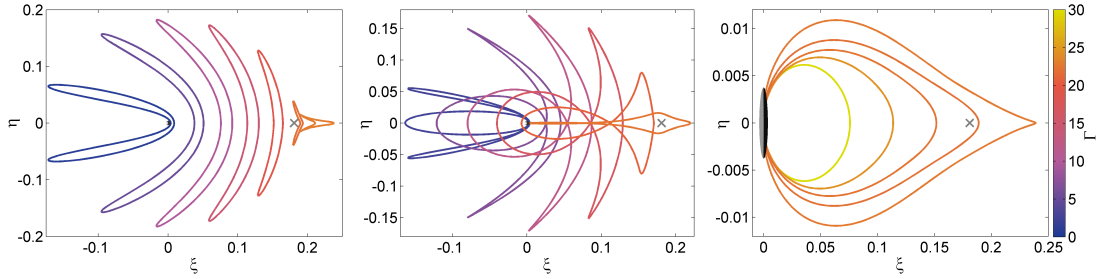

Figure 5.28: Evolution of families a, and g' left and right branches with eclipses. Lightness number $\beta' = 30$.

This modification of the SRP term conserves the symmetries in the model, and, as such, the method to obtain periodic orbits is still valid. However, it introduces a discontinuity in the dynamics, which modifies the solution space. The solution map is plotted in Fig. 5.27 for the cases with high lightness number $\beta' = 30$ and $\beta' \sim 684$. Both families extend beyond the theoretical L_2 point without eclipses, skirting the forbidden region, and the shape of the orbits dramatically changes for the cases spending a considerable time in eclipse (see Figs. 5.28 and 5.29).

5.3.5 Stability of *a* and *g-g'* families of periodic orbits

In previous sections, some orbit family branches have been shown to be unfeasible or non-existent for large lightness numbers. On the other hand, for the feasible branches and families, the stability of the periodic orbits needs to be taken into consideration to have usable and practical orbits for asteroid exploration. Ac-

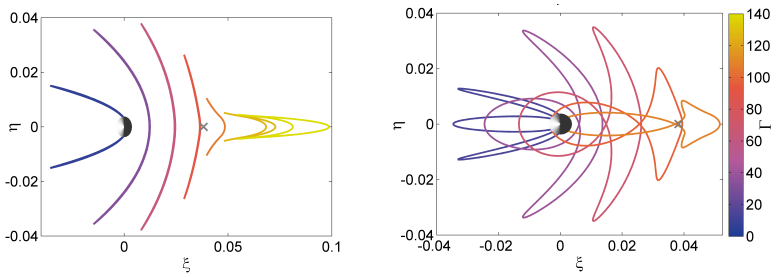

Figure 5.29: Evolution of families a, and g' with eclipses. Extreme case of $\beta' \sim 684$.

cording to Hénon (1969), in the original Hill problem without SRP all a orbits and all g' double periodic are unstable, with two small sections of stable orbits in the simple-periodic branch.

In order to calculate the linear stability using Floquet theory, the state transition matrix is integrated together with the state vector along the trajectory for one orbital period (Scheeres, 2012e). The monodromy matrix Φ_M is then obtained by mapping the transition matrix after one revolution to the selected surface of section. The symmetries of the problem and the choice in initial conditions (a perpendicular crossing point of the ξ-axis with positive $\dot{\eta}_0$) implicitly select $\eta = 0$ as the surface of section. This results in a reduced state vector $\vec{\rho}* = (\xi, \zeta, \dot{\xi}, \dot{\zeta})$ in which the η and $\dot{\eta}$ coordinates have been eliminated.

For the problem at hand the monodromy matrix results in a sparse 4×4 matrix, where the in-plane and out-of-plane dynamics are decoupled. It can then be split into two 2×2 matrixes and the stability for each type studied separately. The simplified condition for linear stability is then given by $|Tr(\Phi_{M,2\times2})| < 2$ (Scheeres, 2012e).

With this stability criteria, family a remains always highly unstable, as was the case when solar radiation pressure was not introduced. The stability index (trace of the 2×2 monodromy matrix) is over two orders of magnitude larger than 2.

Orbits in family g' present more interesting properties, with points of critical stability and in the worst case regions of mild instability (the stability index remains close to 2). Figures 5.30 and 5.31 present the stability index for family g' as a function of the ξ_0 crossing scaled with the ξ position of the L_2 point. In the plots, orbits are stable for a stability index between -2 and 2. For the left branch of family g', including the double-periodic section, orbits are mostly in-plane unstable for low lightness number, but become stable as the lightness

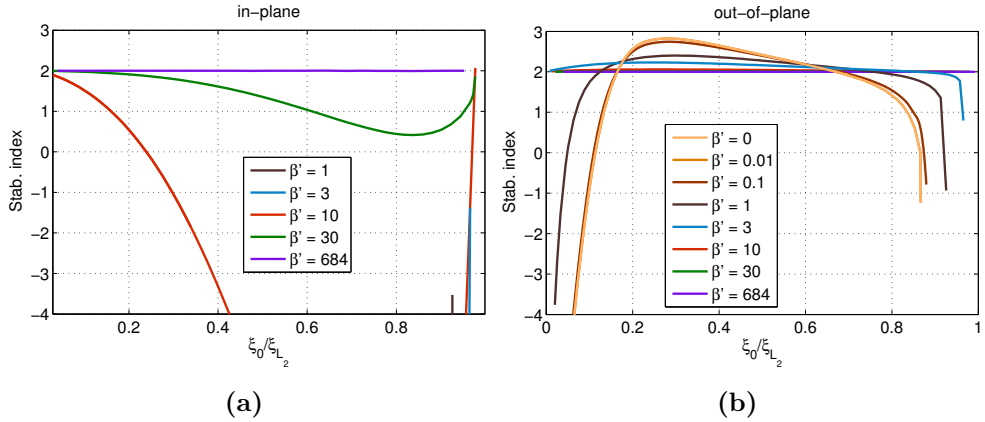

(a) **(b)**

Figure 5.30: Stability of family g' left branch, in-plane (a) and out-of-plane (b)

number increases towards realistic values close to 30 (see Fig. 5.30a), with the extreme case of large lightness numbers tending towards a stability index equal to 2. Conversely, when considering out-of plane stability (see Fig. 5.30b), the family displays somewhat opposite behaviour: it presents regions of stability for low lightness numbers for certain ranges of ξ-axis crossings. It becomes unstable though as the lightness number increases, and the extreme case tends again to a stability index equal to 2.

On the other hand, the right branch of family g', which is always simple-periodic, seems stable for most of the range when the lightness number is not zero, both in-plane and out-of plane (see Fig. 5.31). That is also the case in the original Hill problem, and it is not surprising as this branch comprises quasi-circular orbits of reduced size around the secondary. Regrettably, these orbits intersect the surface of the secondary for large lightness numbers, questioning their applicability for asteroid exploration. Note also that the behaviour of this branch without SRP is intrinsically different for low ξ_0 crossings, as it includes a different section of the $g - g$' family.

The region of stability around the $g - g$' family is nonetheless very narrow in the Hill problem, as shown in the Poincaré section in Simó and Stuchi (2000). This behaviour is unfortunately unaffected with the introduction of SRP, and the stable regions are surrounded by a chaotic region which includes escape trajectories.

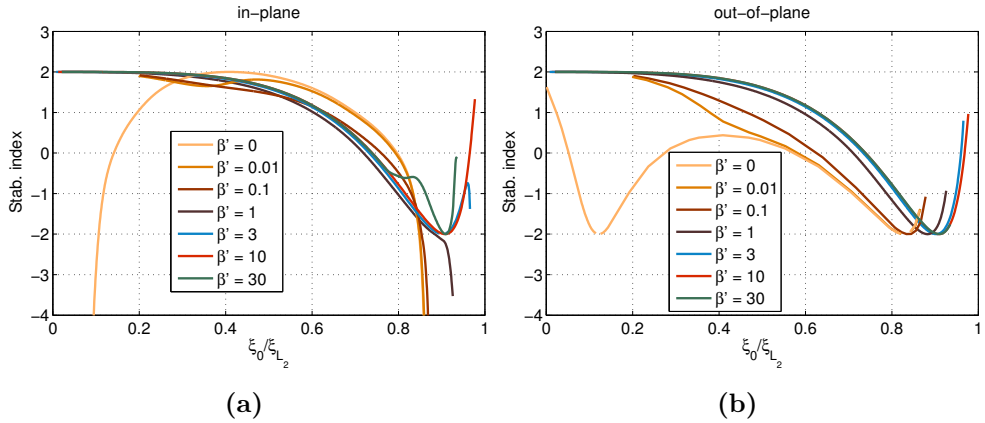

Figure 5.31: Stability of family g' right branch, in-plane (a) and out-of-plane (b)

5.3.6 Discussion and model limitations

The analysis presented uses simplified dynamics to study a particular set of planar periodic orbit families in the extended Hill problem with solar radiation pressure. These families of orbits are of particular interest for the exploration of small minor bodies, as the mass ratio is consistent with the Hill approximation and the lightness numbers involved are higher than in usual missions around planets or other larger bodies. They provide alternatives to the current orbit and hovering strategies around asteroids.

Given the instability of the orbits presented, often resulting in escape solutions after a small number of revolutions, a strategy that combines hovering points away from the asteroid with approach and escape trajectories connected to the g' orbits through their associated manifolds would allow for a combination of distant and close-up observations. These unstable manifold trajectories can be of use providing access or escape to and from a hypothetical stand-off point at a safe distance from the asteroid.

The analysis in this section limits itself to the set of simple-periodic or double-periodic families studied by Hénon (1969). In the course of the study, various exotic and complex orbits were found belonging to higher order periodicity families, still in the planar case (see Fig. 5.31 for a sample of the trajectories found, mostly for low lightness numbers). The higher multiplicity exploration of the Hill problem by Hénon (2003) led to a series of new families, labelled Ha to Hg, some of them stable, albeit without the inclusion of solar radiation pressure. Families up to multiplicity 81 with solar radiation pressure were already reported and

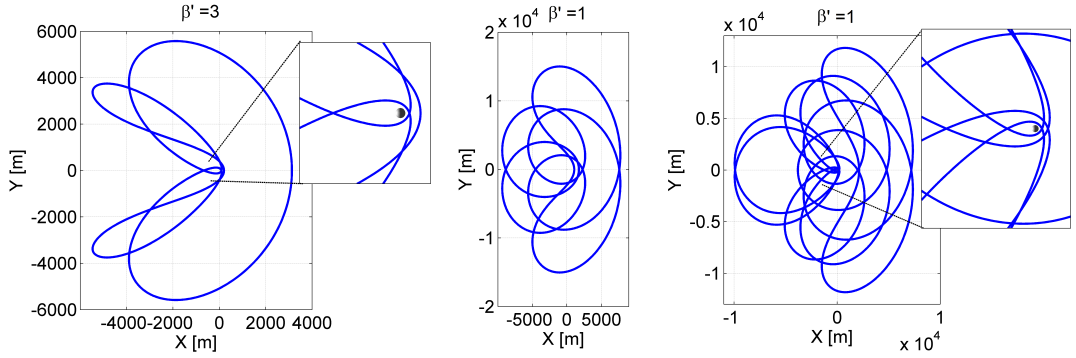

Figure 5.32: Higher multiplicity family examples: 3-periodic, 5-periodic and 10-periodic.

studied in the literature (Papadakis, 2006). The orbit family evolution, feasibility and stability analysis could be extended to these set of N-periodic families. Despite the beauty of the wide range of solutions, their prospective usefulness is questionable, due to frequent passes close to the asteroid, which could compromise the safety of a spacecraft when perturbations are taken into consideration. An additional possible set of families of interest are three-dimensional periodic orbits bifurcating from the planar ones or from known three-dimensional families such as Halo orbits (Katherine and Villac, 2010).

Perhaps the biggest objection to the applicability of the planar symmetric orbit families described in this chapter to asteroid exploration is that the simple dynamical model used may not effectively represent the range of feasible orbits in a more realistic and complete model. The most obvious extension to this problem is the Elliptic Restricted Three Body Problem (Broucke, 1969), or its limiting case the elliptic Hill problem, with the addition of SRP, to account for a more representative case of an asteroid in an elliptical orbit around the Sun. The existence of the a and g' family in the elliptic Hill problem has been demonstrated in the literature (Ichtiaroglou, 1980, 1981). Voyatzis et al. (2012) perform a more detailed analysis of the elliptic Hill problem, extending by continuation to eccentric orbits planar families including stable branches of the higher multiplicity families reported by Hénon (2003). Most orbits are unstable but regions of regular motion can be found around certain families. These orbits could be extended to the case with solar radiation pressure, and their stability properties checked.

However stable the symmetric solutions presented are, this behaviour can quickly change with the introduction of additional perturbations in higher fidelity models. Of particular concern is the non-sphericity perturbation, due to the highly irreg-

ular shape and mass distribution of asteroids. In a related paper (García Yárnoz et al., 2013), the author shows that orbits of the double periodic g' branch could be found that require limited controllability, for a particular case with a rotating tri-axial ellipsoid. These orbits comprise a retrograde section close to the asteroid, which is least affected by the rotation of the ellipsoid, assuming this rotation is also prograde. Resonant orbits with the asteroid rotation would reduce the required control.

5.4 Solutions for system implementation

Given the uncertainty in the mass, shape and associated gravity field of most asteroids, adjustable spacecraft area or reflectivity would be a desired feature for orbiters that intend to use SRP enabled exotic orbits. In the previous sections, solutions that require varying effective areas depending on the initial conditions and the orbit direction have been described. Possible system implementations for the required SRP control are here discussed.

The ratio of the areas required for the 3-revolution retrograde and the 2-revolution prograde orbits presented in Section 5.2 is of the order of 1.6. A system with varying areas of this order could be implemented in multiple ways (see Fig. 5.33 *left*). Various variable effective area solutions include (but are not limited to): solar panels of varying orientation with respect to the Sun (a) (e.g., a tilt angle α of 50° would provide the required ratio of 1.6), additional deployable solar panels as shown in solution (b), or complex variable geometry sails such as the quasi-rhombic pyramid proposed by Ceriotti et al. (2014) (c), or adaptable deployable inflatable membranes (Clark et al., 2012) (d).

These solutions have, however, implications for other subsystems. The solar panels would need to be sized in order to accommodate the significant reduction in available input power when the effective sun-lit area is reduced. This can pose a potential drawback for the power subsystem design and the overall mass budget. Concerning attitude control, most of these solutions have a stable equilibrium attitude with respect to the Sun: the slanted surfaces point away from the Sun direction while the bus remains Sun-pointing. This self-stabilizing attitude would need to be taken into consideration when designing the spacecraft, in particular for the location of radiators and Sun-shields, and for the payload enclosures. In the example of the quasi-rhombic pyramid, visual spectrum cameras inside the

pyramid would allow observing the illuminated faces of the asteroid while they would face away from it when on the dark side. Additional visual and/or infrared cameras may be required in the lateral faces in order to observe the unlit areas of the asteroid. The small thrusters required to alternate the orbiting direction of the spacecraft need always to thrust in the Sun direction, which also constrains their location on the spacecraft.

Up to this point the reflectivity or solar pressure parameter Q is assumed equal to 1, corresponding to a perfectly absorbing surface. An alternative to variable effective area is to modify in a controlled way the SRP perturbation through the use of reflective surfaces coated with electro-chromic material than can vary the material reflectivity when an electrical current is applied (schematic in Fig. 5.33 *right*). The benefit of such an approach is a faster and more flexible variation of the SRP effect that removes the risk of having movable parts. Current electro-chromic devices such as the patches used in the Ikaros solar sail mission demonstrated a variation in the reflectivity by a factor of 1.4 (Funase et al., 2010), which is close to the desired values. However, the area covered by these devices in the case of Ikaros is small, which results in small variations of the total force. There are nonetheless proposals in literature to cover the full solar sail with similar devices, to utilise them for shape changing or for attitude control by selective variation of the reflectivity across the surface (Borggräfe et al., 2014).

In practice, a combination of both variable surface and variable reflectivity may be required. A variable surface would be useful to account for the great uncertainties in the geometry and gravity field of such small bodies before the close approach, and until proper characterisation of the target body is complete. Variable reflectivity devices would still be required for faster modifications once the characterisation is complete, and for fine control. The variations required by the alternating orbiter trajectories between prograde and retrograde orbits presented here could be partly provided by the electro-chromic devices, while larger variations depending on the orbit geometry with respect to the body axes would be performed with a variable area mechanism. For the $g - g$' families, small variations through electro-chromic coating would probably suffice.

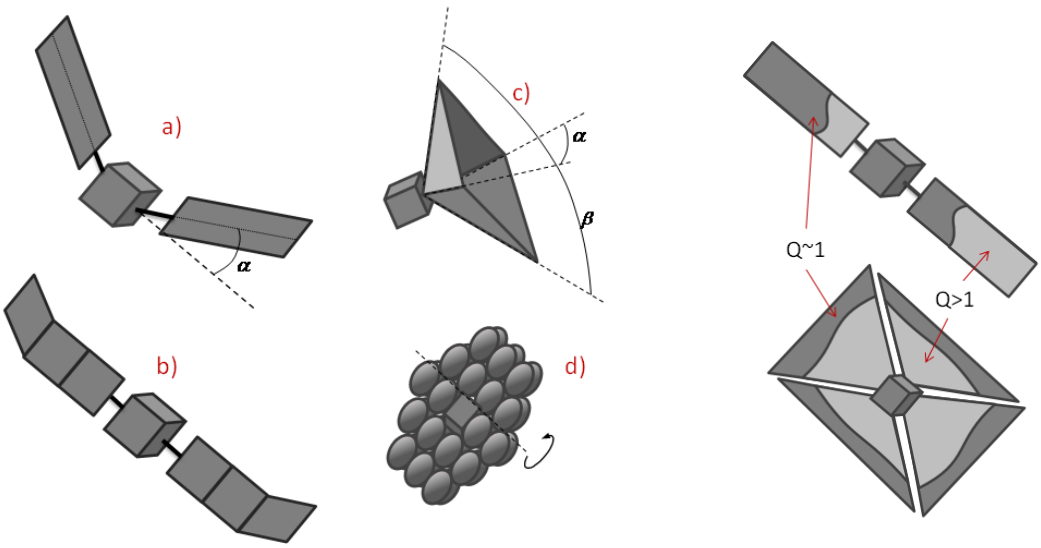

Figure 5.33: *Left:* Variable effective surface mechanisms. Tilting panels (a), additional deployable panels (b), varying quasi-rhombic pyramidal configuration (c), or self-inflating adaptable membrane (d). *Right:* Variable reflectivity through electro-chromic coatings modifies the SRP perturbation without changing the area.

5.5 Summary

Proximity phases for spacecraft orbits around small minor bodies are highly perturbed by the solar radiation pressure (SRP) perturbation. Current strategies in the literature for characterisation and proximity operations at small asteroids provide partial coverage of the sunlit side of an asteroid or incur high fuel costs for orbit maintenance. This chapter puts forward solutions to circumvent these problems, allowing coverage of the regions in the orbital plane of the asteroid, including passes over the sub-solar and anti-solar points.

An alternating orbiter solution is presented, which combines retrograde and prograde orbits and takes advantage of the natural evolution of the orbit eccentricity to reduce the size and frequency of manoeuvres required when compared to more traditional hovering strategies. Additional solutions of interest have been presented, including possible free return trajectories for a "hopper" spacecraft.

The effect of eclipses and non-sphericity perturbations has been analysed for this alternating orbiter strategy. Trajectories with different combinations of prograde and retrograde sections have been shown to be effective to reduce the adverse influence of resonances with the rotation of a non spherical asteroid.

A second solution proposes the use of planar symmetric periodic closed orbits that benefit from inversions of the orbit direction due to the natural dynamics. These solutions belong to the well-known a and $g - g$' families of the Hill problem, which have been extended in this chapter to levels of solar radiation pressure perturbation characteristic of minor bodies. Some of these families have been shown to be partly unfeasible or highly unstable for realistic asteroid densities and the lightness numbers characteristics of small bodies.

Altogether, double-periodic g' orbits are perhaps the best candidates for temporary orbiters in the equatorial plane. They provide good coverage of the sub-solar point and the whole XY plane, without close approaches to the asteroid surface that could compromise the safety of the spacecraft. For the range of lightness numbers associated with small asteroid spacecraft ($\beta' \sim 20 - 30$), they are stable in the planar motion and present a mild instability for out-of-plane motion. Furthermore, their orbits are more robust against the introduction of the non-sphericity perturbation due to the retrograde motion close to the asteroid (and prograde away from it), assuming that the asteroid rotational motion is prograde.

The two proposed strategies require a variation of the effective area of the spacecraft, depending on the desired trajectories, the asteroid characteristics, or the initial conditions. The required SRP control and area variation can be achieved by a number of different variable area or variable reflectivity devices.

Chapter 6

MICRO-SCALE: Winnowing on asteroids

On the morning of his departure he put his planet in perfect order. He carefully cleaned out his active volcanoes. He possessed two active volcanoes; and they were very convenient for heating his breakfast in the morning. He also had one volcano that was extinct. But, as he said, "One never knows!" So he cleaned out the extinct volcano, too. If they are well cleaned out, volcanoes burn slowly and steadily, without any eruptions. Volcanic eruptions are like fires in a chimney.

On our earth we are obviously much too small to clean out our volcanoes. That is why they bring no end of trouble upon us.

The little prince also pulled up, with a certain sense of dejection, the last little shoots of the baobabs. He believed that he would never want to return

Saint-Exupéry (1943), *The Little Prince*

Unlike in the little prince's home world, there are no reported volcanoes on asteroids, and of course none are expected to be found (though one could argue that there are dramatic eruptions on comets, and there is definitely volcanic activity

in some outer planet moons). However, asteroids are far from being geologically dead bodies, and movement of regolith and transient atmospheres of dust can be generated by multiple causes. Most rubble pile asteroids are speculated to have gone through several stages of surface disruption and re-shaping since their formation (Hirabayashi and Scheeres, 2012; Walsh et al., 2011), due to planetary encounters, impacts, or spin-up disruption, for example through YORP. Several processes for regolith migration and segregation have been suggested for asteroid Itokawa (Miyamoto et al., 2008, 2007), causing major re-consolidation of its surface. In addition, particles and small rocks are regularly ejected from asteroids (Scheeres et al., 2002), due to rotational fission, micro-meteoroid impacts, or other processes such as electrostatic levitation.

These phenomena may constitute challenges, but also opportunities if engineered appropriately for material processing. Understanding dust and ejecta dynamics in the vicinity of asteroids is key for future science missions and, in the long-term, for asteroid exploitation. This chapter analyses the feasibility of manipulating asteroid material by means of solar radiation pressure. A novel method is proposed for passively sorting material as a function of its grain size or density, where solar radiation pressure is used as a passive in-situ 'mass spectrometer'. A simplified analysis shows that, in principle, this method allows an effective sorting of regolith material. This could have immediate applications for a sample return mission, and for industrial scale in-situ resource utilization to separate and concentrate regolith according to particle size or composition.

6.1 Motivation and background

Asteroids are regarded as prime targets for space exploration missions. In addition, they may well be the most affordable source of in-situ resources to underpin future space exploration ventures (Sanchez and McInnes, 2011a).

To date, in-situ observations of asteroids (e.g., Itokawa, Eros) indicate that all Near-Earth Objects (NEOs) visited thus far, including very small bodies, are not bare lumps of rock (Michel, 2013). A very fine layer of regolith material is likely to have a ubiquitous presence on most asteroid surfaces. The formation of this layer of regolith is usually explained by the effect of impact cratering and sandblasting through micro-meteoroid bombardment (Clark et al., 2002). The presence of this fine dust, coupled with weak and irregular gravitational and electrostatic

forces, increases the risk of triggering transient dust atmospheres during asteroid operations that can potentially degrade instrumentation, damage mechanisms and reduce visibility and communications. The future exploitation of asteroid material would need to take into account the dynamical behavior of dust under solar radiation pressure (SRP) in order to minimize the risk of such transient dust atmospheres. Considerable efforts have been made to understand the perturbing forces and space environment in the vicinity of cometary and asteroid bodies (Richter and Keller, 1995; Scheeres et al., 2010). These perturbing forces will have direct implications for the operations of spacecraft around and on small bodies. On the other hand, they also represent an opportunity, if engineered for practical benefit, to devise novel methods for asteroid resource exploitation.

As noted before, extra-terrestrial resource exploitation is by no means a new idea. It was first proposed well over a century ago by the first pioneers of astronautics (Tsiolkovsky, 1903), and in the past decades it was given a comprehensive treatment by Lewis (1996). Ross (2001) further discusses the feasibility of extra-terrestrial mining applied to the NEO population. The concept is presently back in the spotlight due to the founding of two companies with the final objective of mining asteroids: Planetary Resources Inc. and Deep Space Industries. If in-situ industrial scale exploitation is ever considered, various separation and material processing techniques would need to be implemented.

On Earth, industrial separation processes for mineral processing (Kelly and Spottiswood, 1982) range from the more traditional gravity concentration devices to numerous 'modern' methods including magnetic and electrostatic separation or, more recently, automated ore sorting (Salter and Wyatt, 1991). Methods based on gravity or centrifugal separation are still used extensively in mineral processing as a first step to generate mineral concentrates for further treatment, or to discard waste, due to their simplicity and high capacity (Burt and Mills, 1984). However, most of these gravity-driven separation methods are clearly no longer applicable in microgravity, or have a reduced performance, whereas others may require large-scale in-situ machinery.

There is an abundant literature on proposals for the exploitation and processing of lunar regolith (Haskin et al., 1986; Lewis, 1996). Magnetic separation techniques have been tested and proven useful on lunar simulants generated in the laboratory (Graham et al., 2010; Stoeser et al., 2011). Both reports show that paramagnetic pyroxene silicates and non-magnetic plagioclases can be effectively

sorted with magnetic separation. So-called dry methods are effective down to particle sizes of 150 μm, whereas for smaller particles the use of slurries is needed (Graham et al., 2010), possibly due to cohesion. Further tests carried out in simulated lunar gravity on parabolic flights on tribocharged lunar silicate simulants (Quinn et al., 2013) demonstrated the effectiveness of magnetic and electrostatic techniques in low gravity. Analogous processes could be applied to asteroids (O'Leary et al., 1979), given the similarities in the silicate minerals present in both types of regolith, the vacuum and low-gravity environment. The higher ferro-metallic content in asteroid regolith would suggest that techniques based on magnetic separation are even more suited for asteroid resource exploitation to separate metals. Although this may be true, they require large, complex machinery for the separation, and for the previous steps of grinding and feeding. These methods would benefit from a prior regolith size separation or mineral concentration process. With this intention, new methods that take advantage of the low-gravity and vacuum environment of asteroids could be utilized.

This chapter proposes and performs a feasibility analysis of one such novel method for sorting asteroid material, exploiting the dynamical interaction of regolith particles with solar radiation pressure. Separation is achieved by differential solar radiation pressure on ejected particles of different area-to-mass ratios. The concept is analogous to the separation process of 'winnowing' in agriculture, used for many thousands of years for separating grain from chaff due to differential atmospheric drag, again for materials with different area-to-mass ratio. This method has potentially attractive applications for large-scale industrial exploitation of asteroids, such as allowing a first, coarse, in-situ separation of different regolith particle sizes, or pre-concentration and separation of different materials based on their density. Future asteroid engineering and mining endeavours would benefit from this sorting technique, where solar radiation pressure is used as a passive in-situ 'mass spectrometer'. This process could be used in combination with, or as a first stage of a more complex process exploiting electrical or magnetic effects for more precise sorting.

6.1.1 Exploiting solar radiation pressure for material sorting

Regarding the dynamical environment of asteroids, and depending on an asteroid's size and its spin state, the effective ambient gravitational acceleration

experienced by dust grains on small bodies can range from micro-gravity to milli-gravity (Scheeres et al., 2010), much lower than on the Moon. Under such conditions, the SRP perturbation becomes the largest non-gravitational force affecting single grains that have been lifted from the asteroid's surface, either naturally by micrometeoroid impacts or electrostatic forces, or by mechanical means. Dust grains with a large area-to-mass ratio can escape from the asteroid (Scheeres et al., 2002), whereas those with smaller area-to-mass ratios will remain bounded. Their trajectories will nevertheless be significantly perturbed, even when ejected at low initial velocities. Based on this effect of differential SRP influence on dust grains, a method can be designed for passively sorting asteroid material as a function of grain size or density. The proposed idea consists of one surface element that collects and scoops loose regolith directly from the asteroid surface and expels it at a small velocity (either before or after grinding it), and one or several collectors that capture sorted particles as they fall back to the surface. A similar natural process, caused by electrostatic levitation (Lee, 1996), is believed to be responsible for the movement and concentration of fines (particles smaller than 40 μm) on shaded or shallow areas on asteroid surfaces. This process has been suggested as a possible explanation for the dust ponds observed at Eros (Robinson et al., 2001).

In the following sections, simplified models will be used to describe the trajectories of dust particles in the vicinity of an asteroid considering the third body perturbation of the Sun and solar radiation pressure perturbation. Preliminary conclusions can then be drawn from the analysis regarding the prospect of actively engineering and exploiting the forces experienced by dust grains in the vicinity of asteroids. Two separation strategies are presented, and the effect of uncertainties in the initial conditions on the separation is analysed.

The preliminary analysis presented in this chapter does not consider the modelling of additional perturbations, among them inter-particle forces, leaving it for future work. However, given the low gravity and vacuum conditions around asteroids, these additional forces acting on dust grains, particularly cohesion between individual particles, are likely to reduce the efficiency of the proposed sorting method. The implications of inter-particle forces are discussed in the final section of the chapter.

6.2 Zero velocity curves in photo-gravitational CR3BP

The problem to be tackled consists of particles of asteroid material under the influence of the gravitational attraction of Sun and asteroid, as well as SRP perturbations. It has been modelled according to the photo-gravitational CR3BP in a co-rotating frame described in Section 2.3.1. Higher order gravitational perturbations of the asteroid, any inter-particle forces, and eclipses are neglected at this stage of the investigation.

Recalling equations 2.12 and 2.13, it is possible to calculate for particles ejected from the surface of an asteroid zero velocity curves (corresponding to $J = 2U$), which depend on the lightness number β, as defined in Eq. 2.11. Assuming spherical particles of constant density ρ and radius r, the lightness number β can also be expressed as:

$$\beta = \frac{L_S Q}{4\pi c \mu_S} \frac{S}{m} = \frac{3 L_S Q}{16 \pi c \mu_S r \rho} \tag{6.1}$$

This parameter will prove useful in describing the different orbiting regimes of particles in the vicinity of an asteroid. Clearly, β is proportional to the particle's area-to-mass ratio, so for a fixed density, β increases when the particle radius decreases. Therefore, for small dust grains, SRP can provide a significant perturbing force.

Figure 6.1 represents the zero velocity curves for different particle sizes ejected with a fixed velocity from a hypothetical 10 km radius asteroid at 1 AU from the Sun, along with a set of example trajectories for a particular ejection site on the equator. The axes correspond to a co-rotating or synodic frame (see Fig. 2.1). The asteroid is assumed to be rotating with a 4 hour period around the z-axis, and the ejection velocity direction is selected radially outwards, normal to the asteroid surface. The average NEO density of 2.6 g/cm^3 (Chesley et al., 2002) is considered for the asteroid, whereas estimates on the particle radius are provided assuming spherical grains of constant density of 3.2 g/cm^3, representing a relatively low density olivine. If the composition and structure of the asteroid is uniform, this implies a macro-porosity of 19%, close to the average S-type asteroid (Britt et al., 2002). For ejection velocities above 11.2 m/s the zero velocity curves are open around L_2 for all values of β. An ejection velocity of 10.34 m/s was selected so that all particles with β lower than 5×10^{-3} (which corresponds to particles

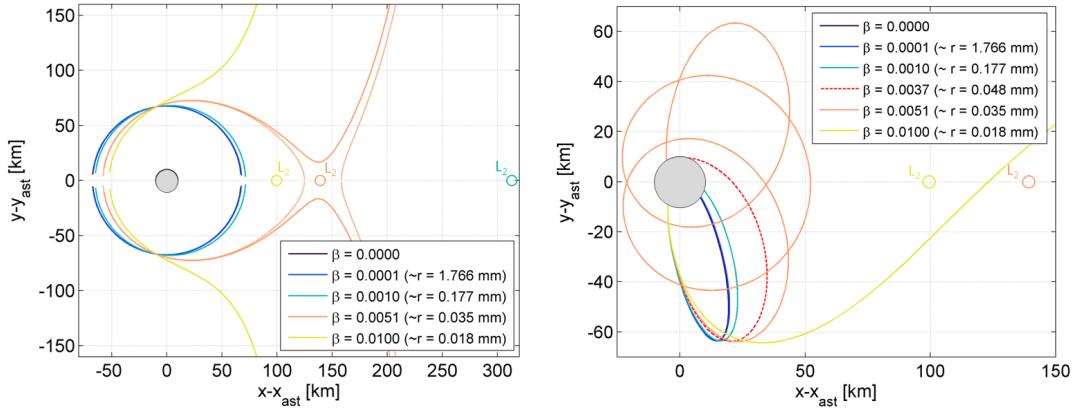

(a) **(b)**

Figure 6.1: Zero velocity curves (a) and trajectories in the co-rotating frame (b) for ejection velocities of 10.34 m/s from a 10 km asteroid with a 4 hour rotational period, for different values of β. Particle size estimation are given assuming spherical grains of constant density and $Q = 1$. Zero velocity curves are open for all particles with β larger than 0.0051. All particles with β lower than 0.0037 impact before one revolution for this particular ejection site (*dashed red line*).

larger than approximately 35 μm radius) have closed zero velocity curves. The ejection velocity that ensures closed curves for a given particle size increases with the rotation period (e.g., for a fast rotator with shorter 3 hour period, a correspondingly lower ejection velocity of 9.5 m/s has similar effects).

The range of lightness numbers selected covers from large boulders down to particles of size tens of μm. Smaller particles are likely to levitate naturally, or potentially escape when ejected due to the SRP perturbation (an example of this can be observed in Fig 6.1b). Two values of lightness number β are particularly relevant: the value of β for which the zero velocity curves open (5×10^{-3} in this particular case), which sets an upper bound on particle size for dust to escape, and the one that ensures an impact before one revolution.

The first value sets a theoretical limit for particles to escape, based solely on energy considerations. However, this is a necessary but not sufficient condition for escape, as reaching escape conditions depends not only on the energy level, but also the solar longitude of the ejection site and the orbital geometry in general.

The positions on the x-axis of the two collinear libration points of the Sun-asteroid system, x_1 and x_2, can be calculated by solving the system in Eq. 6.2 for each particular lightness number, and from there the associated value of the integral

of motion J is obtained. These conditions represent the equilibrium solutions of Eq. 2.12 such that:

$$x_1 - \frac{(1-\mu)(1-\beta)}{(x_1+\mu)^2} + \frac{\mu}{(x_1+\mu-1)^2} = 0 \rightarrow J_1 = 2U(x_1)$$
$$x_2 - \frac{(1-\mu)(1-\beta)}{(x_2+\mu)^2} - \frac{\mu}{(x_2+\mu-1)^2} = 0 \rightarrow J_2 = 2U(x_2) \tag{6.2}$$

Given these values of the Jacobi constant J, and equating them to Eq. 2.13 , substituting the potential energy of points on the surface of the asteroid, the ejection velocity required for the zero velocity curves to be open through the L_1 or L_2 points can be obtained. Because of the influence of the SRP perturbation, it is the L_2 point that offers the lowest energy for the zero velocity curves to be open, and thus also the lowest ejection velocity for escape trajectories of the dust grains. The main effect of SRP on the location of the libration points is to displace both the L_1 and L_2 points towards the Sun, resulting in an L_2 point closer to the surface of the asteroid (see Fig 6.1a). It could then be assumed that there is a particle size at which the L_2 point would be on the surface of the asteroid, and any smaller particles lifted from the surface with an infinitesimally small velocity at the correct time in a rotational period of the asteroid may escape. In reality, that region is in eclipse and SRP would only affect particles that are still orbiting when the Sun comes into view.

It is then possible to calculate a guaranteed return velocity, for a given value of β, that ensures closed zero velocity curves and eventual impact with the surface. Figure 6.2 plots this velocity for a 10 km asteroid rotating along the z-axis assuming vertical ejection along the equator, where the asteroid's rotation provides the largest contribution to the total kinetic energy, and thus an easier escape at lower velocities. This guaranteed return velocity shows small variations with the longitude of the ejection site. Ejection longitudes are measured along the equator with respect to the anti-solar direction.

In contrast, the value of β that ensures impact before one revolution is highly dependent on the point of ejection, and the relative geometry of the orbit with respect to the Sun. Certain ejection sites will have all particles directly impact under the perturbation of solar radiation pressure, whereas others will have a limiting β that allows multiple revolutions. Figure 6.3 represents the impact time in a longitude-latitude grid of the ejection site for the selected vertical ejection velocity of 10.34 m/s. The lightness number β is set to 0.0045 to ensure closed

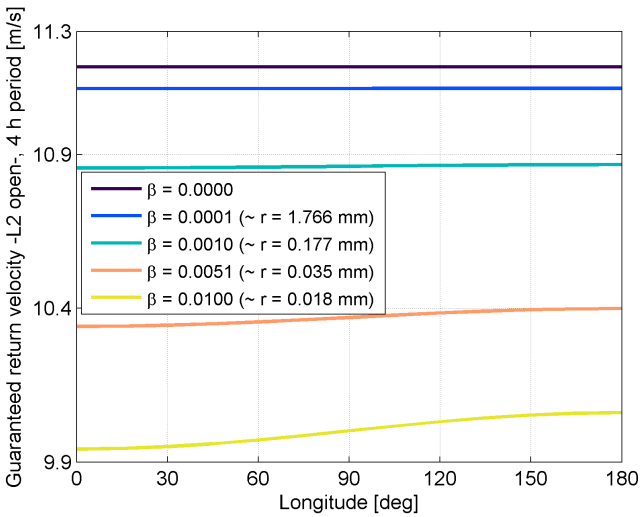

Figure 6.2: Guaranteed return velocity for dust particles ejected radially outwards along the equator of a 10 km asteroid with a 4 h rotational period, for different values of β. The longitude of the ejection site is measured along the equator with respect to the antisolar direction.

zero velocity curves and impact of all particles. Figure 6.3b gives the impact time in number of periods calculated with the initial osculating semi-major axis at ejection. The semi-major axis, and therefore also the period, is larger at the equator. For most of the surface of the asteroid the impact time is less than one initial period, while there is a region in the longitude's third quadrant that allows multiple revolutions. As expected, it is the region near the equator that has the highest probability of generating ejecta that perform more than one revolution. Also, the longitude's first and second quadrant, where the SRP acts against the velocity reducing the pericentre height, have shorter impact times than the third and fourth quadrant where the effect of the SRP perturbation contributes to raising the pericentre height.

It is difficult to draw more significant conclusions from this general form of the equations of motion, or to predict the impact of the dust without full numerical propagation for each particular case, which is time consuming. For this reason, a semi-analytical approximation is used in this chapter to study the behaviour and various regimes of ejected dust in the vicinity of an asteroid.

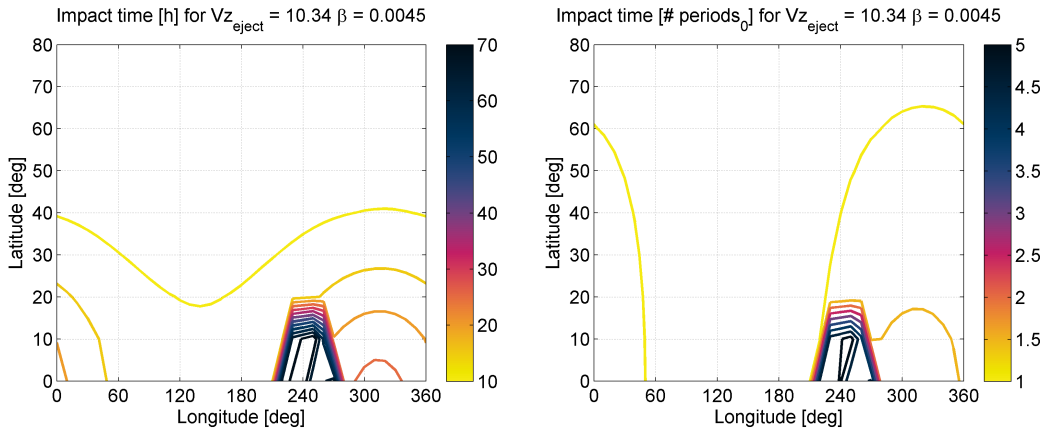

(a) **(b)**

Figure 6.3: Re-impact time on a 10 km asteroid with a 4 h rotational period, for dust particles of β=0.0045 ejected radially outwards with 10.34 m/s ejection velocity. Re-impact time is given in hours (a) and number of initial periods (b).

6.3 Phase-space graphs from orbit-averaged equations

Although the orbit-averaged equations of motion described in Section 2.3.4 are not the most appropriate tool to propagate trajectories of dust close to escape or impact, the phase-space plots introduced are still a useful visualisation tool to study the behaviour of dust particles.

The graph in Fig. 6.4a is obtained by plotting the previously generated trajectories in an eccentricity-ϕ space, with the solar phase angle ϕ definition given by Eq. 2.16. Initial ejection eccentricities range from 0.965 for an equatorial ejection, up to 1 for a polar ejection. It can be easily appreciated that the eccentricity increases along the trajectory when ϕ is larger than 180°, and decreases when ϕ is between zero and 180°. Only a few trajectories with initial solar phase angle ϕ around 90° and latitudes close to the equator perform multiple revolutions. As an illustration, the evolution of a particular multi-revolution equatorial trajectory is plotted in Fig. 6.4b. The osculating ellipses are represented at ejection (A), impact (D) and two intermediate points when crossing the eccentricity value of 0.6. For this particular example, the eccentricity drops down to 0.5 before increasing back to values close to 1 causing an impact, while the solar phase angle evolves from 120° ((A)) to close to 240° ((D)), as the pericentre rotates. This eccentricity-solar phase graph closely resembles the phase space in the work by Oyama et al.

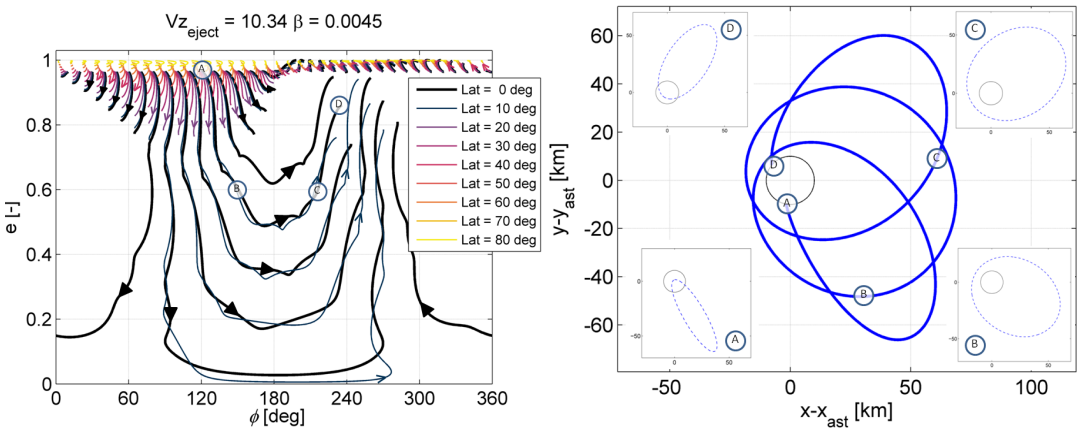

Figure 6.4: Eccentricity-ϕ plot (a) of dust trajectories for different latitude-longitude ejection sites on a 10 km asteroid with a 4 hour rotational period, for dust particles of $\beta = 0.0045$ ejected radially outwards with 10.34 m/s ejection velocity. An example equatorial trajectory is plotted (b), along with the osculating ellipses at ejection (A), impact (D) and two intermediate points along the trajectory.

(2008) for the limiting case with infinite SRP-gravity ratio.

Figure 6.5 plots the comparison between the numerical propagation of ejected dust trajectories in the equatorial plane, and the isolines of constant Hamiltonian that the orbit-averaged elements should follow according to the orbit-averaged equations. The ejection velocity of this particular plot is 9.5 m/s and the rotation period of the asteroid 3 hours.

While the initial argument of pericentre of the ejected dust can be arbitrarily chosen by selecting an ejection site/time, the rest of the initial osculating orbital elements a_0, e_0 and true anomaly ν_0 of the ejected particles are calculated as:

$$a_0 = \frac{R}{2 - \frac{R}{\mu_A}\left(v_{eject}^2 + \left(\frac{2\pi}{T_A}R\right)^2\right)} \tag{6.3}$$

$$e_0 = \sqrt{\left(v_{eject}\frac{2\pi}{T_A}R^2\right)^2\left(\frac{4\pi^2}{{T_A}^2}R^3 - \mu_A\right)^2} \Big/ \mu_A \tag{6.4}$$

$$\nu_0 = \arccos\left(\left(\frac{4\pi^2}{{T_A}^2}R^3 - \mu_A\right) \Big/ e_0\mu_A\right) \tag{6.5}$$

with R being the asteroid radius, T_A its rotational period and v_{eject} the ejection velocity, once again assumed normal to the surface of the asteroid.

The initial eccentricity e_0 calculated from Eq. 6.4 is 0.93 for these ejection conditions. No equilibrium points are found in the phase-space, due to the high SRP perturbation when compared to the cases studied by Oyama et al. (2008) and Colombo et al. (2011). This is consistent with the notion that no stable traditional equatorial orbits can be found around small bodies when high SRP is included. The eccentricity eventually increases up to values that cause an impact, or in the case of very high area-to-mass ratio, up to a possible hyperbolic escape. Still, the orbit-averaged equations correctly predict the trends in the eccentricity evolution. For the initial conditions selected, there is an increase in eccentricity for all points with $\phi > 180°$, resulting in a decrease in pericentre height and immediate impact before one revolution of all particles ejected in two full quadrants of the asteroid.

The region around $\phi = 90°$ (which corresponds to ejection points with negative y in the third quadrant of longitude as seen in Fig. 6.3) contains both trajectories that impact and others that perform multiple revolutions. The eccentricity is decreasing in all cases, but only for a small range of initial phase angles does the pericentre height rise above the asteroid radius which allows the resulting trajectory to perform multiple revolutions. To better illustrate this multi-revolution regime, a thick blue dashed horizontal line is plotted in Fig. 6.5, which represents a critical eccentricity given by:

$$e_{crit} = 1 - \frac{R}{a_0} \tag{6.6}$$

corresponding to a value of 0.708 for the initial conditions selected in the figure. For eccentricities above this value and the initial semi-major axis, the osculating pericentre is below the asteroid surface, which results in an impact. As the variation of a over one revolution is zero, and ejection/impact takes place close to pericentre, this approximation is accurate enough.

The apocentres and pericentres in the numerical trajectories have been indicated with $\times$ and $\circ$ markers. Any pericentre taking place above the critical eccentricity line implies an impact. It can be observed that whenever the eccentricity is lower than the critical value by the first pericentre, the dust particle manages to perform multiple revolutions, until after a few loops the eccentricity grows again above the critical one. The maximum reduction in eccentricity over one revolution does not take place exactly at $\phi = 90°$ (see the markers for the first pericentres), and

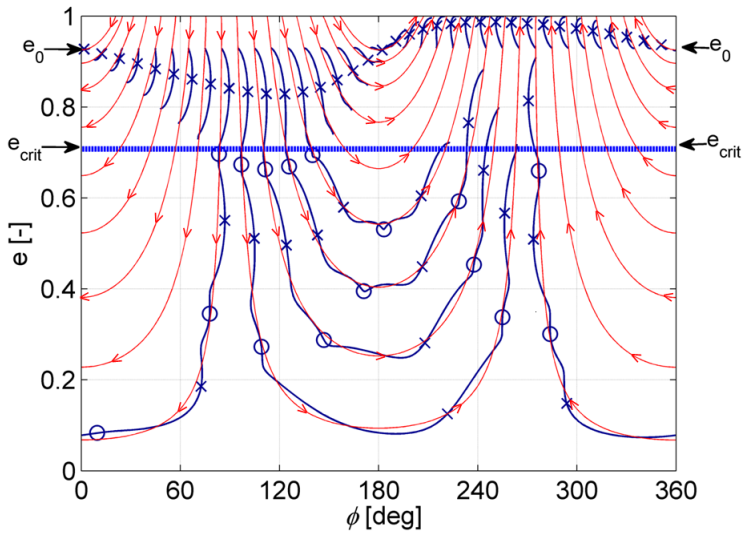

Figure 6.5: Isolines of constant Hamiltonian (*red with arrows*) and numerical propagation of ejected dust (*dark blue with* × *and* ∘ *markers*) plotted in the eccentricity-ϕ phase space. Apocentres and pericentres of the numerical trajectories are indicated with × and ∘ markers respectively. Vertical ejection velocity is 9.5 m/s, $\beta = 0.0045$, and the rotation period is 3 h.

the region of multi-revolution ejecta is thus not centred around it but shifted to the right on the plot.

A series of operational guidelines can then already be drawn from these results with regards to the selection of the extraction site, to determine the solar longitudes where operations are safer to avoid impact of dust on crewed missions or equipment. If transient dust atmospheres are to be avoided, solar longitudes close to $\phi = 270°$ $(= -90°)$ would be preferred. Operations at other solar longitudes are still feasible if the forces used ensure the ejection velocity of dust stays well below the limit that allows multi-revolution trajectories.

6.3.1 Time integration

The Hamiltonian system in Eq. 2.19 can be transformed into full canonical form with the simple change of variable (Hamilton and Krikov, 1996):

$$k = \sqrt{1 - \bar{e}^2} \tag{6.7}$$

resulting in:

$$\begin{cases} \dfrac{k}{\partial\lambda_{SUN}} &= \dfrac{\partial H}{\partial\phi} \\ \dfrac{\partial\phi}{\partial\lambda_{SUN}} &= -\dfrac{\partial H}{\partial k} \end{cases} \tag{6.8}$$

It can be demonstrated that the tidal term is of the same order as SRP only for distances of the order of 20 asteroid radii, while the trajectories of interest stay bounded well below this distance. If the tidal term is neglected, Oyama et al. (2008) showed that it is possible to integrate the system to obtain the time needed for a particle to travel along a line of constant Hamiltonian H^* between two values of k (or eccentricity), obtaining:

$$t - t_0 = \frac{-1}{\sqrt{\frac{d^3}{\mu_S}(1+J^2)}} \left(\arccos \frac{(1+J^2)k - H^*}{J\sqrt{1+J^2-H^*}} - \arccos \frac{(1+J^2)k_0 - H^*}{J\sqrt{1+J^2-H^*}} \right) \tag{6.9}$$

As a result, it is possible to plot isolines of transfer time on the phase-space graphs, in particular the isolines corresponding to the time until apocentre or pericentre, to determine if the next pericentre takes place before or after critical eccentricity is reached.

To obtain the orbital period it is also necessary to take into account the variation in argument of pericentre due to SRP. The Lagrange planetary equation for the derivative of time with respect to true anomaly, which includes a term related to the variation in ω, is:

$$\frac{dt}{d\nu} = \sqrt{\frac{a^3}{\mu_A}} \frac{(1-e^2)^{3/2}}{(1-e\cos\nu)^2} \left[1 - \beta \frac{\mu_S}{\mu_A} \frac{a^2}{d^2} \frac{(1-e^2)}{e(1-e\cos\nu)^2} \left(\cos\phi + \frac{\sin\nu\sin(\phi+\nu)}{1+e\cos\nu} \right) \right] \tag{6.10}$$

Integrating over one revolution considering the mean values of semi-major axis and eccentricity, the orbital period can be approximated as:

$$T \approx 2\pi \sqrt{\frac{\bar{a}^3}{\mu_A}} \left(1 - \frac{1}{2}\beta \frac{\mu_S}{\mu_A} \frac{\bar{a}^2}{d^2} \frac{12+13\bar{e}^2}{4\bar{e}} \cos\phi \right) \tag{6.11}$$

A similar approach can be followed to obtain the first semi-period until apocentre. Plotting on the phase space the isolines of Eq. 6.9 corresponding to the time from initial true anomaly to apocentre and pericentre calculated analytically (see Fig. 6.6), they are a good match for the apsides points calculated with numerical

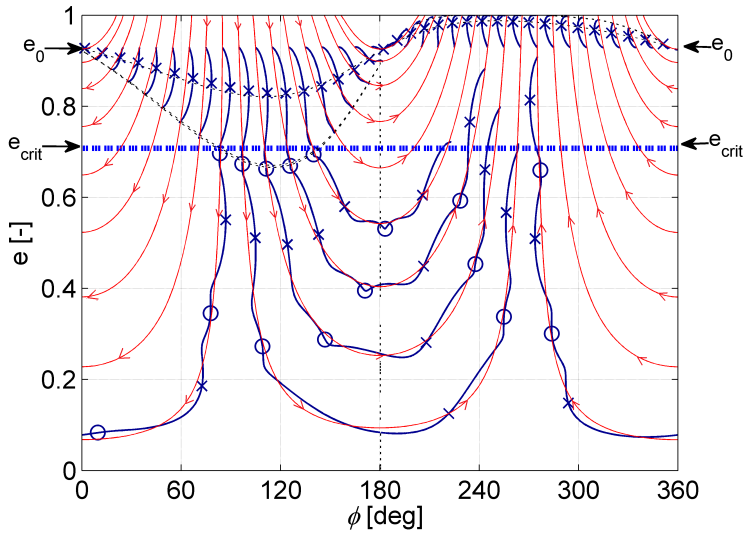

Figure 6.6: Apocentre and pericentre analytical time estimation (*dashed black lines*) on the eccentricity-ϕ phase space. Vertical ejection velocity is 9.5 m/s, $\beta = 0.0045$, and the rotation period of the asteroid is 3 h.

propagation. This allows an accurate analytical prediction of the conditions for a particle to perform multiple revolutions. The region in the phase space where the isolines of time to pericentre are below the critical eccentricity line corresponds to multi-revolution trajectories. It is important to note that the critical eccentricity varies with the semi-major axis along the orbit, so there can be pericentres close to the limiting values on either side that may impact or fly-over depending on the value of the osculating semi-major axis at the impact time for the two extreme cases.

6.4 Material sorting applications

One of the benefits of the differential effect of solar radiation pressure on ejected dust particles is the possibility to engineer these forces in order to passively separate material as a function of lightness number β. This processing of material can be considered either for separation of the same material as a function of grain size on an asteroid of uniform composition (the larger the grain, the lower the β), or alternatively, after a grinding process to reduce all materials to a similar grain size, as a method of separation of two materials with different densities (again the higher the density of the material, the lower the β). This SRP sorting

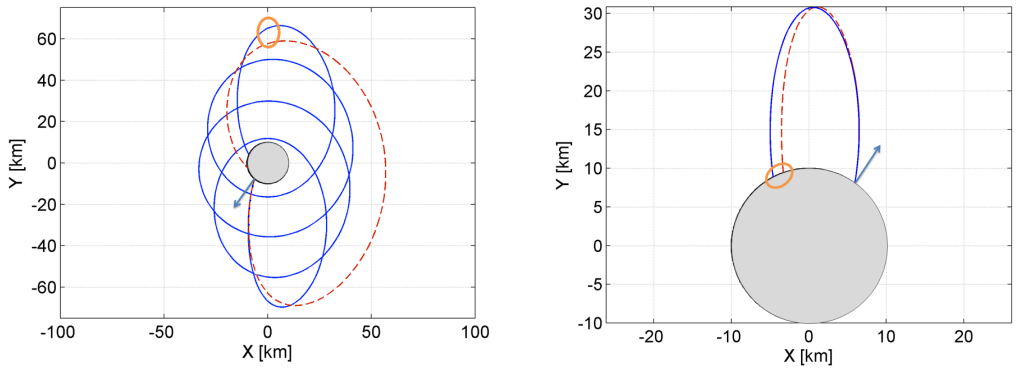

(a) **(b)**

Figure 6.7: Schematic representation of separation strategies with a hovering spacecraft collection point (a) and a ground-based collection point (b) for a heavier particle (*solid blue*) and a lighter one (*dashed red*). X-Y axes are parallel to the co-rotating frame axes and centred on the asteroid.

concept takes advantage of the low gravity on asteroids, which would render other techniques such as classical gravity concentration processes infeasible.

Two possible strategies for collecting the separated material can be devised (see Fig. 6.7): a hovering spacecraft that collects on-orbit the material that has been lifted from the surface by a surface element or rover, or several collection points on ground at pre-calculated distances. In both methods, particles are assumed to be ejected from the surface at the same speed. Each method has preferred ejection points on opposite sides of the asteroid ($\phi = \pm 90°$). The surface element can then collect material and, if needed, grind it for one asteroid revolution, and then eject it at the appropriate time depending on the selected strategy.

6.4.1 On-orbit collection

In the first method, the preferred ejection point is close to $\phi = 90°$, where SRP contributes to increasing the pericentre height and multiple orbit revolutions are possible. The collection point should be hovering at a certain distance on the Y-axis. Once an ejection velocity has been selected, there is a minimum value of β that will avoid impact in the first revolution, essentially discriminating a maximum size of the grains of interest (larger grains would fall back onto the asteroid). The rest of the material would travel following isolines of constant H until eventually reaching the desired height on the Y-axis for collection. Figure 6.8

shows superimposed on an eccentricity-ϕ phase plot the lines that correspond to a particular height over the Y-axis on the asteroid assuming a constant mean semi-major axis. Only for certain ejection sites close to $\phi = 90°$ does the eccentricity evolution along the constant Hamiltonian isolines allow the particles to reach heights over 55 km on the Y-axis after a number of revolutions. The thick blue line shows a propagated trajectory of this type, where the eccentricity decreases down to 0.1 (almost circular), before it increases again when the phase angle shifts to values close to 270°. The sixth apocentre for this trajectory is well above 60 km.

The passive separation takes place in time, as larger particles (particles with smaller lightness number) require more revolutions and thus longer times to reach the collection area. This is shown in Fig. 6.9a: the time to come back to the initial eccentricity levels increases with decreasing β. The plot shows the time evolution of the eccentricity for different values of β and the same ejection site at the equator and $\phi = 90°$, a rotation period of 3 hours, and an ejection velocity of 9.5 m/s. Particles with $\beta = 0.004$ impact before the first pericentre.

It is possible to analytically estimate the time until collection by calculating with Eq. 6.9 the time to reach the eccentricity of the intersection of the constant H isoline for ejection with $\phi = 180°$ or $\phi = 0°$. Obtaining the intersection point is straightforward by substituting the phase angle ϕ in Eq. 2.17. Figure 6.9b shows a comparison between the analytical estimates and the numerical propagated trajectories. The collection point for each β is assumed as the point when the eccentricity reaches the value at the first apocentre again, and is indicated with markers in Fig. 6.9a. The first lighter particles arrive one day after ejection, while the heavier particles can take over 70 hours.

The main difficulty concerning this strategy is the large variation in height at the Y-axis crossing for orbiting particles of different β. A non-planar case would have the added difficulty of the evolution of the orbital plane. Very large collectors (of the order of hundreds of metres for an asteroid of radius 10 km) would be required in order to capture a significant number of particles, or an elaborate station keeping strategy that changes height with time would be needed in order to compensate for these variations. This greatly increases the complexity of operations for a hypothetical collection on-orbit. The ejection velocities involved are also higher than for a ground based collection point.

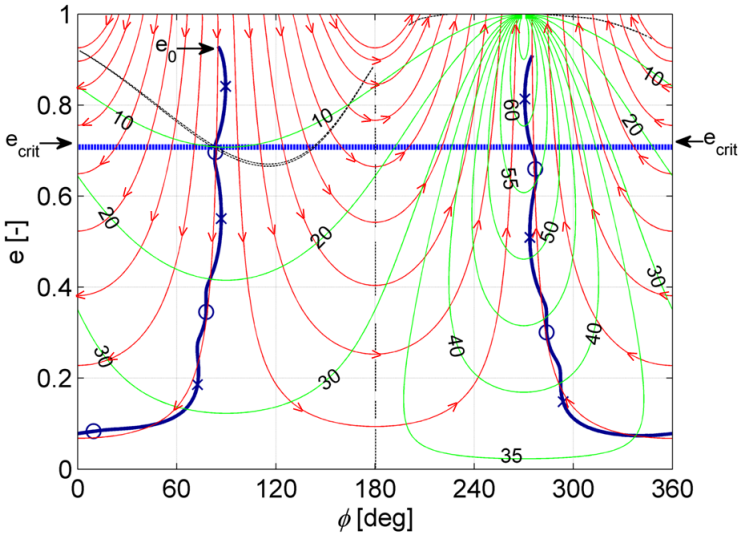

Figure 6.8: Eccentricity-ϕ phase space graph with isolines of constant height over the Y-axis in km (*number-labeled green contours*). Vertical ejection velocity is 9.5 m/s, $\beta = 0.0045$, and the rotation period of the asteroid is 3 h. For ejection sites close to $\phi = 90°$ trajectories can reach heights over 55 km on the Y-axis when the phase angle shifts to 270° after a number of revolutions.

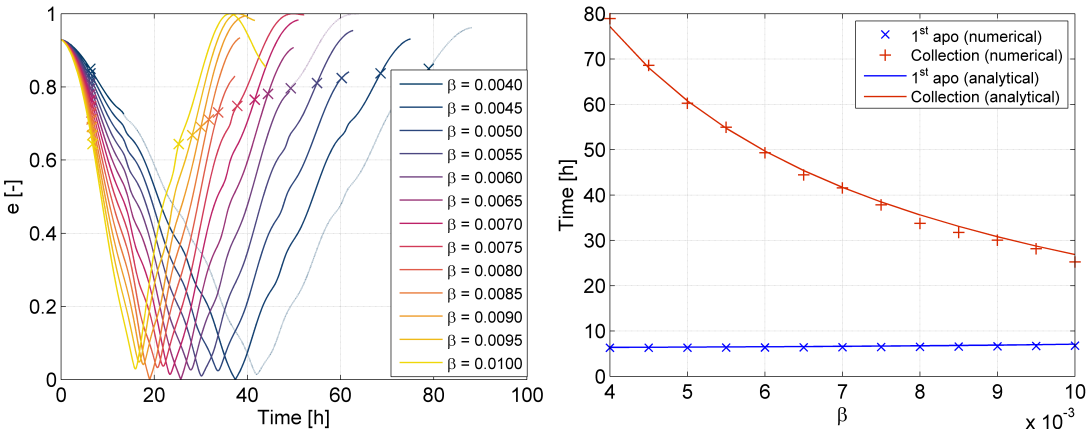

(a) **(b)**

Figure 6.9: (a) Evolution of the eccentricity with time for $\phi = 90°$ and different values of β. Markers indicate the first apocentre and collection point. Discontinuous lines indicate there has been an impact on the surface. (b) Time to collection and analytical approximation as a function of β.

6.4.2 On-ground collection

The second method envisages a series of collector points spaced on the surface of the asteroid (or a collector band or strip extended over some distance). The differential separation of particles as a function of β is performed in space, rather than in time. The preferred ejection point is in this case close to or equal to $\phi = -90°$ (pericentre on the negative Y-axis), which corresponds to trajectories where the SRP reduces the pericentre height and thus impact is assured before one revolution for most values of β.

Figure 6.10 shows the distance between impact points for two regolith particles of different sizes and densities as a function of the ejection velocity. A separation line of 1 m is indicated for reference. The ejection velocity increases with the desired separation. This ejection velocity has been scaled in the X-axis with the radius of the asteroid. For asteroids in the size range of 100 m to 10 km the required ejection velocities for the same separation densities scale well with the radius. Periods selected range from very fast rotators (2.5 h), close to the spin limit, to slow ones (100 h). Only in the case of fast rotators (dark blue lines) if the ejection velocity increases there is actually a clear bifurcation between the separation at a 1 km asteroid (*dashed*) and the 10 km one (*continuous line*) for the range of velocities plotted, and there can even be cases with particles escaping. For a smaller 100 m asteroid the bifurcation takes place at lower relative ejection velocities but in all cases it is well above the 1 m separation horizontal line.

Figure 6.10a assumes spherical particles of constant average density of 3.2 g/cm ^{3} (homogeneous asteroid of a low density olivine) for the suggested ejection site and different rotational periods of the asteroid. If the desired separation between two such particles of size 1 mm and 1 cm is 1 m, the graph shows that, for an asteroid rotating with a 2.5 h period, the required ejection velocity would be 2 m/s on a 10 km asteroid. This velocity would more than double in the case of a non-rotating asteroid ($\sim$ 4.5 m/s). If the size of the particles desired for separation is one order of magnitude lower (0.1 mm and 1 mm), the ejection velocities range from 0.5 to 1.7 m/s for the same separation distance. These velocities are almost one order of magnitude lower than the ones suggested for a hovering spacecraft collection point.

Figure 6.10b assumes instead a differentiated asteroid with two materials to be separated. The regolith is assumed to have been previously ground to grains of

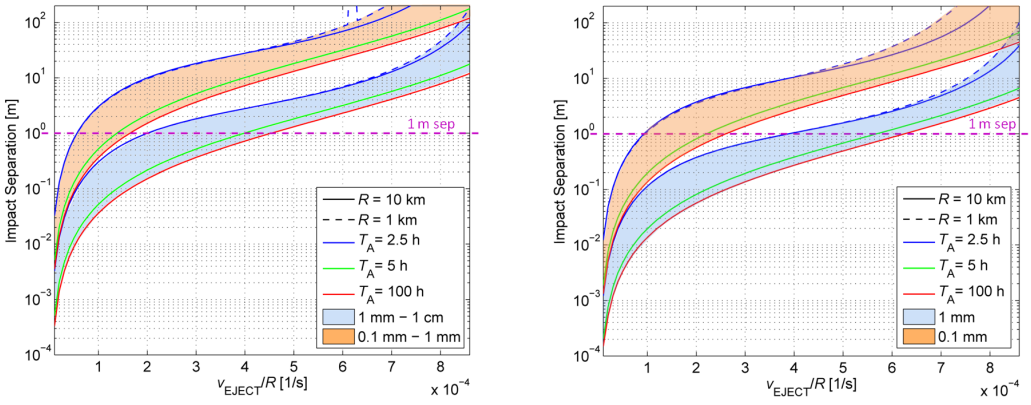

Figure 6.10: Impact point separation between 1 mm-1 cm (*blue patch*) and 0.1 mm-1 mm (*orange patch*) grains of homogenous density of 3.2 g/cm^3 (a), and between grains of different densities (2.68 and 3.74 g/cm^3) of the same size, 1 mm in blue, 0.1 mm in orange (b). Particles are ejected with a phase angle ϕ of 270 degrees for different asteroid rotation periods. *Dashed* and *solid lines* indicate the 1 km and 10 km asteroid respectively.

the same size (1 mm or 0.1 mm). Assuming 1 mm grains composed of plagioclase (average density of 2.68 g/cm^3) and a denser olivine or pyroxene (3.74 g/cm^3), the ejection velocities required for a 1 m separation on a 10 km asteroid range from 4 to 6.2 m/s depending on its rotation rate. For finely ground 0.1 mm particles, these velocities are reduced to 1 to 2.6 m/s. As the required ejection velocities scale with the radius, on a 1 km size asteroid they would be one order of magnitude lower.

In addition to the lower ejection velocities, other benefits of ground based collection when compared to on-orbit collection is that eclipses have little or no influence in the trajectories of the particles as the preferred ejection sites result in effectively eclipse-free trajectories except for a short interval at ejection. Other perturbations, such as higher order harmonics of the gravity field for the usually irregularly shaped asteroids would affect all particles equally, regardless of the β value, so the differential effect of SRP would still cause a separation in impact points of the same order. Non-planar trajectories would be affected in a similar way over one revolution, and the only concern of an ejection point away from the equator would be a higher required ejection velocity, similar to the case of a slowly rotating asteroid.

6.5 Effect of uncertainties

One of the concerns that arises when evaluating the ground based collection method is the sensibility of the separation to errors or uncertainties in the ejection conditions. When compared to the calculation of trajectories for a single asteroid or spacecraft, the hypothetical propagation of thousands to millions of regolith particles make necessary the introduction of a dispersion analysis to confirm the first-order feasibility of the separation method proposed. As the relative difference in grain size or density is small, errors in velocity at ejection may induce greater dispersion on the grains than the solar radiation pressure perturbation.

The separation caused by velocity errors was calculated for various asteroid sizes and rotation periods. Figure 6.11 shows the impact point separation for an error in the velocity modulus of 1% (a) and an error in the ejection direction of 0.33° (b). Only in-plane errors were considered. The colour patches representing the separation by solar radiation pressure calculated in the previous section are superimposed for comparison. Lines above colour patches indicate that errors induced by dispersions at ejection are larger than the desired separation. Because of this, there is a limiting asteroid size for each ejection velocity for which the SRP induced separation is no longer effective compared to errors in velocity. The separation induced by errors in angle (see Fig. 6.11b) has actually a minimum at a particular velocity for each case, which lies close to the required ejection velocity to obtain an orbital period for the grains equal to the rotational period of the asteroid. Close to this velocity, an error in the ejection angle causes an error in semi-major axis that barely modifies the impact time. As the particles perform a revolution at approximately the same time as the surface, there is a particular velocity for which errors in angle would result in the same impact point at the surface, only slightly before or after in time.

For a better understanding of the implications of these results, the previous figures are simplified to focus on specific examples for separation of 0.1 mm and 1 mm particles on a slow and a fast rotator, as shown on Fig. 6.12. Two particular examples are highlighted (indicated by vertical lines with circles).

For the case of a fast rotating asteroid with a period of 2.5 h (*blue square,* ①), the required ejection velocity for a separation of 1 m is equal to $0.06 \times R$ m/s. Assuming velocity modulus errors of 1%, the separation between equal particles would be of the order of 20 m for a 10 km asteroid, 2 m for a 1 km one, and

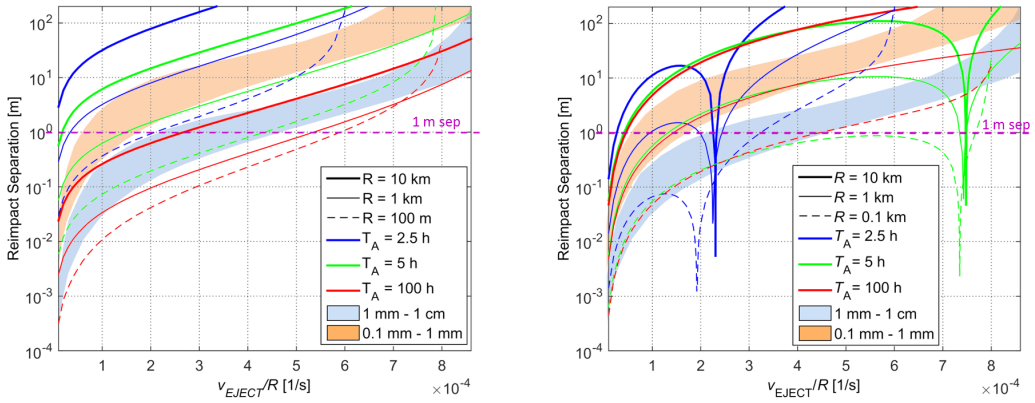

Figure 6.11: Impact point separation for errors in ejection velocity modulus of 1% (a), and errors in ejection angle (in-plane) of 0.33° (b). Line-styles indicate asteroid size; colours its rotation period. The colour patches indicating the separation by differential SRP are also included for reference.

0.2 m for asteroids of 100 m radius (see circles along the vertical line of constant ejection speed). When these circles are above the SRP induced separation of 1 m, they are coloured in black, indicating that the dispersion errors are larger (in the case of a 10 km asteroid by more than one order of magnitude) and the method is infeasible. If dispersion errors are smaller than the desired separation, the corresponding circle is coloured in grey.

For a slowly rotating asteroid (period of 100 h, ②), the separations due to errors in velocity modulus are of the order of 0.5, 0.07 and 0.02 m for asteroids of 10, 1 and 0.1 km radius respectively. In this case all dispersion induced errors are below the desired separation, although for the case of a 10 km asteroid, they would be of the same order of magnitude.

While the dispersions in a slow rotator for asteroids up to 1 km seem acceptable for implementing SRP particle sorting, they would render it useless for larger asteroids of 10 km radius, or for fast-rotators.

Figure 6.12b corresponds to the equivalent plot for errors in the ejection velocity angle. When considering the same two examples as in the previous case, the separation induced by errors in ejection angle is of the order of 4, 0.4 and 0.03 m for the fast-rotator case ①, and 10, 1 and 0.1 m for the slow-rotator ②. This seems to indicate that only asteroids of up to 100 m radius (or slightly larger) are good candidates for the sorting method proposed (grey circles in both examples),

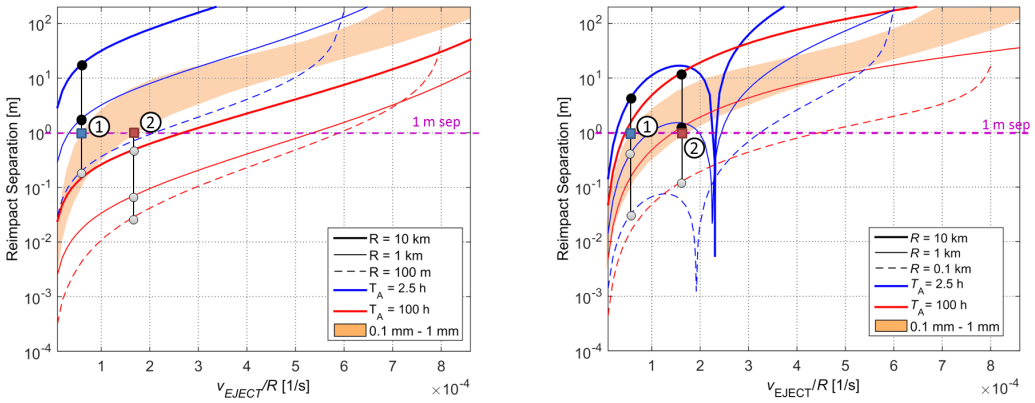

Figure 6.12: Fast versus slow rotators examples with errors in ejection velocity modulus of 1% (a), and errors in ejection angle (in-plane) of 0.33° (b).

as for all other cases separations due to dispersions are larger or of the same order of magnitude as SRP induced ones.

In order to have a more comprehensive analysis of the effect of additional uncertainties, such as variations in the grain size or the densities of the materials, Monte Carlo simulations with 10000 shots were run for a 100 m radius fictitious asteroid rotating with a period of 5 h and with regolith that has previously been ground to a particle radius of 100 μm.

For the composition of the asteroid, an ordinary chondrite S-type asteroid is assumed, containing mostly silicates (in general olivine-pyroxene with densities ranging from 3.2 to 4.37 g/cm^3) and a few traces of metal (of density 7.3 to 7.7 g/cm^3) (Britt et al., 2002). Table 6.1 lists the material composition as well as the assumed mean density and dispersion for five selected materials: Fe-Ni metallic grains, a high density orthopyroxene (opx), two olivine (ol) silicates of medium and low density, and a plagioclase silicate. The average grain density is 3.52 g/cm^3 for this particular mix, which is well within the range of ordinary chondrite meteorites of L or H type (Consolmagno et al., 2008; Flynn et al., 1999).

Table 6.2 presents additional variables with uncertainties in the Monte Carlo simulation. The velocity modulus is selected to obtain a nominal separation of 1 m for an asteroid with a rotation period of 5 hours for 100 μm particles of the materials selected in the previous section (see Fig. 6.10b). The errors in velocity modulus follow a normal distribution with a 3σ uncertainty of 3% of the velocity modulus. Errors in ejection angle are assumed in two orthogonal

Table 6.1: Regolith composition and densities. opx: orthopyroxene, ol: olivine.

Material	Regolith, %	Mean density* [g/cm^3]	1-σ standard dev. [g/cm^3]
Fe-Ni	2%	7.50	0.07
High density opx	15%	3.95	0.10
Medium density ol	50%	3.50	0.10
Low density ol	28%	3.20	0.05
Plagioclase	5%	2.68	0.04

* Data available at http://webmineral.com [retrieved 29 Jan. 2013]

directions (along the longitude and latitude) with a 3-σ standard deviation of 1°. The particles in the regolith are assumed to be ground prior to ejection down to a fine dust with radius of 100 μm. The distribution of particle size is assumed to follow a log-normal distribution of parameters μ_{log} and σ_{log} of -9.21 and 0.05, which corresponds to a mode in particle radius of 100 μm. The mean value is slightly higher and the standard deviation is approximately 5 μm, as can be seen in Table 6.2.

Table 6.2: Uncertainties in Monte Carlo simulation.

		Mean	1-σ standard dev.
Velocity modulus	[cm/s, %]	2.35	1%
Error angle	[deg]	0.00	0.33
Particle radius	[μm]	100.38	5.22

Figure 6.13 shows the results of one Monte Carlo run with 10000 shots. Figure 6.13a represents the trajectory in the Sun-asteroid co-rotating frame, with the Sun along the negative X-axis. Metallic particles are the least affected by SRP and fall closer to the trajectory without perturbations (*red dashed line*). In Fig. 6.13c the same trajectories are plotted in a local horizontal frame with the x_{loc}-axis tangent to the longitude lines on the asteroid (in this case the equator) and the z_{loc}-axis normal to the surface. The Sun direction rotates but it is also close to the negative x_{loc}-axis due to the selected ejection point with phase angle. From the point of view of the ejector (i.e., Fig. 6.13c), the particles start travelling upwards along the local vertical up to a height of about 5 metres, and then start falling behind as the asteroid rotates, with the closest heavier particles falling around 3 m in the anti-solar direction and the lightest particle considered

impacting 7 m away from ejection. A trajectory without SRP is also plotted (*red dashed line*) for comparison. The impact points are represented on Fig. 6.13b and 6.13d. Figure 6.13b shows the displacement along the x_{loc}-axis as a function of the particle density, while Fig. 6.13d plots the impact point in the local horizontal frame. The theoretical impact point without SRP is also indicated in both plots. The main effect of errors in velocity in the y_{loc} direction is a displacement of the impact point in the same direction. Its influence in the separation or mixing of particles is limited.

The separation as a function of density is particularly effective for metallic particles, due to their well differentiated density. There is a much less clear separation among different silicate materials, although a gradient in density along the x_{loc}-axis is evident, from heavier pyroxene-olivine mixtures to lighter silicates of the plagioclase–feldspar family. The distances involved (of teh order of 1 m) are also acceptable from an engineering point of view: a 10 metre collector band extended from the ejection module could be deployed to collect material, or a rover could sweep the impact area in strips perpendicular to the x_{loc} direction.

6.6 Discussion and modelling limitations

The analysis presented so far represents a first feasibility study of the concept of passive sorting of material on asteroids by means of solar radiation pressure. This analysis already shows that ground based collection of material is a promising technique. It would be particularly suited for concentrating materials with well differentiated densities, or to coarsely separate grain sizes.

For the case of material separation as a function of density prior grinding is needed. A possible implementation would consist of regolith grinders that operate for a full asteroid revolution and eject the material only at the desired solar longitude. The collectors would be static, placed a few metres away or even attached to the ejector. Similar to mining terrestrial processes, the collectors could consist of simple mounds, strips of material, or "pools" on the surface where material accumulates for later collection or processing. The process can be repeated iteratively with the material in these mounds being ejected again from a different location for further refinement.

On the other hand, for regolith particle size separation, no grinding is required. The regolith collected could be directly ejected by a moving system that advances

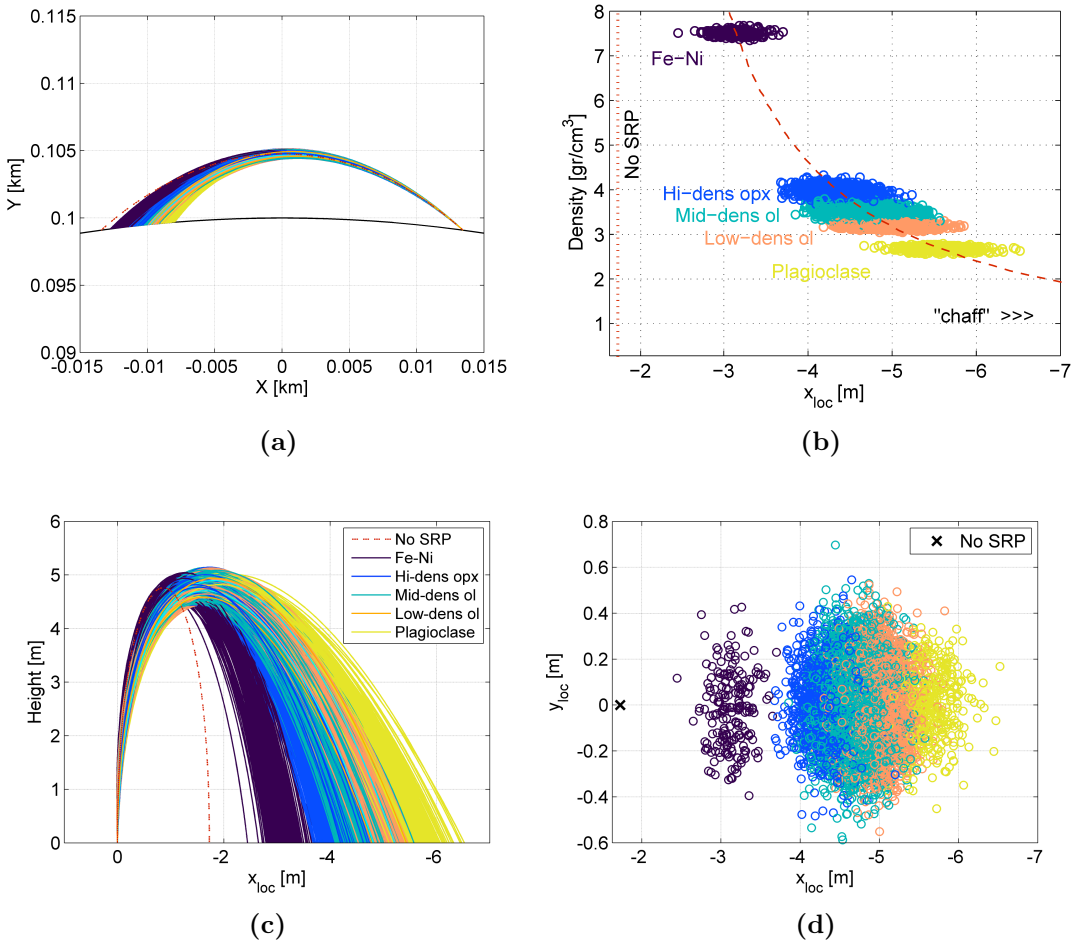

Figure 6.13: Monte Carlo run with 10000 ejected particles of different materials. Plot (a) shows trajectories in the Sun-asteroid co-rotating frame; (b) shows the separation as a function of density; (c) plots the height versus the local horizontal frame separation along the x-axis; (d) shows the impact points in a local horizontal frame.

ideally at the same rate that the asteroid rotates (at a rate of a few millimetres or centimetres per second depending on the asteroid period). However, surface mobility at the required speeds is at best questionable in the microgravity conditions and rough uneven surfaces of asteroids (Richter, 1998). Legged rovers with gripping mechanisms are currently under development for movement on very steep surfaces on Mars or the microgravity conditions of asteroids (Chacin and Tunstel, 2012; Parness, 2011). They would enable steady locomotion on asteroids and the ability to traverse obstacles, but would be unlikely to deliver the required speeds to allow a continuous ejection system that keeps up with the asteroid rotation. Large industrial ventures may consider the installation of complex machinery and systems such as rails to enable locomotion on asteroids for exploitation.

Alternatively, both for density and regolith size separation, a possible solution is moving rovers that return to a designated ejection point at the appropriate time to eject the collected and/or ground material. These rovers could use the gripping-motion systems noted earlier, but at much lower speeds. The ejection sites could be pre-selected to take advantage of the local topography for better separation or ease of collection.

The main benefit of the separation method in itself is the simplicity of its physical principle. This is an advantage for implementation, which can be modular and scalable, with potential for high throughput. Because of this, one of the possible applications is the concentration of materials or grain sizes prior to or in combination with more sophisticated processing techniques specific to each material type or particle size. It would comprise the first step of an industrial process similar to gravity concentration on Earth. Nevertheless, further work on the numerical validation of these semi-analytical results is desirable in order to ensure the efficacy of the method presented in a more complete dynamical model of a small body.

First of all, the use of the CR3BP for numerical propagation instead of a more complex model including the eccentricity of the asteroid orbit around the Sun has a minor influence on the results, as the timescales of the trajectories considered are short compared to the period of a NEO orbit around the Sun. In addition, the analytical results correspond to a simplified planar case and, although an extension to low inclination is possible and the general behaviour is not expected to change, a three-dimensional model is required for large inclination trajectories for ejecta from higher latitudes or from asteroids where the rotation axis is not

perpendicular to the Sun-line. For these cases, the closed-form solution of the radiation pressure approximation (RPA) by Richter and Keller (1995) could allow an analytical extension of the problem to three dimensions. The RPA approach has already been used in the literature to study stable orbits of ejecta from small bodies (Scheeres and Marzari, 2000). It may however not be best suited to study the trajectories of interest, as the model fails if the number of revolutions is small, as in this case.

The irregular shape of asteroids has also an important effect on the method proposed, not only due to unmodelled gravitational perturbations that may render some of the multi-revolution trajectories presented infeasible (Scheeres et al., 1998, 1996), but also due to the changes in the impact point position and direction as a function of the local geometry. Higher order gravitational terms should affect all particles independently of their lightness number, so their influence on the SRP induced separation is expected to be limited for the on-ground collection method where a full revolution does not take place. However, the shape of the asteroid will change the departure and impact conditions significantly.

Regarding the solar radiation pressure force modelling and the material properties, the same reflectance was assumed for all materials by setting the radiation pressure scattering coefficient $Q = 1$, corresponding to complete absorption. The lightness number β is proportional to Q/ρ and material dependant variations in the radiation pressure coefficient would affect the separation between particles. However, reflectance spectra analysis from meteorite metal-silicate mixtures (Cloutis et al., 2009) show that the absolute reflectance of orthopyroxene and olivine silicates is greater than that of denser metallic mixtures, thus having the effect of a greater gap in β values, and theoretically increasing the impact separation between metallic and silicate particles. The simple 'cannon-ball' model used for SRP is considered accurate enough to study particle evolution, where the shape and effective area and the attitude of the particle are not known. In addition, as pointed out earlier, eclipses would not affect the on-ground collection scheme as preferred ejection points result on effectively eclipse-free trajectories (except for the ejection instant). However, if strategies involving multi-revolution trajectories are implemented, eclipses need to be considered. They influence the evolution of eccentricity (and all other orbital elements) in the phase space plots and may result in earlier or later impact.

Additionally, inter-particle forces are of great relevance when separation methods are to be implemented, and they need to be taken into consideration. Scheeres et al. (2010) provide a scaling of these forces as a function of particle size that proves useful to discriminate between the various perturbations.

Self-gravity can in general be ignored for particle sizes below a few centimetres. However, that is not the case for electrostatic forces. In fact, it was theorised (Lee, 1996; Robinson et al., 2001) that they provide a natural mechanism for segregating and accumulating particles smaller than 100 μm on craters and shaded areas through electrostatic levitation, if sufficient charging time is provided. These predicted smooth deposits of material in ponds were confirmed by observation at Eros (Robinson et al., 2001), and the levitation and transport mechanism was reproduced by simulation (Colwell et al., 2005; Hughes et al., 2008). The proposed sorting method is in fact an enhanced extension of this natural "electrostatic winnowing" for larger particles, with the ejection of particles not necessarily performed by electrostatic means.

The ejection sites selected are close to the terminator of the body, where electrostatic forces are expected to be larger (Scheeres et al., 2010), and dust levitation is most likely to take place naturally. The use of electrostatic forces as an aid or as the main ejection mechanism could therefore be considered, using artificial electric fields to accelerate tribocharged particles. However, for the on-orbit collection case, the velocities employed for the ejection are much larger than the ones induced by natural electrostatic forces. In the case of on-ground collection the ejection takes place on the dark side of the asteroid close to sunrise, where none or little electrostatic charge would build up, so it is also unlikely to be a useful mechanism if no artificial charging and electric fields are generated. Nonetheless, natural electrostatic forces need to be taken into account in this case, as the ejection velocities are low enough that very small particles may remain levitating after ejection, and collection takes place on the Sun-lit side where electric charges are building up. In addition, due to the different magnetic and electrical properties of the regolith components (ferromagnetic for the iron-nickel particles, paramagnetic for pyroxenes, non-magnetic for plagioclases) the final portion of their trajectories near the collection point will be influenced differently by the building up electrical charge on the surface, depending on the accumulated charge for each particle and its size.

Of greater concern are the cohesive/adhesive inter-particle forces in contact, which in theory significantly contribute to the internal strength of rubble piles (Sánchez and Scheeres, 2013). Due to cleaner surfaces in vacuum and thus better contact between particles, cohesion can be up to 5 orders of magnitude larger than SRP at 1 AU for millimetre sized particles (Scheeres et al., 2010). Two or more regolith grains in contact after being lifted from the surface are likely to remain together. Depending on the varying packing efficiency or porosity of bundles of grains held together by cohesion (Yang et al., 2007), the effective area-to-mass ratio may vary significantly, and with it the SRP force.

The main limitation on the model and analysis presented with regards to cohesion is therefore the assumption that each dust grain is treated as an independent particle, neglecting the formation of aggregates or clusters of particles due to cohesion or adhesion. Particle aggregates will have varying area-to-mass ratio depending on the shape and structure of the aggregate, and the orientation with respect to the incoming radiation. For example, for the simplest case of two particles (see Fig. 6.14), the effective area-to-mass ratio, and corresponding lightness number β^*, can vary between 0.5 and 1 times the original value for a single particle due to the orientation of the particles. In a more complex three-dimensional aggregate of a larger number of particles, the effective lightness number decreases with the equivalent radius of the cluster r_{eq}, and increases with porosity Φ (for higher porosities the mass per volume decreases). The effect of shape and orientation, represented in the following equation by a factor f, can result in large variations that are difficult to predict. More complex six degrees-of-freedom Monte-Carlo analysis considering different sizes of aggregates, and varying orientation and rotation would need to be designed.

$$\beta^* \sim f \frac{1}{1-\Phi} \frac{r}{r_{eq}} \beta \tag{6.12}$$

Aggregates with very high porosities can be formed in low-gravity conditions (Yang et al., 2007), depending on the force ratio. The force for two particles of the same radius can be expressed as (Scheeres et al., 2010):

$$F_c = \frac{A_H {S_c}^2}{48 {\Omega_O}^2} \frac{r}{2} \tag{6.13}$$

where A_H is the Hamaker coefficient, S_c the cleanliness ratio (which can be assumed close to 1 for vacuum conditions, 0.1 in "dirtier" environments), and Ω_O

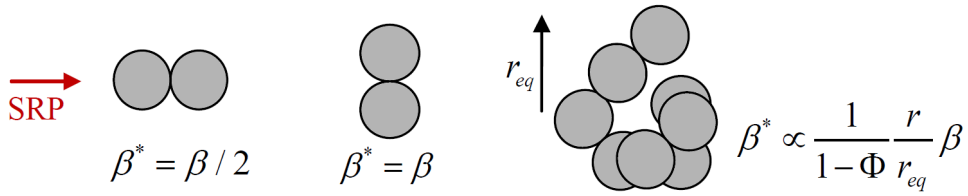

Figure 6.14: Effective lightness number for different configurations of aggregates.

is a constant equivalent to the diameter of a O^{-2} ion ($\sim 1.32 \times 10^{-10}$ m).

The force ratio between cohesive and gravity forces, or Bond ratio, is of the order of 10^6 for particles of 100 μm on a 100 m radius asteroid with a rotation period of 5 hours. This corresponds to porosities of the order of 0.9 according to Yang et al. (2007), or if the packing efficiency definition of Valverde and Castelllanos (2006) is used, to values for this packing efficiency between 0.1 and 0.18. Due to these high porosities, the decrease in lightness number is not as dramatic as initially could be expected. Aggregates of equivalent radius up to 10 times a single grain can have area-to-mass ratios of the same order as independent particles. In general, the effective lightness number will be smaller than that of a single particle, and the graph in Fig. 6.13b will be displaced towards the left. There will be further mixing due to the fact that aggregates may consist of particles of different materials. The fact that the attraction force between a small particle and a larger grain is always greater than the forces between equal sized small particles (Sánchez and Scheeres, 2013) could also inhibit the application to size separation.

In addition, complex models of particle cloud propagation may be required to take into account shading effects and collisions between ejected particles. Collisions may have the beneficial effect of evening out velocities at ejection. They may also break up clusters held together by cohesion if a joint receives an impact with sufficient kinetic energy, or, on the contrary, contribute to the build-up or restructuring of these aggregates, as shown in Richardson (1995) and Dominik and Tielens (1997). The complexity of these interactions is beyond the scope of this chapter. Moreover, shading between particles may significantly reduce the SRP induced separation. Both effects are a function of the particle density in the cloud, which depends on the design of the ejection mechanism, and its mass flow rate.

Finally, bouncing and migration of particles after impact will affect the separation. If such a concentration method is implemented, special emphasis needs to be put on the design of the collectors to avoid undesired post-impact effects.

In general, cohesion represents the biggest drawback for the method proposed for finely ground particles, though it is unlikely that it will completely negate the segregation or concentration effect of solar radiation pressure as a function of size or density. The strength of cohesive/adhesive forces is indeed an inherent problem for all separation techniques in vacuum and low-gravity environment, and other separation techniques that can be extrapolated from their terrestrial equivalent to the asteroid environment would suffer the same impediments.

6.7 Summary

The engineering of the solar radiation pressure (SRP) perturbation is a promising method for separation of dust grains around small bodies. Simplified models to describe the behaviour of particles ejected at low velocities from an asteroid surface have been described and applied to a spherical rotating asteroid. The planar Hamiltonian approach and the phase space graphs introduced have proven to be useful tools to study and understand the behaviour of dust, and they allow prediction of the conditions to perform multiple revolutions or to impact as a function of the ejection site and the size of the particle.

A novel passive SRP separation method has been proposed, and possible variations of the collection strategy were discussed, both on-orbit and on-ground. The analysis suggests that the winnowing-like method with collection on ground can be an effective mechanism for material processing on asteroids of sizes up to 100 m diameter, while the on-orbit collection presents greater challenges. The method has the benefit of simplicity of the physical principle. Similarly to gravity concentration on Earth, a method with low separation efficiency but simple principle and high throughput, the application of the SRP separation method for an initial pre-concentration of regolith sizes or materials is suggested, prior to more complex processing methods. However, the efficacy of such a method would greatly depend on the properties of the material, the conditions in each particular asteroid, and the effect of inter-particle forces that have not been taken into consideration. Also, surface mobility on asteroids in microgravity conditions represents a technological challenge for any collection strategy. Further analysis

and demonstration of the concept through simulations with more complex models and/or microgravity and vacuum chamber laboratory tests would be of great value to assess the viability of SRP induced material separation.

Chapter 7

Conclusions

"But you must not forget it. You become responsible, forever, for what you have tamed."

Saint-Exupéry (1943), *The Little Prince*

This chapter concludes the thesis with general remarks regarding the thesis outcomes, a summary of its main findings, and a discussion on future work and possible extensions.

7.1 General remarks

This thesis has proposed exploiting natural forces and dynamics in the vicinity of minor bodies to devise novel asteroid manipulation methods. The research reported links the abundant research on astrodynamics in literature with new applications that attempt to push forward the boundaries of space engineering. It intends to open the field of asteroid manipulation beyond the pre-conceived idea that the only useful purpose is asteroid deflection. Even though the range of topics treated is diverse, there is a common thread through all of them: exploiting natural astrodynamics for the manipulation of asteroids can be applied across all length-scales resulting in either reduced costs and improved efficiency, such as in methods for asteroid capture or spin state control presented, or in new applications or alternative solutions to traditional problems, such as new orbiting strategies or material separation techniques proposed.

There are however risks associated with the manipulation of asteroids or any other solar system body. Because of this, there is a level of liability for manipulation

concepts and macro-engineering endeavours when put into practice. In general, the larger the scale of the manipulation, the higher the risk of undesired side-effects. This clearly implies that it is in the case of capture, or macro-scale manipulation, that stricter precautions need be taken. The potential for scientific return from controlled manipulation of asteroids and comets is inmense, but so is the responsibility that comes along with it.

It is also important to highlight that asteroid manipulation is a concept in its infancy, and even though this thesis has tried to lay the foundations of a promising research field, there is still much to be done. As such, the models presented have simplifying assumptions, but nevertheless they can be considered initial proofs of concept. This work has much to gain from synergies with other fields such as minor body and solar system science, planetary protection, and space resource utilisation. At the same time, any advances in the possibility of asteroid manipulation will contribute to the future research in those fields.

7.2 Summary of the main findings

This section lists again the main findings and major contributions of the thesis, presented according to length-scale:

7.2.1 Macro-scale: exploiting 3^{rd} body perturbation and manifold dynamics for the capture of asteroids

- For the first time exploiting manifold dynamics has been analysed for the capture of small asteroids into libration point orbits (LPOs) about the Earth's collinear L_1 and L_2 points
- A new subfamily of NEOs has been defined: the Easily Retrievable Objects (EROs), containing minor bodies in Earth-like orbits that can be captured at moderate Δv costs into LPOs. An associated quantifiable and ordered classification based on their potential for capture has been established
- A robust methodology for systematic pruning of the Minor Planet Centre NEO database and optimisation of capture trajectories through the hyperbolic invariant stable manifolds has been implemented and tested

- Despite the incomplete census of very small objects, the ERO catalogue has already been populated with twelve candidates, assuming a threshold cost of 500 m/s and a double impulsive burn strategy. Twenty-five capture opportunities over the next 30 years to vertical Lyapunov, planar Lyapunov, and halo orbits have been optimised and presented

- The most promising ERO candidate is asteroid 2006 RH120, which could be captured with a single impulse of 58 m/s to a southern halo family orbit. 2006 RH120 is also the only Temporarily Captured Orbiter of the Earth confirmed to date

- Analysis shows that the retrieval of an entire small 2–7 m asteroid or a similar sized portion of a larger one is feasible in terms of energy

- The selected capture target orbits could in addition serve as natural gateways to families of orbits in the Earth–Moon system through homoclinic and heteroclinic connections between collinear points, the Earth and the Moon

7.2.2 Macro- to Meso-scale: exploiting tidal torques for asteroid spin state and structure manipulation during swing-bys

- Tidal torques can be used to modify the spin or configuration of minor bodies during a swing-by of a planet or moon in the capture phase of an asteroid retrieval mission

- The net effect of the tidal torque is highly dependant on the initial spin state, the geometric configuration at the pericentre of the swing-by, the mass of the central body, and the distance of the swing-by

- Undesired spin-up of a captured asteroid during a swing-by can be avoided by inducing a small retrogade rotation (with respect to the orbital motion)

- A fast rotating asteroid (with a prograde rotation faster than three times the true anomaly variation rate at pericentre) does not suffer either from spin-up or de-spin

- Asteroids with a residual prograde rotation (with rotation rates smaller than the true anomaly variation at pericentre) can be de-spun during an Earth swing-by, depending on the mass of the central body and the shape of the asteroid, by tuning the relative attitude of the asteroid at pericentre passage

- Asteroid spin-up can be achieved in a similar manner for prograde slow-rotating asteroids, to spin rates of the order of the true anomaly variation rate at pericentre, usually higher than the mass shedding limit for low altitude flybys of massive bodies

- Induced spin-up can be employed ultimately to break-up a contact binary or fragment a rubble pile, for scientific reasons or exploitation purposes

- Analysis indicates that binary asteroids are unlikely to maintain their binary structure after a close encounter with a massive body (for the case of the Earth, less than 10 Earth radii), except for particular geometrical configurations

7.2.3 Meso- to Micro-scale: exploiting solar radiation pressure for novel asteroid exploration orbiting strategies

- Solar radiation pressure (SRP) perturbations allow the design and generation of highly non-Keplerian orbits with rapidly varying eccentricity in the vicinity of very small minor bodies

- Two orbiting solutions have been presented that allow coverage of key regions in the orbital plane of an asteroid, including passes over the sub-solar and anti-solar points. These solutions are complementary to hovering strategies and other well-known families of orbits associated with the terminator plane

- The first solution presented is an alternating orbiter solution, which reverses its orbit direction after a number of revolutions and takes advantage of the natural evolution of the orbit eccentricity to reduce the size and frequency of manoeuvres required

- The alternating orbiter strategy provides complementary coverage to terminator and quasi-terminator orbits, can reduce the fuel consumption by a factor of 10 when compared with hovering and pseudo-hovering strategies, and has advantages for gravity field characterisation when compared to hovering or multiple flybys

- Trajectories that combine high-altitude prograde and low-altitude retrograde sections (with respect to the asteroid rotation) have been shown to be effective in reducing the adverse influence of resonances with the rotation of a non spherical asteroid

- The second solution proposes the use of planar symmetric periodic a and $g - g$' orbit families of the Hill problem, which benefit from inversions of the orbit direction due to the natural dynamics of the problem

- These families of orbits have been extended for the first time to the levels of solar radiation pressure perturbation characteristic of minor bodies

- The evolution, feasibility and stability of these families for realistic asteroid densities and lightness numbers has been presented. Most families are shown to be unstable

- Despite their mild vertical motion instability, double-periodic g' orbits have been proposed for temporary orbiters in the equatorial plane, because of their good coverage of the asteroid's surface on the orbital plane, and their robustness against non-sphericity perturbations

- Additional solutions such as free return trajectories for "hopper" spacecraft have been presented

- To account for required spacecraft effective surface changes, variable surface area and/or variable reflectivity devices are proposed to enable these orbiting concepts

7.2.4 Micro-scale: exploiting solar radiation pressure for asteroid material separation and sorting

- A novel winnowing-like method to separate asteroid material as a function of the density or particle size has been proposed

- On-ground collection strategies have been shown to be more promising than on-orbit collection.
- The on-ground collection method is only applicable to small-sized asteroids (of the order of 100 m diameter or smaller)
- The method allows the partial separation of metallic particles from less dense silicate ones by ejecting and collecting the regolith material close to the terminator at sunrise. For a 100 m radius asteroid, separations of the order of 1 m between metallic rich and silicate rich material can be achieved with ejection velocities of 2.35 cm/s
- Inter-particle forces such as cohesion will lower the method's effectiveness depending on the material properties and the type of aggregates it forms
- Even with a reduced efficiency, possible applications for pre-concentration of regolith sizes prior to more complex sorting methods are suggested

7.3 Future work

After presenting the major contributions of the thesis, further analyses and lines of research can be devised to build upon or complement its results, or improve the fidelity of the models used.

7.4 Further applications of the methods

In particular, the methods proposed can be extended or applied to additional problems:

- *Generation and extension of temporary captures:* The dynamical features through which naturally occurring moonlets are temporarily captured in the Earth–Moon system are not significantly different from the method used to capture EROs. In fact, the only confirmed Temporarily Captured Orbiter (TCO) is also the best ERO candidate (Granvik et al., 2011). TCOs follow a transit orbit delimited by L_1 or L_2 manifold tubes to enter and exit their bounded phase around the Earth. If fully capturing EROs in Libration Point Orbits (LPO) is considered too costly or deemed unnecessary

for scientific purposes, artificially turning one ERO into a TCO should be a more cost-effective solution that provides observation opportunities and direct access to an asteroid during a prolonged period of time. The efforts to further extend the lifetime of a TCO in its captured phase (Urrutxua et al., 2014; Verrier and McInnes, 2015) could also be applied to these artificially generated moonlets. For that purpose, and to correctly reproduce temporary captured phases, Urrutxua et al. (2014) show that higher fidelity models are required.

- *NEO and TCO access from Libration Point Orbits:* A similar strategy to that employed for ERO capture, but inverted starting from an LPO orbit and escaping through the hyperbolic invariant unstable manifold, can be adapted to generate transfers from the Earth libration points to Near–Earth Objects on their original orbits. Due to the much lower masses to be accelerated (essentially the spacecraft), the cap on the total Δv cost for such a transfer could be raised. This strategy has been used for the transfer of the Chinese probe Chang'e 2 to asteroid Toutatis (Zoua et al., 2014). Asteroids can thus become end-of-life extension targets for current or future telescopes and spacecraft near L_1 or L_2, such as JAXA's technology demonstrator DESTINY. In addition, this method can also be applied to access newly discovered natural TCOs. Given their typically highly eccentric retrograde trajectories, transfers from the libration points can prove more economical than direct access from Earth. Granvik et al. (2011) estimate that at any given time there should be at least two 1-metre sized objects temporarily captured, which can also become attractive end-of-life options for libration point spacecraft.

- *Extended concepts for tidal de-spin:* As a minor addendum to the analysis of tidal torque exploitation, the effects of close encounters on the spin and structure of an asteroid could be enhanced by artificial means. A possible implementation would be by modifying the shape of the asteroid with deployable tethers (a variation of the concept proposed in Bombardelli, 2007). If the tethers are movable or rotating, they can also be utilised to slightly modify the spin state of the asteroid prior to the swing-by and its attitude at pericentre, to minimise or maximise the tidal disruption.

- *Comprehensive study of the Hill problem at high SRP:* From a purely mathematical point of view, it can be argued that the mapping of the periodic

orbit families of the Hill problem with high solar radiation pressure presented in Chapter 5 is not complete. Important families such as the c family of planar Lyapunov orbits around L_1, or the f family of distant retrograde orbits have not been included in the analysis. The main reasons for the omission are the limited applicability to real missions to asteroids: due to the L_1 point migration sunward away from the asteroid at high levels of SRP, these associated families would not be particularly suited for asteroid observations. However, for completeness, the evolution of the full map of planar solutions of the Hill problem can be extended to include the missing families, as well as their stability. In addition, particular attention could be paid to vertical stability bifurcations that lead to 3-dimensional families which are believed to connect with halo orbits, among other. Finally, extension to higher multiplicity orbit families could also be addressed.

7.4.1 Improvements of the models

Furthermore, the simplified models presented can be developed to include additional dimensions and other perturbations:

- *Maintenance and improvement of the Easily Retrievable Objects catalogue:* With the advances in telescope optics and detection methods, new asteroids and comets are being discovered on a daily basis, and thus the number of Near–Earth Objects in the Minor Planet Centre database is expected to grow exponentially. Automation of the database download, pruning methods and transfer trajectory optimisation will allow an up-to-date derived catalogue of capture opportunities for Easily Retrievable Objects (ERO). Indeed, with the increase in completeness of the asteroid census, several very low-cost opportunities are expected to be found each year. The main benefit of such a capture catalogue for the international community, and the growing asteroid mining industry, is a quick access to nominal and backup targets for exploration, scientific or resource exploitation probes. In addition, improved dynamical models should be implemented to allow for higher fidelity transfers. In that respect, at least the implementation of the Elliptic Restricted 3-Body Problem would be advisable, to take into account the eccentricity of the Earth's orbit, and the lunar third body perturbation need be considered. Although the list of EROs and their associated costs is

not expected to differ significantly with improved models, the high fidelity transfers would clearly be required for a real capture mission.

- *Analysis of tidal torques exploitation in three dimensions:* The analysis presented in Chapter 4 is limited to planar cases, with the rotation axis of the asteroid or the binary perpendicular to the swing-by plane. The models presented can be extended to three dimensions, allowing for more complex interactions between the orbit and the rotational state of the asteroid or binary pair. In principle, induced tumbling and de-tumbling of asteroids during swing-bys, or their avoidance, could be achieved with these new models. However, the practicality and effectiveness of such strategies would need to be confirmed. The effect on the binary component orbits is also expected to include orbital plane changes induced by the tidal torques.

- *Alternating orbiter applicability for future missions:* The alternating orbiter strategy problem has been tackled in this thesis from a theoretical perspective. These orbits can, in principle, be applied to current planned missions to asteroids, such as Hayabusa 2. On one hand, it would require a higher fidelity model of the asteroid's orbit, gravity field and rotational state to correctly reproduce the orbital perturbations on the spacecraft. On the other hand, more flexible strategies can be envisaged, for example by releasing the symmetry constraint imposed on the orbit currently. The manoeuvre size, direction and frequency could be tuned to perform global coverage of the spacecraft, not limited to the orbital plane, and certainly not requiring a symmetric pattern.

- *Additional material separation studies:* The regolith sorting method proposed in Chapter 6 has been modelled from an astrodynamics perspective, with limited discussion on the effect of material properties and forces such as cohesion. To objectively estimate its efficiency, it would require a thorough comparison with other methods, such as electrostatic or magnetic separation, including as detailed mechanical and material modelling as possible. Experimental validation of these regolith sorting concepts could also be foreseen.

Bibliography

Abell, P. A., Barbee, B. W., Mink, R. G., Adamo, D. R., Alberding, C. M., Mazanek, D. D., Johnson, L. N., Yeomans, D. K., Chodas, P. W., Chamberlin, A. B., Benner, L. A. M., Drake, B. G. and Friedensen, V. P. (2012). The Near-Earth Object Human space flight Accessible Targets Study (NHATS) list of Near-Earth Asteroids: Identifying potential targets for future exploration, *44^{th} annual meeting of the Division for Planetary Sciences of the American Astronomical Society*, Vol. 1659, Reno, NV, USA.

Adamo, D. R., Giorgini, J. D., Abell, P. A. and Landis, R. R. (2010). Asteroid destinations accessible for human exploration: A preliminary survey in mid-2009, *Journal of Spacecraft and Rockets* **47**(6): 994–1002.

A'Hearn, M. F., Belton, M. J. S., Delamere, A. and Blume, W. H. (2005). Deep Impact: A large-scale active experiment on a cometary nucleus, *in* C. T. Russell (ed.), *Deep Impact Mission: Looking Beneath the Surface of a Cometary Nucleus*, Springer Netherlands, Dordrecht, the Netherlands, pp. 1–21.

Alessi, E. M. (2010). *The Role and Usage of Libration Point Orbits in the Earth-Moon System*, PhD thesis, Universitat de Barcelona, Barcelona, Spain.

Alessi, E. M., Colombo, C., Sanchez Cuartielles, J. P. and Landgraf, M. (2013). Out-of-plane extension of resonant encounters for escape and capture, *64^{th} International Astronautical Congress*, IAC-13.C1.9.1, Beijing, China.

Andrés de la Fuente, J. I. (2007). *Enhanced Modelling of LAGEOS Non-Gravitational Perturbations*, PhD thesis, Technische Universiteit Delft, Delft, the Netherlands.

Aravind, P. K. (2007). The physics of the space elevator, *American Journal of Physics* **75**(2): 125–130.

Augustine, N. R., Austin, W. M., Chiba, C., Kennel, C. F., Bejmuk, B. I., Crawley, E. F., Lyles, L. L., Chiao, L., Greason, J. and Ride, S. K. (2009). Seeking a human spaceflight program worthy of a great nation, *Technical Report 396093main_HSF*, Review of U.S. Human Spaceflight Plans Committee.

Baileya, N. J., Swinerda, G. G., Morleya, A. D. and Lewis, H. G. (2006). Near Earth Object impact simulation tool for supporting the NEO mitigation decision making process, *Proceedings of the International Astronomical Union* **2**(S236): 477–486.

Balmino, G. (1994). Gravitational potential harmonics from the shape of an homogeneous body, *Celestial Mechanics and Dynamical Astronomy* **60**: 331–364.

Baoyin, H.-X., Chen, Y. and Li, J.-F. (2010). Capturing Near Earth Objects, *Research in Astronomy and Astrophysics* **10**(6): 587–598.

Barbee, B. W., Espositoy, T., Elfego, P. I., Hur-Diaz, S., Mink, R. G. and Adamo, D. R. (2010). A comprehensive ongoing survey of the Near-Earth Asteroid population for human mission accessibility, *AIAA Guidance, Navigation, and Control Conference*, AIAA 2010-8368, Toronto, Canada.

Barucci, M. A., Cheng, A. F., Michel, P., Benner, L. A. M., Binzel, R. P., Bland, P. A., Böhnhardt, H., Brucato, J. R., Bagatin, A. C., Cerroni, P., Dotto, E., Fitzsimmons, A., Franchi, I. A., Green, S. F., Lara, L.-M., Licandro, J., Marty, B., Muinonen, K., Nathues, A., Oberst, J., Rivkin, A. S., Robert, F., Saladino, R., Trigo-Rodriguez, J. M., Ulamec, S. and Zolensky, M. (2012). MarcoPolo-R near–earth asteroid sample return mission, *Experimental Astronomy* **33**(2-3): 645–684.

Barucci, M. A., Yoshikawa, M., Michel, P., Kawagushi, J., Yano, H., Brucato, J. R., Franchi, I. A., Dotto, E., Fulchignoni, M., Ulamec, S. and Team, M. P. S. (2009). MARCO POLO: near–earth object sample return mission, *Experimental Astronomy* **23**(3): 785–808.

Batkhin, A. B. (2013a). Symmetric periodic solutions of the Hill's problem. I, *Cosmic Research* **51**(4): 275–288.

Batkhin, A. B. (2013b). Symmetric periodic solutions of the Hill's problem. II, *Cosmic Research* **51**(6): 452–464.

Battin, R. H. (1999). *An Introduction to the Mathematics and Methods of Astrodynamics, Revised Edition*, AIAA Education Series, New York, NY, USA.

Belbruno, E. and Marsden, B. G. (1997). Resonance hopping in comets, *The Astronomical Journal* **113**(4): 1433–1444.

Belló, M., Gómez, G. and Masdemont, J. J. (2010). Invariant manifolds, Lagrangian trajectories and space mission design, *in* E. Perozzi and S. Ferraz-Mello (eds), *Space Manifold Dynamics – Novel Spaceways for Science and Exploration*, Springer-Verlag, New York, NY, USA, pp. 1–96.

Bewick, R., Sanchez, J. P. and McInnes, C. R. (2012). The feasibility of using an L_1 positioned dust cloud as a method of space-based geoengineering, *Advances in Space Research* **49**(7): 1212–1228.

Binzel, R. P., Lupishko, D., di Martino, M., Whiteley, R. J. and Hahn, G. J. (2002). Physical properties of Near–Earth Objects, *in* W. Bottke, A. Cellino, P. Paolicchi and R. P. Binzel (eds), *Asteroids III*, University of Arizona Press, Tucson, AZ, USA, pp. 255–271.

Blackburn, E. P., Sabroff, A. E., Bohling, R. F., DeBra, D. B., Dobrotin, B., Fischell, R., Fleig, A. J., Kelly, J., Fosth, D., O'Neill, S., Spenny, C. H., Perkel, H., Roberson, R. E., Scott, E. D. and Tinling, B. (1969). Spacecraft gravitational torques, *Technical Report NASA SP-8024*, NASA.

Bombardelli, C. (2007). Artificial spin-up and fragmentation of sub-kilometre asteroids, *58th International Astronautical Congress*, IAC-07.A3.4.09, Hyderabad, India.

Bombardelli, C., Urrutxua, H., Cano, J., Cacciatore, F., Bastante, J., Foerstner, R., Falke, A., Ahedo, E., Herrera, J. and Peláez, J. (2013). KABOOM: Kinetic Asteroid-Binary-Object Orbit Modification, *Technical Report 12/X03 ESA/4000107023/12/F/MOS*, UPM, ESA GSP SysNOVA Initiative.

Bombardelli, C., Urrutxua, H., Gálvez, A. and Carnellix, I. (2012). The SIROCO asteroid deflection demonstrator, *AAS/AIAA Space Flight Mechanics Meeting*, AAS 12-227, Charleston, SC, USA.

Bookless, J. and McInnes, C. (2006). Dynamics and control of displaced periodic orbits using solar-sail propulsion, *Journal of Guidance, Control, and Dynamics* **29**(3): 527–537.

Bookless, J. P. (2006). *Dynamics, Stability and Control of Displaced Non-Keplerian Orbits*, PhD thesis, University of Glasgow.

Borggräfe, A., Ceriotti, M., Heiligers, J. and McInnes, C. (2012). Coupled orbit and attitude dynamics of a reconfigurable spacecraft with solar radiation pressure, 63rd *International Astronautical Congress*, IAC-12.C1.9.10, Naples, Italy.

Borggräfe, A., Heiligers, J., Ceriotti, M. and McInnes, C. R. (2014). Distributed reflectivity solar sails for extended mission applications, *in* M. Macdonald (ed.), *Advances in Solar Sailing*, Springer-Verlag Berlin Heidelberg, pp. 331–350.

Borum, A., Burns, J., Wentzel, P. and Andreyev, A. (2012). Asteroid capture using a binary exchange mechanism, *Virginia Space Grant Consortium Student Research Conference*, Williamsburg, VA, USA.

Bottke, W., Cellino, A., Paolicchi, P. and Binzel, R. P. (2002a). An overview of the asteroids: The Asteroids III perspective, *in* W. Bottke, A. Cellino, P. Paolicchi and R. P. Binzel (eds), *Asteroids III*, University of Arizona Press, Tucson, AZ, USA, pp. 3–15.

Bottke, W. F., Morbidelli, A., Jedicke, R., Petit, J.-M., Levison, H. F., Michel, P. and Metcalfe, T. S. (2002b). Debiased orbital and absolute magnitude distribution of the Near-Earth Objects, *Icarus* **156**(2): 399–433.

Bottke, W., Nolan, M., Greenberg, R. and Kolvoord, R. (1994). Collisional lifetimes and impact statistics of near-Earth asteroids, *in* T. Gehrels, M. Matthews and A. Schumann (eds), *Hazards Due to Comets and Asteroids*, University of Arizona Press, Tucson, AZ, USA, p. 336357.

Bottke, W., Vokrouhlicky, D., Broz, M., Nesvorný, D. and Morbidelli, A. (2001). Dynamical spreading of asteroid families by the Yarkovsky effect, *Science* **294**: 16931696.

Brasser, R. and Wiegert, P. (2008). Asteroids on Earth-like orbits and their origin, *Monthly Notices of the Royal Astronomical Society* **386**: 2031–2038.

Britt, D. T., Yeomans, D., Housen, K. and Consolmagno, G. (2002). Asteroid density, porosity, and structure, *in* W. Bottke, A. Cellino, P. Paolicchi and R. P. Binzel (eds), *Asteroids III*, University of Arizona Press, Tucson, AZ, USA, pp. 485–500.

Brophy, J., Culick, F., Friedman, L., Allen, C., Baughman, D., Bellerose, J., Betts, B., Brown, M., Casani, J. and Coradini, M. (2012). Asteroid retrieval feasibility study, *Technical report*, Keck Institute for Space Studies, Caltech, JPL.

Broschart, S. B., Lantoine, G. and Grebow, D. J. (2014). Quasi-Terminator Orbits near primitive bodies, *Celestial Mechanics and Dynamical Astronomy* **120**(2): 195–215.

Broschart, S. B. and Scheeres, D. J. (2005). Control of hovering spacecraft near small bodies: Application to asteroid 25143 Itokawa, *Journal of Guidance, Control, and Dynamics* **28**(2): 343–354.

Broschart, S. B. and Scheeres, D. J. (2007). Boundedness of spacecraft hovering under dead-band control in time-invariant systems, *Journal of Guidance, Control, and Dynamics* **30**(2): 601–610.

Broucke, R. (1969). Stability of periodic orbits in the elliptic, restricted three-body problem, *AIAA Journal* **7**(6): 1003–1009.

Broucke, R. A. (1968). Periodic orbits in the restricted three-body problem with earth-moon masses, *Technical Report JPL TR 32-1168*, JPL, Caltech.

Brown, P., Spalding, R. E., ReVelle, D. O., Tagliaferri, E. and Worden, S. P. (2002). The flux of small near–Earth objects colliding with the Earth, *Nature* **420**: 294–296.

Burt, R. O. and Mills, C. (1984). *Gravity Concentration Technology*, Elsevier, Amsterdam, The Netherlands.

Byram, S. M. and Scheeres, D. J. (2008). Spacecraft dynamics in the vicinity of a comet in a rotating frame, *AIAA/AAS Astrodynamics Specialist Conference*, AIAA 2008-7202, Hololulu, HI, USA.

Canalias, E. and Masdemont, J. J. (2006). Homoclinic and heteroclinic transfer trajectories between Lyapunov orbits in the Sun-Earth and Earth-Moon systems, *AIMS Discrete and Continuous Dynamical Systems - Series A (DCDS-A)* **14**(2): 261 – 279.

Cardiff, E. H. and Englander, J. A. (2013). Asteroid retrieval propulsion and flight dynamics concepts, *33rd International Electric Propulsion Conference*, IEPC-2013-455, Washington DC, USA.

Carnelli, I., Gálvez, A. and Izzo, D. (2006). Don Quijote: a NEO deflection precursor mission, *NASA Workshop: Near–Earth Object Detection, Characterisation and Threat Mitigation*, ACT-RPR-MAD-2006-NASANEOWS, Vale, CO, USA.

Ceriotti, M. and Cuartielles, J. P. S. (2013). Orbit control of asteroids in libration point orbits for resource exploitation, *64th International Astronautical Congress*, IAC-13.C1.4.3, Beijing, China.

Ceriotti, M., Harkness, P. and McRobb, M. (2014). Variable-geometry solar sailing: the possibilities of the quasi-rhombic pyramid, *in* M. Macdonald (ed.), *Advances in Solar Sailing*, Springer-Verlag Berlin Heidelberg, pp. 899–919.

Chacin, M. and Tunstel, E. (2012). Gravity-independent locomotion: Dynamics and position-based control of robots on asteroid surfaces, *in* A. Dutta (ed.), *Robotic Systems - Applications, Control and Programming*, InTech, Rijeka, Croatia, pp. 314–338.

Chandrasekhar, S. (1963). The equilibrium and the stability of the Roche ellipsoids, *The Astrophysical Journal* **138**: 1182–1213.

Chernikov, Y. A. (1970). The photogravitational restricted three-body problem, *Soviet Astronomy - AJ* **13**(1): 176–181.

Chesley, S. R., Chodas, P. W., Milani, A., Valsecchi, G. B. and Yeomans, D. K. (2002). Quantifying the risk posed by potential Earth impacts, *Icarus* **159**: 423–432.

Chesley, S. R., Ostro, S. J., Vokrouhlický, D., Čapek, D., Giorgini, J. D., Nolan, M. C., Margot, J.-L., Hine, A. A., Benner, L. A. M. and Chamberlin, A. B. (2003). Direct detection of the Yarkovsky effect by radar ranging to asteroid 6489 Golevka, *Science* **302**(5651): 1739–1742.

Chodas, P. W. and Chesley, S. R. (2001). 2000 SG344: The story of a potential Earth impactor, *Bulletin of the American Astronomical Society* **33**: 1196.

Clark, B. E., Hapke, B., Pieters, C. and Britt, D. (2002). Asteroid space weathering and regolith evolution, *in* W. F. Bottke, A. Cellino, P. Paolicchi and R. P. Binzel (eds), *Asteroids III*, University of Arizona Press, Tucson, AZ, USA, pp. 585–599.

Clark, R., Sinn, T., Lucking, C., Donaldson, N., Brown, R. H. and Parry, T. (2012). Strathsat-R : Deploying inflatable CubeSat structures in micro gravity, *63rd International Astronautical Congress*, Naples, Italy.

Clarke, A. C. (1945). Extra-terrestrial relays – Can rocket stations give worldwide radio coverage?, *Wireless World* **L1**(10): 305–308.

Cloutis, E. A., Hardersen, P. S., Reddy, V., Gaffey, M., Bailey, D. T. and Craig, M. A. (2009). Metal-orthopyroxene and metal-olivine mixtures: spectral reflectance properties and implications for asteroid spectroscopy, *40th Lunar and Planetary Science Conference*, The Woodlands, TX, USA.

Colombo, C., Lücking, C. and McInnes, C. R. (2011). Orbital dynamics of high area-to-mass ratio spacecraft with J_2 and solar radiation pressure for novel Earth observation and communication services, *Acta Astronautica* **87**(1): 137–150.

Colwell, J. E., Gulbis, A. A., Horanyi, M. and Robertson, S. (2005). Dust transport in photoelectron layers and the formation of dust ponds on Eros, *Icarus* **175**: 159–169.

Consolmagno, G., Brittb, D. and Macke, R. (2008). The significance of meteorite density and porosity, *Chemie der Erde* **68**: 1–29.

Cuk, M. (2007). Formation and destruction of small binary asteroids, *The Astrophysical Journal* **658**: 57–69.

Dankowicz, H. (1993). Some special orbits in the two-body problem with radiation pressure, *Celestial Mechanics and Dynamical Astronomy* **58**: 353–370.

Darwin, G. (1897). Periodic orbits, *Acta Mathematica* **21**(1): 99–242.

Davidsson, B. J. R. (2001a). Tidal splitting and rotational breakup of solid spheres, *Icarus* **142**: 525–535.

Davidsson, B. J. R. (2001b). Tidal splitting and rotational breakup of solid biaxial ellipsoids, *Icarus* **149**: 375–383.

Domingo, V., Fleck, B. and Poland, A. I. (1995). The SOHO mission: An overview, *Solar Physics* **162**(1-2): 1–37.

Dominik, C. and Tielens, A. G. G. M. (1997). The physics of dust coagulation and the structure of dust aggregates in space., *The Astrophysical Journal* **480**: 647–673.

Dormand, J. R. and Prince, P. J. (1980). A family of embedded Runge-Kutta formulae, *Journal of Computational and Applied Mathematics* **6**(1): 19–26.

Doyle, D., Pilbratt, G. and Tauber, J. (2009). The Herschel and Planck space telescopes, *Proceedings of the IEEE* **97**(8): 1403–1411.

Edward, T. L. and Stanley, G. L. (2005). Gravitational tractor for towing asteroids, *Nature* **438**: 177–178.

Elvis, M. (2014). How many ore-bearing asteroids?, *Planetary and Space Science* **91**: 20–26.

Elvis, M. and Esty, T. (2014). How many assay probes to find one ore-bearing asteroid?, *Acta Astronautica* **96**: 227–231.

Fang, J. and Margot, J.-L. (2012). Binary asteroid encounters with terrestrial planets: timescales and effects, *The Astronomical Journal* **143**(25): 1–8.

Farinella, P. and Chauvineau, B. (1993). On the evolution of binary Earth-approaching asteroids, *Astronomy and Astrophysics* **279**: 251–259.

Farquhar, R. W. (1967). Station-keeping in the vicinity of collinear libration points with an application to a lunar communications problem, *Science and Technology Series: Space Flight Mechanics Specialists Symposium* **11**: 519–535.

Flynn, G. J., Moore, L. B. and Klock, W. (1999). Density and porosity of stone meteorites: Implications for the density, porosity, cratering, and collisional disruption of asteroids, *Icarus* **142**: 97–105.

Funase, R., Mori, O., Tsuda, Y., Shirasawa, Y., Saiki, T., Mimasu, Y. and Kawaguchi, J. (2010). Attitude control of IKAROS solar sail spacecraft and its flight results, *61st International Astronautical Congress*, IAC-10.C1.4.3, Prague, Czech Republic.

García Yárnoz, D., Sanchez Cuartielles, J. and McInnes, C. (2013). Applications of solar radiation pressure dominated highly non-Keplerian trajectories around minor bodies, *64th International Astronautical Congress*, IAC-13.C1.9.6, Beijing, China.

Gates, M., Stich, S., McDonald, M., Muirhead, B., Mazanek, D., Abell, P. and Lopez, P. (2014). The asteroid redirect mission and sustainable human exploration, *65th International Astronautical Congress*, IAC-14.A5.1.1, Toronto, Canada.

Giancotti, M., Campagnola, S., Tsuda, Y. and Kawaguchi, J. (2014). Families of periodic orbits in Hill's problem with solar radiation pressure: application to Hayabusa 2, *Celestial Mechanics and Dynamical Astronomy* **120**(3): 269–286.

Gibbings, A., Vasile, M., Hopkins, J.-M., Burns, D. and Watson, I. A. (2012). Potential of laser-induced ablation for future space applications, *Space Policy* **28**(3): 149–153.

Gil-Fernandez, J., Cabral, F., Prieto, T., Escorial, D., Barrena, V., Amata, G. B., Lavagna, M. and Filipetto, D. (2013). BEAST (Binary Asteroid Orbit Modification), *Technical Report 12/X03 ESA/4000106980/12/F/MOS*, GMV, ESA GSP SysNOVA Initiative.

Glassmeier, K.-H., Boehnhardt, H., Koschny, D., Kührt, E. and Richter, I. (2007). The Rosetta mission: Flying towards the origin of the solar system, *Space Science Reviews* **122**(1-4): 1–21.

Gómez, G., Llibre, J., Martínez, R. and Simó, C. (2000). *Dynamics and Mission Design Near Libration Points - Fundamentals: The Case of Collinear Libration Points*, Vol. 1 of *World Scientific Monograph Series in Mathematics*, World Scientific Publishing, Singapore.

Gómez, G. and Mondelo, J. M. (2001). The dynamics around the collinear equilibrium points of the RTBP, *Physica D: Nonlinear Phenomena* **157**(4): 283–321.

Graham, J. N., Lambson, R. S., Nordwick, S. M., Dahlgren, E. J. and Young, C. A. (2010). Benefication of terrestrial resources for the production of lunar simulant separates, *Workshop on the Lunar Applications of Mining and Mineral Beneficiation*, 2009LPI_40.1332C, Butte, MT, USA.

Granvik, M., Vaubaillon, J. and Jedicke, R. (2011). The population of natural Earth satellites, *Icarus* **218**(1): 262–277.

Greenstreet, S., Ngo, H. and Gladman, B. (2011). The orbital distribution of Near-Earth Objects inside Earth's orbit, *Icarus* **217**: 355–366.

Hamilton, D. P. and Krikov, A. V. (1996). Circumplanetary dust dynamics: Effects of solar gravity, radiation pressure, planetary oblateness, and electromagnetism, *Icarus* **123**: 503–523.

Haskin, L. A., Podnieks, E. R., Roepke, W. W., Agosto, W. N., Rowley, J. C., Neudecker, J. W., Meek, T. T., Vaniman, D. T., Cocks, F. H., Wright, R. A., Blacic, J. D., Allton, J. H., Galindo, C., J., Watts, L. A., Pettit, D. R. and Lewis, W. (1986). Lunar material and processes, *in* W. Mendell (ed.), *Lunar Bases and Space Activities of the 21st Century*, The Lunar and Planetary Institute, Houston, TX, USA.

Hasnain, Z., Lamb, C. and Ross, S. D. (2012). Capturing Near-Earth asteroids around Earth, *Acta Astronautica* **81**: 523–531.

Heiligers, J., Ceriotti, M., McInnes, C. and Biggs, J. (2011). Displaced geostationary orbit design using hybrid sail propulsion, *Journal of Guidance, Control and Dynamics* **34**(6): 1852–1866.

Heiligers, J., Diedrich, B., Derbes, B. and McInnes, C. (2014). Sunjammer: Preliminary end-to-end mission design, *SPACE2014 – AIAA/AAS Astrodynamics Specialist Conference*, AIAA 2014-4127, San Diego, CA, USA.

Hénon, M. (1965). Exploration numérique du problème restreint. II. Masses égales, stabilité des orbites périodiques, *Annales d'Astrophysique* **28**: 992–1007.

Hénon, M. (1969). Numerical exploration of the restricted problem. V. Hill's case: Periodic orbits and their stability, *Astronomy and Astrophysics* **1**: 223–238.

Hénon, M. (1973a). Vertical stability of periodic orbits in the restricted problem. I. Equal masses, *Astronomy and Astrophysics* **28**: 415–426.

Hénon, M. (1973b). Vertical stability of periodic orbits in the restricted problem. II. Hill's case, *Astronomy and Astrophysics* **30**: 317–321.

Hénon, M. (2003). New families of periodic orbits in Hill's problem of three bodies, *Celestial Mechanics and Dynamical Astronomy* **85**(3): 223–246.

Hénon, M. (2005). Families of asymmetric periodic orbits in hill's problem of three bodies, *Celestial Mechanics and Dynamical Astronomy* **93**(1-4): 87–100.

Hirabayashi, M. and Scheeres, D. J. (2012). Fission and surface disruption limits for rapidly rotating asteroids: The case of Kleopatra, *Asteroids, Comets, Meteors 2012. LPI Contributions* **1667**.

Hopkins, J., Dissel, A., Jones, M., Russell, J. and Gaza, R. (2010). Plymouth Rock: An early human mission to Near Earth Asteroids using Orion spacecraft, *Technical report*, Lockheed Martin Corporation.

Howell, K. C. (2001). Families of orbits in the vicinity of collinear libration points, *Journal of the Astronautical Sciences* **49**(1): 107–125.

Howell, K. C. and Pernicka, H. J. (1993). Stationkeeping method for libration point trajectories, *Journal of Guidance, Control, and Dynamics* **16**(1): 151–159.

Hu, W. and Scheeres, D. J. (2002). Spacecraft motion about slowly rotating asteroids, *Journal of Guidance, Control, and Dynamics* **25**(4): 765–775.

Hughes, A. L. H., Colwell, J. E. and DeWolfe, A. W. (2008). Electrostatic dust transport on Eros: 3-D simulationa of pond formation, *Icarus* **195**: 630–648.

Ichtiaroglou, S. (1980). Elliptic Hill's problem: The continuation of periodic orbits, *Astronomy and Astrophysics* **92**: 139–141.

Ichtiaroglou, S. (1981). Elliptic Hill problem: Families of periodic orbits, *Astronomy and Astrophysics* **98**: 401–405.

Jacobson, S. A. and Scheeres, D. J. (2011). Dynamics of rotationally fissioned asteroids: Source of observed small asteroid systems, *Icarus* **214**(1): 161–178.

Jewitt, D., Agarwal, J., Li, J., Weaver, H., Mutchler, M. and Larson, S. (2014). Disintegrating asteroid p/2013 r3, *The Astrophysical Journal Letters* **784**(1).

Kanavos, S. S., Markellos, V. V., Perdios, E. A. and Douskos, C. N. (2002). The photogravitational Hill problem: Numerical exploration, *Earth, Moon and Planets* **91**: 223–241.

Katherine, Y.-Y. L. and Villac, B. (2010). Periodic orbits families in the Hill's three-body problem with solar radiation pressure, *Advances in the astronautical sciences* **136**(1): 285–300.

Kawaguchi, J., Fujiwara, A. and Uesugi, T. (2008). Hayabusa - Its technology and science accomplishment summary and Hayabusa-2, *Acta Astronautica* **62**(10-11): 639–647.

Keller, H. U., Barbieri, C., Lamy, P., Rickman, H., Rodrigo, R., Wenzel, K.-P., Sierks1, H., A'Hearn, M. F., Angrilli, F., Angulo, M., Bailey, M. E., Barthol, P., Barucci, M. A., Bertaux, J.-L., Bianchini, G., Boit, J.-L., Brown, V., Burns, J. A., Büttner, I., Castro, J. M., Cremonese, G., Curdt, W., Deppo, V. D., Debei, S., Cecco, M. D., Dohlen, K., Fornasier, S., Fulle, M., Germerott, D., Gliem, F., GuizzoS., G. P., Hviid, F., Ip, W.-H., Jorda, L., Koschny, D., Kramm, J. R., Kührt, E., Küppers, M., Lara, L. M., Llebaria, A., López, A., López-Jimenez, A., López-Moreno, J., Meller, R., Michalik, H., Michelena, M. D., Müller, R., Naletto, G., Origné, A., Parzianello,

G., Pertile, M., Quintana, C., Ragazzoni, R., Ramous, P., Reiche, K.-U., Reina, M., Rodríguez, J., Rousset, G., Sabau, L., Sanz, A., Sivan, J.-P., Stöckner, K., Tabero, J., Telljohann, U., Thomas, N., Timon, V., Tomasch, G., Wittrock, T. and Zaccariotto, M. (2007). OSIRIS - The scientific camera system onboard Rosetta, *Technical Report OSIRIS_SSR*, OSIRIS Space Science Review Instrument Paper.

Kelly, E. G. and Spottiswood, D. J. (1982). *Introduction to Mineral Processing*, Wiley-Interscience, New York, NY, USA.

Kidder, S. Q. and Vonder Haar, T. H. (1990). Notes and correspondence - On the use of Molniya orbits for meteorological observation of middle and high latitudes, *Journal of Atmospheric and Oceanic Technology* **7**: 517–522.

Kleiman, L. A. (1968). *Project Icarus: an MIT Student Project in Systems Engineering*, The MIT Press, Cambridge, MA, USA.

Koon, W. S., Lo, M. W., Marsden, J. E. and Ross, S. D. (2000). Heteroclinic connections between periodic orbits and resonance transitions in celestial mechanics, *Chaos* **10**(2): 427–469.

Koon, W. S., Lo, M. W., Marsden, J. E. and Ross, S. D. (2008). *Dynamical systems, the three-body problem and space mission design*, Marsden Books, Online book.

Kwiatkowski, T., Kryszczynska, A., Polinska, M., Buckley, D. A. H., O'Donoghue, D., Charles, P. A., Crause, L., Crawford, S., Hashimoto, Y., Kniazev, A., Loaring, N., Colmenero, E. R., Sefako, R., Still, M. and Vaisanen, P. (2009). Photometry of 2006 RH120: an asteroid temporary captured into a geocentric orbit, *Astronomy and Astrophysics* **495**: 967–974.

Landau, D. and Strange, N. (2011). Near-Earth Asteroids accesible to human exploration with high-power electric propulsion, *AAS/AIAA Astrodynamics Specialist Conference*, AAS 11-446, Girdwood, AK, USA.

Lantoine, G., Broschart, S. B. and Grebow, D. J. (2013). Design of quasi-terminator orbits near primitive bodies, *AAS/AIAA Astrodynamics Specialist Conference*, AAS 13-815, Hilton Head, SC, USA.

Lara, M. and Russell, R. (2006). Concerning the family "g" of the restricted three-body problem, *IX Jornadas de Trabajo en Mecanica Celeste*, Jaca, Spain.

Lara, M., Russell, R. and Villac, B. (2007). Classification of the distant stability regions at Europa, *Journal of Guidance, Control, and Dynamics* **30**(2): 409–418.

Lee, P. (1996). Dust levitation on asteroids, *Icarus* **124**: 181–194.

Lewis, J. S. (1996). *Mining The Sky: Untold riches from asteroids, comets and planets*, Helix Books/Perseus Books, Reading, Massachusetts, USA.

Little, J. M. and Choueiri, E. (2013). Electric propulsion system scaling for asteroid capture-and-return missions, *49th AIAA/ASME/SAE/ASEE Joint Propulsion Conference*, AIAA 2013-4125, San Jose, CA, USA.

Lo, M. W. and Ross, S. D. (1999). Low-energy interplanetary transfers using Lagrangian points, *NASA Tech Brief* **23**(11).

Lo, M. W. and Ross, S. D. (2001). The lunar L_1 gateway: Portal to the stars and beyond, *AIAA Space 2001 Conference*, AIAA 2001-4768, Albuquerque, NM, USA.

Lunan, D. (2014). *Incoming Asteroid! What Could We Do About It?*, Astronomers' Universe, Springer Science+Business Media, New York, NY, USA.

Mainzer, A., Grav, T., Bauer, J., Masiero, J., McMillan, R. S., Cutri, R. M., Walker, R., Wright, E., Eisenhardt, P., Tholen, D. J., Spahr, T., Jedicke, R., Denneau, L., DeBaun, E., Elsbury, D., Gautier, T., Gomillion, S., Hand, E., Mo, W., Watkins, J., Wilkins, A., Bryngelson, G. L., Del Pino Molina, A., Desai, S., Gómez Camus, M., Hidalgo, S. L., Konstantopoulos, I., Larsen, J. A., Maleszewski, C., Malkan, M. A., Mauduit, J., Mullan, B. L., Olszewski, E. W., Pforr, J., Saro, A., Scotti, J. V. and Wasserman, L. H. (2011). NEOWISE observations of Near-Earth Objects: Preliminary results, *The Astrophysical Journal* **743**(2).

Markellos, V. V., Roy, A. E., Velgakis, M. J. and Kanavos, S. S. (2000). A photogravitational Hill problem and radiation effect on Hill stability of orbits, *Astrophysics and Space Science* **271**: 293–301.

Marzari, F., Rossi, A. and Scheeres, D. (2011). Combined effect of YORP and collisions on the rotation rate of small Main Belt asteroids, *Icarus* **214**(2): 622–631.

Massonnet, D. and Meyssignac, B. (2006). A captured asteroid: Our David's stone for shielding Earth and providing the cheapest extraterrestrial material, *Acta Astronautica* **59**: 77–83.

Matukuma, T. (1930). On the periodic orbits in Hill's case, *Proceedings of the Imperial Academy of Japan* **6**(1): 6–8.

Matukuma, T. (1932). Periodic orbits in Hill's case. Second paper, *Proceedings of the Imperial Academy of Japan* **8**(5): 147–150.

Matukuma, T. (1933). Periodic orbits in Hill's case. Third paper, *Proceedings of the Imperial Academy of Japan* **9**(8): 364–366.

Mazanek, D. D., Merrill, R. G., Brophy, J. R. and Mueller, R. P. (2014). Asteroid Redirect Mission concept: A bold approach for utilizing space resources, *65th International Astronautical Congress*, IAC-14.D3.1.8, Toronto, Canada.

McInnes, C., Macdonald, M., Angelopolous, V. and Alexander, D. (2001). Geosail: Exploring the magnetosphere using a small solar sail, *Journal of Spacecraft and Rockets* **38**(4): 622–629.

McInnes, C. R. (1999). *Solar Sailing. Technology, Dynamics and Mission Applications*, Springer-Praxis Books in Aeronautical Engineering, Springer-Verlag, Berlin, Germany.

Melosh, H. J., Nemchinov, I. V. and Zetzer, Y. I. (1994). Non-nuclear strategies for deflecting comets and asteroids, *in* T. Gehrels (ed.), *Hazards due to comets and asteroids*, University of Arizona Press, Tucson, AZ, USA.

Melosh, H. and Stansberry, J. (1991). Doublet craters and the tidal disruption of binary asteroids, *Icarus* **94**(1): 171–179.

Michalodimitrakis, M. (1980). Hill's problem: families of three-dimensional periodic orbits, *Astrophysics and Space Science* **68**(1): 253–268.

Michel, P. (2013). Physical properties of Near-Earth Objects that inform mitigation, *Acta Astronautica* **91**(1): 6–13.

Michel, P., Zappala, V., Cellino, A. and Tanga, P. (2000). Estimated abundance of Atens and asteroids evolving on orbits between Earth and Sun, *Icarus* **143**: 421–424.

Miele, A. (2010). Revisit of the theorem of image trajectories in the Earth–Moon space, *Journal of Optimization Theory and Applications* **147**(3): 483–490.

Mingotti, G., Sánchez, J. P. and McInnes, C. (2014). Combined low-thrust propulsion and invariant manifold trajectories to capture NEOs in the Sun-Earth circular restricted three-body problem, *Celestial Mechanics and Dynamical Astronomy* **120**(3): 309–336.

Miyamoto, H., Kargel, J. S., Fink, W. and Furfaro, R. (2008). Granular processes on Itokawa, a small near-Earth asteroid: implications for resource utilization, *Proceedings of the SPIE* **6960**: 1–8.

Miyamoto, H., Yano, H., Scheeres, D. J., Abe, S., Barnouin-Jha, O., Cheng, A. F., Demura, H., Gaskell, R. W., Hirata, N., Ishiguro, M., Michikami, T., Nakamura, A. M., Nakamura, R., Saito, J. and Sasaki, S. (2007). Regolith migration and sorting on asteroid Itokawa, *Science* **316**(5827): 1011–1014.

Moons, M. (1996). Review of the dynamics in the Kirkwood gaps, *Celestial Mechanics and Dynamical Astronomy* **65**(1): 175–204.

Morbidelli, A. and Vokrouhlický, D. (2003). The Yarkovsky-driven origin of near–Earth asteroids, *Icarus* **163**(1): 120–134.

Murdoch, N., Abell, P., Carnelli, I., Carry, B., Cheng, A., Drolshagen, G., Fontaine, M., Galvez, A., Koschny, D., Kueppers, M., Michel, P., Reed, C. and Ulamec, S. (2012). Asteroid Impact & Deflection Assessment (AIDA) mission. Opportunities and tests in a US-Europe space mission cooperation., *Interim release*, ESA.

Murray, C. D. and Dermott, S. F. (1999). *Solar System Dynamics*, Cambridge University Press, Cambridge, United Kingdom.

Nocedal, J. and Wright, S. J. (2006). Sequential quadratic programming, *Numerical Optimization*, second edn, Springer Series in Operations Research and Financial Engineering, Springer-Verlag, New York, NY, USA, pp. 530–563.

Nugent, C. R., L., M. J., R., C. S. and Vokrouhlický, D. (2012). Detection of semimajor axis drifts in 54 near–Eearth asteroids: new measurements of the Yarkovsky effect, *The Astronomical Journal* **144**(60): 1:13.

O'Leary, B., Gaffey, M. J., Ross, D. J. and Salkeld, R. (1979). Retrieval of asteroidal materials, *in* B. Gossett (ed.), *Space Resources and Space Settlements.*, University Press of the Pacific, Los Altos, CA, USA, chapter IV-2.

Öpik, E. J. (1951). Collision probabilities with the planets and the distribution of interplanetary matter, *Proceedings of the Royal Irish Academy. Section A: Mathematical and Physical Sciences* **54**(A): 165–199.

Oyama, T., Yamakawa, H. and Omura, Y. (2008). Orbital dynamics of solar sails for geomagnetic tail exploration, *Journal of Spacecraft and Rockets* **45**(2): 316–323.

Paolicchi, P., Burns, J. A. and Weidenschilling, S. J. (2002). Side effects of collisions: Spin rate changes, tumbling rotation states, and binary asteroids, *in* W. Bottke, A. Cellino, P. Paolicchi and R. P. Binzel (eds), *Asteroids III*, University of Arizona Press, Tucson, AZ, USA, pp. 517–526.

Papadakis, K. E. (1996). Families of periodic orbits in the photogravitational three-body problem, *Astrophysics and Space Science* **245**: 1–13.

Papadakis, K. E. (2006). The planar photogravitational Hill problem, *International Journal of Bifurcation and Chaos* **16**(6): 1809–1821.

Parness, A. (2011). Anchoring foot mechanisms for sampling and mobility in microgravity, *Proceedings of the IEEE International Conference on Robotics and Automation*, Shanghai, China, pp. 6597–6599.

Pater, I. d. and Lissauer, J. J. (2010). *Planetary Sciences*, 2nd edn, Cambridge University Press, New York, NY, USA.

Pearson, J., Oldson, J. and Levin, E. (2006). Earth rings for planetary environment control, *Acta Astronautica* **58**(1): 44–57.

Perko, L. M. (1982). Periodic solutions of the restricted problem that are analytic continuations of periodic solutions of Hill's problem for small $\mu > 0$, *Celestial mechanics* **30**(2): 115–132.

Pop, V. (2006). *Unreal Estate: The Men Who Sold the Moon*, Exposure Publishing, Burguess Hill, United Kingdom.

Pop, V. (2008). *Who Owns the Moon? Extraterrestial Aspects of Land and Mineral Resources Ownership*, Vol. 4 of *Space Regulations Library*, Springer, New York, NY, USA.

Pop, V. (2013). Legal considerations on asteroid exploitation and deflection, *in* V. Badescu (ed.), *Asteroids. Prospective Energy and Material Resources*, Springer-Verlag Berlin Heidelberg, pp. 659–680.

Poynting, J. H. (1904). Radiation in the solar system: its effect on temperature and its pressure on small bodies, *Philosophical Transactions of the Royal Society of London. Series A* **202**(346-358): 525–552.

Pravec, P., Harris, A. W. and Michalowski, T. (2002). Asteroid rotations, *in* W. Bottke, A. Cellino, P. Paolicchi and R. P. Binzel (eds), *Asteroids III*, University of Arizona Press, Tucson, AZ, USA, pp. 113–122.

Qiao, D. (2014). Trajectory options for low-cost missions to Easily Retrievable Objects, *2nd IAA Conference on Dynamics and Control of Space Systems*, IAA-AAS-DyCoSS2-14-06-06, Rome, Italy.

Quinn, J. W., Captain, J. G., Weis, K., Santiago-Maldonado, E. and Trigwell, S. (2013). Evaluation of tribocharged electrostatic beneficiation of lunar simulant in lunar gravity, *Journal of Aerospace Engineering* **26**(1): 37–42.

Richardson, D. C. (1995). A self-consistent numerical treatment of fractal aggregate dynamics, *Icarus* **115**: 320–335.

Richardson, D. C., Bottke, W. F. and Stanley, G. L. (1998). Tidal distortion and disruption of Earth-crossing asteroids, *Icarus* **134**: 47–76.

Richardson, D. L. (1980). Halo orbit formulation for the ISEE-3 mission, *Journal of Guidance, Control, and Dynamics* **3**(6): 543–548.

Richter, K. and Keller, H. U. (1995). On the stability of dust particle orbits around cometary nuclei, *Icarus* **114**: 355–371.

Richter, L. (1998). Principles for robotic mobility on minor solar system bodies, *Robotics and Autonomous Systems* **23**(1-2): 117–124.

Robertson, H. P. (1937). Dynamical effects of radiation in the solar system, *Monthly Notices of the Royal Astronomical Society* **97**(6): 423–437.

Robinson, M. S., Thomas, P. C., Veverka, J., Murchie, S. and Carcich, B. (2001). The nature of ponded deposits on Eros, *Nature* **413**: 396–400.

Ross, S. D. (2001). Near-Earth asteroid mining, *Caltech internal report*, Space Industry Report, Caltech.

Rubincam, D. P. (1995). Asteroid orbit evolution due to thermal drag, *Journal of Geophysical Research* **100**(E1): 1595–1594.

Rubincam, D. P. (2000). Radiative spin-up and spin-down of small asteroids, *Icarus* **148**: 2–11.

Ruprecht, J. D., Stuart, J. S., Woods, D. F. and Shah, R. Y. (2014). Detecting small asteroids with the space surveillance telescope, *Icarus* **239**: 253–259.

Russell, R. P. (2006). Global search for planar and three-dimensional periodic orbits near Europa, *Journal of the Astronautical Sciences* **54**(2): 199–226.

Saint-Exupéry, A. (1943). *The Little Prince*, Reynal & Hitchcock, New York, NY, USA.

Salter, J. D. and Wyatt, N. P. G. (1991). Sorting in the minerals industry: past, present and future, *Minerals Engineering* **4**(7-11): 779–796.

Sanchez Cuartielles, J. P., Alessi, E. M., García Yárnoz, D. and McInnes, C. (2013). Earth resonant gravity assists for asteroid retrieval missions, *64th International Astronatical Congress*, IAC-13.C1.7.8, Beijing, China.

Sanchez Cuartielles, J. P., Colombo, C., Vasile, M. and Radice, G. (2009). Multicriteria comparison among several mitigation strategies for dangerous Near–Earth Objects, *Journal of Guidance, Control, and Dynamics* **32**(1): 121–142.

Sanchez, J. P. and Colombo, C. (2013). Impact hazard protection efficiency by a small kinetic impactor, *Journal of Spacecraft and Rockets* **50**(2): 380–393.

Sanchez, J. P., García-Yárnoz, D., Alessi, E. M. and McInnes, C. R. (2012a). Gravitational capture opportunities for asteroid retrieval missions, *63rd International Astronautical Congress*, IAC-12.C1.5.13, Naples, Italy.

Sanchez, J. P., García-Yárnoz, D. and McInnes, C. R. (2012b). Near-Earth Asteroid resource accessibility and future capture missions opportunities, *Global Space Exploration Conference*, GLEX-2012.11.1.5, Washington D.C., USA.

Sanchez, J. P. and McInnes, C. R. (2011a). Asteroid resource map for near-Earth space, *Journal of Spacecraft and Rockets* **48**(1): 153–165.

Sanchez, J. P. and McInnes, C. R. (2011b). On the ballistic capture of asteroids for resource utilization, *62nd International Astronautical Congress*, IAC-11.C1.4.6, IAF, Cape Town, South Africa.

Sanchez, J. P. and McInnes, C. R. (2013). Available asteroid resources in the Earth's neighbourhood, *in* V. Badescu (ed.), *Asteroids: Prospective Energy and Material Resources*, Springer-Verlag Berlin Heidelberg, pp. 439–458.

Sánchez, P. and Scheeres, D. J. (2013). Granular cohesion and fast rotators in the NEA population, *International Conference on Micromechanics of Granular Media. AIP Conference Proceedings*, Vol. 1542, Sidney, Australia, pp. 955–988.

Scheeres, D. (2007). Orbit mechanics about small asteorids, *20th International Symposium on Space Flight Dynamics*, Annapolis, MD, USA.

Scheeres, D. J. (1994). Dynamics about uniformly rotating triaxial ellipsoids: Application to asteroids, *Icarus* **110**: 225–238.

Scheeres, D. J. (1999). Satellite dynamics about small bodies: Averaged solar radiation pressure effects, *Journal of the Astronautical Sciences* **47**: 26–46.

Scheeres, D. J. (2012a). Controlled hovering motion at an asteroid, *Orbital Motion in Strongly Perturbed Environments: Applications to Asteroid, Comet and Planetary Satellite Orbiters*, Springer-Verlag Berlin Heidelberg, pp. 243–254.

Scheeres, D. J. (2012b). Introduction and background, *Orbital Motion in Strongly Perturbed Environments: Applications to Asteroid, Comet and Planetary Satellite Orbiters*, Springer-Verlag Berlin Heidelberg, pp. 4–13.

Scheeres, D. J. (2012c). Modelling small body environments, *Orbital Motion in Strongly Perturbed Environments: Applications to Asteroid, Comet and Planetary Satellite Orbiters*, Springer-Verlag Berlin Heidelberg, pp. 23–59.

Scheeres, D. J. (2012d). Solar radiation pressure: Exact analysis, *Orbital Motion in Strongly Perturbed Environments: Applications to Asteroid, Comet and Planetary Satellite Orbiters*, Springer-Verlag Berlin Heidelberg, pp. 255–275.

Scheeres, D. J. (2012e). Solution and characterization methods, *Orbital Motion in Strongly Perturbed Environments: Applications to Asteroid, Comet and Planetary Satellite Orbiters*, Springer-Verlag Berlin Heidelberg, pp. 143–169.

Scheeres, D. J., Benner, L. A. M., Ostrob, S. J., Rossi, A., Marzari, F. and Washabaugh, P. (2005). Abrupt alteration of asteroid 2004 MN4's spin state during its 2029 Earth flyby, *Icarus* **178**: 281–283.

Scheeres, D. J., Durda, D. D. and Geissler, P. E. (2002). The fate of asteroid ejecta, *in* W. Bottke, A. Cellino, P. Paolicchi and R. P. Binzel (eds), *Asteroids III*, University of Arizona Press, Tucson, AZ, USA, pp. 527–544.

Scheeres, D. J., Hartzell, C. M., Sánchez, P. and Swift, M. (2010). Scaling forces to asteroid surfaces: The role of cohesion, *Icarus* **210**: 968–984.

Scheeres, D. J. and Marzari, F. (2000). Temporary orbital capture of ejecta from comets and asteroids: Applications to the Deep Impact experiment, *Astronomy and Astrophysics* **356**: 747–756.

Scheeres, D. J., Ostro, S. J., Hudson, R., DeJong, E. M. and Suziki, S. (1998). Dynamics of orbits close to asteroid 4179 Toutatis, *Icarus* **132**: 53–79.

Scheeres, D. J., Ostro, S. J., Hudson, R. S. and Werner, R. A. (1996). Orbits close to asteroid 4769 Castalia, *Icarus* **121**: 67–87.

Scheeres, D. J., Ostro, S. J., Werner, R. A., Asphaug, E. and Hudson, R. S. (2000). Effects of gravitational interactions on asteroid spin states, *Icarus* **147**: 106–118.

Scheeres, D. J. and Schweickart, R. L. (2004). The mechanics of moving asteroids, *Planetary Defense Conference*, AIAA-2004-1446, Orange County, CA, USA.

Scheeres, D., Miller, J. and Yeomans, D. (2003). The orbital dynamics environment of 433 Eros: A case study for future asteroid missions, *Technical Report IPN Progress Report 42-152*, JPL / InterPlanetary Network Directorate, Los Angeles, CA, USA.

Schuerman, D. W. (1980). The restricted three-body problem including radiation pressure, *The Astrophysical Journal* **238**: 337–342.

Schunová, E., Jedicke, R., Walsh, K. J., Granvik, M., Wainscoat, R. J. and Haghighipourb, N. (2014). Properties and evolution of NEO families created by tidal disruption at Earth, *Icarus* **238**: 156–169.

Shah, R., Woods, D. F., Faccenda, W., Johnson, J., Lambour, R., Pearce, E. C. and Stuart, J. S. (2013). Asteroid detection with the space surveillance telescope, *Advanced Maui Optical and Space Surveillance Technologies Conference (AMOSTech)*, Maui, HI, USA.

Shapiro, I. I., A'Hearn, M., Vilas, F. and et.al. (2010). Defending planet Earth: Near-Earth Object surveys and hazard mitigation strategies, *Technical Report ISBN 9780309149686*, National Research Council.

Simmons, J. F. L., McDonald, A. J. C. and Brown, J. C. (1985). The restricted 3-body problem with radiation pressure, *Celestial Mechanics* **35**: 145–187.

Simó, C. (1973). Solución del problema de Lambert mediante regularización, *Collectanea Mathematica* **24**(3): 231–247.

Simó, C., Gómez, G., Llibre, J., Martínez, R. and Rodríguez, J. (1987). On the optimal station keeping control of halo orbits, *Acta Astronautica* **15**(67): 391–397.

Simó, C. and Stuchi, T. (2000). Central stable/unstable manifolds and the destruction of KAM tori in the planar hill problem, *Physica D: Nonlinear Phenomena* **140**: 1–32.

Sincarsin, G. B. and Hughes, P. C. (1983). Gravitational orbit-attitude coupling for very large spacecraft, *Celestial Mechanics* **31**: 143–161.

Steinberg, E. and Sari, R. (2011). Binary YORP and evolution of binary asteroids, *The Astronomical Journal* **141**(2/55): 1–10.

Stoeser, D., Benzel, W., Schrader, C., Edmunson, J. and Rickman, D. (2011). Notes on lithology, mineralogy, and production for lunar simulants, *Technical Report NASA/TM2011216454*, NASA.

Strange, N., Landau, D. and Chodas, P. (2014). Identification of retrievable asteroids with the Tisserand criterion, *SPACE 2014 – AIAA/AAS Astrodynamics Specialist Conference*, AIAA 2014-4458, AIAA/AAS, San Diego, CA, USA.

Strömgren, E. (1922). Forms of periodic motion in the restricted problem and in the general problem of three bodies, according to researches executed at the Observatory Copenhagen, *Publikationer og mindre Meddeler fra Kobenhavns Observatorium* **39**: 3–29.

Struck, C. (2007). The feasibility of shading the greenhouse with dust clouds at the stable lunar Lagrange points, *Journal of the British Interplanetary Society* **60**: 82–89.

Szebehely, V. (1967). *Theory of orbits*, Academic Press, New York, NY, USA.

Szebehely, V. and Nacozy, P. (1967). A class of E. Strömgren's direct orbits in the restricted problem, *The Astronomical Journal* **72**(2): 184–190.

Takahashi, Y. and Scheeres, D. J. (2011). Small-body postrendezvous characterisation via slow hyperbolic flybys, *Journal of Guidance, Control, and Dynamics* **34**(6): 1815–1827.

Tancredi, G. (1997). An asteroid in an Earth-like orbit, *Celestial Mechanics and Dynamical Astronomy* **69**(1-2): 119–132.

Toth, J., Veres, P. and Kornos, L. (2011). Tidal disruption of NEAs - a case of Pribram meteorite, *Monthly Notices of the Royal Astronomical Society* **415**: 1527–1533.

Tsiolkovsky, K. E. (1903). The exploration of cosmic space by means of reaction devices, *The Scientific Review* **5**.

Tsirogiannis, G. A. and Markellos, V. V. (2013). A greedy global search algorithm for connecting unstable periodic orbits with low energy cost, *Celestial Mechanics and Dynamical Astronomy* **117**(2): 201–213.

Urrutxua, H., Scheeres, D. J., Bombardelli, C., Gonzalo, J. L. and Pelaez, J. (2014). What does it take to capture and asteroid? A case study on capturing asteroid 2006 RH120, *24^{th} AAS/AIAA Space Flight Mechanics Meeting*, AAS 14-276, Santa Fe, NM, USA.

Vallado, D. A. (2007). *Fundamentals of Astrodynamics and Applications*, third edn, Microcosm Press & Springer, Hawthorne, CA / New York, NY, USA.

Valverde, J. M. and Castelllanos, A. (2006). Random loose packing of cohesive granular materials, *Europhysics Letters* **75**(6): 985–991.

Vasile, M., Gibbings, A., Vetrisano, M., Sanchez Cuartielles, J.-P., Garcia Yarnoz, D., Burns, D., Hopkins, J.-M., McInnes, C., Colombo, C., Eckersley, S., Wayman, A., Branco, J., di Sotto, E. and Guerreiro, L. (2013). LightTouch^2, effective solutions to asteroid manipulation, *Technical Report 12/X03 ESA/4000107024/12/F/MOS*, University of Strathclyde, ESA GSP SysNova Initiative.

Vasile, M. and Locatelli, M. (2009). A hybrid multiagent approach for global trajectory optimization, *Journal of Global Optimization* **44**(4): 461–479.

Veres, P., Jedicke, R., Wainscoat, R., Granvik, M., Chesley, S., Abe, S., Denneau, L. and Grav, T. (2009). Detection of Earth-impacting asteroids with the next generation all-sky surveys, *Icarus* **203**(2): 472–485.

Verrier, P. (2013). Connections between Halo families and prograde families in the Earth–Moon CRTBP, *(unpublished)*, University of Strathclyde, Glasgow, UK, pp. 1–11.

Verrier, P. and McInnes, C. (2015). Low-energy capture of asteroids onto Kolmogorov-Arnold-Moser tori, *Journal of Guidance, Control, and Dynamics* **38**(2): 330–335.

Villac, B. F. (2003). *Dynamics in the Hill problem with applications to spacecraft maneuvers*, PhD thesis, The University of Michigan, Ann Arbor, MI, USA.

Voyatzis, G., Gkolias, I. and Varvoglis, H. (2012). The dynamics of the elliptic Hill problem: periodic orbits and stability regions, *Celestial Mechanics and Dynamical Astronomy* **113**(1): 125–139.

Wallace, M. S. and Broschart, S. (2013). Circular-orbit maintenance strategies for primitive body orbiters, *AAS/AIAA Astrodynamics Specialists Conference 2013*, AAS 13-816, Hilton Head, SC, USA.

Walsh, K. J., Michel, P. and Richardson, D. (2011). Collisional and rotational disruption of asteroids, *Advanced Science Letters* **4**: 311–324.

Walsh, K. J., Richardson, D. C. and Michel, P. (2012). Spin-up of rubble-pile asteroids: Disruption, satellite formation, and equilibrium shapes, *Icarus* **220**(2): 514–529.

Yang, R. Y., Zou, R. P., Dong, K., An, X. Z. and Yu, A. (2007). Simulation of the packing of cohesive particles, *Computer Physics Communications* **177**: 206–209.

Zagouras, C. and Markellos, V. V. (1977). Axisymmetric periodic orbits of restricted problem in three dimensions, *Astronomy and Astrophysics* **59**: 79–89.

Zoua, X., Lia, C., Liua, J., Wanga, W., Lia, H. and Pinga, J. (2014). The preliminary analysis of the 4179 Toutatis snapshots of the Chang'e-2 flyby, *Icarus* **229**: 348–354.